SCHOOL OF INDUSTRIAL AND MANUFACTURING SCIENCE

PhD Thesis

By

Iain Johnstone

Academic Year 2001 - 2002

A CRITICAL STUDY OF HIGH EFFICIENCY DEEP GRINDING

Supervisors: - Prof. D. Stephenson and Prof. J. Corbett

"Come forth, the sky is wide and it is a far cry to the worlds ends"...."There is a road which leads to the Moon and Great Waters, and it has no end; but it is a fine road, a braw road – who will follow it?...."

John Buchan

Excerpts from: The Rime of True Thomas

Abstract

The recent years, the aerospace industry in particular has embraced and actively pursued the development of stronger high performance materials, namely nickel based superalloys and hardwearing steels. This has resulted in a need for a more efficient method of machining, and this need was answered with the advent of High Efficiency Deep Grinding (HEDG). This relatively new process using Cubic Boron Nitride (CBN) electroplated grinding wheels has been investigated through experimental and theoretical means applied to two widely used materials, M50 bearing steel and IN718 nickel based superalloy. It has been shown that this grinding method using a stiff grinding centre such as the Edgetek 5-axis machine is a viable process.

Using a number of experimental designs, produced results which were analysed using a variety of methods including visual assessment, sub-surface microscopy and surface analysis using a Scanning Electron Microscope (SEM), residual stress measurement using X-Ray Diffraction (XRD) techniques, Barkhausen Noise Amplitude (BNA) measurements, surface roughness and Vickers micro-hardness appraisal.

It has been shown that the fundamentals of the HEDG process have been understood through experimental as well as theoretical means and that through the various thermal models used, grinding temperatures can be predicted to give more control over this dynamic process.

The main contributions to knowledge are made up of a number of elements within the grinding environment, the most important being the demonstration of the HEDG effect, explanation of the phenomenon and the ability to model the process. It has also been shown that grinding is a dynamic process and factors such as wheel wear will result in a continuous change in the optimum grinding conditions for a given material and wheel combination. With the significance of these factors recognised, they can be accounted for within an industrial adaptive control scenario with the process engineer confident of a more efficient use of time and materials to produce a higher quality product at lower cost.

Author's Profile

The author gained a wide experience level within the aerospace industry through twelve years service with the Royal Air Force and seven years working in various, sometimes, exotic places around the world.

The author read a first degree in Automotive Engineering and was awarded his B. Eng honours degree by the University of Hertfordshire. The culmination of studies undertaken was a final year research project entitled the Optimisation of a Twin Wing Assembly. This thesis won third prize when entered into a national competition by the Institute of Vehicle Engineers.

Having been successful in applying for a Masters in Research place at Cranfield University the author was rather taken aback when Professor Stephenson telephoned and asked if he would rather attempt a PhD course.

He did.

Acknowledgements

Professors D. Stephenson and J. Corbett for their uncompromising encouragement throughout this experience.

One should never forget or underestimate the few who gave the "above and beyond" support, namely Dr. John Barnes, Martin Faulkner, Paul Morantz and Andy Roberts.

The technical staff who collectively attempted to aid myself in various ways throughout the whole three year term. These technical types were as follows Andy Baldwin, John Hedge, Tim Prior, Andrew Dyer and Christine Kimpton are all due acknowledgements, some more than others for their unwavering and of course stress-free assistance which covered a variety of situations.

One should always acknowledge the sponsors involved in the project these were; Rolls Royce, SKF Italy, Saint-Gobain, Castrol, Renold Precision Technologies, Jones & Shipman, Wanner International and the Engineering and Physical Sciences Research Council for the funding of this research programme.

A special thank you goes to Miss Karen Moir who has been in the forefront of many a diverse evening.

Author's Publications

I declare that this doctoral thesis and the work contained therein was the sole work of the author except where explicitly stated otherwise in the text. The following articles were published during the period of research. Certain material and concepts from these publications, where necessary, will be presented within the body of this work.

Johnstone, I., Jin, T. Baldwin, A., Corbett J. and Stephenson, D.J. (2002). High Efficiency Deep Grinding (HEDG) of M50 Bearing Steel. *International Journal of Machine Tools & Manufacture*, In Press

Stephenson, D. J., Laine, E., Johnstone, I., Baldwin, A. & Corbett, J., (2001). Burn threshold studies for super abrasive grinding using electroplated CBN wheels. In: 4th International Machining & Grinding Conference, Troy, MI., USA 7th - 9th May 2001.

Table of Contents

Table of Figures

Table of Tables

Nomenclature

(Further details of nomenclature are contained in the text as appropriate)

a_e	*Depth of Cut*
C	*Temperature constant for workpiece conduction*
c	*Specific heat capacity*
D	*Wheel diameter*
E	*Young's modulus of elasticity (Pascals)*
ε	*Measured strain*
e	*Effective or real value*
e_c	*Specific energy (power/volume removal rate = energy/unit volume)*
fin	*Value on finished grinding surface*
F_t	*Tangential grinding force*
F_z	*Normal grinding force*
G	*Giga*
G Ratio	*Grinding Ratio (Material Removed / Wheel Wear)*
k	*Thermal conductivity*
l	*Half-width of heat source*
l_c	*Contact length along inclined plain*
l_i	*Contact length along arc*
max	*Maximum value*
M	*Mega*
P	*Grinding power*
Pe	*Peclet number* ($v_w.l_c/2\alpha$)
T	*Temperature*
q	*Heat flux entering an element (power per unit contact area)*
Q'_w	*Specific material removal rate*
Q_w	*Material removal rate*
R	*Fraction of total heat entering a process element*
r_o	*Wear flat contact radius*
s	*Suffix used for grinding wheel*
σ	*Calculated stress (Pascals)*
t	*Suffix used for total*
U	*Specific grinding energy*
v_s	*Grinding wheel speed*

v_w	*Work piece in feed rate*
w	*Suffix used for work piece*
α	*Thermal diffusivity (k/ρc)*
β	*Geometric mean thermal property (√(kρc))*
λ	*wavelength*
ϕ	*Angle of inclination of heat source relative to horizontal*
ρ	*Density*

List of Abbreviations

Al_2O_3	*Aluminium Oxide*
Alox	*Aluminium Oxide*
BNA	*Barkhausen Noise Amplitude*
CBN	*Cubic Boron Nitride*
CDCF	*Continuous Dressing Creep Feed Grinding*
CONCAWE	*CONservation of Clean Air and Water in Europe.*
emf	*ElelectroMagnetic Force*
EP	*Electroplated*
EU	*European Union*
HEDG	*High Efficiency Deep Grinding*
LD	*Lethal Dosage*
MRes	*Masters in Research*
NDT	*Non Destructive Testing*
Pa	*Pascals*
PCBN	*Poly Crystalline Cubic Boron Nitride*
PCD	*Poly Crystalline Diamond*
SEM	*Scanning Electron Microscope*
SiC	*Silicon Carbide*
VAR	*Vacuum Arc Re-Melted*
VIM	*Vacuum Induction Melted*
XRD	*X Ray Diffraction*

In Memory of my Father

CHAPTER 1 INTRODUCTION

Abrasive machining has been used in industry for many years but now technological advances have encouraged this technology to the forefront of new and exciting areas of research. As custom designed grinding centres, more versatile grinding wheels and highly engineered grinding fluids become available the requirement of research to ascertain the efficiency of these new processes and systems has become a feasible option. As industry requires more efficient use of time and resources this research program and subsequent thesis is concerned with the development of high efficiency deep grinding and associated technologies.

The aim of this introduction is to provide the necessary background for the development of the thesis in the chapters that follow, with particular emphasis on grinding technology related to the Edgetek Machine (see Chapter 3) and the HEDG process. In addition, the correlation of a wide array of responses is investigated with a view to enhance the future working practices regarding HEDG.

1.1 Background

High efficiency deep grinding (HEDG) is a relatively new grinding technology. HEDG, whilst combining the mechanics of high-speed and creep-feed grinding, offers the possibility of achieving very efficient grinding, with values of specific energy much lower than in high-speed and creep-feed grinding, Tawakoli (1993).

As the material removal rate is increased, both the volume of grinding chips and the amount of heat increase, which suggests that there should be an upper limit of material removal rate. This is readily observed in creep-feed grinding when feed rate is increased. With HEDG, the material removal rates are increased substantially compared to creep-feed grinding, and thermal damage to the workpiece could be a serious concern. However, the thermal phenomena occurring during HEDG are thought to be very different from those experienced in shallow, high-speed and creep-feed grinding. To reduce the flow of heat into the workpiece a combination of high wheel speeds and sufficiently high feed rates and depths of cut are used. Tawakoli (1993) stated that high wheel speeds result in short contact times between the abrasive grits and the workpiece, and Rowe (2001) reported that the bulk of the heat is

removed with the grinding chips and the grinding fluid. As the feed rate is increased both the chip thickness and material removal rate increase although the specific grinding energy decreases. A significant reduction in specific grinding energy is required in order to limit workpiece temperature rise. The HEDG process reduces the transmission of heat to the finished surface due to the combined effects of large inclination angles and high work speeds. This in theory allows very high removal rates to be achieved, without causing thermal damage to the finished component. Thus, a fundamental understanding of the mechanical and thermal performance of HEDG is essential in order to determine the boundaries for HEDG and achieve a robust and reliable model, which validates the HEDG concept.

Rowe (2001) stated that the initial concept of HEDG was proposed by Gühring in 1967. The concept was developed further by Werner and Tawakoli during the 1980's and 90's. Tawakoli stated quite clearly in his book that HEDG does not conform to the conventional mode of grinding. The idea that when the depth of cut is increased with elevated feed rates accompanied by higher wheel speeds, a lower grinding work piece temperatures results even today sounds outlandish. With this in mind, this revolutionary grinding method is required to be tested on various materials using a number of different grinding parameters.

The following chapters provide the necessary background to research area and then summarise the work carried out, results generated and conclusions drawn.

1.2 Reasons for this research

Grinding or the ability to use abrasive particles to reduce the size of a component or change its shape has been used for centuries. Even with the advent of machines specifically designed for high efficiency deep grinding operations modern conservative attitudes still prevail, so that conventional grinding techniques such as creep feed grinding and reciprocating grinding are the main uses for these relatively stiff grinding centres. This research was started in order to provide manufacturing industry with the confidence that the HEDG process could be operated under industrial production conditions. Industrial collaborations across the entire process chain were involved with the project.

Table 1.1 gives details of the individual sponsors and associated business.

Rolls Royce	Gas Turbines
SKF Italy	Aerospace Bearings
Castrol	Grinding Fluids
Saint Gobain	Abrasive Wheels
Wanner International	High Pressure Pumps
Renold Precision Technologies	Edgetek Grinding Centre
Jones & Shipman	Edgetek Grinding Centre

Table 1.1: Sponsors & Associated Interest

Each sponsor was interested in their own area of expertise in relation to the research. Each wished to gain more information as to how their product would react to the vigorous environment of high efficiency deep grinding. The research therefore focused on both the fundamental principles of HEDG and the industrial application of the technology.

1.3 Aims & Objectives

The Edgetek test programme was initiated in July 1999. The aims and objectives at that point were to monitor different aspects of the grinding process during a number of predefined tasks. These tasks, which are shown in Appendix A, were decided by the sponsors, to take into account various aspects of grinding while retaining a HEDG bias. These decisions also indicated that such parameters as types of grinding fluid, grit sizes and grinding mode should be pursued for different material types. The main criterion was one of safety when the types of grinding fluid were chosen. As the final tests were to manufacture actual aerospace components, it was decided to minimise the possibility of corrosion by omitting sulphur and chlorine based additives. In addition, it was decided to test the efficiency of the three main types of grinding fluid within the project. These were mineral grinding fluid, synthetic ester based grinding fluid and water based grinding fluid. The grit sizes were chosen to cater for the materials used within the project. M50 bearing steel is an extremely hard material of Rockwell Hardness (R_c) 62, and was machined with a B151 grit. The other nickel based superalloy materials were both ground using the B252 CBN grit; the first was IN718 a tough creep resistant material and the second MAR-M-002 an equi-axed

material used in the manufacture of high pressure turbine blades in axial flow gas turbine engines. The aspect of up or down grinding was decided upon using the work carried out by Tawakoli. Tawakoli states that for specific material removal rates of 0 to 20mm^2/s and above 70mm^2/s then down grinding should be used. For the specific material removal rates from 20-70mm^2/s then Tawakoli advocates the use of up grinding. Although the methodology changed during the project timescale the main aims were kept intact as they were seen to retain their importance throughout the study.

Thus the objectives of this project were to:

- identify the mechanisms of HEDG such that process parameters can be optimised to assess maximum material removal rates and acceptable surface integrity.

- demonstrate that the HEDG effect exists e.g. specific grinding energy and workpiece surface temperature reduce with high material removal rates.

- produce predictive tools which can be used within industry, and within areas of adaptive control scenarios to enhance the final quality of the ground components.

1.4 Research Rationale

During the initial acceptance tests the Edgetek machine performed as expected. With the initial testing completed loop stiffness tests were concluded with the stiffness being calculated at 98N/μm at a distance of 200mm from the z-axis.

A modified programme of work based on a number of Taguchi 2 level factorial experiments was undertaken. This type of design of experiments enables the interactions between the most important variables to be considered when using the minimum number of tests, which indicate by arithmetical means the possible direction of the most optimised parameters.

In optimising the grinding process for M50 tool steel and IN718 nickel based superalloy, the grinding fluid system and the grit wear characteristics proved to be amongst the most sensitive parameters. It is well documented in the technical literature that the fundamental characteristics of the grinding fluid delivery system have to be understood before any significant headway can be gained.

Following this work a more appropriate value of the parameters were identified, and a number of experiments were undertaken to investigate different aspects of grinding. For example how the generation of wear flats affected levels of specific grinding energy and the subsequent calculated temperatures over a wide range of specific material removal rates.

Using the burn threshold technique devised by Malkin (1974) the experimental data gave a clear indication of when surface burn should occur in relation to the energy required. Theoretical calculations were investigated using previously published material by Rowe et al (2001). This thermal modelling is designed to predict the onset of surface burn for any given set of parameters. Additional work was required to measure temperatures within the grinding zone during grinding operations, using up and down grinding. These measurements were then correlated with the predicted temperatures, residual stress measurements and surface integrity studies.

Finally components were manufactured using the information obtained during this investigation. The components were nickel based superalloy turbine blade roots and M50 steel bearing rings.

1.5 Structure of Thesis

The work is presented in 10 chapters, the first being the introduction. The initial step in this research was to give background information into HEDG, and give reasons why the research was undertaken, list the aims and objectives and describe the research rationale. Chapter 2 (Literature Review) details the results of an extensive literature review to highlight the main results arising from the research carried out within the field. Chapter 3 (Edgetek Machine) describes the acceptance tests carried out on the Edgetek 5-axis machine. Chapter 4 (Experimental Technique) gives details

of the experimental method followed, regarding the initial tests followed when investigating the HEDG process, and using a host of associated engineering analysis techniques. Chapter 5 (M50 Bearing Steel) and Chapter 6 (IN718 Nickel Based Superalloy) give details of the results of the grinding experiments, and discusses them in relation to M50 steel and IN718 respectively. Chapter 7 (Validation Experiments) describes and discusses the experiments used to investigate the influence of each grinding mode and the thermal measurement experiments which were used to corroborate the trends found previously. Chapter 8 (Component Manufacture) describes and gives the results of two ground components manufactured, using techniques developed within this study. Chapter 9 provides a summary discussion, where the grinding response of the different workpiece materials is compared, the thermal characteristics of the HEDG process reviewed and some industrial implications discussed. Chapter 10 (Conclusions & Recommendations) lists the conclusions arising from the research and recommends further areas of work to extend knowledge of the HEDG process. There are fourteen appendices added to this thesis. Appendix A lists the particulars of the Edgetek research program as a whole. Appendices B, C and D give material mechanical and thermal data. Appendix E details the results from the Taguchi style screening tests. Appendices F and G list the experimental parameters used during the tests carried out on M50 bearing steel and IN718 nickel based superalloy respectively. Appendix H lists the procedure followed when carrying out the thermal modelling. Appendices I & J list the results from the bearing and turbine component manufacture phases respectively. Appendix K contains the external report funded by the turbine manufacturer to study blade roots formed both at Cranfield and at the manufacturer's plant. Appendices L, M and N are datasheets for the three grinding fluids used in this work.

1.6 Summary

This chapter has provided a general introduction to this research study. It has discussed the reasons why this research is relevant to today's engineering industry and the aims and objectives.

Chapter two gives a detailed review of the up to date literature available.

CHAPTER 2 LITERATURE REVIEW

Chapter Two includes the key areas of theory underlying the research topic. The processes involved have been divided into nine parts. Firstly grinding and the associated process involved in the work described in this thesis are discussed in part 2.1; part 2.2 discusses the abrasives available and the abrasives used in the project; 2.3 looks into the grinding wheel technologies; 2.4 explores the project materials; 2.5 considers the cutting fluids used currently and various associated aspects. Part 2.6 reviews surface integrity testing by techniques such as X-Ray Diffraction and Barkhausen Noise techniques which are both used for different styles of stress measurement. Part 2.7 discusses the thermal modelling, and adaptive control systems are reviewed in 2.8. The Chapter is then summarised in part 2.9.

The aim of this review is to highlight recent research relating to high efficiency deep grinding (HEDG) and to show that the project aims and objectives are viable. It should be stressed that very little on HEDG has been reported in the literature and it is therefore concluded that the research undertaken in this work is particularly timely because of a desire to reduce manufacturing costs and improve process efficiency.

2.1 Grinding

Mankind's relentless pursuit of a finer finish to his tools regardless of shape or purpose has been an on going quest since time immemorial.

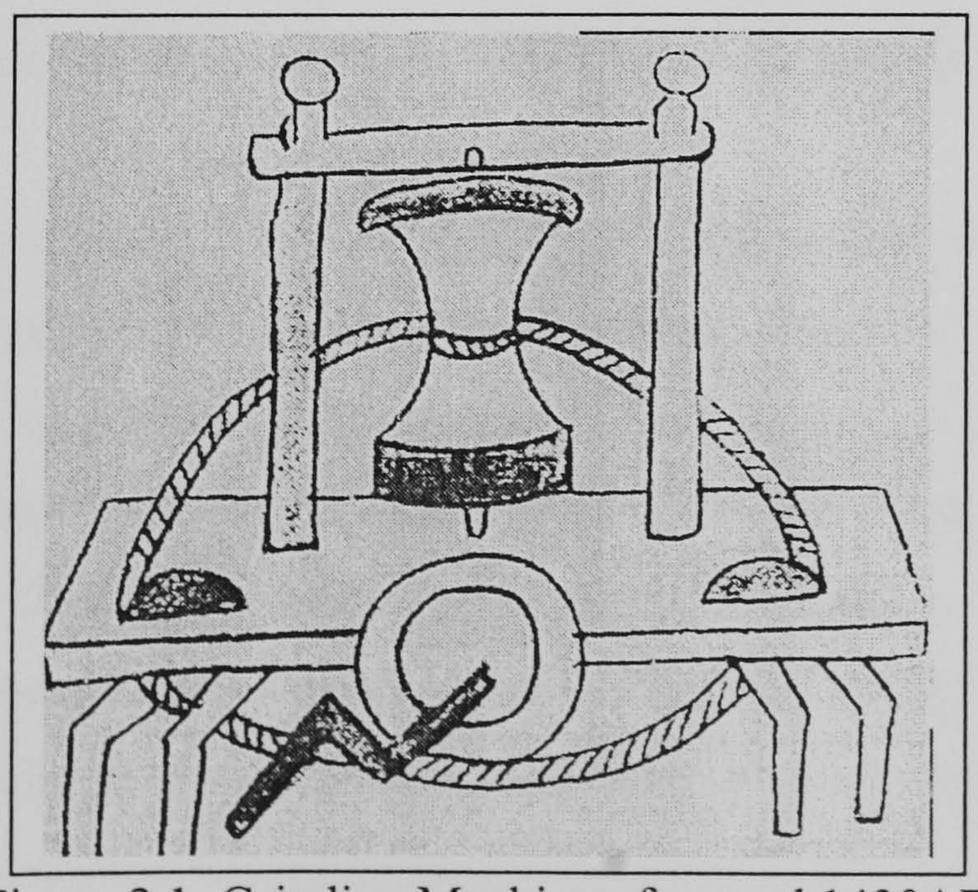

Figure 2.1: Grinding Machine of around 1430AD

Figure 2.1 (After Woodbury 1959) depicts the first known "Grinding Machine", where the work was held as well as being worked upon. With the advent of the industrial revolution, mechanical innovation took grinding, in many shapes and form, to mass production levels. By the end of the 1890's more specialised machines were being produced to fill niche markets. Woodbury (1959) concluded his book aptly by stating, "Grinding…. brought profound changes in the way in which we all live".

The grinding principle uses hundreds of thousands of extremely hard, single cutting grits. These grits cut exceptionally small chips from the parent material or work piece.

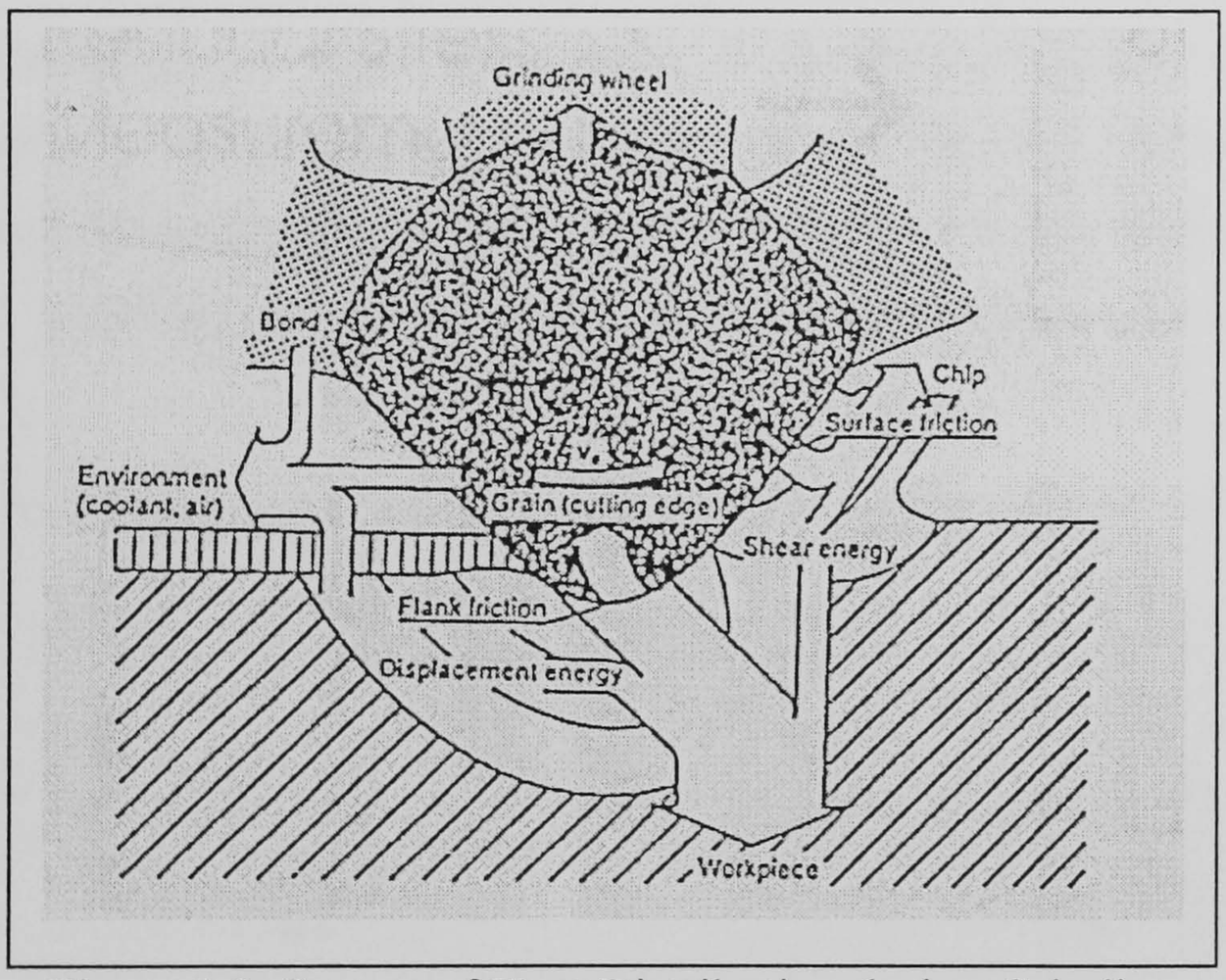

Figure 2.2: Source of Heat Distribution during Grinding

With any mechanical process there is a release of energy and in this process the main release is in the manner of excessive heat as depicted in figure 2.2 (after König 1999). Here it is clearly shown that energy is released by various sources of heat. These result from elastic and plastic deformation when the grit ploughs through the material. In addition, when wear flats appear on the grit's cutting face then a sliding action occurs creating a friction component. Further, as the chip itself is cut there is a release of energy from the shearing action along the shear planes of the worked material. The heat

energy released is therefore routed via the chip, workpiece, grit, wheel and grinding fluid. Therefore, with the use of grinding fluids the grinding temperature is reduced.

Grinding, which in theory is a continuous metal removal method, has been described in numerous texts as a finishing process. Today's attitudes have altered through diligent research and the acceptance of ideas that have thrust grinding into the metal cutting arena. With the advent of new technologies such as superabrasive grits, extremely stiff machining centres and a greater all round understanding of the grinding processes involved, ideas such as HEDG are now more widely accepted.

2.1.1 Grinding Mode

Up and down grinding, are words that describe the direction of rotation of the grinding wheel in relation to the direction of workpiece travel. Figure 2.3 shows the general principles where the up grinding wheel direction is opposite to the workpiece direction and in down grinding the wheel rotates in the same direction as the workpiece movement.

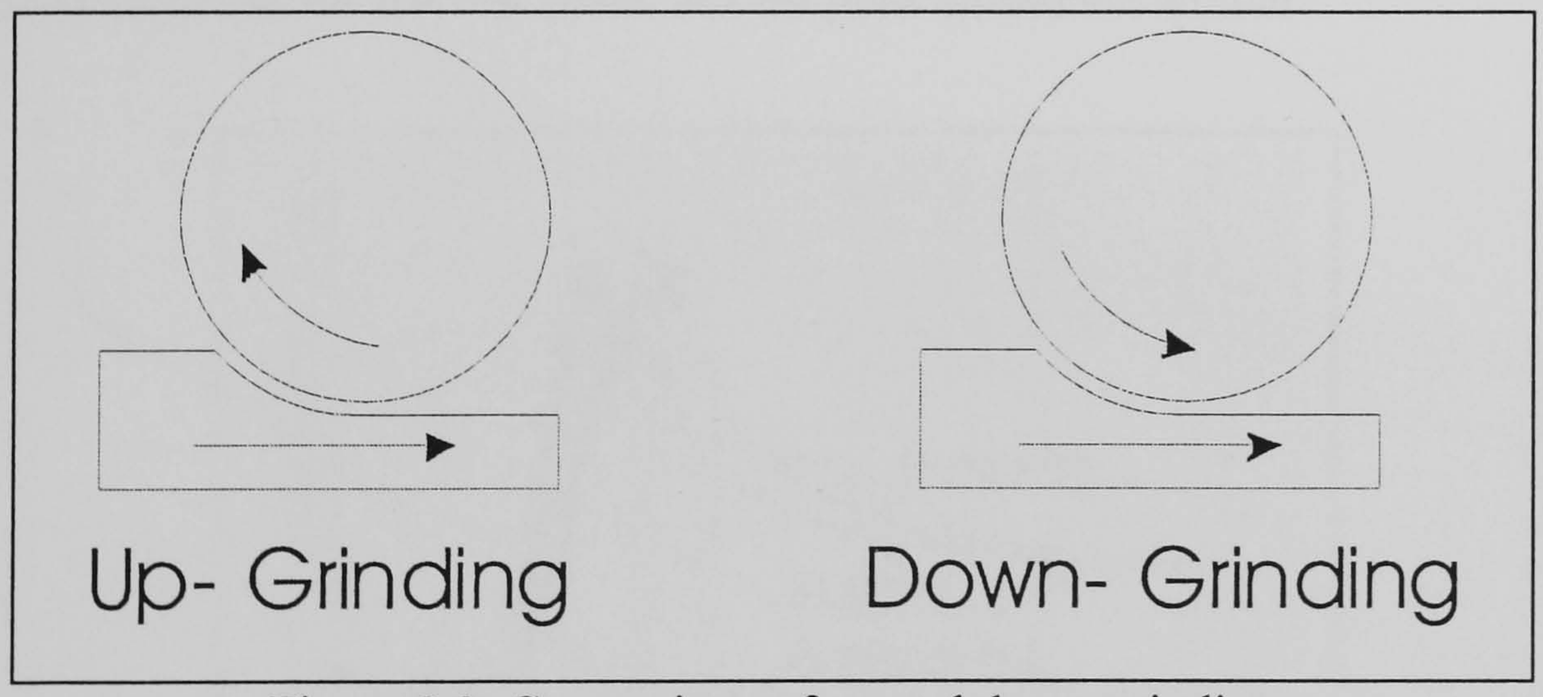

Figure 2.3: Comparison of up and down grinding

Both Malkin (1974) and Shaw (1996) have discussed the two grinding regimes and both have put forward pros and cons for both concepts. Shaw states that the tangential forces calculated from the spindle power are less in the down grinding mode than up grinding and this relates to a slightly lower power requirement for this type of grinding. Shaw also describes how in down grinding the chip's maximum undeformed thickness is produced when a grain enters the contact zone, and the shock of maximum work at the

initial contact point could have a detrimental influence on wheel wear. Andrew et al (1985) describes how in down grinding the power required is lower than up grinding, also that wheel wear is reduced and subsequently the grinding ratio (The ratio of volume of material removed to volume of wheel removed) is increased using this mode.

Tawakoli (1993) explains that the grinding fluid application is more effective when up grinding as it is applied at the point at which the chip is just starting to be formed and is instantly lubricating the finished surface. He then goes on to describe how the measured temperatures were lower when using down grinding to attain specific material removal rates of up to $20mm^2/s$ and also those greater than $70mm^2/s$. Tawakoli advocates up grinding through the mid range, of 20 to $70mm^2/s$.

Wager & Gu (1991) investigated this topic with a view to shallow surface grinding. It was stated that although up grinding has a longer contact length and subsequent peak temperatures are higher the differences were not as great as the differences in force suggest. This is shown in Figure 2.4 where the characteristics of the temperature traces are slightly different for the two cases, but the peak values are similar.

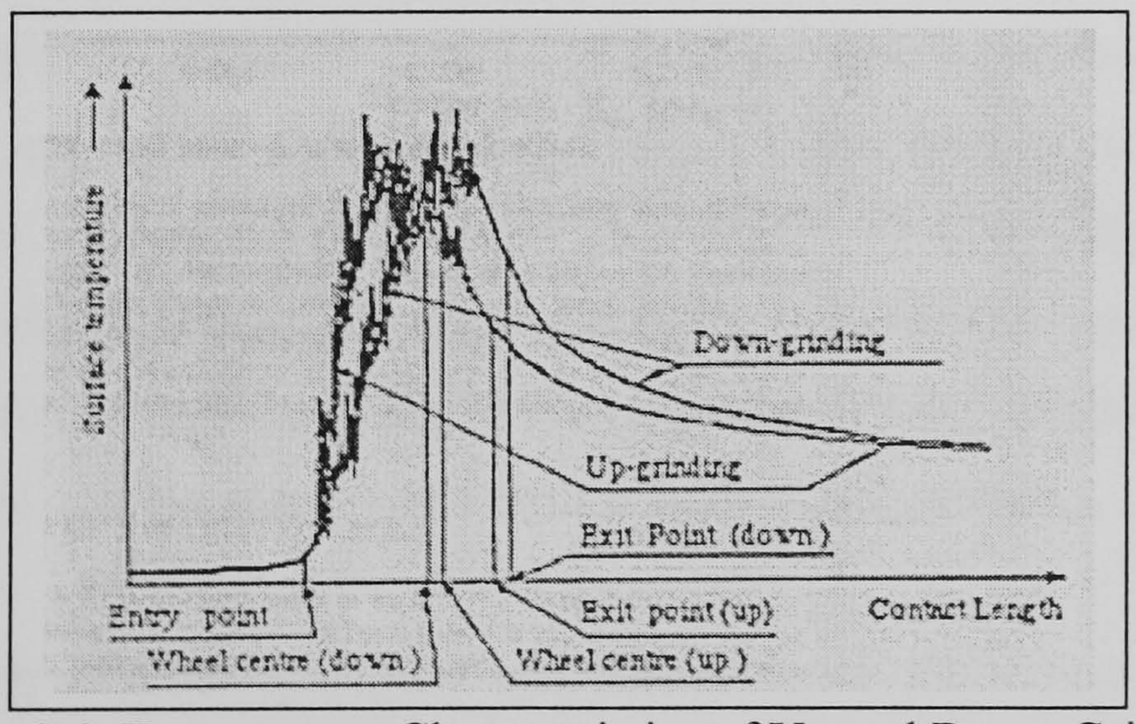

Figure 2.4: Temperature Characteristics of Up and Down Grinding

Rowe (2001) advises that up grinding gives lower temperatures for the intermediate metal removal rates due to convection cooling of the workpiece. Rowe advocates for high material removal rates down grinding could be best as the grits impact the contact surface with greater impact forces enhancing the friability of the grits and thus maintaining the sharp cutting edges on the grits.

2.1.2 Creep Feed Grinding

Creep feed grinding entered large-scale industrial use in the late 1960's and early 1970's. This type of grinding originated from two different types of machining process, namely milling and electrolytic grinding and is characterised by slow feed rates and extremely high depths of cut Malkin (1989). This grinding process can be divided into the two main grinding process areas, the first, finish or form-grinding and the second a form of stock removal grinding. The process studied in this research is the latter where high material removal rates are attained with good levels of surface integrity.

During the 1980's and 1990's intensive efforts were made to increase stock removal rates and improve work quality. As shown in table 2.1 creep feed grinding increased the specific stock removal rate (Q'_w, which equates to the product of depth of cut – a_c and work piece feed rate V_w) in comparison to reciprocating grinding by increasing the depth of cut but retaining the low feed rates to maintain low finished surface temperatures.

2.1.3 High Speed Grinding

During the 1960's the peripheral speeds of grinding wheels increased, from which, evolved a concept called high speed grinding. This method of metal removal demonstrated that increased specific metal removal rates were possible, albeit with the unwanted side effect of higher grinding temperatures. As further research investigated this type of grinding it was found that these temperatures were reduced with the use of grinding fluid and with the use of cubic boron nitride (CBN) wheels.

Both Tönshoff & Falkenberg (1996) and Yui & Lee (1996) showed that with an increase in peripheral wheel speed the grinding force (F_t) reduced and with increased depth of cut, the unit of energy used to remove a cubic mm of material or specific grinding energy (J/mm^3) was also reduced. Hwang et al (2000) noted that the lower overall values of specific energy were seen to be proportional to the higher wheel speeds, and this was attributed to the shorter contact time between the work piece and the grit at high wheel speeds. This concurs with Shaw (1972) who stated that the un-

deformed chip thickness is directly proportional to work piece feed rate and inversely proportional to wheel speed.

2.1.4 High Efficiency Deep Grinding

As more efficient ways of metal removal were required, a number of different methods were investigated. High efficiency deep grinding is a hybrid of two well known grinding processes, these being high speed grinding and creep feed grinding. Grinding processes are compared (Inasaki et al 1993) in Figure 2.5, which shows the possibilities when using superabrasive electroplated wheels. The figure depicts the increase in stock removal rates, without dressing the wheel, and associated productivity improvements.

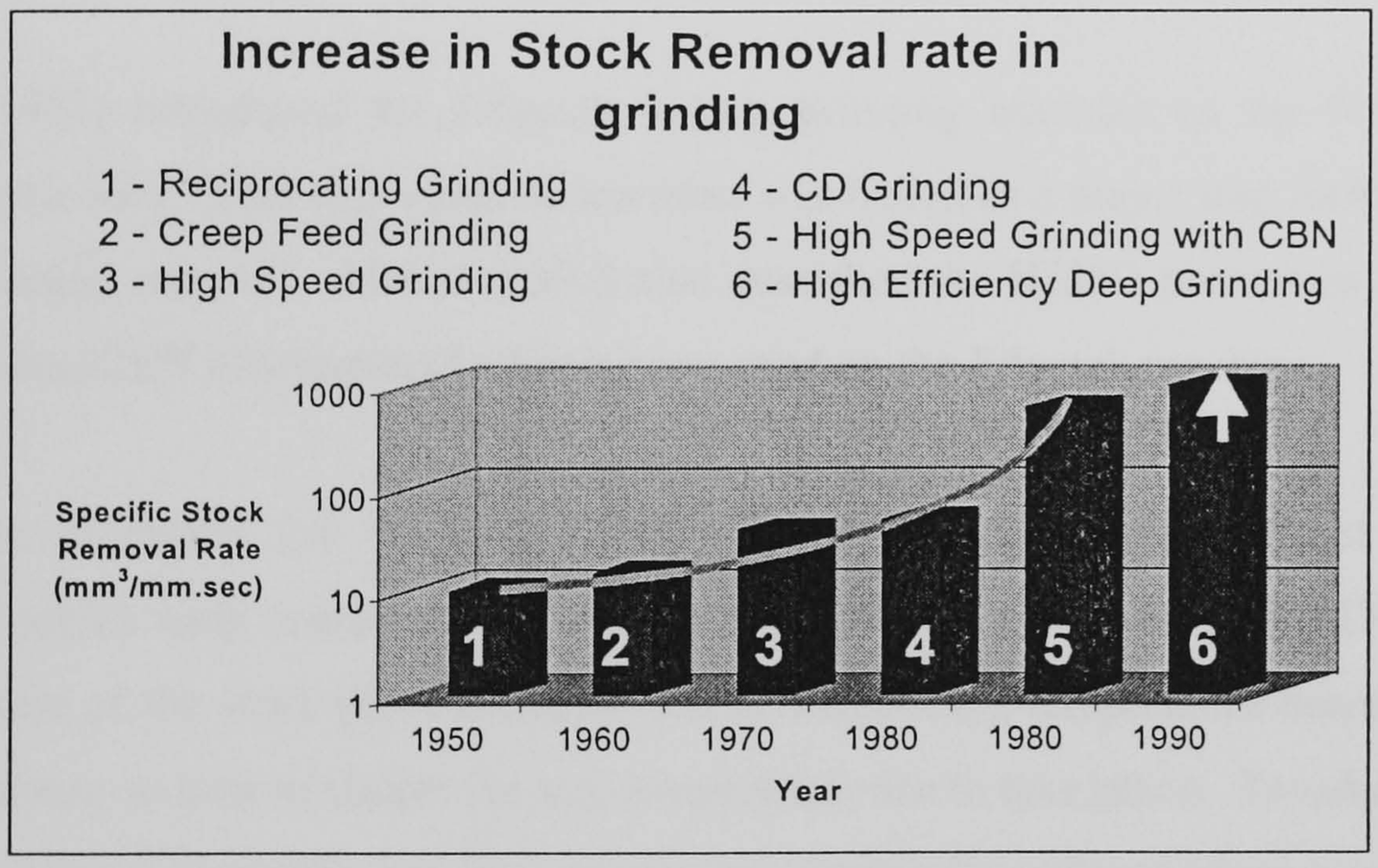

Figure 2.5: Increase of Stock Removal Rate in Surface Grinding

Work by Tawakoli (1993) reported that HEDG is characterised by increases in all the following parameters: wheel speed, depth of cut and work feed-rate thus permitting extremely high stock removal rates.

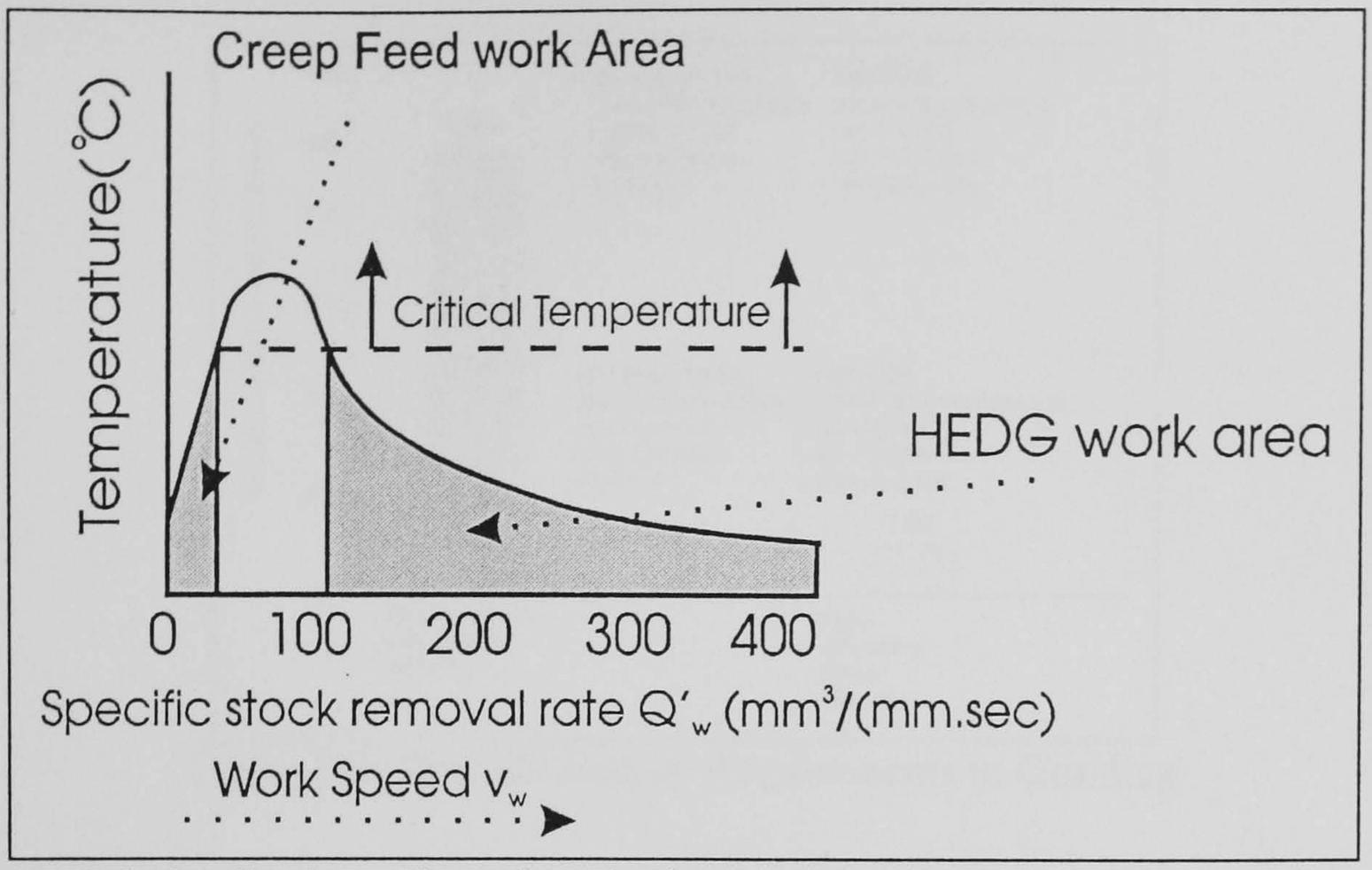

Figure 2.6: Qualitative effect of work piece speed and relative stock removal rate

Mason (1993) introduced the Edgetek 5-Axis grinding machine as the first HEDG grinding machine. This stiff versatile machine was hailed as a major step forward in the world of metal removal. Mason (1997) also described the HEDG process as a form of milling when CBN electroplated wheels were used on the Edgetek machine.

As shown in Figure 2.6 Tawakoli (1993) stated that there were distinct areas of operation which both creep feed grinding and HEDG occupied. In the HEDG area as the feed rate of the work piece increases the corresponding temperature decreases, due to the decrease in time available for any temperature rise to take place. Tawakoli (1993) also found that the specific grinding energy was drastically reduced when using HEDG in comparison to creep feed grinding; this is illustrated in Figure 2.7.

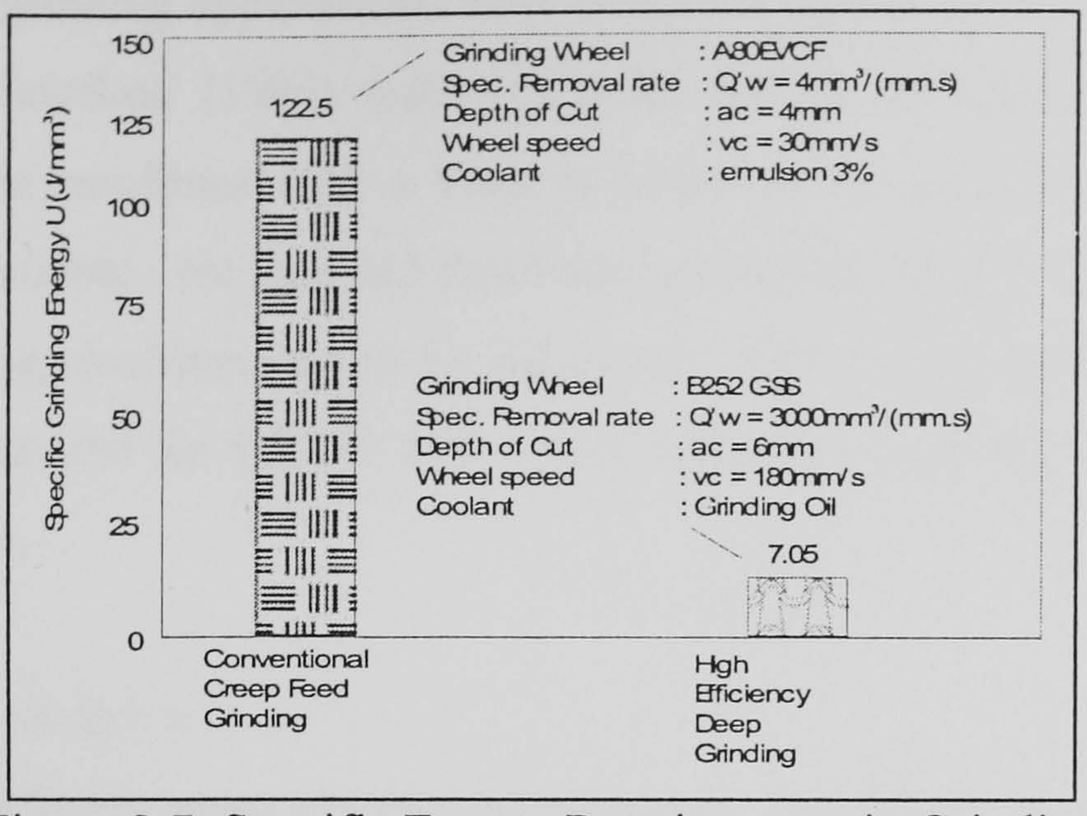

Figure 2.7: Specific Energy Requirements in Grinding

Werner (1994) reported that as the maximum grinding wheel speed increased the theoretical temperatures experienced within the grinding contact zone should decrease and therefore HEDG was a viable concept under the correct conditions. This was also reported by Tawakoli (1993) who compared different grinding regimes as shown in Table 2.1.

	Reciprocating Grinding	*Creep Feed Grinding*	*HEDG*
Depth of Cut a_c (mm)	LOW 0.001 – 0.05	HIGH 0.1 - 30	HIGH 0.1 – 30
Work Speed V_w (m/mm)	HIGH 1 – 30	LOW 0.05 – 0.5	HIGH 0.5 – 10
Wheel Speed V_s (m/s)	LOW 20 - 60	LOW 20 - 60	HIGH 80 - 250
Specific Material Removal Rate Q'_w (mm^3/mm.s)	LOW 0.1 - 10	LOW 0.1 - 10	HIGH 50 - 2000

Table 2.1: Comparison between different Surface Grinding Methods

Inasaki et al (1993) noted that with the advent of the CBN technology, as well as the modern day stiff grinding centres, the technological advances being made in the stock removal aspects of surface grinding could be enhanced further. Also, the modern

requirements for grinding applications were stated as high accuracy and high material removal rates. Tawakoli (1996) took this point further; he researched the stiffness requirement of the machines with a view to optimise the process in relation to the machines then available. He reported that basic parameters used in the manufacture of creep feed grinding machines had to be increased. This was primarily due to the fact that the power required for HEDG was 3 to 6 times that required for the creep feed grinding processes.

2.2 Abrasives

There are many different types of grinding abrasive. Two of the most commonly used are aluminium oxide and silicon carbide. These conventional abrasives are still widely used in various grinding processes and are still used effectively in various scenarios where the experience within these industrial areas is extensive. The abrasives used within this project are classed as superabrasives. This classification is reserved for ultra-hard compounds such as Cubic Boron Nitride (CBN) and Poly Crystalline Diamond (PCD). These man made materials are produced by transforming carbon or boron nitride under extreme pressures and temperatures to produce ultra hard abrasive grits.

CBN was first produced by the General Electric Company in the 1950's and was not commercially available until the late 1960's. Depending upon the properties required, CBN wheels are more expensive than the common abrasive wheels and are relatively inert when in contact with steel.

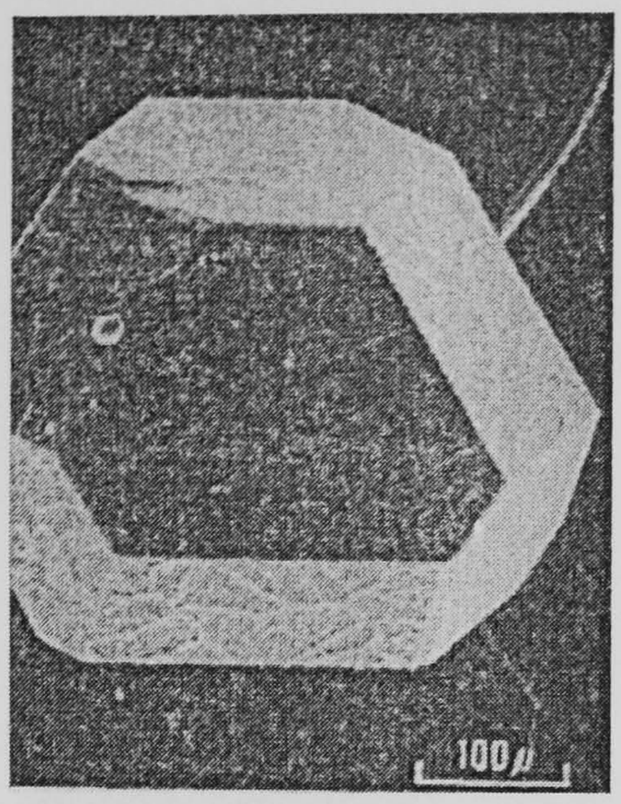

Figure 2.8: SEM Micrograph of MBS Synthetic Diamond (After Shaw 1996)

Figures 2.8 and 2.9 show examples of the highest quality synthetic grits available in diamond and CBN respectively.

Figure 2.9: SEM Micrograph of a single crystal CBN Grit (After Shaw 1996)

Figure 2.10 shows an example of nickel coated CBN-II grit. This CBN-II type grit has obvious imperfections on the surface, the impact of which are reduced due to the coating. This enhances the friability and increases the actual dimensions of the grit.

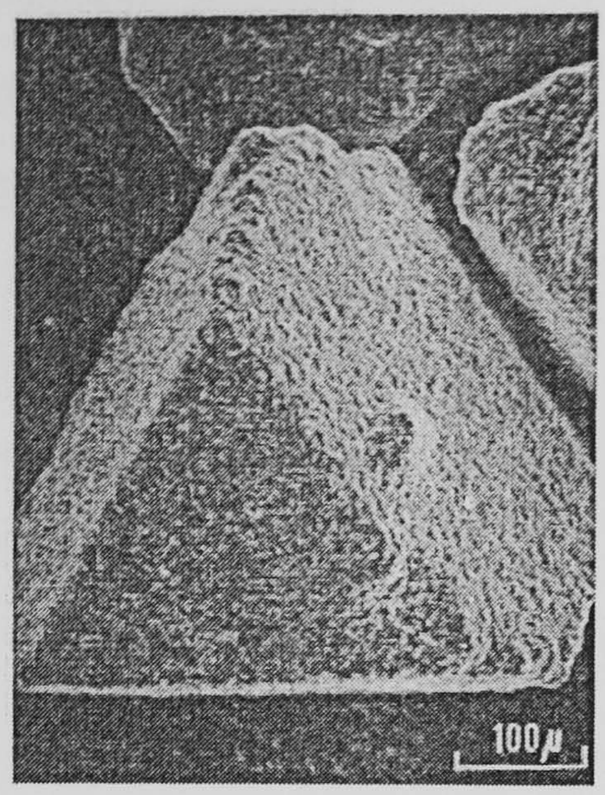

Figure 2.10: SEM Micrograph of Nickel Coated CBN-II Grit (After Shaw 1996)

In addition, Rowe (2001) and Shaw (1996) both reported that, due to CBN's high thermal conductivity the grinding temperature experienced at the finished surface may be far lower than that experimentally measured when using Al_2O_3.

Rowe & Chen (2000) described how the advantages of CBN grits were realised when theoretical temperatures were calculated, which gave the following indications:

- lower final temperatures
- less likelihood of oxidation
- consequently lower residual tensile stresses

This in turn indicated that, for a required temperature, the depth of cut could be increased, or in order to lengthen the wheel life a depth of cut could be retained thus generating a much lower grinding temperature. These findings reinforced work by Bailley & Juchem (1998) who reported that developments in CBN technology have resulted in abrasives which maintain free cutting characteristics during use, and so minimise cutting forces and therefore maintain low temperatures within the cutting zone.

Chou & Evans (1999) cited that CBN grits have half the hardness of PCD which has a superior thermal conductivity of 560 W/mK. The chemical inertness of CBN regarding

ferrous metals makes it more suitable to grind high-speed steels (Bailley 2000). Rowe et al (1995) reported that the thermal conductivity of CBN grit was as high as 240 -1300 W/mK and Alumina as a comparison was 37 W/mK. Morgan et al (1998) also listed the thermal conductivity of CBN to be within 200 and 700 W/mK. These figures represent a range of thermal conductivity values which may be appropriate for different grinding situations. However, exact values are difficult to determine and are sensitive to the specific grade of CBN. Althaus (1985) tested the effect of increasing grit concentration of a CBN grit B64-P100-V wheel in comparison to an aluminium oxide wheel AL100-L5-V when grinding EN31 steel. It was found that in the case of the CBN wheel, the residual stresses increased in magnitude compressively, which was opposite to that observed for the aluminium oxide wheel. The production of wear flats on the aluminium oxide grits contributed to this effect.

2.3 Wheel Technologies

The design and manufacture of grinding wheels is another area of continuous research. The methods of bonding these grits to the wheel include resin, metallic, vitrified bonding and electroplated types. Although all have their own advantages and disadvantages this research is aimed at the use of nickel electroplated CBN wheels. Due to the grits being held in place on a steel hub by an electroplated layer of nickel, these wheels are known to be able to withstand higher rotational speeds than bonded wheels. Klocke & König (1995) noted that with vitrified CBN wheels the conditioning of the grinding wheel abrasive surface is a basic pre-requisite for the efficient use of CBN bonded grinding wheels, where it was found the sharpness of the wheel manifests itself in lower maximum grinding forces. This fact brings forward what could be seen to be an advantage of the electroplated wheel by no longer requiring dressing. However, the application of the grinding fluid is more difficult due to the lack of porosity within the wheel design.

In 1988 Werner & Tawakoli investigated the use of fully plated, partially plated and slotted electroplated CBN wheels when grinding narrow slots in 45NiCr6 which had a Rockwell C hardness of 35HRC. It was reported that in this scenario a slot 25mm deep by 1.5mm wide was cut with a table speed of 600mm/min. These experiments were

reported as indicating that the optimum wheel design utilised a partially plated type with 18 plated segments using B151 CBN grit, 10mm wide and to a height of 1.5mm with an angle of 2°. This design is shown in Figure 2.11.

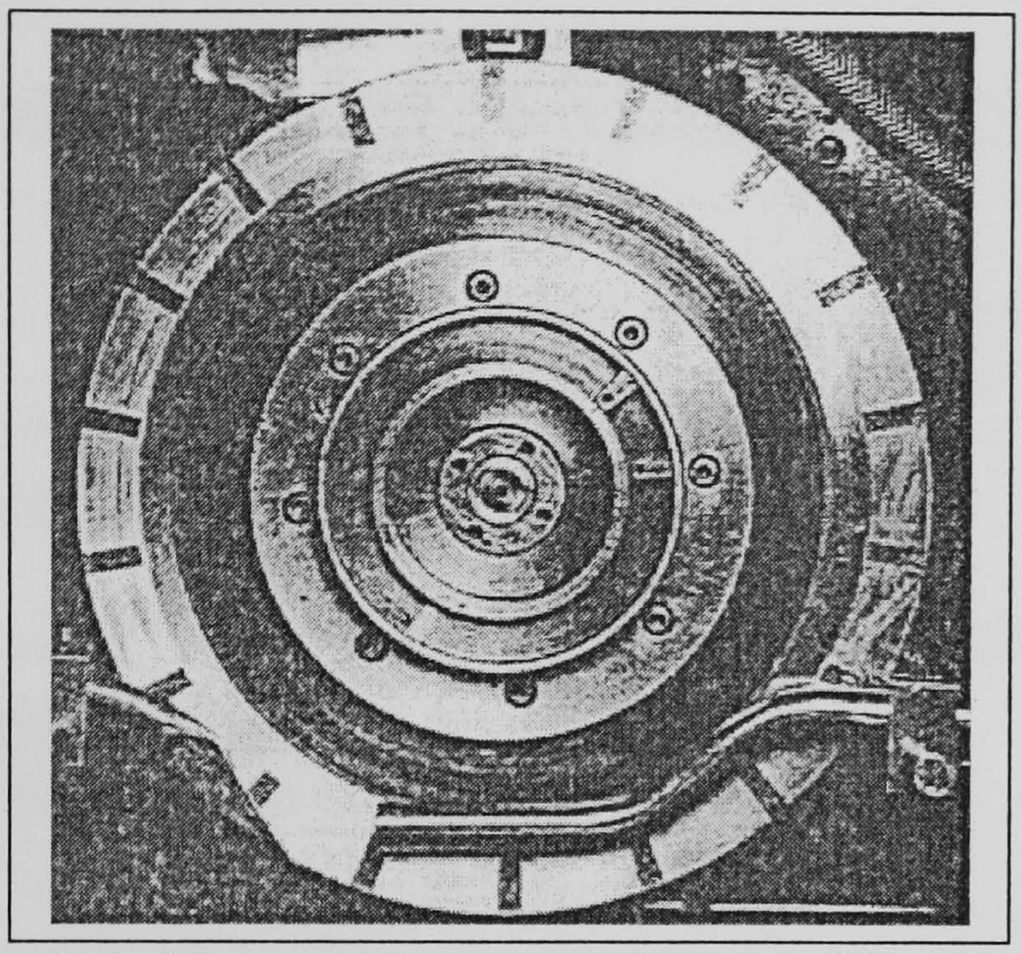

Figure 2.11: Werner & Tawakoli's Optimum Wheel Design

As shown in Figure 2.12 Klocke et at (1997) speculated that although CBN electroplated wheels could not be dressed in the conventional sense the high cutting speeds attainable (>250ms) could enable Q'_w values of 10,000mm^2/s to be achieved.

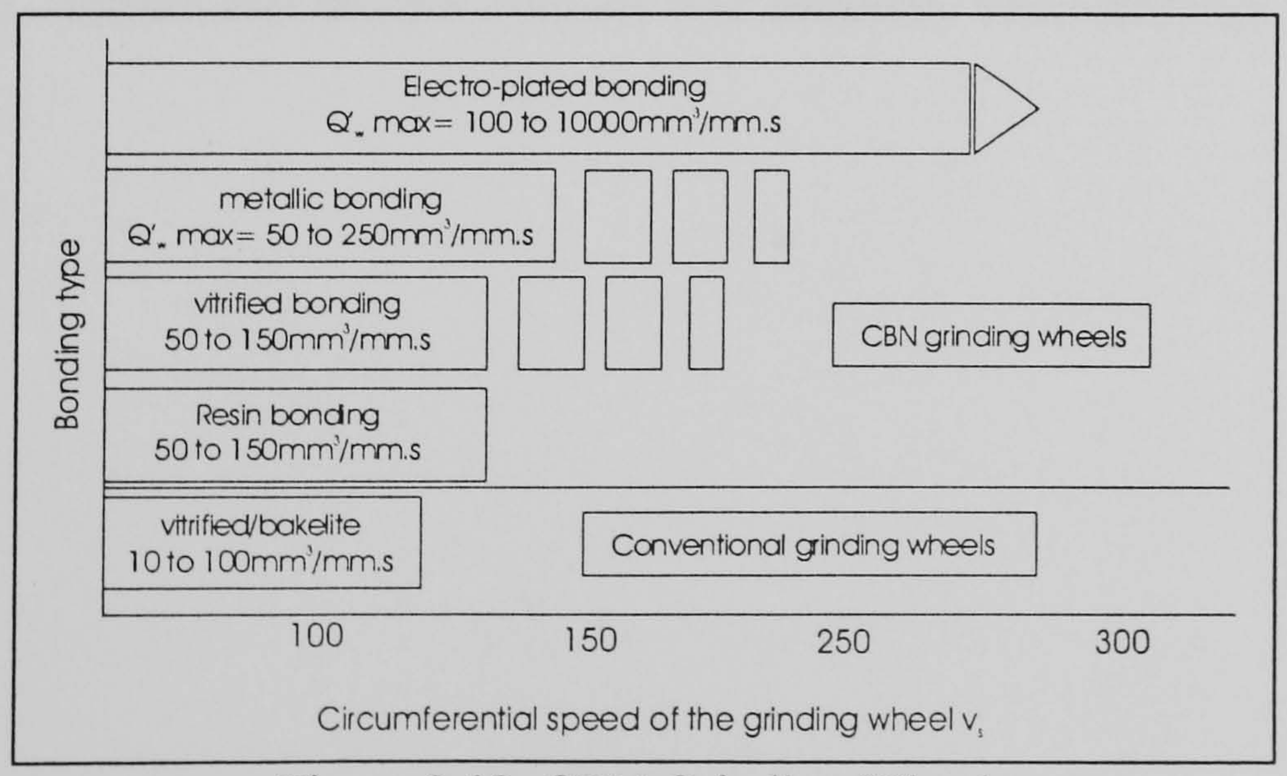

Figure 2.12: CBN Grinding Wheels

Savington (1999) reported that resin and metallic bonds are very closed structure systems and unless outside agents, such as glass spheres were added, no controlled

porosity could assist with chip clearance. Figure 2.13 shows an illustration from Bailley (2000) which compares the concept of a bonded matrix to the electroplated wheels.

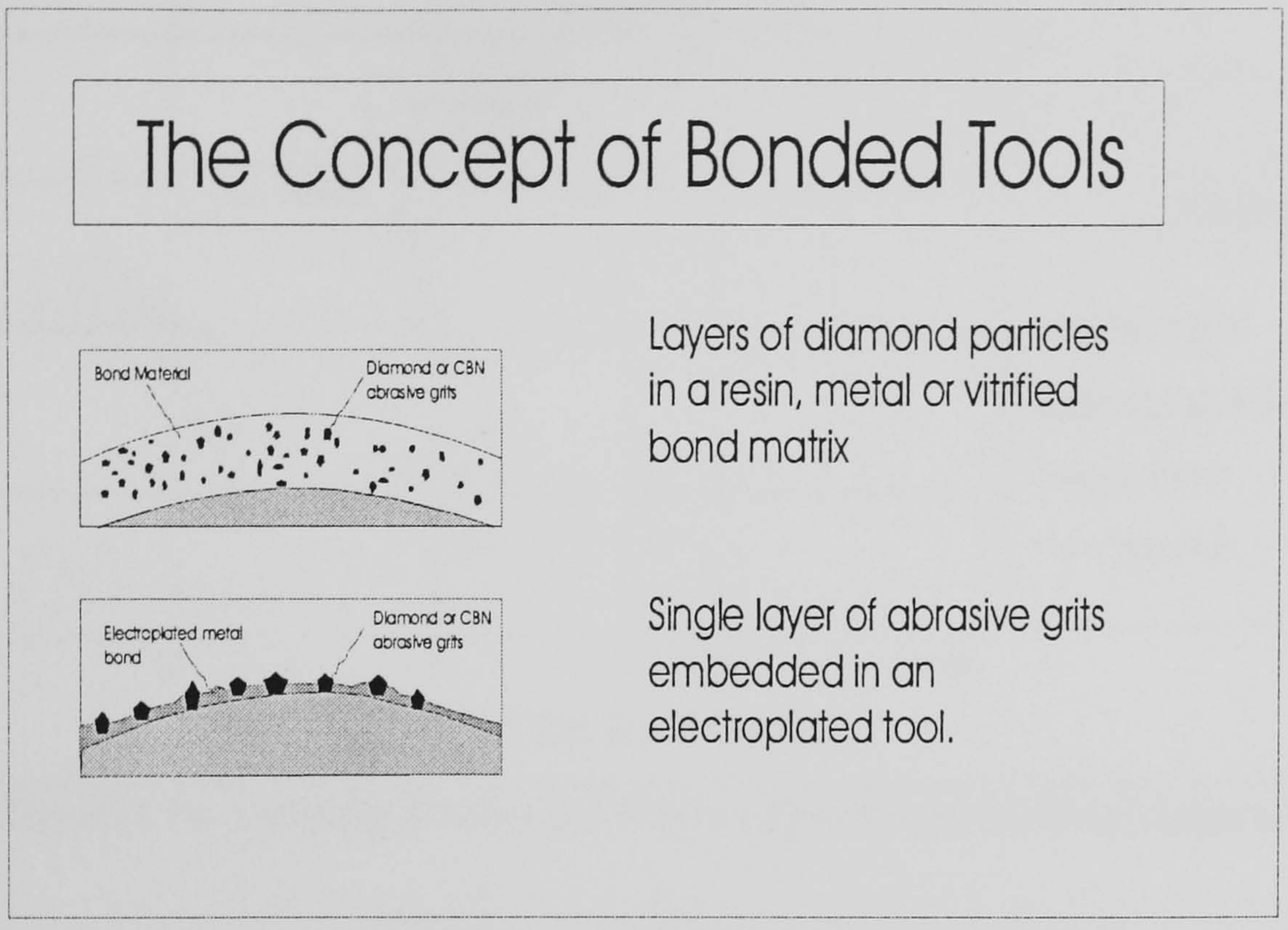

Figure 2.13: The Concept of Bonded Tools

Tönshoff et al (1998) also researched vitrified bonded CBN wheels. They reported that when the workpiece feed rate was increased to 60m/min with a wheel speed of 140m/s the value of normal and tangential cutting forces reduced. Furthermore a Q'_w value of $40mm^3/mm.s$, without any thermal damage was obtained. Their findings are shown in Figure 2.14.

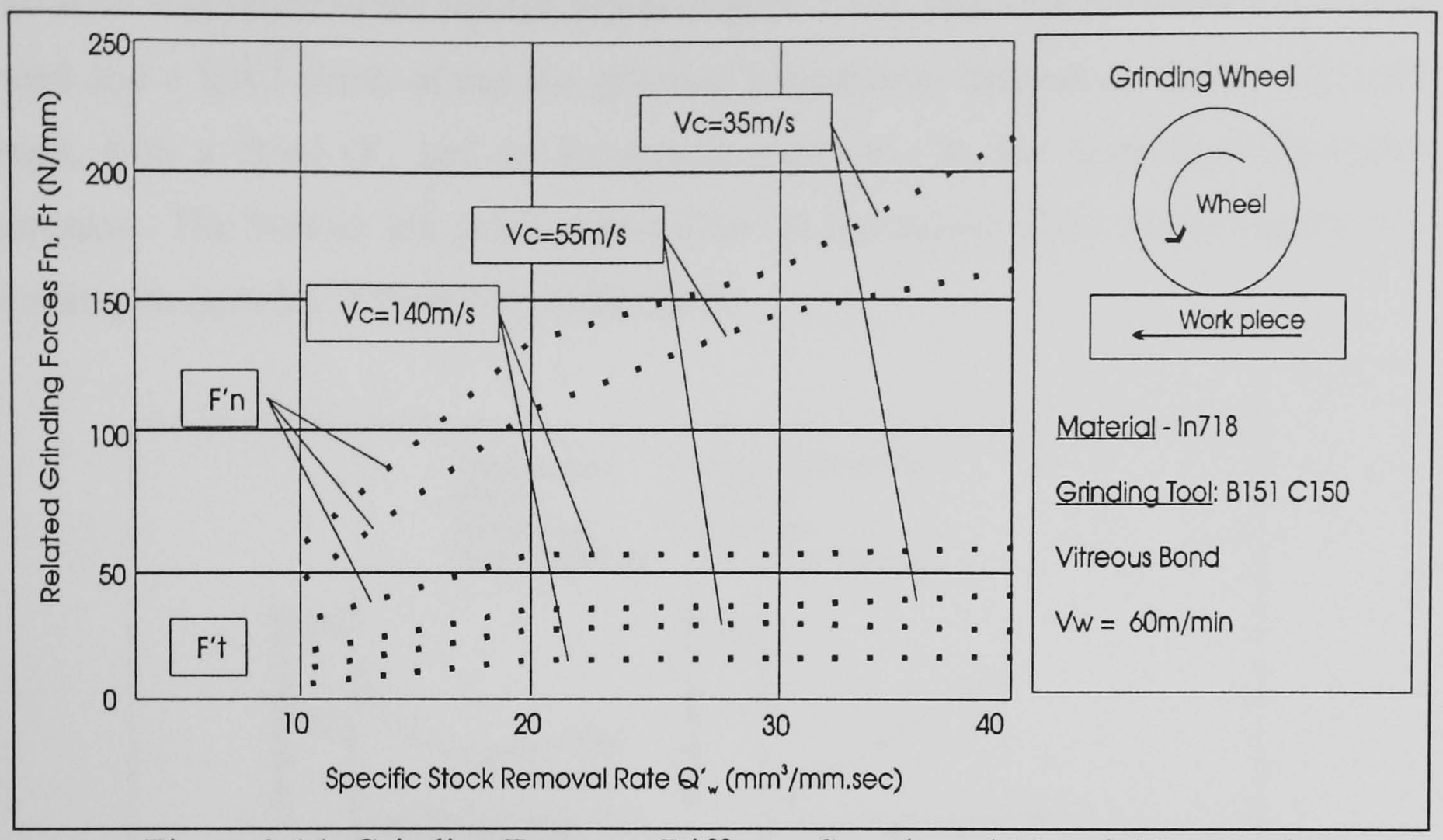

Figure 2.14: Grinding Forces at Different Speeds and Material Removal

Advances in technology are normally financially based. Redington & Joseph (1998) reported that the manufacturing costs per part decreased dramatically with the use of CBN abrasives, particularly when electroplated CBN wheels were used. This was believed to be due to a) the grit's Knoop hardness value of 4800kg/mm^2, b) the enhanced production time due to no longer requiring dressing the wheel and also c) the low power requirement per cut. It was due to these factors that the increased life of the wheel and subsequent reduction in the costs per part were observed.

Porous wheels and slotted electroplated wheels have also been tested and have been shown to increase cooling and lubrication effects, albeit this was done in conjunction with an external supply nozzle. There have been a number of investigations which attempted to deal with different grinding fluid nozzle types and strategies but a comparison of test results has not been possible through the neglect by authors in reporting characteristic data such as flow rate (Brinksmeier et al 1999).

The wheel speed of a solid steel wheel can be increased above that of a bonded type and as shown by Tawakoli (1993), the corresponding grinding temperature should increase and then reduce. Figure 2.15 epitomises the HEDG concept in three simple graphs.

Tawakoli also noted in the top left graph (Figure 2.15), that with the increase of work speed and a fixed depth of cut the grinding temperature decreases. In the top right graph, with a fixed Q'_w and an increasing depth of cut, the grinding temperature increases. The bottom left graph shows how an increasing wheel speed results in a temperature increase followed by a decrease.

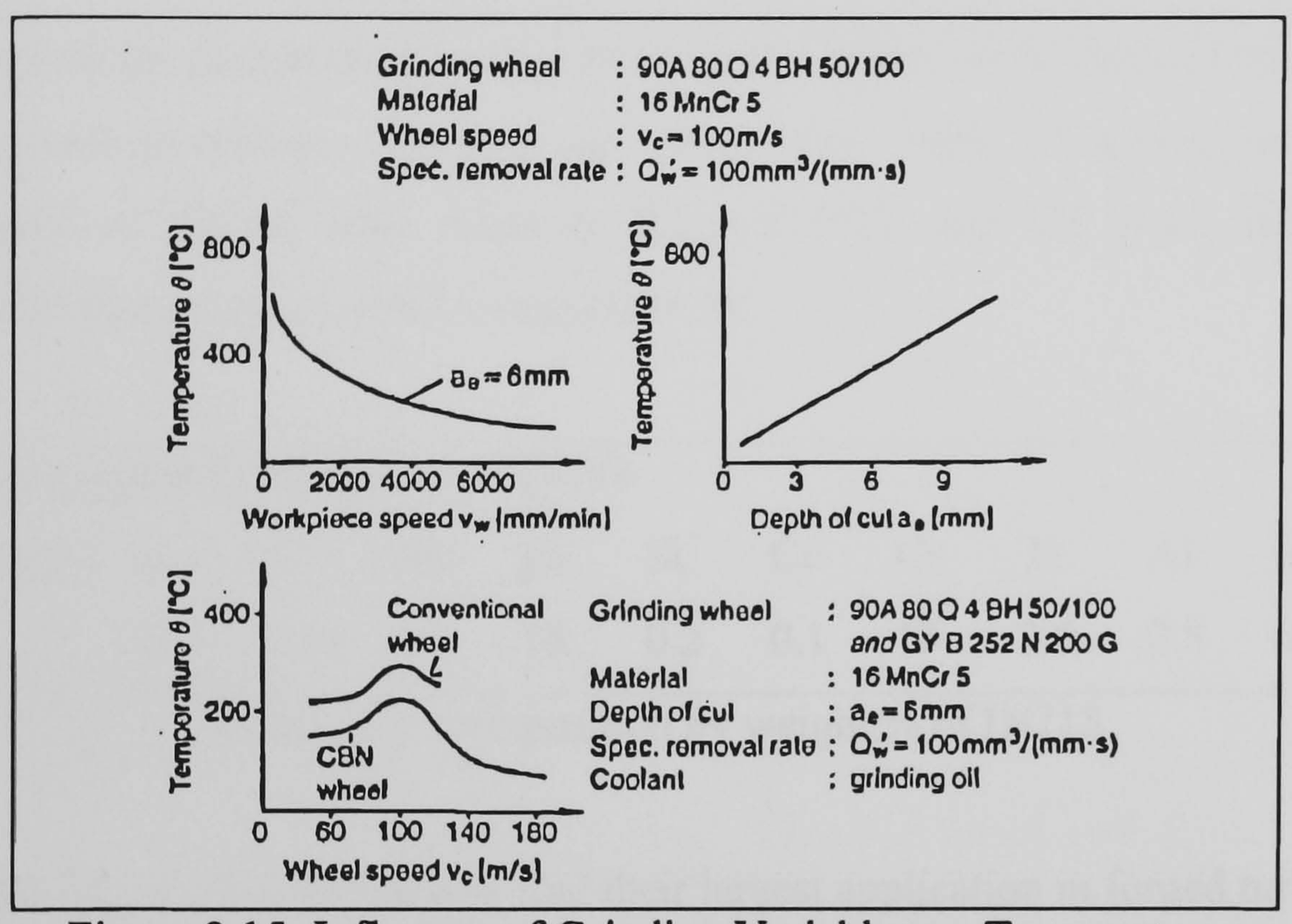

Figure 2.15: Influence of Grinding Variables on Temperature

2.4 Project Materials

As the jet age developed, the use and requirements for superalloys increased. These superalloys can be classified into three main groups: cobalt based, nickel based and nickel-iron based. The success of these alloy types is relatively easy to note, as the aircraft industry has increased the use of nickel based superalloys and the new derivatives are withstanding temperatures of up to 1100°C. The turbine gas-inlet-temperature is a true reflection of the efficiency of the gas turbine engine, and the alloys that perform tasks within these environments have enhanced these efficiencies a great deal. It is to ensure strength retention within these materials over these extremely high operating temperatures that superalloys have been developed.

2.4.1 IN718 Nickel Superalloy

IN718 is a wrought alloy and is an iron-containing alloy, providing moderate-temperature high-strength properties as well as good resistance to strain age cracking in welding. Wrought material is produced in large ingots, which are then rolled, forged and/or extruded to finished sizes and then heat treated to obtain the desired properties. IN718 is vacuum induction melted for a number of reasons that include prevention of the formation of oxides and nitrides, and to avoid the loss of hardening elements such as niobium, titanium and aluminium. Table 2.2 shows the chemical constituents of IN718, after Sims & Hagel (1972), and the main thermal and mechanical properties are listed in Appendix B.

Composition by weight % of IN718										
IN718	Ni	C	Mn	Fe	Si	Cu	Cr	Ti	Al	Nb
	52.5	0.04	0.2	18	0.2	0.1	15	2.5	0.8	0.85

Table 2.2: Composition by weight % of IN718

IN718 as well as other superalloys find their largest application in forged turbine disks due to their creep resistant properties. Kawagoishi et al (1999) also mentioned that IN718 is used in the manufacture of various critical aircraft engine components, for example compressor blades and turbine blades, for the same reason.

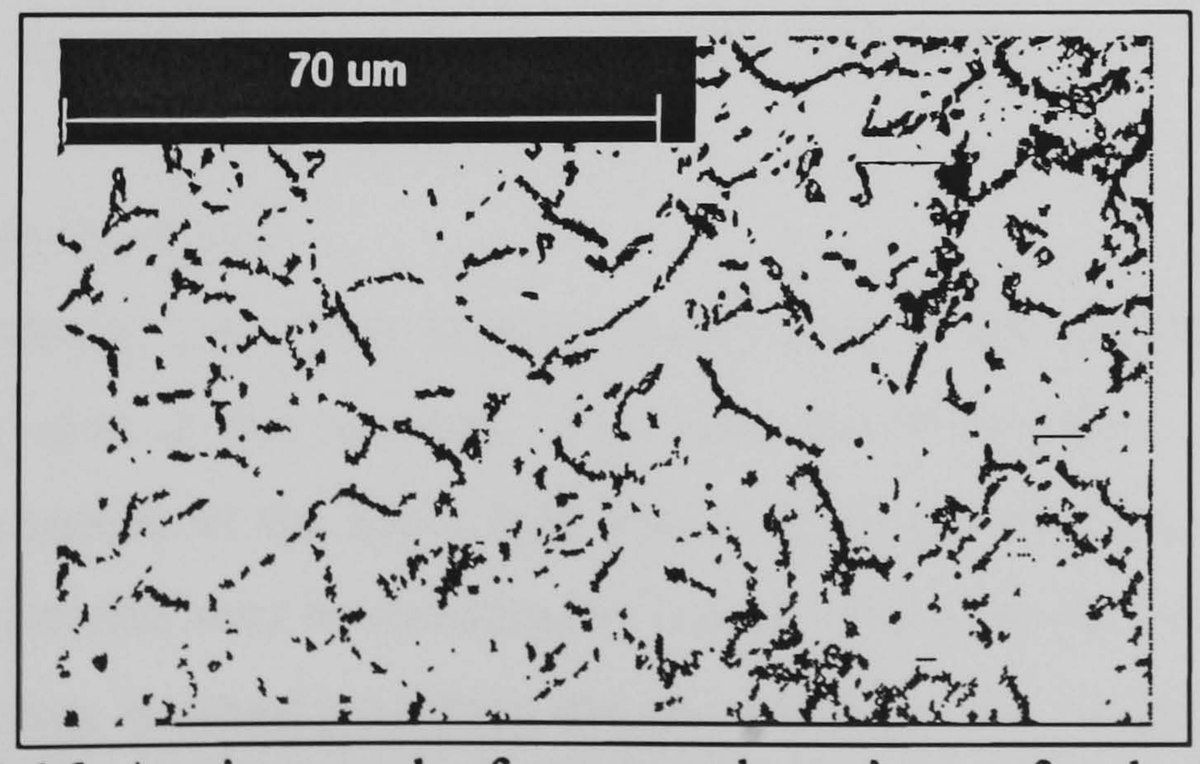

Figure 2.16: A micrograph of an unused specimen of etched IN718.

Figure 2.16 shows the structure of IN718, and a few carbides within the structure at the grain boundaries are clearly visible. These carbides, which occur in superalloys, have a face-centred-cubic lattice, some of which are considered to be the most stable compounds in nature. They occur from a combination of carbon and refractory metals, usually having a formula such as MC (metal carbide) or M_6C_{23}. As IN718 used niobium for strengthening purposes it is expected that the metal in the MC type carbides contain the refractory elements such as niobium and titanium.

With the introduction of more iron replacing nickel, a far more stable and stronger but cheaper alloy was produced, which in this business driven world is a major advantage over the pure nickel based alloys.

IN718 is representative of a group of superalloys where the primary hardening is by ordered body-centred-tetragonal (BCT) lattice γ'. It has been highlighted that BCT γ' would not form in binary nickel-niobium unless some iron was present. It was also shown that IN718 and other iron-nickel based alloys have approximately 2-6% niobium and considerable amounts of iron. However only IN718 has the major strengthening component which has been identified as BCT γ', Sims & Hagel. (1972).

Also, P. L. Tso (1999) described IN718 as being more suited for grinding by CBN wheels than other abrasives, irrespective of what machinability index was considered. The term machinability index can be a measure of a number of responses such as normal grinding force, surface roughness or grinding wheel life.

2.4.2 MAR-M-002

This tough extremely high creep resistant nickel alloy is the second nickel based superalloy to be used in this research. The main use of this alloy is in the high-pressure turbine section of the RB11 high bypass ratio turbo-fan aero engine. This poly crystalline material may be directionally cast or used in single crystal form so as to enhance the creep resistant properties and an example of the structure is shown in Figure 2.17.

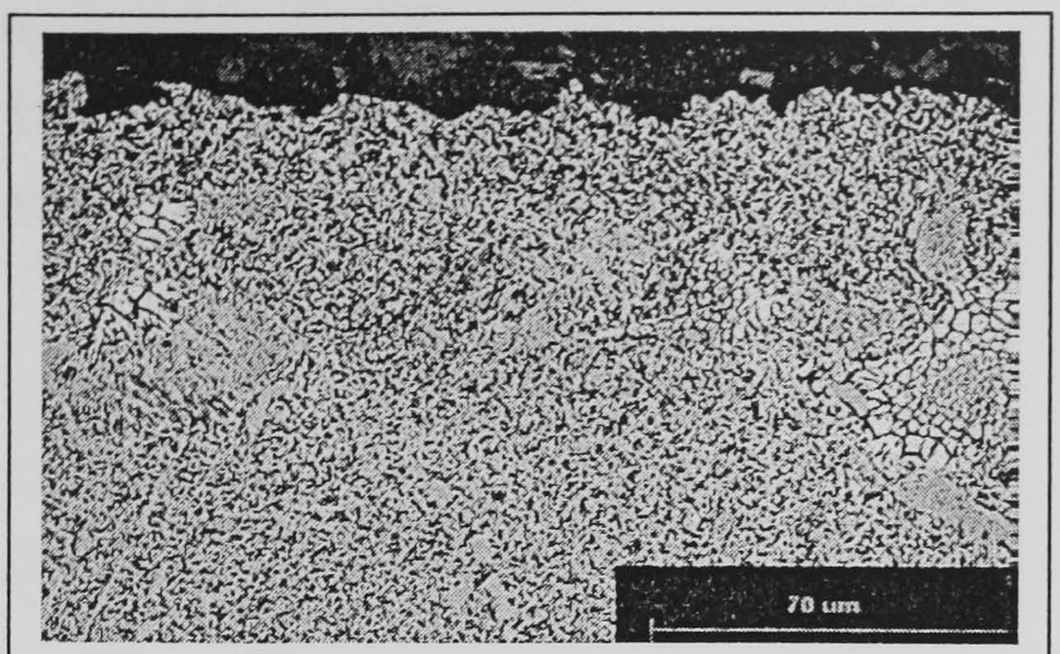

Figure 2.17: Etched sample of unused MAR-M-002

The composition of MAR-M-002 is shown in Table 2.3 and the main thermal and mechanical properties are listed in Appendix C.

Composition by Weight % MAR-M-002												
MAR M 002	Ni	C	Cr	Co	Mo	Ti	Al	B	Zr	Ta	Hf	Fe
	Bal	15	19	10	10	1.5	5.5	0.1	0.05	2.5	1.5	1

Table 2.3: Composition by weight % of MAR M 002

2.4.3 VIM-VAR M50 Bearing Steel

Carpenter VIM-VAR M50 Bearing Steel was also used within this project. The name gives an indication of the refining process that is required, specifically vacuum induction melting (VIM) and vacuum arc re-melting (VAR).

This material has a number of positive properties including excellent resistance to multi axial stresses, good resistance to oxidation and high resistance to softening at high operating temperatures. One of the many uses for this material is in the aerospace industry for bearings within gas turbine engines operating at a service temperature of up to 371°C. The chemical constituents of M50 are shown in Table 2.4 after Metals Handbook (1986), and the main thermal and mechanical properties are listed in Appendix D.

Composition by weight % of M50								
AISI M50	Fe	Cr	Mo	V	Ni	C	Mn	Si
	Bal	4	4.3	1	0.1	0.8	0.25	0.25

Table 2.4: Composition by weight % of M50

M50 has a Rockwell C hardness of 62 to 64 and the manufacturers recommend the cutting fluid is sulphurised mineral oil. However, this was not used within these trials, as a sulphur free mineral oil was the sponsor's choice for two reasons; a) to explore the possibility of using an ecologically friendlier alternative; b) the sponsors use this material primarily in the aviation industry and it was decided to reduce the possibility of the introduction of sulphur and hence a possible source of corrosion.

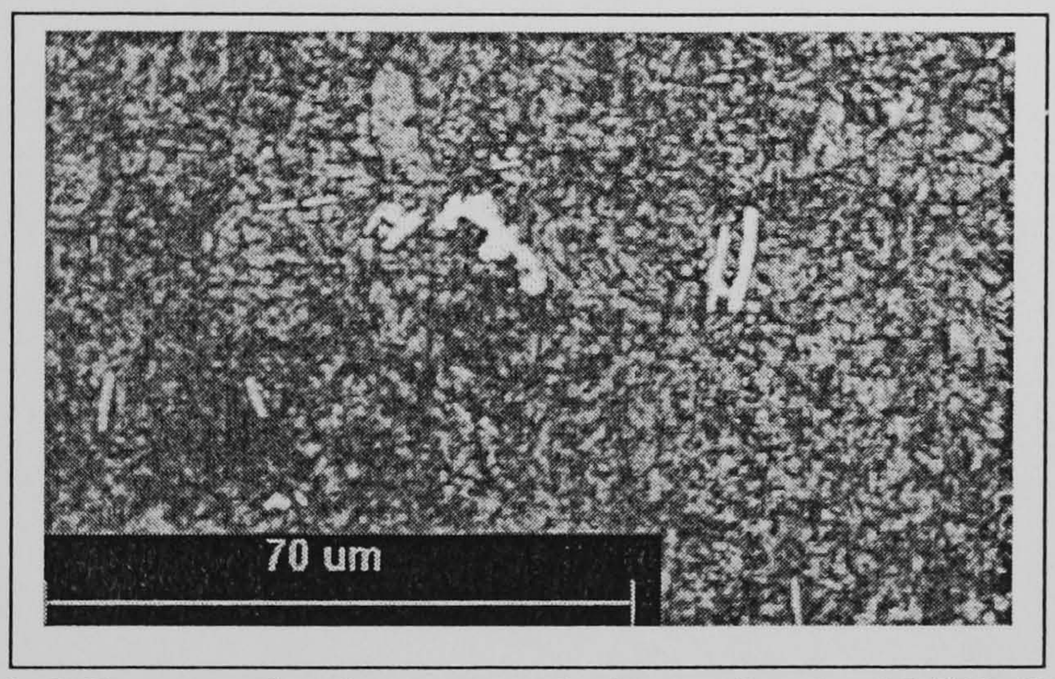

Figure 2.18: Micrograph of an unused piece of etched M50 (Nital Etch).

Figure 2.18 shows a micrograph of an unused specimen of M50 in which a number of carbides can easily be seen. A number of studies have been carried out on these carbides of which there are two types, namely Molybdenum-rich carbide (M_2C carbide) and Vanadium-rich carbide (MC- metal carbide). These carbides have been studied due to their high hardness values which, together with their Young's Modulus values are shown in Table 2.5 below.

Type of carbide	M_2C	MC	M50 Matrix
Young's Modulus (GPa)	302	320	214
Hardness (GPa)	20.4	23.9	7.7

Table 2.5: Young's Modulus of Primary Carbides in M50

Chou and Evans (1997) concluded in their study that these large ultra-hard carbides in the workpiece enhanced fine scale attrition by micro-fracture and fatigue which results in the high wear resistance of the material.

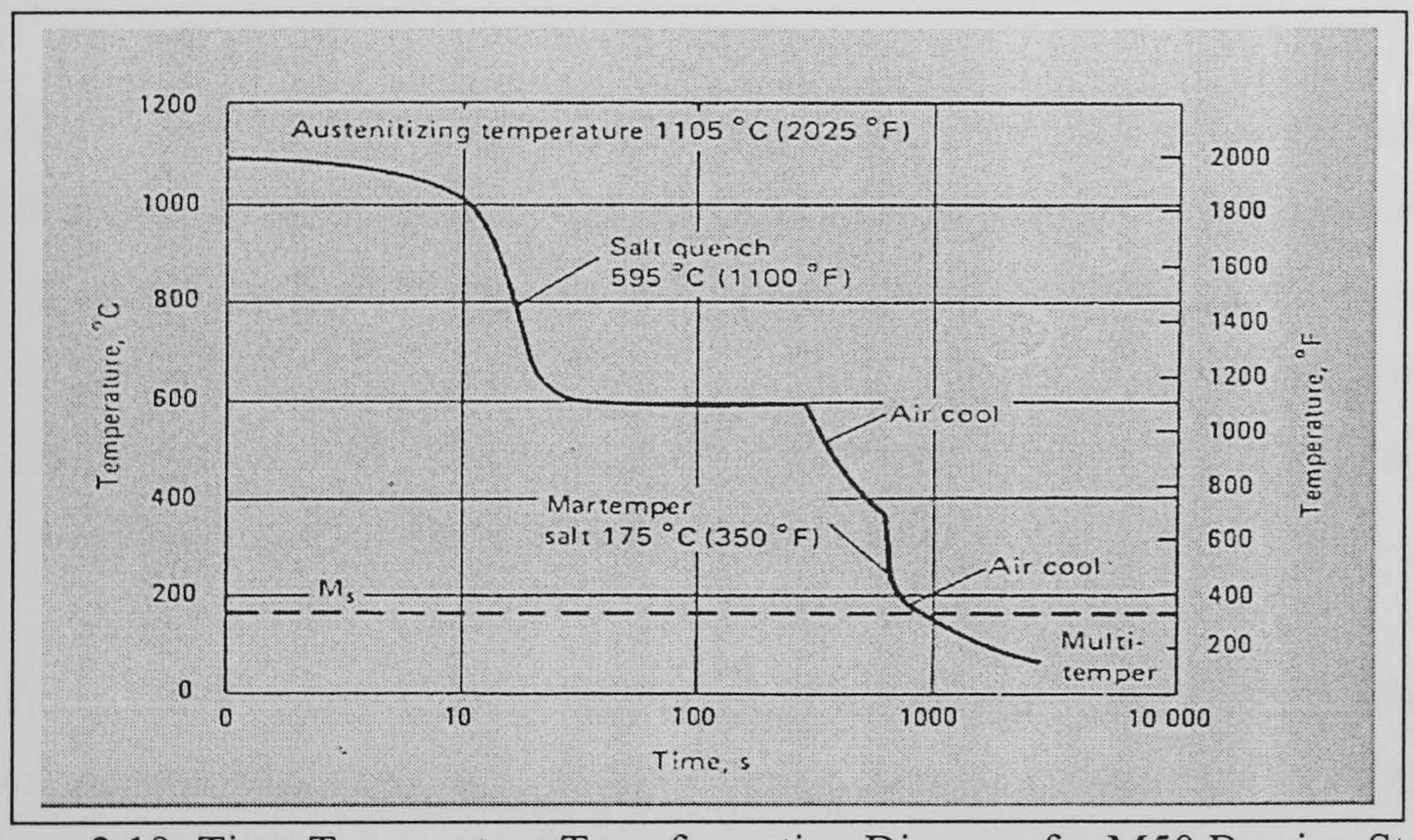

Figure 2.19: Time Temperature Transformation Diagram for M50 Bearing Steel

Figure 2.19 shows the characteristics for heat treating M50 bearing steel.

2.5 Cutting Fluid

Environmental concerns, resulting from public opinion and governmental regulations, are placing increasing constraints on the use and waste provisions for modern day grinding fluids. Waste management is now a basic requirement to take into account when considering the cost of fluid recycling. From an ecological viewpoint a dry grinding process would obviously be desirable. At present this desire will have to wait

for more advanced types of grinding fluid, although in the interim period the use of minimum quantity lubrication (MQL) is the vogue. If the flow rate of grinding fluid can be reduced then it represents a substantial saving to industry, in terms of manufacturing costs, as well as addressing environmental issues. This section investigates the types of grinding fluids, their uses and the state of research into this important field.

2.5.1 Grinding fluid Overview

Of the three grinding fluid types Brinksmeier (1999) reports that neat oil grinding fluid is the most efficient grinding fluid and the most damaging ecologically. Oil based grinding fluids also normally provide enhanced corrosion resistance and lubrication properties. Water based grinding fluids offer a higher efficiency in cooling and washing of the work piece. Other advantages are high chemical stability and transparency.

The addition of different additives to the fluid gives different properties with each additive enhancing specific characteristics of the grinding fluid. The EU released the Dangerous Substances Directive entitled - Directive 75/439/EEC on the disposal of waste oils, which established criteria for products that are potential hazards to the aquatic environment. Bartx (1998) stated that between 13% and 32% of grinding fluids in EU member states were deposited into the environment.

Bienkowski (1993) reported that with the escalation of replacement and displacement costs of these fluids and the tighter governmental regulations and environmental controls, the modern day engineers have to be aware of these issues and re-evaluate their metal working fluid management regimes. Howes et al (1991) also reported that these regimes would impact all stages of grinding fluid selection, use, recycling and disposal in both the factory and external environments.

2.5.2 Biodegradable Research

Biodegradability is the ability of a substance to be decomposed by micro-organisms. In North America a number of research programmes are taking place into a variety of scenarios which although not of a machining nature are heartening none the less, due to the progress being made into this important field (Brinksmeier et al 1999).

Genevro & Heineman (1991) reported that in the past engineers took factors such as work piece material, cutting tool material, tool life, cutting speed, type of machinery operated, method of application and finish desired into account and these were, and still are, all important factors. However these will change with a change in modern attitudes, to include the bigger picture, i.e. to include environmental responsibilities and knowledge of impending health hazards, particularly as new and stricter legislation is introduced.

2.5.3 Grinding fluid Application

There are many factors that influence productivity including grinding fluid type, composition and filtration additives used, grinding fluid supply, grinding fluid application method, flow rate and jet characteristics. As the material chip is formed the grinding fluid in contact with the zone influences the chip formation by the build up of a grinding fluid film. This film reduces frictional forces and cools the material and tool surfaces, so the viscosity and application of a grinding fluid is important to the final product. The general view that oil grinding fluids lubricate better than water based grinding fluids, and water based grinding fluids cool better than oils is constantly vindicated in other studies (Brinksmeier et al, 1999 & Howes 1990).

Recently published research has taken place using various grinding wheel types to compare results using two different types of grinding fluid (water soluble 4% and a mineral oil), minimum quantity lubrication (MQL) and dry grinding. These results indicate that a policy of MQL was of benefit when addressing the related normal and tangential grinding forces and R_z (average peak to valley height) values (Uhlmann & Laufer, 1998). These results are correlated in Brinksmeier's report (1999). Here the inference was that although high grinding fluid delivery pressures could enhance surface finish and residual stresses, there was a possibility that the subsequent normal forces due to hydrodynamic pressures from the elevated flow rate and wheel circumferential speeds disrupted the cutting procedure. When higher cutting speeds were employed, damage to the diamond wheel resulted from thermal stresses and this

curtailed the experiments. When the cutting speeds were reduced to 30m/s and using MQL the forces transmitted were slightly higher compared to those at 15m/s.

Uhlmann & Laufer (1998) reported that it had also been shown, in the case of dry grinding that damage had resulted from insufficient cooling of the work piece, and this indicated that a more efficient level of lubrication was desirable i.e. minimum quantity lubrication. It was noted that the surface roughness decreased with increased cutting speeds. The reason given for this was the smaller chip thickness. At higher cutting speeds energy is absorbed into the work piece material resulting in higher surface temperatures and hence an increase in material ductility and reduction in strength.

2.5.4 Grinding Fluid Delivery Systems

Webster et al (1994) suggest that the various types of grinding fluid delivery systems available today are proving to be highly scientific pieces of equipment, which require careful design and optimisation. The conventional flooding nozzles i.e. the shoe nozzle and the free jet types are at present the most common. Brinksmeier et al (1999) gave examples of different grinding fluid supply strategies which are presented in Figure 2.20, in which Q_{CL} represents the flow rate of grinding fluid in each case.

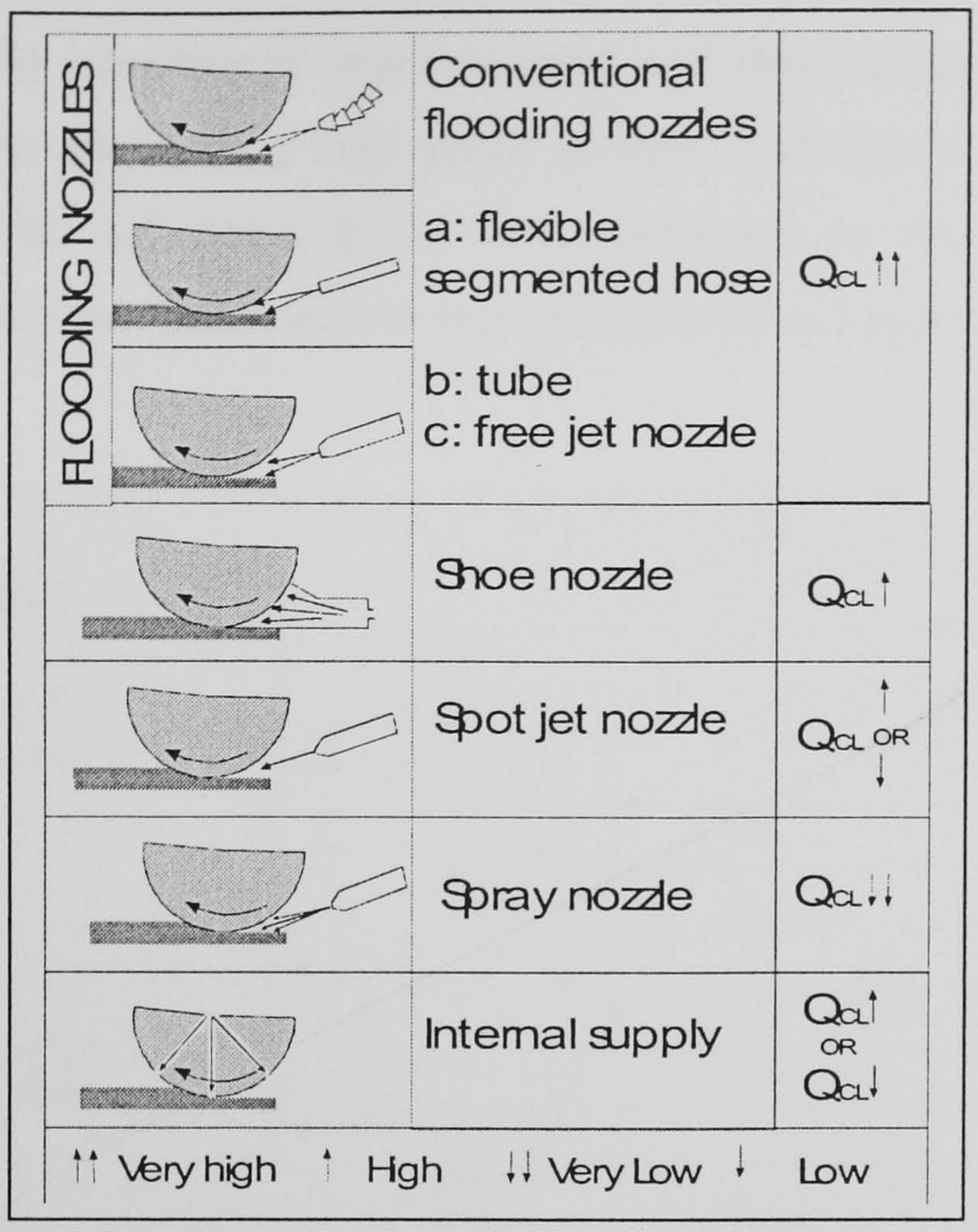

Figure 2.20: Examples for grinding fluid supply strategies

Other research areas have included the positioning of nozzles and their angles in relation to the wheels. Ebbrell et al (1999) showed that nozzles positioned at intermediate and tangential positions, as shown in Figure 2.21, resulted in a more uniform power requirement during the grinding process.

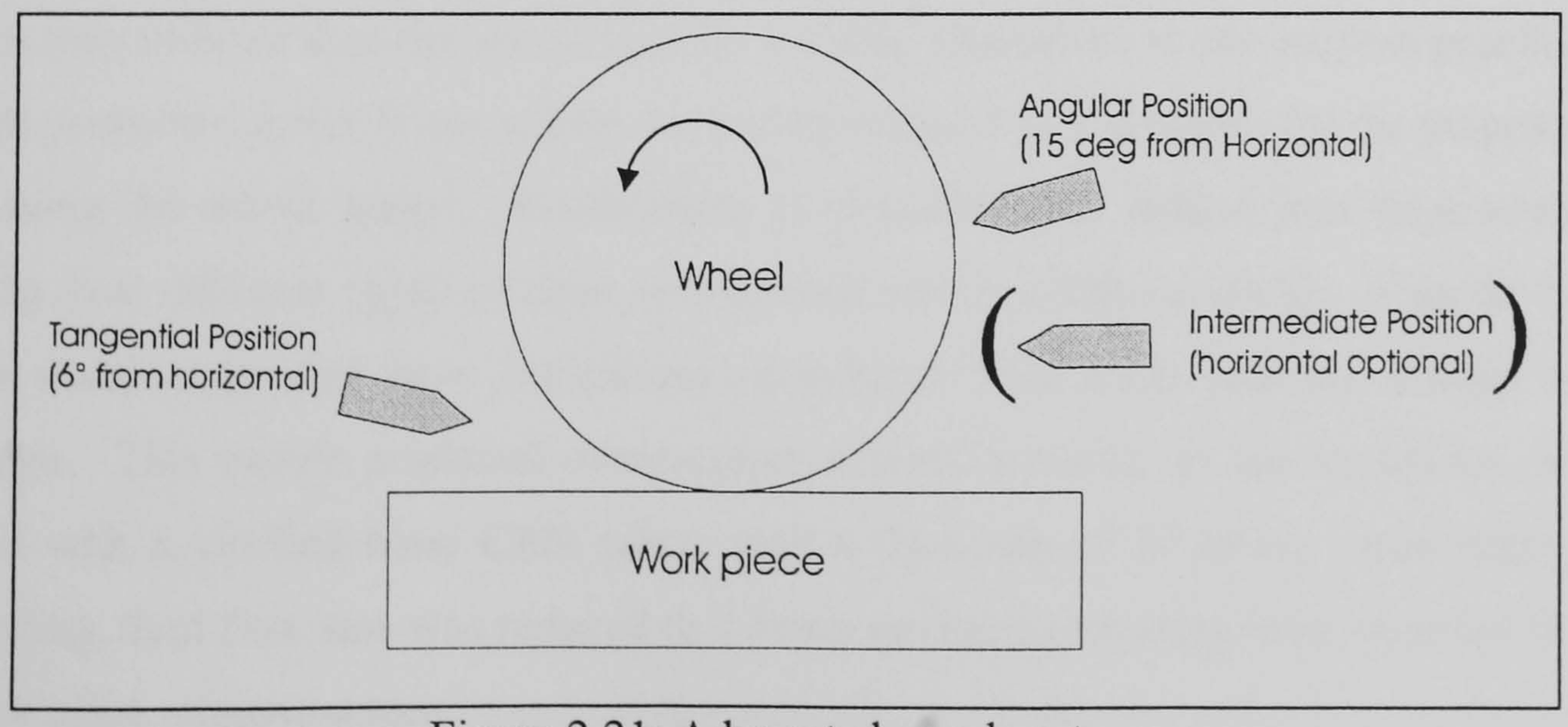

Figure 2.21: Advocated nozzle set up

Klocke et al (2000) investigated experimentally and theoretically the magnitude of hydrodynamic force when using high speed grinding techniques. Using the Navier Stokes equations the calculated forces were compared to measured values. A reasonable correlation was noted and the results are shown in Figure 2.22.

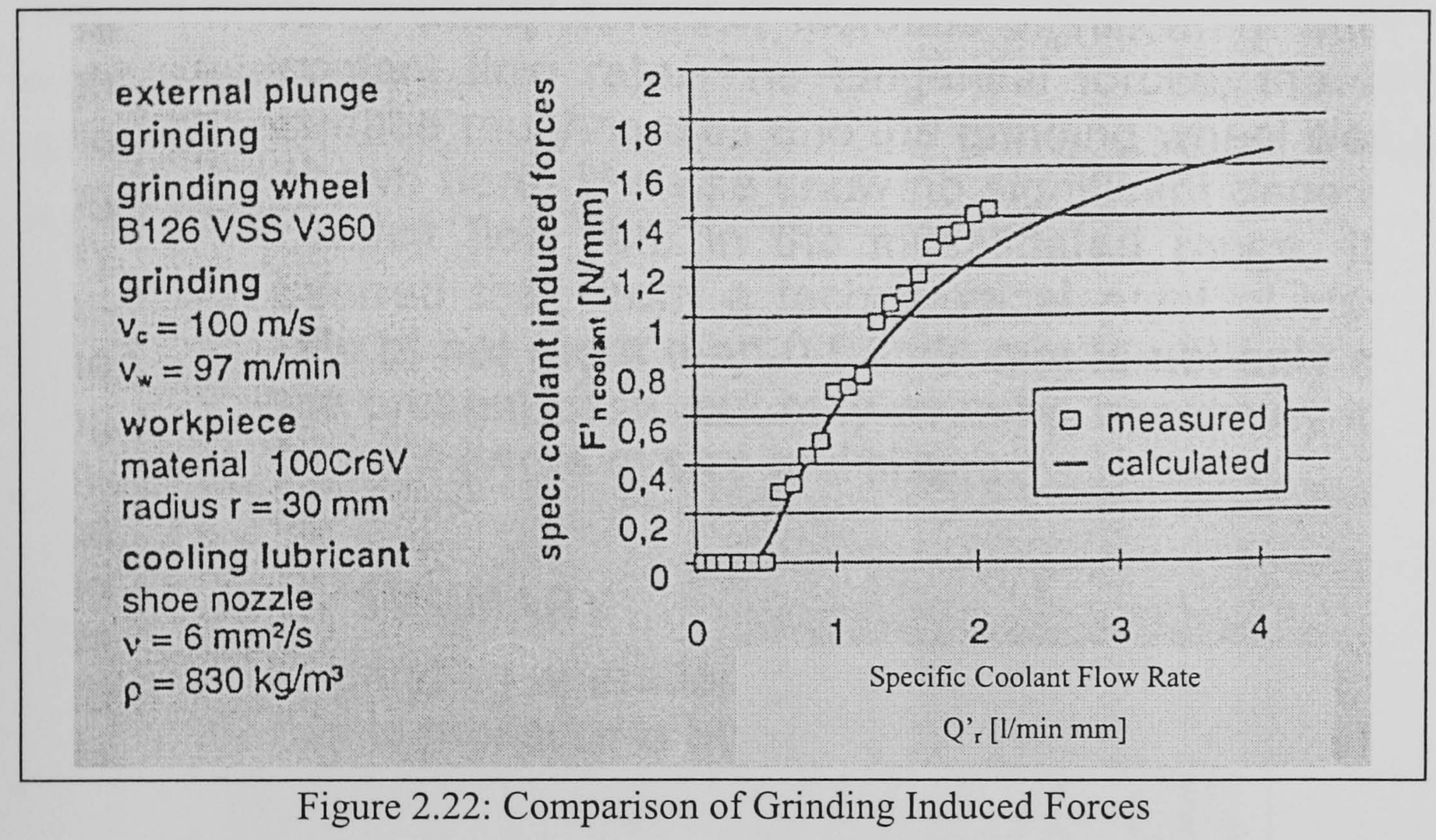

Figure 2.22: Comparison of Grinding Induced Forces

Also the hydrodynamic force measured seemed to increase with an increase in flow rate. In a previous study Werner & Lauer-Schmaltz (1980) also investigated the shoe nozzle, and they found that with this low pressure option wheel loading could easily occur. This may indicate that the shoe could be a viable alternative to the modern practice of high-pressure nozzles if one nozzle were to be retained as a scrubber for the purposes of cleaning the wheel matrix. Brinksmeier et al (2000) also looked into these nozzles, using four different types of shoe nozzle each with a different design of guide vane. The nozzle type that gave indications of reduced fluid swirl was the straight vane design. This nozzle produced compressive residual stresses, in the workpiece, when used with a vitrified bond CBN wheel with a flow rate of 30 l/min. Also when the grinding fluid flow rate was reduced to 5 l/min no thermal damage was observed in the work piece microstructure.

Klocke et al (2000) compared grinding operations performed using shoe nozzles and free flowing nozzles. These trials showed that the use of shoe nozzles could reduce the grinding fluid flow rate by 75%, albeit when used on small Q'_w values of up to $20mm^3/mm.s$.

Ramesh et al (2001) investigated and reported some success in reducing grinding damage with a new shoe nozzle as shown in Figure 2.23. This design incorporated a scraper to reduced the boundary layer or air around the periphery of the wheel. The first drilling was designed to produced a back pressure so that when the actual grinding fluid is applied it adheres to the wheel and is drawn to the contacting surfaces.

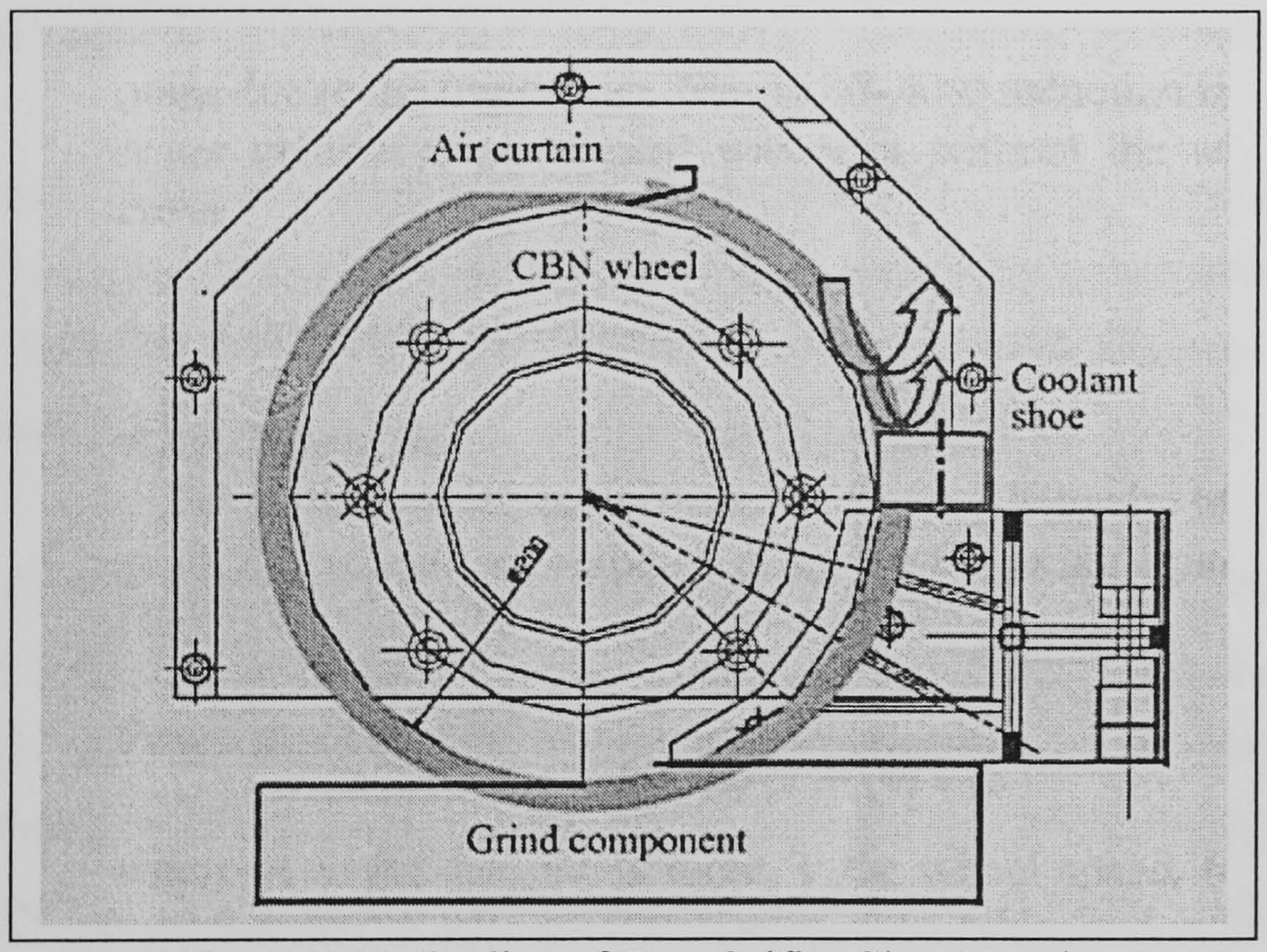

Figure 2.23: Outline of Two Orifice Shoe Nozzle

2.5.5 Contact Zones

The contact zone between the wheel and the work piece has for a long time been identified as a critical factor influencing the ground surface integrity. Webster et al (1995) noted that the actual influence of a grinding fluid on the grinding process is of great importance. The function of the grinding fluid is to reduce friction and enhance swarf removal. There have been studies where the flow rate of the grinding fluid has been varied when using two CBN wheels relevant to the current research, namely, B151 and B252. The results showed that with an increase in flow rate of the mineral oil

grinding fluids from 100 l/min to 130 l/min, the forces normal to the plane increased dramatically. It was not stated if reducing the flow rate would have the reverse effect. (Brinksmeier et al 1993).

2.5.6 Cooling Effectiveness

Through work carried out by Rowe et al (2000) it was stated that the heat generated during grinding is conducted away via the work piece, the abrasive and the grinding fluid. Wang & Kou (1997) reported that it is also assumed that the total heat flux is uniformly distributed over the whole contact region.

The implication of this study was that with adequate fluid injection into the contact zone, the grinding fluid would carry away most of the heat entering the contact area.

Gu & Wager (1990) also considered that the variations in depths of cut altered the grinding fluid effectiveness, i.e. the deeper the cut the greater the temperature increase. Although the initial study in this area was based upon creep feed grinding techniques more research into this field would be of great benefit to HEDG.

Campbell (1997) reported on a study in which sensors were used to develop the required amount of hydrodynamic pressure for the purpose of optimising a grinding process. Also in this study the same piece of equipment was used to test the efficiency of a number of nozzles of various sizes. This study concluded that when used in a shallow surface grinding environment, a 12mm diameter nozzle with a flowrate of 0.3ltr/min gave a higher overall cooling effectiveness compared to a smaller diameter nozzle using the same fluid flowrates.

2.5.7 Grinding fluid Research

Of the three oil types to be used within the confines of this project the mineral oil has the most environmental risks attached to it.

If mineral oils are to be used with this process then development of successful minimum quantity lubrication strategies is therefore a priority. Nozzle design is a further area

where considerable developments could be of benefit. The importance of variables such as nozzle type, flow rate, delivery pressure and nozzle angle/position are all critical in the optimisation of the grinding fluid delivery system.

In addition to technical requirements, aspects of toxicology and industrial medicine will exert an important influence on the formulation of future grinding fluids. The high disposal costs reported will inevitably rise further and this will be one way in which governmental controls will be wielded and should result in the use of products which incorporate environmentally friendly labelling, higher service life and constant long term properties as well as in better maintenance procedures. As biodegradability of oils becomes more widely required, the market demand should result in wider availability and cost reduction. Table 2.6 summarises in general terms the state of grinding research in the various fields of interest and ranges of general parameters used, volunteered by Prof. John Webster.

Name	Source	Mode	Q'_w	Fluid	Vs	Material	Pressure	Specific Flow Rate	Wheel Type
			(mm^2/s)	type	(m/s)		(bar)	(ltr/min.mm)	
Mindek	ASME COGEN	CDCF		Emulsion	30	Inco 718		10	Alox
Werner	SME	CDCF	4	Emulsion	26	M2 steel	13.5	7	Alox
Howes	Supergrind	CDCF	4.3	Emulsion	30	MAR	4		Alox
Pearce	IGT Conference	CDCF		Emulsion	30			5	Alox
Minke	SME	Surface	167	Oil	125	Low Carbon Steel	7	26	Alox Segments
Malkin	SME	Surface		Emulsion	30	Cold Roll Steel		3.6	Alox
Marchand	Supergrind	Creep Feed	6	Emulsion	50	738 Inco	5	11	CBN EP
Marchand	Supergrind	Creep Feed	7.5	Emulsion	200	738 Inco	11	12	CBN EP
Howes	Supergrind	Creep Feed	4.3	Emulsion		M2	6.5	46	Vit CBN
Meyer	SME	Creep Feed	1	Oil		C45	2	10	CBN EP
Meyer	SME	Flat Slot		Oil		Steel	8	174	Diamond
Tawakoli	SME	HEDG		Oil		Steel	14	14	CBN EP
Spur	SME	Surface	16	Various		Silicon Nitride	10	3.75	Diamond MSL
Meyer	SME	Cyl Slot	37	Oil	140	Case Hard Steel	13	94	CBN EP
Meyer	SME	CAM	4.2	Oil	100	Cast Iron	8	7	Vit CBN
Kovach	SME	Cylindrical	8.6		178	Silicon Nitride	27	340	Diamond MSL
Guhring	Book on HSG	Cylindrical	300	Oil	180	Steel	30	12.5	CBN EP
Konig	SME	Cylindrical	40	Oil	90	Chrome Moly	20	13-40	CBN
Meyer	SME	Crank	180	Oil	140	Cast Iron	25	8	CBN EP

Table 2.6: Summary of Current Grinding fluid Research

2.6 Evaluation of Surface Integrity

This section reviews the techniques used and provides a background to the metallurgical analyses required for the characterisation of workpiece surfaces. Shaw (1996) stated that finished components have been studied since the 1960's and a number of reviews have taken place since, including Fields et al (1971 & 1974).

2.6.1 Surface Characterisation

Surface analysis encompasses many techniques to study various aspects of the ground surface. Each individual technique gives an insight to the quality of the finished component. Tönshoff (1992) reported that the surface roughness gave a keen measure of the quality of the workpiece. Also the morphology of the finished surface can indicate a number of machining induced imperfections such as chatter. These vibrations can be damped out by a number of means including using reduced feed rates, depths of cut and wheel speeds and also external parameters such as using softer wheels.

2.6.2 Measures of Surface Roughness

There are a number of main measures of surface roughness or texture which are chosen to highlight different aspects of the surface in question. Also different countries use different surface parameters as their own standard.

Table 2.7 below gives an insight as to the variance of use for these parameters after Mainsah (2001).

Parameter Designation	Country	Parameter Description
R_a	UK,USA & ISO	Average Roughness
R_q	UK,USA & ISO	Root Mean Square Roughness
R_t	Germany & Russia	Maximum peak to valley height

Table 2.7: The Main 2D Surface Roughness Parameters

There are numerous surface measures used around the world but as stated by Mainsah (2001) only a few have been fully accepted by all. The main surface measures are described here and more in depth descriptions and explanations can be found in the relevant international standards, these being ISO 4287, 1996; ANSI/ASMEB46.1, 1985 and DIN 4772, 1979.

The average roughness of a surface is called R_a and it measures the absolute roughness as the deviation of the profile from a mean line.

R_a is derived as:

$$R_a = \frac{1}{L}\int_0^L |z| dx \qquad \text{Eqn 2.1}$$

R_q is used as a measure of the root mean square deviation of a profile about a mean line.

R_q is derived as:

$$R_q = \frac{1}{L}\int_0^L |z^2| dx \qquad \text{Eqn 2.2}$$

R_t is another common measurement and is described by Mainsah (2001) as being an extreme value parameter. R_t is the height between the lowest and highest points of the surface in question. This measurement is therefore susceptible to significant one off anomalies.

Examples of the measurements not described here but that are available in the international standards are measurements for slope, skew and average curvature of a surface.

There are a number of three dimensional measurements also available to both measure the surface quality and map the surface topography of samples. Although there is no international standard for these measurements there are a number, which are being

accepted internationally. These include S_a, which is used to denote the three dimensional equivalent of R_a and S_q which has the same relationship to R_q.

2.6.3 Sub-Surface Characterisation

Fields & Kahles (1971) describe how samples should be cut, polished and etched so that the grain boundaries of the samples can be studied.

Tönshoff (1991) stated that the influences of mechanical and thermal effects arising from grinding a material's surface and sub-surface grain structure are described by the surface and sub-surface analysis of a sample. In order to view the grain structure of a sample normally involves mounting and polishing the surface to a mirror like finish through various processes and examining light reflected from it at magnifications of 50 to 1500. If the surface is lightly chemically etched in an appropriate solution, the grain boundaries and constituent phases will be attacked at different rates and will be visible. This makes it possible to establish which phases are present as well as their shape, size, and distribution. Metallography is of particular value in the analysis of samples which have failed or have performed in an unexpected manner.

Another technique of sub-surface integrity is the Vickers Hardness Tester. Devised in the 1920's by engineers at Vickers, it was designed to measure the hardness of a material which was calculated from the size of an impression produced under load by a pyramid-shaped diamond indenter. The pyramid, whose opposite sides meet at the apex at an angle of 136°, is pressed into the surface of the material at loads ranging up to approximately 1000 grams-force, and the size of the impression is measured with the aid of a calibrated microscope.

The Vickers number (HV) is calculated using the following formula:

$HV = 1.854(Load/mm^2)$,

The applied load is usually specified when HV is cited. The Vickers test is reliable for measuring the hardness of metals, and it is also used on ceramic materials.

2.6.4 Microstructure Changes

The area of micro structural change during grinding has been well documented by a number of authors. Shaw et al (1993) and Shaw (1996) discussed the minimum carbon content in steel to be 0.25% by weight in order to obtain untempered martensite.

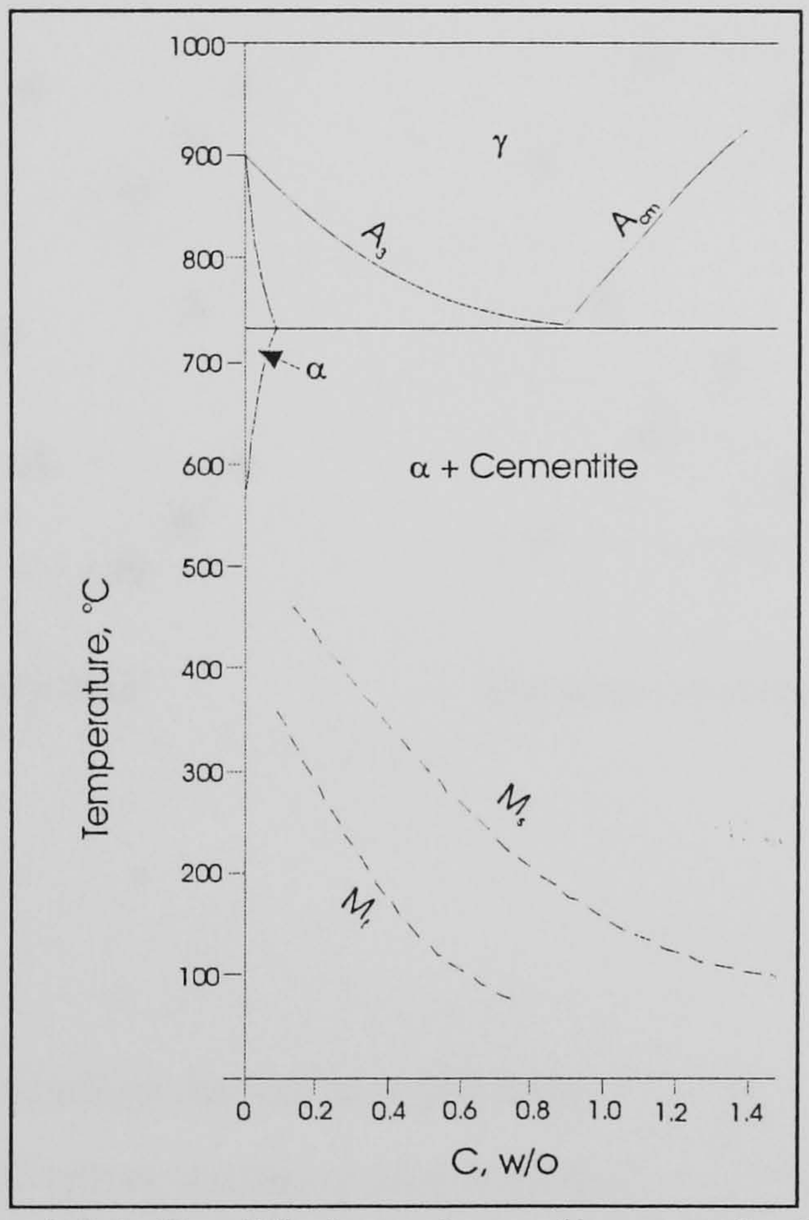

Figure 2.24: Equilibrium phase diagram for Fe-C.

Figure 2.24 shows the equilibrium phase diagram for Fe-C and indicates where the martensitic transformation begins (M_s) and ends (M_f). The critical temperature relating to over temper burn or the onset of an over tempered region was found for ferrous metals in general to be in the region of 450-500°C (Rowe et al 1995). McCormack (2001) outlines the effects of abusive grinding in relation to its effects on the surface of EN31 steel with regards to hardness, martensitic transition temperatures and residual stresses. Figure 2.25 illustrates the changes in molecular structure between alpha and gamma iron.

Shaw et al (1993) and Shaw (1996) describe how during this transition period the ferrous material undergoes a substantial phase change at a rapid rate. The plastic

deformation during the grinding process of γ iron along with the heat generated produces an extremely fast reaction time to produce untempered martensite in the region of 0.1μs.

Figure 2.25: Cells of a) Ferrite and b) Austenite

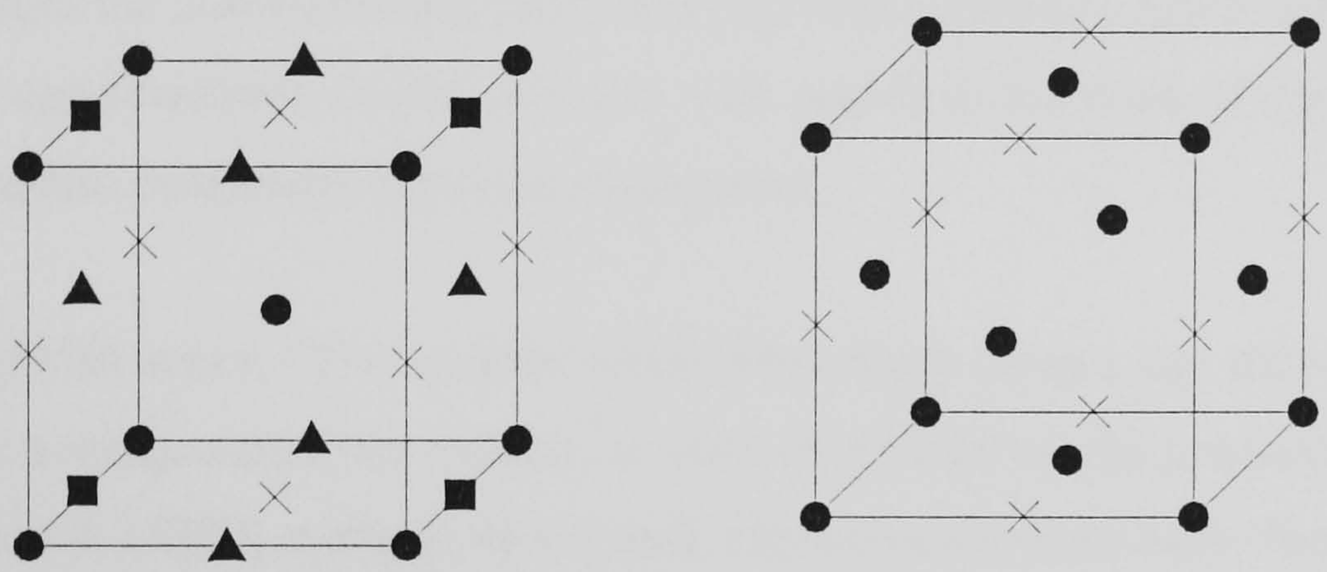

Also Chen et al (2000) states that when abnormally high temperature ranges are experienced the added disadvantages of thermal expansion and contraction and ultimately phase changes within the material could be witnessed. The phase changes could interact with these expansions and contractions which could lead to localised fractures at or near the surface.

2.6.5 The X-Ray Diffraction Residual Stress Measurement Technique

When a component is manufactured some of the energy expended becomes trapped within the structure of the component in the form of residual stresses. As Chen et al (2000) states these residual stresses are formed due to Hertzian compression and shear

forces produced by the action of the grains. These stressed areas may be contained within the grains of the material and are called micro-stresses, or if a large volume of material is stressed in this way, and as such encompasses more than one grain of material, they are called macro-stresses.

Residual stresses can be induced through thermal or mechanical processes or a combination of both. The final design criteria to which the component must conform would dictate the allowable magnitude and sign of acceptable levels of residual stress. All these considerations should be taken with regard to the level of significance on each individual component's service requirement.

Prevey (1986) states, "The residual stress determined using x-ray diffraction is the arithmetic average stress in a volume of material defined by the irradiated area." X-ray diffraction (XRD) methods of residual stress measurement have been used for a number of years particularly in the automotive and aerospace industry. Tönshoff et al (1992) mentions that the magnitude and sign of residual stress in the material surface, are the best indicators of the thermal and mechanical influences on the surface integrity. Kruszynski et al (1991) also endorsed the use of residual stress measurement as being the most representative parameter of all the properties in the surface layer created by grinding. Shaw et al (1996) stated that although residual stress measurements gave an indication of the stress regimes involved on the surfaces of the workpiece, he warned that these results could be misleading as to the real sub-surface residual stress picture.

It is a well-known fact that the measurement of stress can be described as a misnomer as stress is quantified by the measurement of some other intrinsic property such as strain. Hooke's Law relating Young's Modulus of Elasticity, calculated stress and measured strain is shown in Eqn 2.3:

$$E = \frac{\sigma}{\varepsilon} \qquad \text{Eqn 2.3}$$

Where :

E is the Young's Modulus of Elasticity

ε is the measured strain

σ is the calculated stress

Eqn 2.3 is normally used in some form or other to describe the mechanical properties of materials. The only major difference with other means of stress calculation and X-ray diffraction (XRD) techniques, is that with this highly controllable source of X rays and detection, minute changes in stresses within the crystal lattice plain can be detected.

The measurement of residual stress at the surface of the specimen requires the following assumptions to be made:

- a condition called plane stress is present
- the major principal stress is in line with the machined surface

Plane stress is when the stresses are present in the x and y direction but the third axis, being z, has a value of zero. The largest principal stress ($\sigma 1$) is parallel with the grinding direction.

2.6.5.1 Bragg's Law

Figure 2.26 shows waves 1 and 2, in phase with each other, glancing off atoms A and B of a crystal that has a separation distance d between its atomic, or lattice, planes. In this case the number (n) of full wavelengths in question is 2. The reflected angle is equal to the incident angle. The condition for the two waves to stay in phase after both are reflected is that the path length CBD be a whole number (n) of wavelengths. Also, CB and BD are equal to each other and to the distance d times the sine of the reflected angle, or d $\sin\theta$.

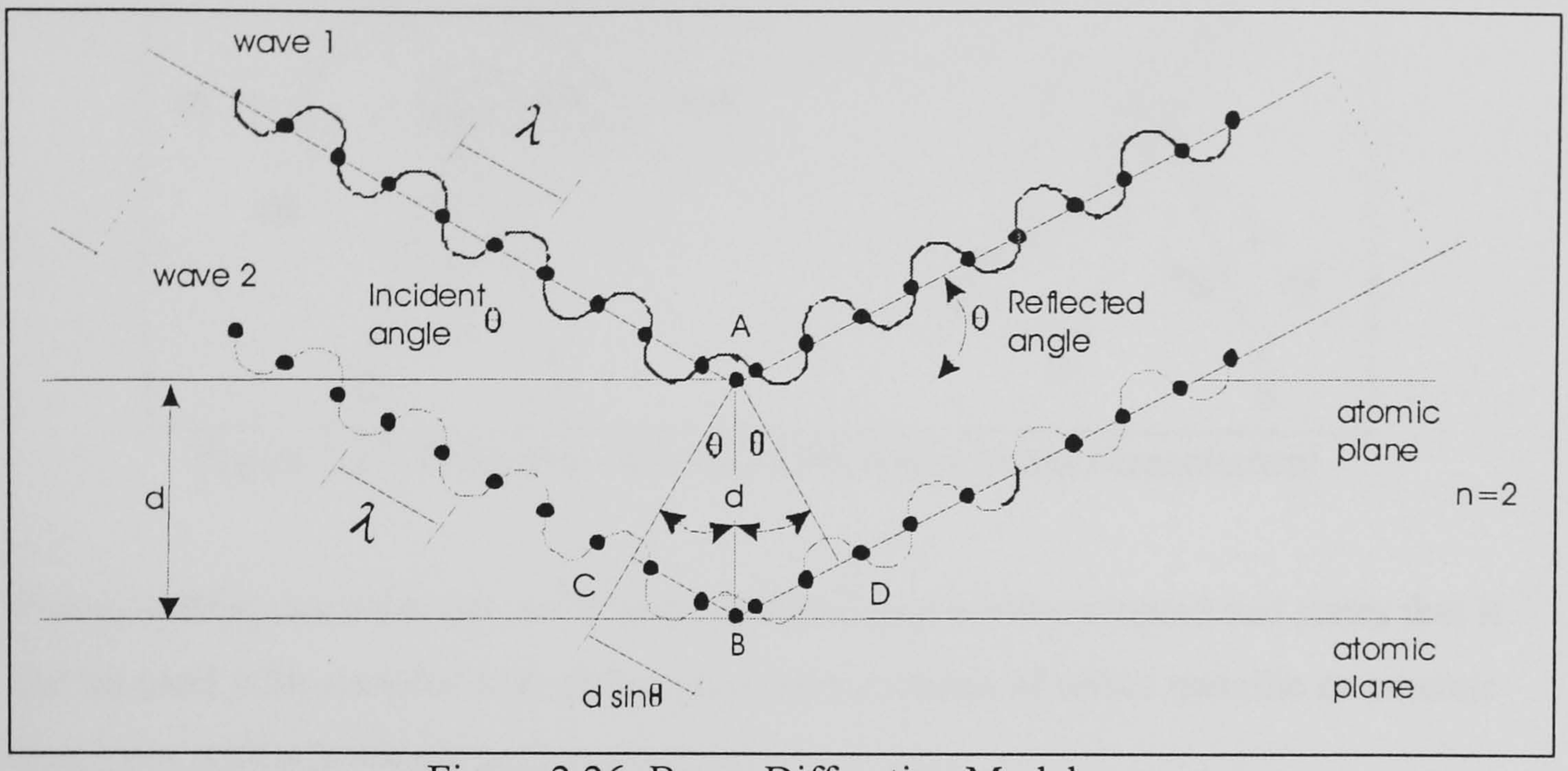

Figure 2.26: Bragg Diffraction Model

Thus, Bragg's law is shown in equation 2.4.

$$n\lambda = 2d \sin\theta \qquad \text{Eqn 2.4}$$

2.6.5.2 Basic Residual Stress Measuring Techniques

Of the four basic styles of residual stress measurement the two angle technique ($\sin^2\Psi$ technique) is widely used in the United Kingdom and Europe. This technique measures the lattice spacing between a maximum and minimum range of the angle 2theta for a number of Ψ angle tilts, an example of which is shown in Figure 2.27 (after Prevey 1986). Once the full angular range has been analysed the Ψ angle is changed so that further lattice structures will be perpendicular to the emitted X-rays. In this way the maximum amount of information relating to any changes in the d-spacing can be gathered over a wide range of Ψ tilts.

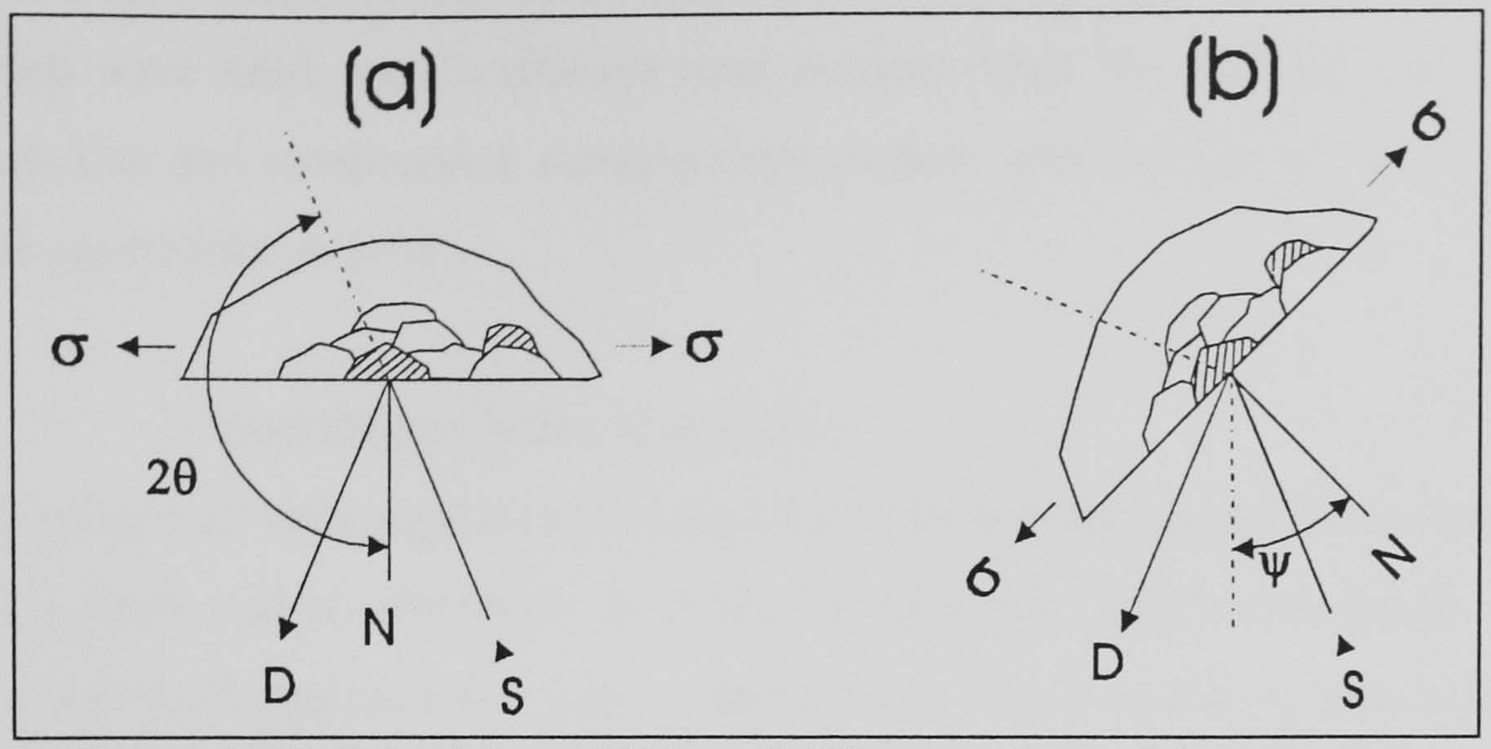

Figure 2.27: Principles of X-Ray Diffraction Stress Measurement

Prevey (1986) describes the $\sin^2\Psi$ technique as being widely adopted and states that it can be used with samples with polycrystalline structures of either metallic or ceramic structures with a moderate to fine grain size.

McCormack (2001) stated that depending upon the stress regime within a component, the magnitude and sign would dictate the life and quality of the component. The onset of tensile stresses was noted to be around a critical stress temperature of approximately 250°C for EN31 steel. Chen et al (2000) also investigated this and found for a medium carbon steel such as EN9 the transition temperature was found to be around 200 °C. This was concurred by Mahdi & Zhang (1996) who stated that the onset of thermal deformation, and therefore residual stress regimes, was around 300°C for EN23 steel when using shallow cut reciprocating grinding processes.

Österle et al (1997) investigated the effects of creep feed grinding on IN738 nickel superalloy material using corundum abrasives and CBN superabrasives. When grinding with CBN grits the microstructure showed that micro cracking had occurred in a re-deposited layer at the surface, and that this layer was only a few microns thick. This was confirmed in the residual stress measurements where an easily removable layer had slight tensile stresses. In a further study Österle et al (1999) studied the effects of grinding a cast nickel based superalloy under different grinding conditions. It was found that although the lubrication delivery system was one of the top priorities due to the low thermal conductivity, the use of CBN superabrasives induced a greater magnitude of compressive stress. These previous studies correlated well with work

carried out by Matsuo et al (1987) which indicated that when comparable grinding parameters were used, tensile stresses were evident when the grinding medium was white alumina and compressive stresses were evident with the use of both CBN and diamond superabrasive grits.

2.6.6 Barkhausen Noise Amplitude

With the advent of more sophisticated amplifiers, the Barkhausen Noise technique has become a more viable alternative to X-Ray Diffraction (XRD) techniques for the quality control of manufactured parts. Barkhausen Noise Analysis, which has also been referred to as the Magneto-elastic or the Micro-magnetic method, is based on a concept of an inductive measurement of a signal that is generated when a magnetic field is applied to a ferrous metal sample. The German scientist Professor Heinrich Barkhausen explained the nature of this phenomenon in 1919 and the technique was subsequently named after him and the signal is called Barkhausen Noise.

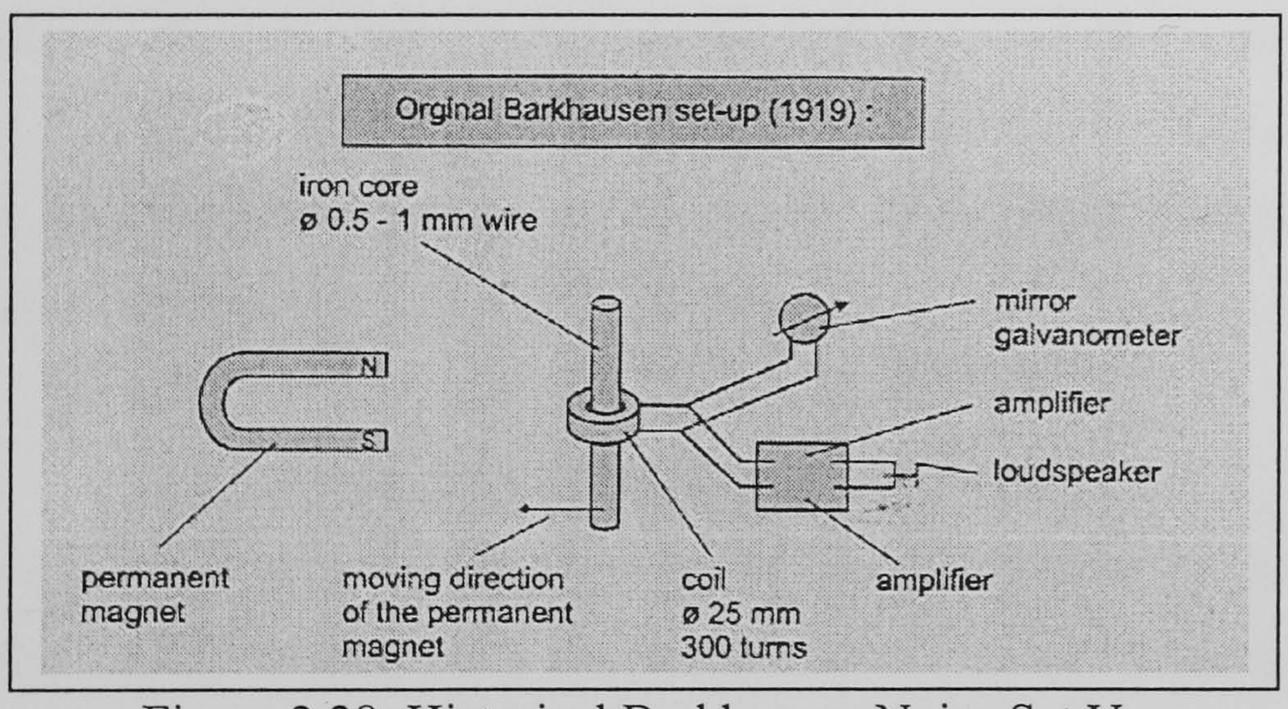

Figure 2.28: Historical Barkhausen Noise Set Up

Figure 2.28 shows the set up used by Prof. Barkhausen, after Karpuschewski, (2000). Barkhausen was the first to note that the changes in magnetic field due to the rearrangement of Bloch-wall domains were not a gradual one but rather a series of jumps (Barkhausen 1919).

This phenomenon is described in the next section which also investigates the use of this technique with regard to the measurement of stresses and micro-structural changes induced by grinding.

2.6.6.1 The Barkhausen Noise Effect

Ferromagnetic materials consist of small magnetic regions called domains. Each domain is similar to individual bar magnets which are magnetized along a natural crystallographic direction and any change in the elastic energy induced by an AC current will induce a stress regime within the microstructure of the material. The domains are separated by boundaries known as Bloch Walls. It was Barkhausen who first noticed that these walls do not have a gradual motion, when polarity changes occur through magnetic inducement, but rather a jerky or jumpy one.

An alternating current induced magnetic field causes these Bloch Walls to oscillate, and for this to take place changes in grain size has to occur. The same is true for an axial tensile load being applied on the ends of a bar; the bar elongates in the direction of the load and reduces in diameter perpendicular to the load. These changes in grain size alter the magnetic field strength induced in the sample. These alterations in the mechanical properties of a piece of steel are felt in shifts in the stress fields within the specimen. Karpuschewski (2000) stated that the Barkhausen output is damped by two occurrences, firstly the existence of compressive stresses within the domains and secondly the material properties dampen the output, for example materials which are of high hardness such as high speed or tool steels.

2.6.6.2 Applications of Barkhausen Noise Analysis

The surface treatment of a material can affect the Barkhausen output, be it heat treatment after material production or mechanical metal removal. It has been widely documented that Barkhausen Noise Techniques have been used as non-destructive testing (NDT) for the location or existence of surface and sub surface abnormalities within a component. Gupta et al (1996) carried out an extensive study in which it was found that a good correlation existed between the Barkhausen effect and visible thermal damage on the surface of ground steels.

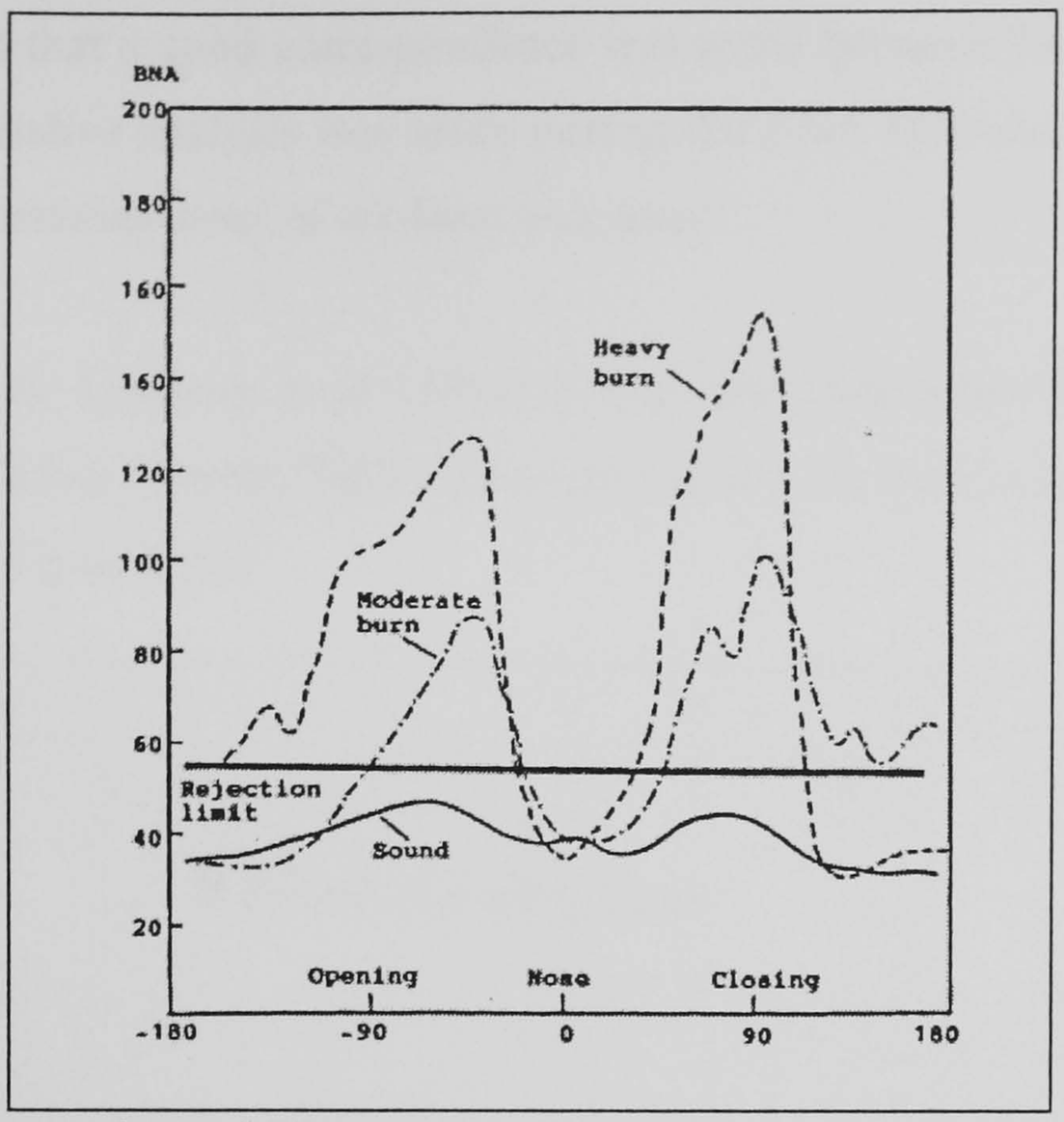

Figure 2.29: Comparison of BNA readings from damaged and undamaged samples.

Fix (2000) investigated the effects of thermal damage on ground steel crankshafts using the Barkhausen Noise response as an output. He found an excellent correspondence between BNA and the variable intensity of grinding burn quantified by Nital etch. These results are shown in Figure 2.29. Hallet (2000) also utilised the BNA effect to optimise the lubrication system of a grinding process using the BNA output as a guide as to the efficiency of the process used when varying different parameters. Hillman (2000) investigated induction hardening depth making comparisons between Eddy Current techniques and Barkhausen Noise.

Hillman reported that a good correspondence was noted between the two techniques and when a qualitative analysis was made putting the BNA Rollscan output into five categories an uncertainty level of ±0.4mm was noted.

During a study by Desvaux et al (1999) it was also concluded that there was a reasonable correlation between XRD measurements and the Barkhausen Noise effect. This is shown in Figure 2.30.

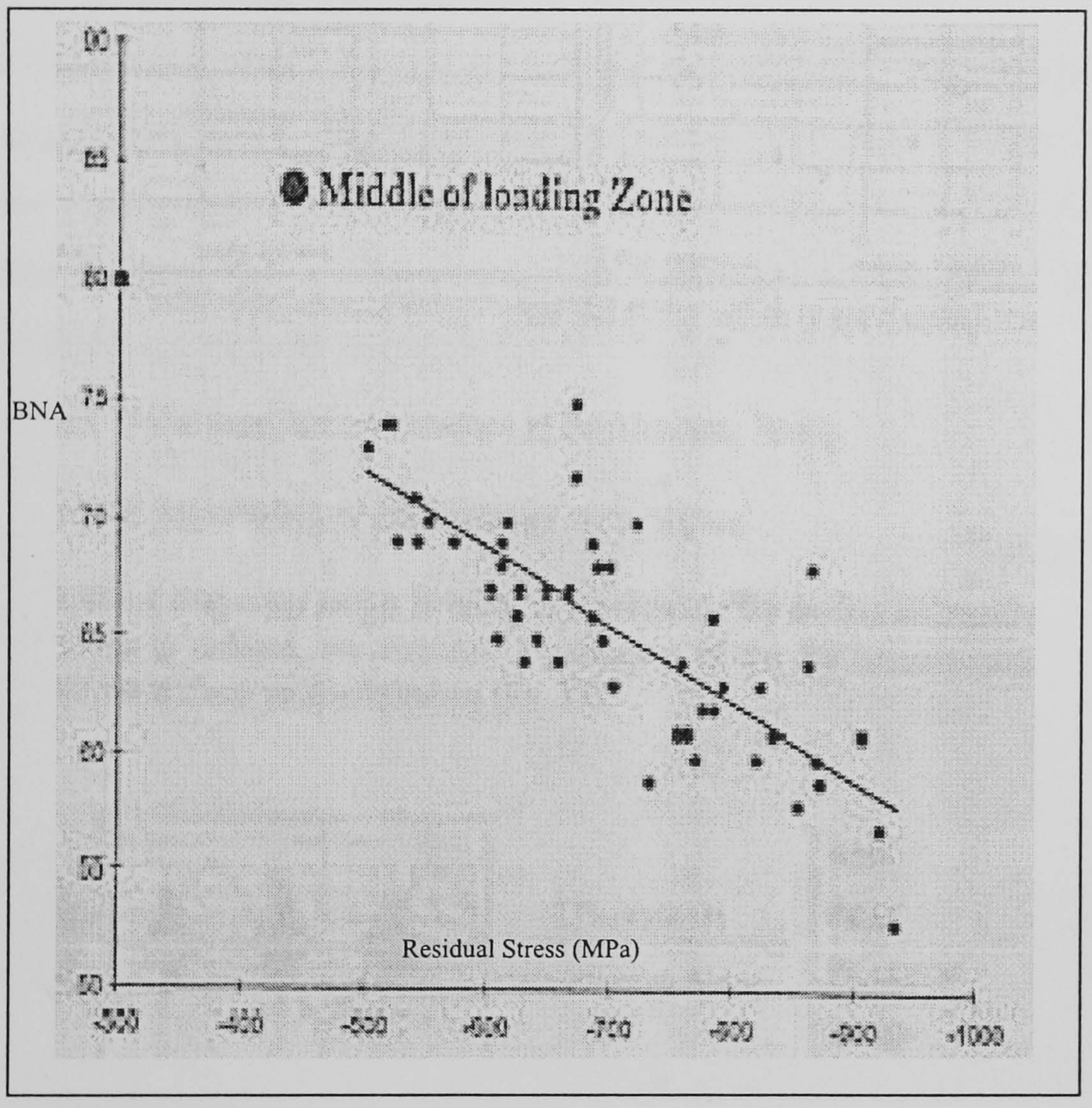

Figure 2.30: Correlation between Barkhausen Noise and XRD Measurements

The Barkhausen Noise concept is becoming more widely acclaimed as a legitimate NDT method alongside the more quantitative techniques. As further research is carried out and the results are shown to be repeatable; the mobility of the equipment, speed of testing, reliability of the readings, ease of use and the amount of training required could make this method of NDT more attractive to a wider range of manufacturers.

2.7 Thermal Modelling

There have been a number of reports / studies carried out regarding the thermal or thermally connected aspects of grinding. These have covered a myriad of individual subjects but all have included the three basic components of the grinding system: the work piece, abrasive and cutting fluid.

2.7.1 Historical Overview

The initial theoretical temperature-measuring model was published by Jaeger (1942). This model was designed to describe grinding with constant feed rates, light depths of cut and the assumption that the majority of the heat generated by the sliding heat source enters the work piece. The model predicts the temperature of sliding contacts assuming a moving source of heat and is shown Equation 2.5.

$$\theta = 0.754\frac{Ruvd}{\beta\sqrt{vl}} \qquad \text{Eqn 2.5}$$

where:

θ	Mean surface temperature
R	Energy partition coefficient
u	Specific grinding energy
v	Feed rate
d	Depth of Cut
l	Wheel / workpiece contact length

$$\beta = (k\rho c)^{0.5} \qquad \text{Eqn 2.6}$$

and β is defined by equation 2.6, relating to the workpiece thermal characteristics as follows:

k	Thermal conductivity
ρ	Density of material
c	Co-efficient of heat capacity

The Jaeger model relates temperature to the specific grinding energy. Malkin (1974) suggested that the total specific grinding energy *u* may be considered in terms of several components, a chip formation energy due to cutting u_{ch}, a ploughing energy u_{pl} and a sliding energy u_{sl}, in the form of:

$$u = u_{ch} + u_{pl} + u_{sl} \qquad \text{Eqn 2.7}$$

Malkin shows that the ploughing and sliding energies may be expressed in terms of the grinding variables such that equation 2.8 can be derived as follows:

$$u = u_0 + Bd_e^{1/4} a_c^{-3/4} v_w^{-1/2} \qquad \text{Eqn 2.8}$$

Where:

$$u_0 = 0.45u_{ch} \qquad \text{Eqn 2.9}$$

Note: d_e represents effective wheel diameter, a_c depth of cut and v_w feed rate.

A plot of specific grinding energy against the function $f = \left(d_e^{1/4} a_c^{-3/4} v_w^{-1/2}\right)$ should yield a linear relationship with the gradient determined by the grinding temperature as

shown schematically in Figure 2.31. Malkin (1974) also reported that a line denoting the boundary between damaged and undamaged specimens can be drawn and the gradient of this line is proportional to the constant maximum grinding zone temperature. Therefore any set of parameters used that resulted in any point being mapped above this line would produce a damaged workpiece.

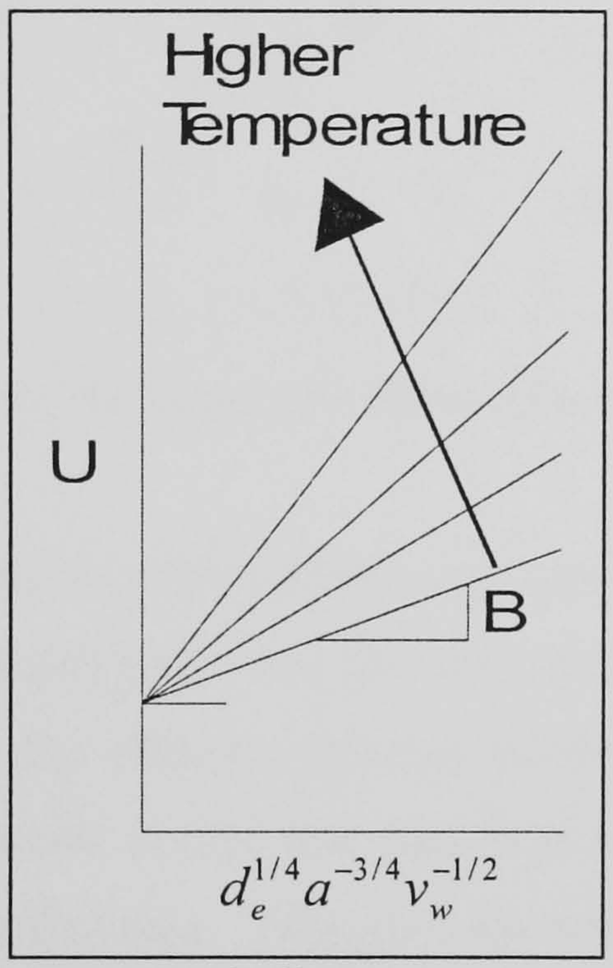

Figure 2.31: Lines of constant grinding zone temperatures. (after Malkin)

The validity of this approach has been demonstrated by Mayer et al at the University of Texas (1999) and Stephenson et al (2001). An example is shown in Figure 2.32 that depicts the boundary condition between burn and no burn regions for ground X53 steel.

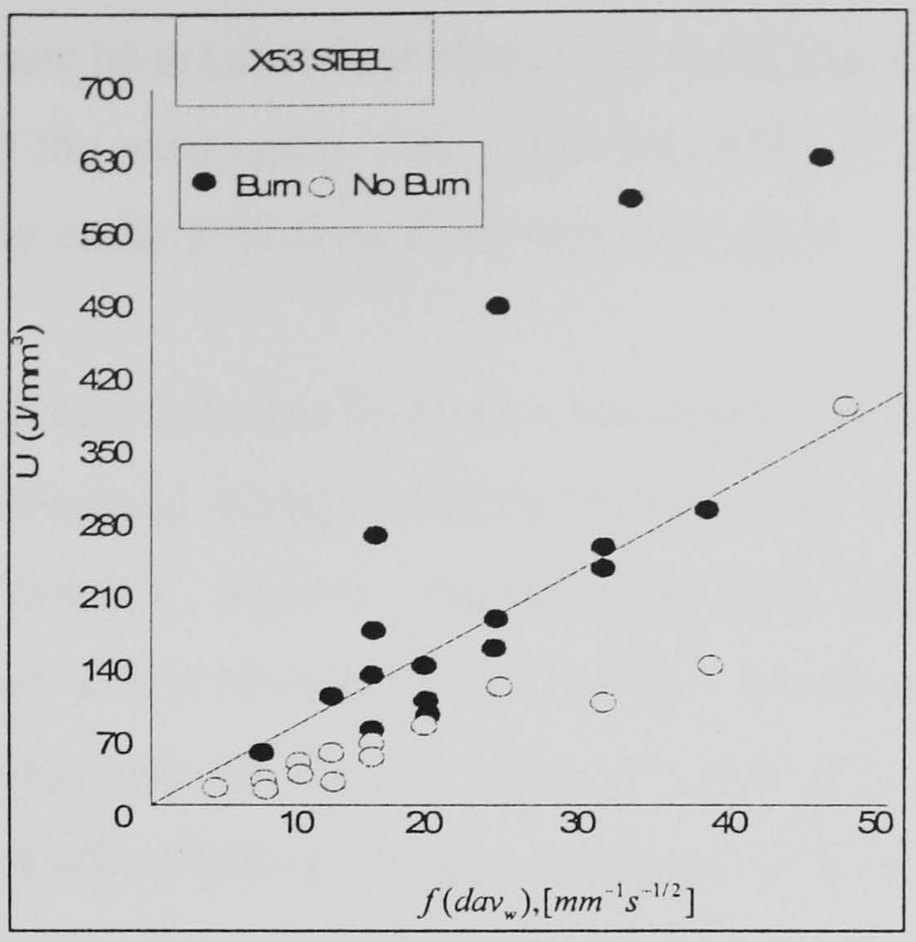

Figure 2.32: Specific Energy U versus $f(da_c v_w)$ for X53 steel

Rowe et al (1995) concluded an experimental investigation into the heat transfer in grinding by stating that the partition ratio for CBN grit was lower than aluminium oxide abrasives. Also that the effective thermal conductivity of CBN grains was within a range of 87-240W/mK which was significantly lower than the theoretical value of 1300W/mK used at that time. This gives an indication of the amount of heat generated, and which is conducted away from the workpiece using this superabrasive.

There have been many studies into mathematical modelling of the grinding process and the temperature partitions therein. Wang et al (1998) reported that the during creep feed tests the fraction of total grinding energy entering the work piece reduced due to the high depth of cut and low work piece feed rate. This is in line with the characteristic temperature to specific material removal rate curve, on which the rise in temperature eventually reaches a critical value where burn is inevitable.

Guo et al (1999) investigated the energy partitioning when grinding with vitrified CBN wheels. Using the moving heat source theoretical temperature equation by Carswell & Jaeger (1942) experimental means were used to evaluate the energy partitioning coefficients using an AISI 52100 bearing steel with a Rockwell C hardness of 60. Energy partitions were found to be within a range of 4.0% - 8.5%.

Many assumptions have been taken from this model including one from Outwater and Shaw (1952). Here the assumption was made that 65% of the shear energy was removed with the chip while 35% flowed into the work piece.

Hahn (1955) deduced that Outwater & Shaw's reasoning was flawed due to the total amount of energy witnessed during grinding which could not be dissipated using Outwater & Shaw's theories. He noted that there had to be sliding between the work piece and grain, which would account for this energy. At this point we have the first indication of the modern idea of grinding where it is generally accepted that there is ploughing, sliding and chip forming energies associated with the grinding process.

Rowe realised that HEDG did not have the same characteristics as shallow grinding as the finished surface could be a reasonable distance form the contact surface. To this end Rowe (2000) published his ideas using an inclined plane, to depict the contact length, as shown in Figure 2.33. Rowe used Equation 2.5 and introduced a new co-ordinate structure to predict temperatures of both finished and contact surfaces at any point along the contact length.

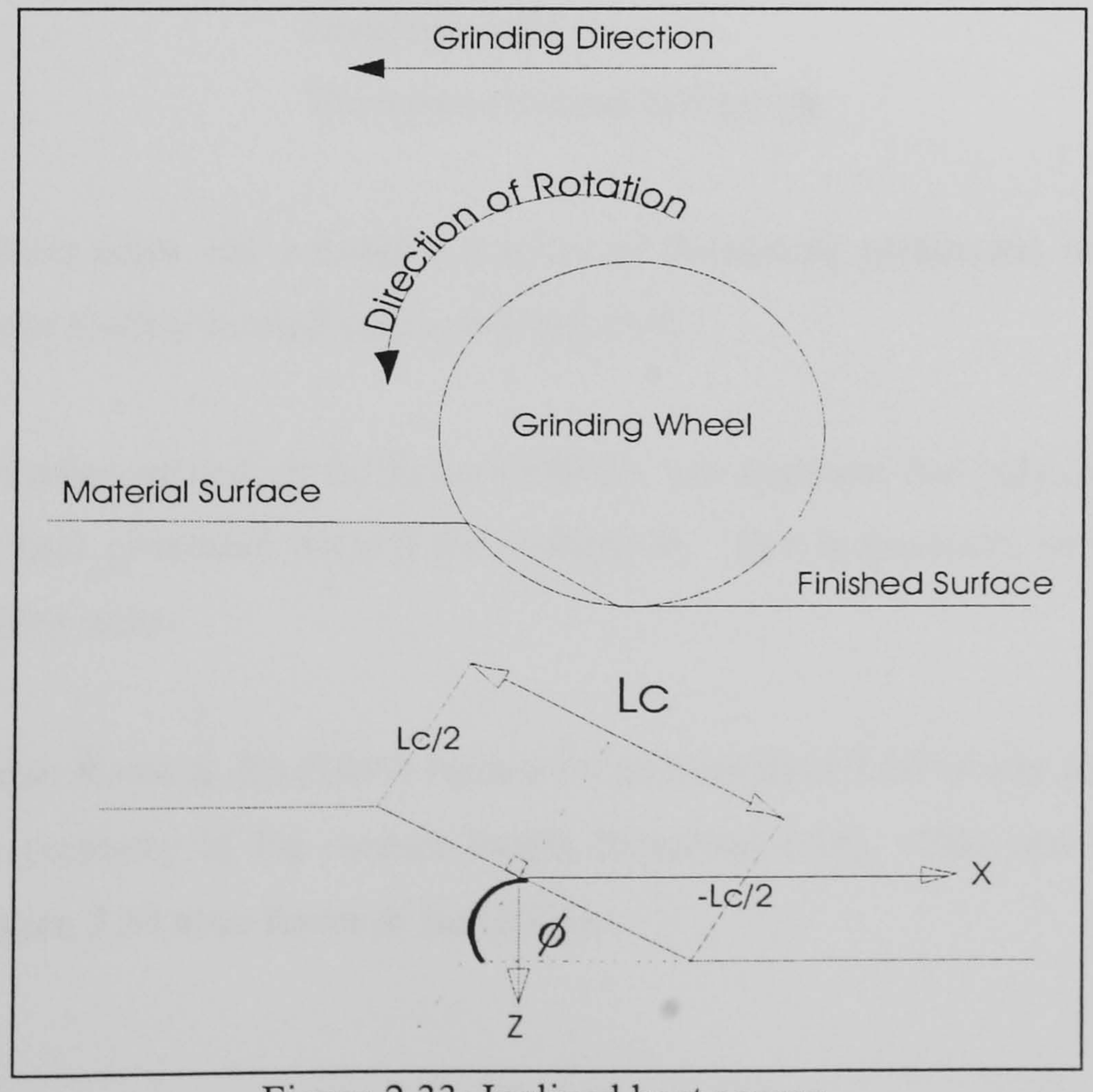

Figure 2.33: Inclined heat source.

Further work by Rowe (2001) refined the model by Carslaw & Jaeger (1959), into the form as shown in Equation 2.10.

$$T = \int_{-lc/2}^{+lc/2} \frac{q}{\pi k} . e^{\frac{\upsilon(x - a\cos\phi)}{2\alpha}} . K_o \left\{ \frac{\upsilon\left[(x - a\cos\phi)^2 + (z - a\cos\phi)^2\right]^{1/2}}{2\alpha} \right\} da \qquad \text{Eqn.2.10}$$

where:

T	Calculated temperature in degrees Centigrade
q	Average heat flux along the length of the contact length
e	Exponential function
k	Thermal conductivity of the workpiece
K_o	Bessel Function of the Second Order Zero
lc	Contact length
υ	Feed rate
x	X co-ordinate
z	Z co-ordinate
φ	Grinding angle
α	Workpiece thermal diffusivity

This expression takes into account a number of fluctuating parameters such as how the heat source q alters throughout the contact zone.

In the case studies carried out by Rowe (2000) it was apparent that only a percentage of the total heat generated entered the workpiece. This is generally known as the energy partition ratio.

In a later paper Rowe & Jin (2001) further refined equation 2.10 to take into account the circular geometry of the contact length (Equation 2.11). This new concept is shown in Figure 2.34 after Rowe & Jin (2001).

$$T = \frac{1}{\pi k}\int_0^{lc} q.e^{\frac{v_f(x-l_i\cos\phi_i)}{2\alpha}}.K_o\left\{\frac{v_f\left[(x-l_i\cos\phi_i)^2+(z-l_i\cos\phi_i)^2\right]^{1/2}}{2\alpha}\right\}dl_i \quad \text{Eqn.2.11}$$

where:

T	Calculated temperature in degrees Centigrade
q	Average heat flux along the length of the contact length
e	Exponential function
k	Thermal conductivity of the workpiece
K_o	Bessel Function of the Second Order Zero
l_i	Portion of Total Contact length Analysed
υ_f	Feed rate
x	X co-ordinate
z	Z co-ordinate
φ_i	Grinding angle
α	Workpiece thermal diffusivity

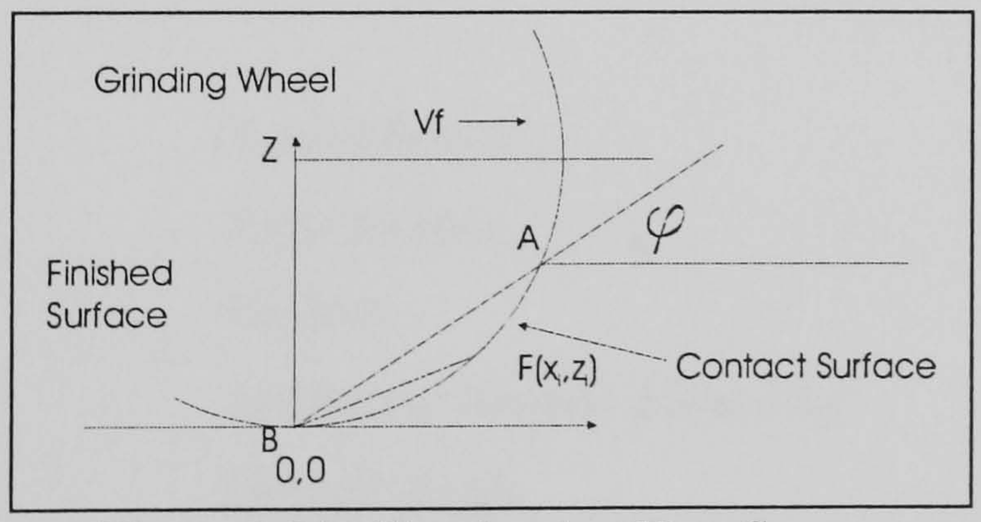

Figure 2.34: Circular Arc Heat Source

This paper gave the equation for the heat flux to be as follows:

$$q = \bar{q}(n+1)(l_i / l_c) \qquad \text{Eqn. 2.12}$$

Where n=0 for a uniform heat source and n=1 for a triangular heat source. $\bar{q}$ is the mean heat flux along the total contact arc AFB.

The calculated outcome of Eqn 2.11 can be expressed as a dimensionless number when using the following expressions:

$$X = \frac{v_f x}{4\alpha} \qquad \text{Eqn 2.13}$$

$$Z = \frac{v_f z}{4\alpha} \qquad \text{Eqn 2.14}$$

The Peclet Number is calculated using:

$$L = \frac{v_f l_c}{4\alpha} \qquad \text{Eqn 2.15}$$

Where:

x	X co-ordinate
z	Z co-ordinate
v_f	Feedrate
α	Workpiece thermal diffusivity
l_c	Contact length

2.8 Adaptive Control Systems

The concept of adaptive control is to constantly update grinding parameter input to an electronic controller, in order to automatically maintain or achieve higher grinding performance in comparison to basic manual control methods.

There have been a number of studies carried out into various types of adaptive control. Shaw (1975) carried out a study into the cost savings made possible when more control of the grinding parameters were set. Through various methods he concluded that there were indeed major efficiencies to be made, albeit concessions had to be made regarding total wheel and total grinding process costs. Shibata et al (1980) reported that by using two parameters such as feed rate and depth of cut in a feedback loop via a computer, the conveyer-type belt grinding process could be controlled to give a more predictable output. Malkin & Koren (1980) used a computer to record the responses from a plunge grinding process and investigated how these affected the next set of results. In such research it was found that the results suggested a 70% improvement in the process metal removal rate when the burning power limit was kept below its maximum value. Malkin (1981) interfaced a cylindrical grinder to a computer where the parameters, work, wheel speed and in-feed were constantly upgraded by the computer which received grinding power data on a continuous basis. Malkin stated that this system maintained a faster in-feed and wheel velocity, which resulted in a higher quality surface finish and reduced the roughing time through the accelerated spark out conditions. Lezanski et al (1993) undertook research using a multi sensor approach on a cylindrical grinding platform using vibration, out of roundness, normal and tangential forces and acoustic emissions. It was stated that the reduced out of roundness error in the finished components was a major achievement but also that more work was required in this area.

Varghese et al (2000) researched the concept of an intelligent wheel design. The wheel had an integrated acoustic emission sensor and a force sensor and showed that this type of intelligent equipment could be of major use in the overall application of adaptive control systems.

2.9 Summary

As previously described HEDG is a fast metal removal procedure and as such requires a lubricating grinding fluid in the contact zone. Because there is less time for a build up of heat there is a smaller requirement for cooling, and it is the reduction in friction that is more important. If mineral oils are to be used for grinding processes such as HEDG, then ecological considerations will dictate that the quantities of these

lubricants being used must be reduced to far lower quantities than current levels. The development of successful minimum quantity lubrication strategies for high speed grinding and HEDG are therefore a priority.

Nozzle design is a further area where developments could be of considerable benefit. The importance of variables such as nozzle type, flow rate, delivery pressure and nozzle angle/position are all critical in the optimisation of the grinding fluid delivery system. It is reported in various papers and has been witnessed in the current Edgetek programme, that the hydrodynamic forces pose a severe threat to the quality of the finished work piece.

This literature survey has shown a distinct lack of previously published material regarding HEDG and the practices used within the process. It has highlighted areas where research could contribute significantly to its understanding and these areas include correlation between responses to measured outputs such as temperature and residual stress measurement, assessed by the use of Barkhausen noise levels.

Adaptive control techniques could benefit the overall use of HEDG if advances of knowledge of the process led to the development of a working model for CNC grinding centres.

Thus the aim of this project has been to understand the mechanism of HEDG such that process parameters can be optimised to assess maximum material removal rates together with acceptable surface integrity.

CHAPTER 3 THE EDGETEK 5-AXIS GRINDING CENTRE

The previous chapter developed the up to date literature of the day and presented this data in such a way as to clarify where the research should be guided. This chapter sets out and discusses the prerequisite testing methodology carried out in this study in six parts. Part 3.1 describes and gives the specifications of the Edgetek Grinding Centre, Part 3.2 explains the experimental procedure used, 3.3 views the calibration techniques. Part 3.4 investigates the first mode of natural frequency, with 3.5 discussing the static loop stiffness results, with the idle power tests described in Part 3.6. Finally the chapter is summarised in Part 3.7.

3.1 The Edgetek Grinding Centre

The Edgetek Grinding Centre is shown in Figure 3.1 and a manufacturer's specification is given in Table 1.1

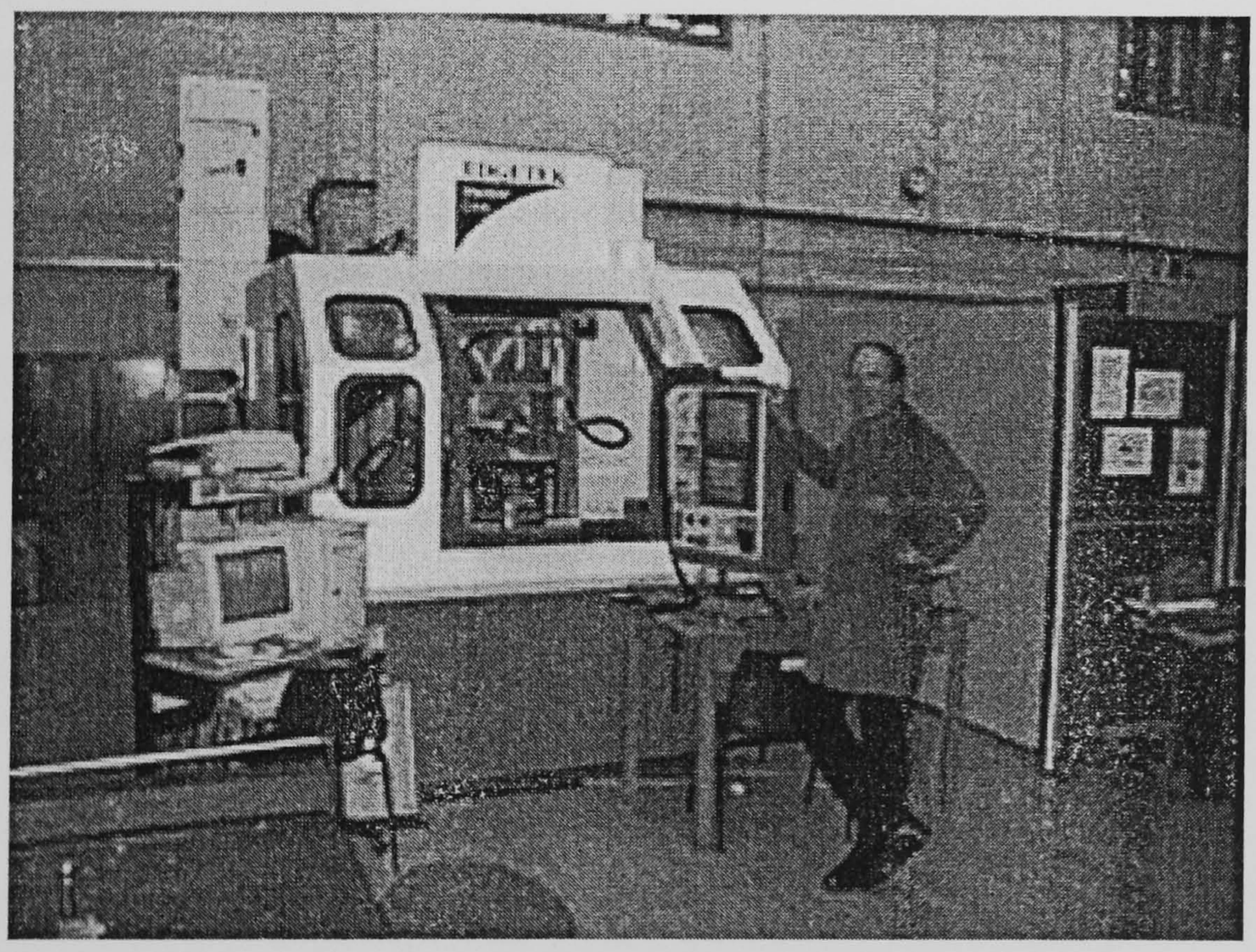

Figure 3.1: The Edgetek Machine

The Edgetek grinding centre is a 5 axis grinding machine with a 26kW spindle and runs from 0 – 14000rpm. The base and column are manufactured from a cast-polymer material which absorbs vibration from heavy cutting forces more effectively than cast iron. The Edgetek's Standard Specifications are listed in Table 3.1.

X-Axis Travel	427mm
Y-Axis Travel	350mm
Z-Axis Travel	305mm
B-Axis Rotary	317.5mm Diameter
5th Axis	A or Rotary tilt versions
Spindle Power	27kW Standard up to a 50kW maximum
Spindle RPM	14,000 rpm, higher rpm's available
Way System	Schneeberger Hi-precision Linear Roller Bearing Ways
Position Feedback	Heidenhain Linear Scales on X,Y & Z
Feedrate	0 to 66mm/s
Rapid Traverse	0 to 126mm/s
Voltage	200-230 volts 3 phase 50Hz
Machine Weight	6800kg
GE Fanuc 16M CNC Control	
Hand held Manual Pulse Generator	
Air/Oil Mist Lubricated Ways and Spindle Bearings	
Air Line Dryer	
Two Zone Programmable Coolant Valves	
Full Splash Guard Enclosure	
Slideways	± 0.005mm per 300mm positioning
	0.005mm per 300mm repeatability
	0.001mm resolution
B Axis Rotary	± 20 ARC seconds 0.001' Resolution, 360,000 positions

Table 3.1: Standard Edgetek Specifications

3.2 Experimental Procedure

During the initial four months of this programme after the machine was delivered to Cranfield University and commissioned in October 1999 initial work concentrated on the following:

- Modification of the machine including grinding fluid supply system, power measurement and force measurement
- Calibration of axis movements
- First mode of natural frequency
- Measurement of static stiffness
- Quantify Power required to Maintain Spindle Speeds

It was only when this phase was complete could a steady foundation be relied upon for the main experimental and analytical stages.

Using the above areas of research it will be shown that the HEDG process is viable for the materials tested and the derived temperature model is a functional and worthwhile tool.

3.3 Calibration of Axis Movements

Tests were carried out to ascertain if any backlash was present in the system and in particular the X, Y and Z axes. This was done by moving the cross-slide using the hand wheel control and ensuring that a calibrated capacitance gauge registered this movement. The position of the digital read out was noted and another movement was initiated. When this second movement registered the system was stopped immediately. The difference between the two digital readings would indicate the backlash in the system.

The incremental procedure was as follows. An input of 4 microns was requested and the actual movement registered by the capacitance gauges was then noted. Therefore any difference between the digital read-out and the capacitance gauge would infer an error.

Carriage tests were carried out between the two gauges, the distance between the pair being 90mm. The capacitance gauges were zeroed to one specific point either side of a parallel spacer. As the readings were taken together, and averaged, this ensured that the travel between each gauge could be monitored and any error halved between the two readings. The spacer was earthed to the control unit to reduce any spurious readings.

All the results from these tests were within the limits stated by the machine manufacturer.

3.4 First Mode of Natural Frequency

Natural frequencies within an assembly are areas of frequencies, which resonate together to cause vibrations of high amplitude. Natural frequencies are always present and so with respect to machine tools the aim was to find where they are and if possible to avoid them.

In accordance with the classical approach as described in BS 6897 Part 2 1990, a shaker unit was independently mounted from the machine so as to have no influence on the frequencies sensed. The procedure for this test was to use the shaker to excite the spindle over a range of frequencies with the output being sensed by an accelerometer and then compared to the input. When this output reaches an extraordinary high peak and the phase angle changes by 180°, this is the first mode of natural frequency. It was hoped to test the machine further up the frequency range to ascertain the second and perhaps the third mode.

The set up was initially used with an input range of 100mVpk to 800mVpk. Two resonating frequencies were detected, these being at 456.7Hz and 1.34kHz. However, these were both higher than the specification for the Edgetek spindle. The actual frequency range being explored was narrowed to the Edgetek machine's fundamental

operating range (0-14,000 rpm), which equated to 0Hz up to 233Hz. With no further resonating frequencies being found an independent force dynamometer was incorporated into the system in an attempt to maximise any vibrations.

Again no discernable vibrations were noted, therefore the equipment used was not sensitive enough to detect the vibration. Attempts were made to procure a larger shaker unit but none was available.

3.4.1 Spindle Frequency Test

Additional frequency tests were carried out using the spindle motor essentially as a shaker with an eccentric load. Via a program the spindle motor was driven up through 0 – 7000 rpm, while the frequency waveform was monitored. Throughout this procedure no significant dynamic change in vibration amplitude was noted.

3.5 Static Loop Stiffness

Zhang (2001) clearly stated that one of the most important parameters which affect the workpiece integrity of a grinding process is the machine loop stiffness. The static loop stiffness measurement of the Edgetek machine was designed to indicate the stiffness of the machine as a complete unit. This test was carried out using a Micrometer screw, capacitance gauges and the force dynamometer.

Figure 3.2 illustrates the set-up used to find the static loop stiffness which is advised by BS 6897: Part 2. When a function was performed then any deformation or deflection, between the spindle and work piece, was deemed a movement of the machine as a whole.

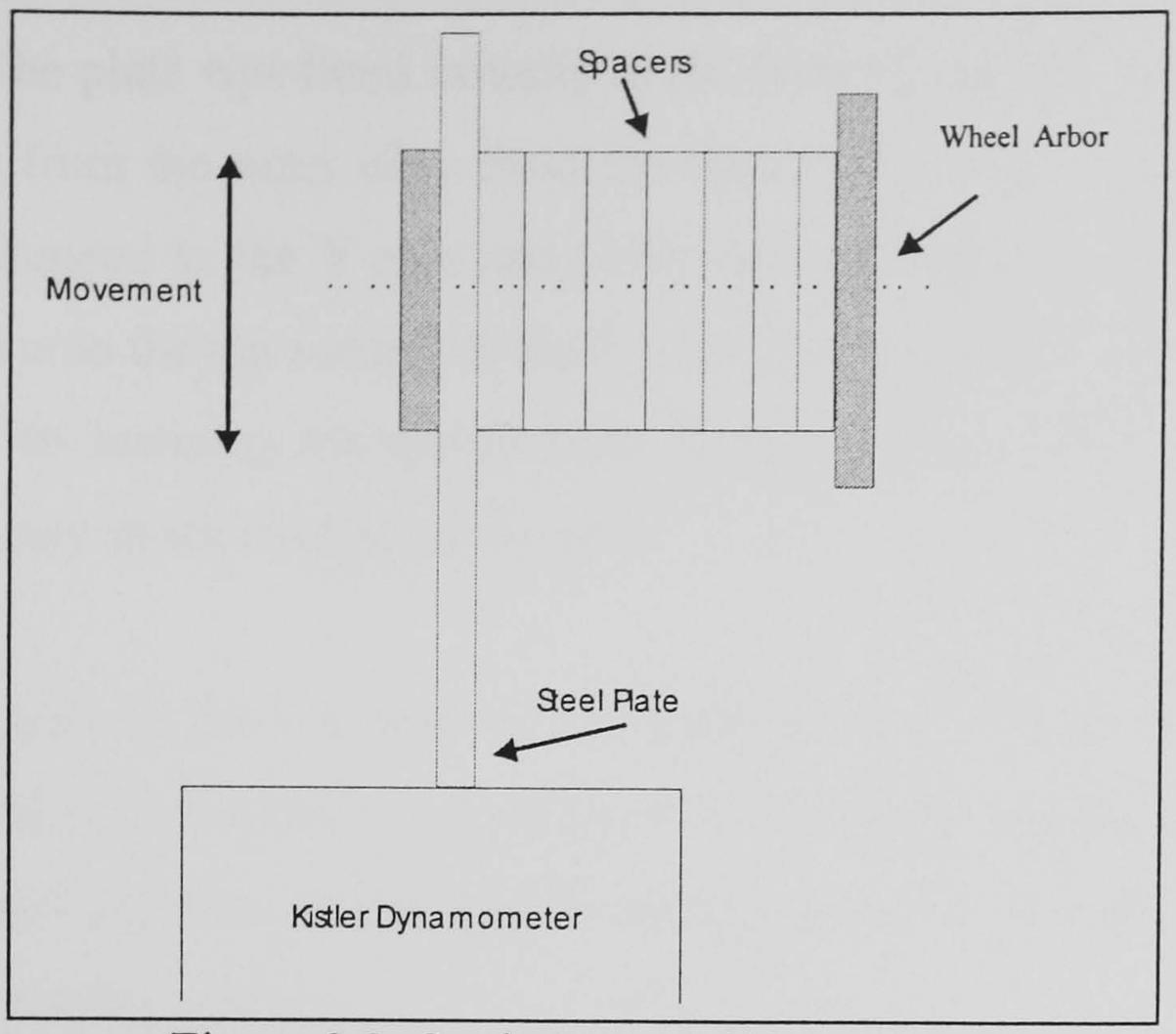

Figure 3.2: Static Loop Stiffness Setup

The calibration procedure for the Kistler dynamometer was as follows. The software was initiated and calibrated weights were placed on the dynamometer. From a starting point of zero the 1kg increments were used up to a maximum of 5kg. A large amount of time was allowed to elapse to test the equipment for any leakage from the piezo crystal. The plot shown in Figure 3.2 shows the forces registered from the applied weights.

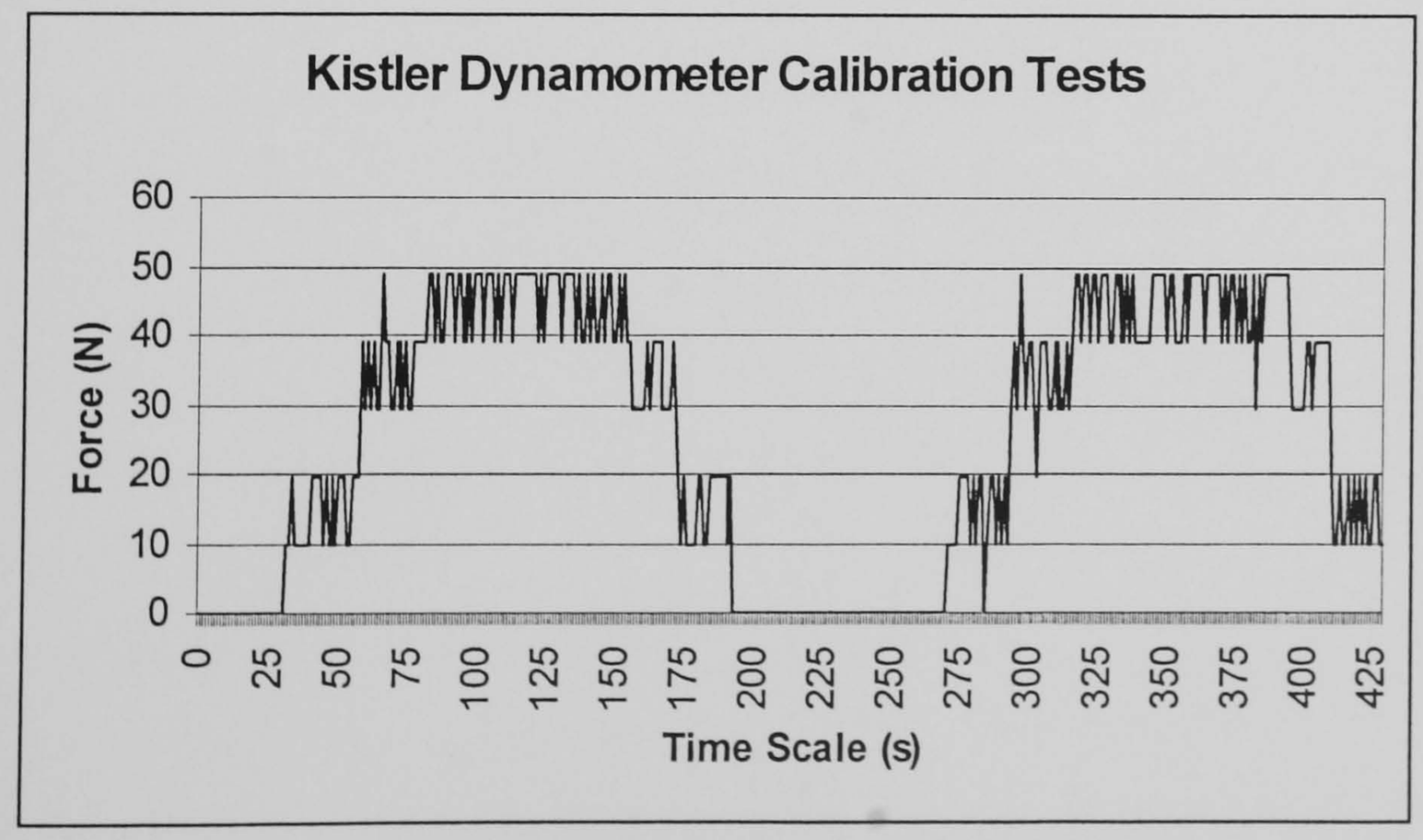

Figure 3.3: Kistler Dynamometer Calibration Chart

A steel plate was manufactured which incorporated a hole of the same diameter as the wheel arbor. The plate was fitted initially to the front of the arbor and so the neutral axis lay 10mm from the inner edge from the front of the arbor. Also a LVDT was magnetically clamped to the Y axis and positioned and zeroed. The steel plate was then positioned onto the top surface of the Kistler Dynamometer. A slight pre-loading was introduced by lowering the spindle/plate to make contact with the Kistler unit in order to reduce any shock loading of the unit.

With the equipment in place a number of 'bedding–in' oscillations were performed. This was to reduce the possibility of hysteresis affecting the results. The spindle was then lowered 5μm and then returned to the starting position, then lowered 10 μm and returned to the starting position.

This procedure was repeated up to and including 50μm movement. During this time the actual deflection was recorded using a calibrated LVDT, and the forces exerted were recorded using the Kistler Dynamometer. The difference between the actual movement of the spindle and the requested movement equalled the deflection within the machine as a whole. This procedure was repeated for various positions along the arbor and the results are shown in Figure 3.4. The illustration of the arbor used behind the graph is not drawn to scale and is purely for information purposes only, to show the loop stiffness at various points along the length of the arbor.

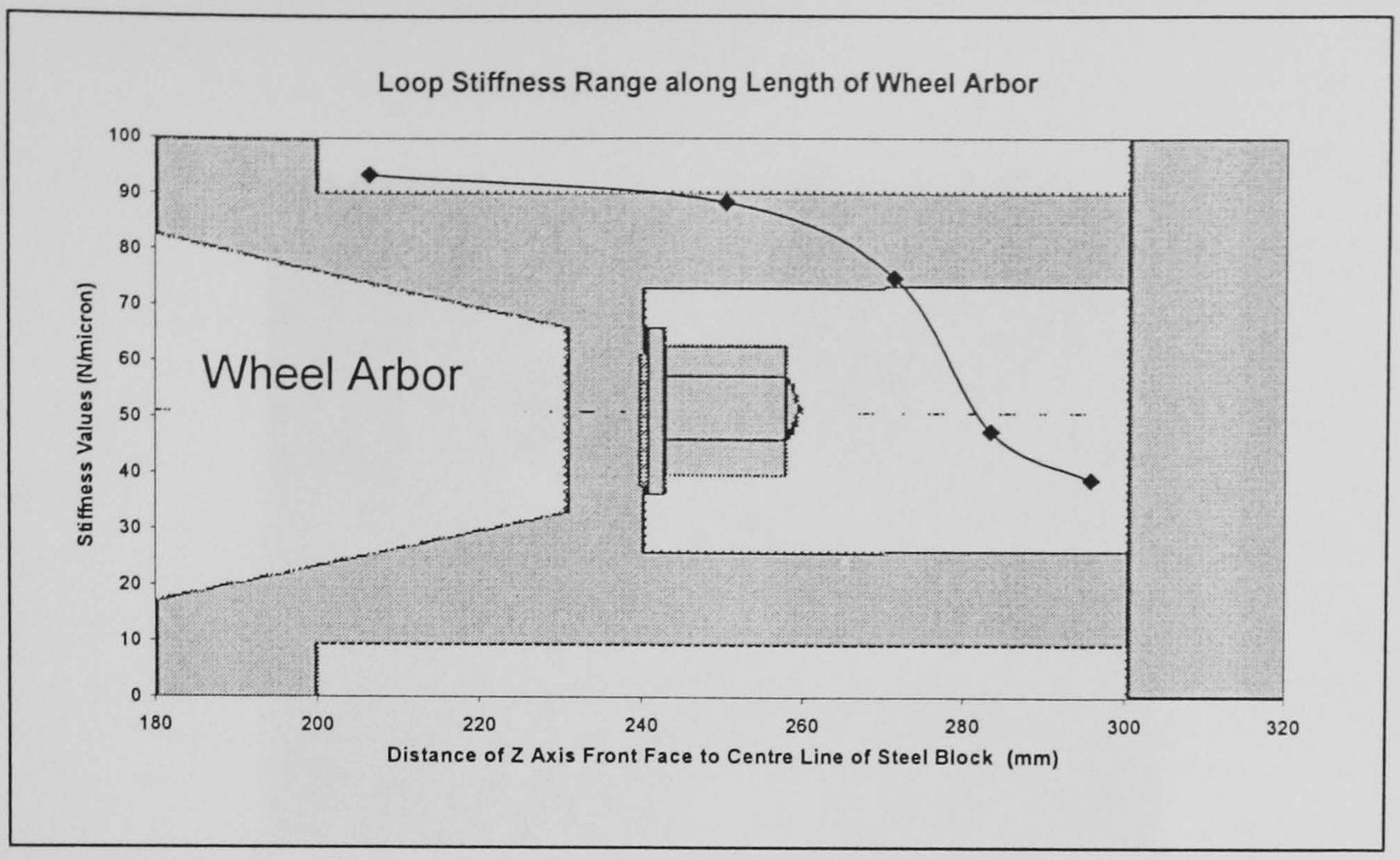

Figure 3.4: Static Loop Stiffness Results

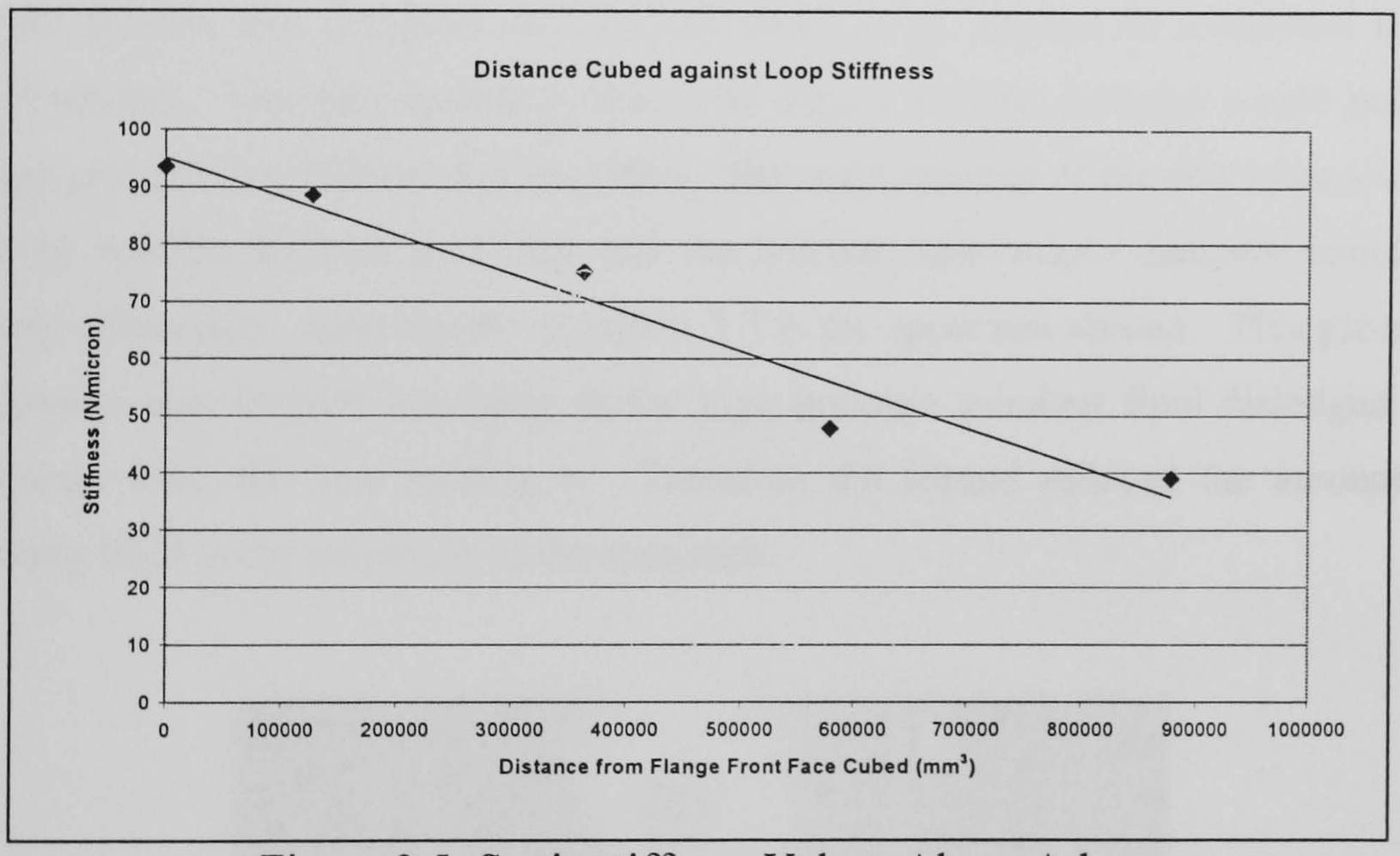

Figure 3.5: Static stiffness Values Along Arbor

In theory the stiffness should vary according to the cubed distance along the arbor. Figure 3.5 shows the linear relationship obtained for the present set-up.

The initial grinding fluid system, shown in Figure 3.6, was judged to be inefficient in providing a laminar flow of grinding fluid as a turbulent flow was noted. Therefore it was also apparent that the nozzle design was ineffective in directing the grinding fluid flow directly into the grinding zone. The datasheets for the three grinding fluids used are shown in Appendices L to N.

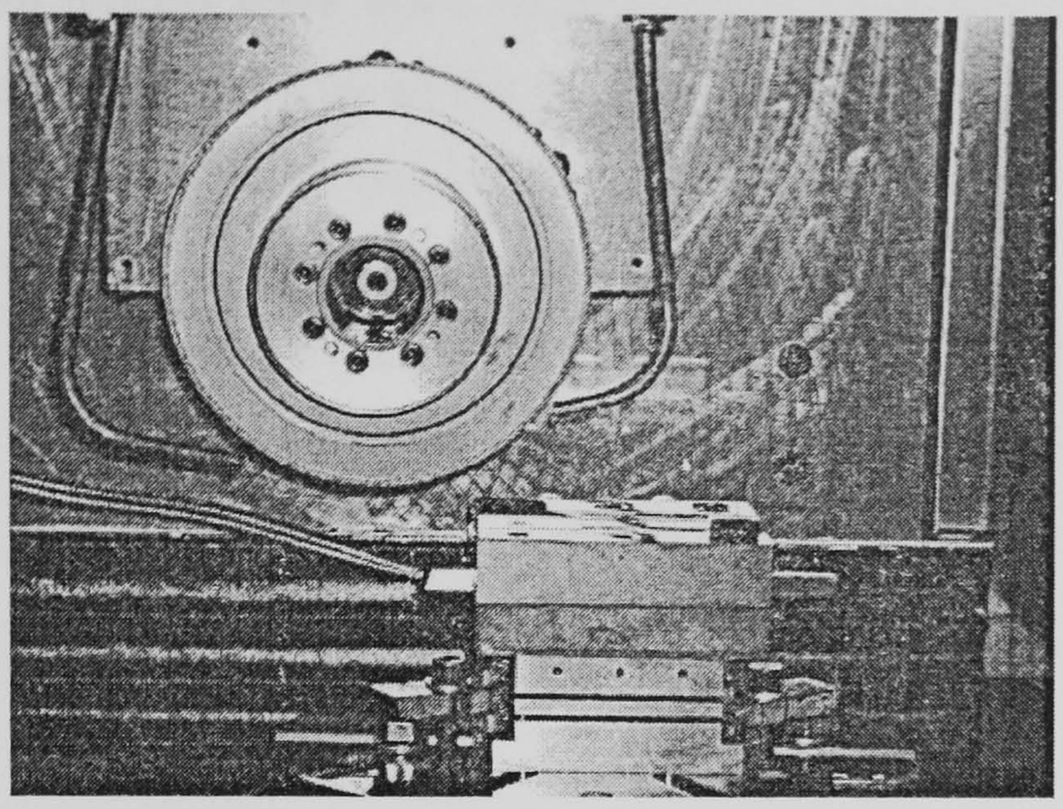

Figure 3.6: Original grinding fluid system

A new system was designed and manufactured in an attempt to overcome these shortcomings. The new system is shown in Figure 3.7 and includes a new nozzle design provided by Webster & Cui (1995). The main features of the new system were that the nozzles position in 3 axes and the laminar flow nozzle diameter could be closely controlled. Also shown in Figure 3.7 is the specimen shroud. This piece of equipment was deemed necessary as the high pressure grinding fluid dislodged the specimen from the vice holding it. Therefore the shroud reduced the amount of grinding fluid to the underside of the specimen.

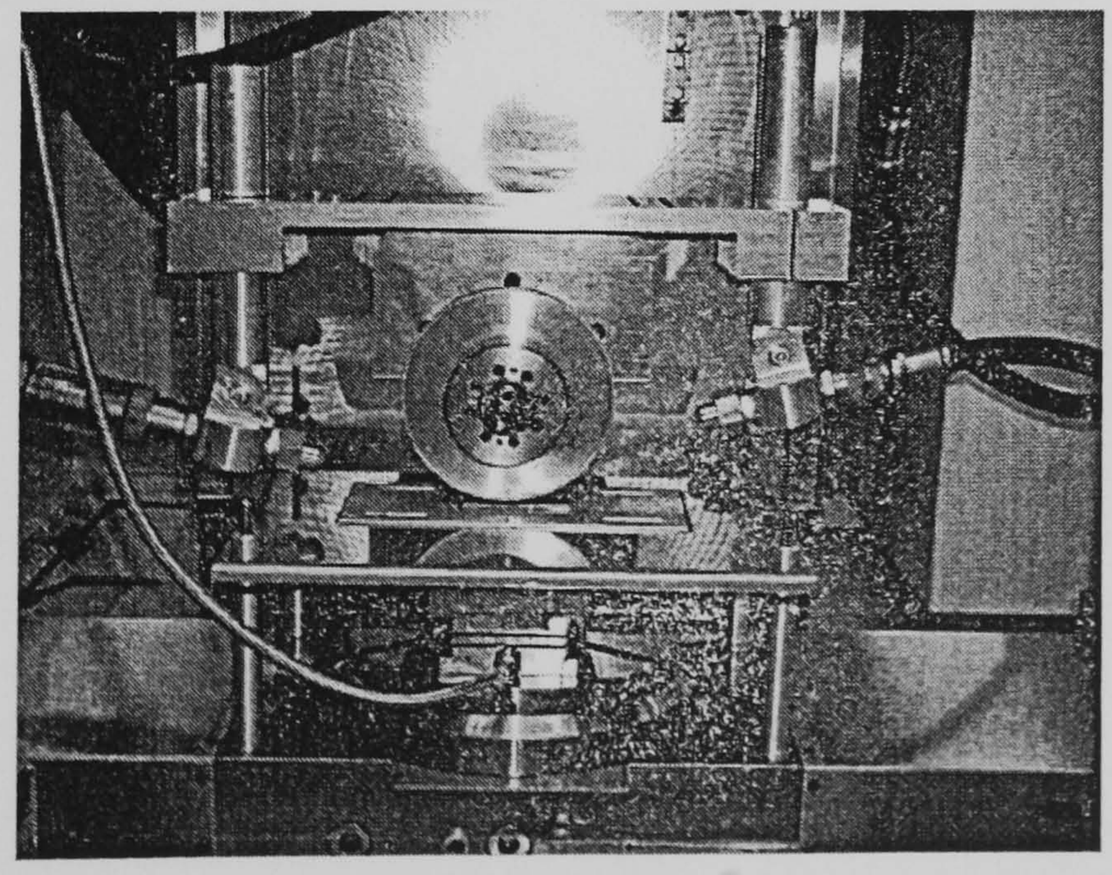

Figure 3.7: The Modified Grinding Fluid Delivery System

3.6 Idle Power Requirement

With any unknown process there lies a requirement to know the power required to maintain a certain desired velocity of the grinding fluid. This was simply done by running the wheel up to a desired speed waiting 10 seconds for any fluctuations in the readings to subside and taking a power reading. The spindle power was measured using a Universal Power Cell, which utilised three balanced Hall Effect devices. Each device sensed changes in phase and after applying a vector multiplication of the current flow and voltage the output is shown via a calibrated multi-meter in percent of total spindle power. The results are tabulated in Table 3.2 and the results are shown in Figure 3.8.

Wheel Speed (rpm)	Power Required (% of 27kW)	Wheel Speed (rpm)	Power Required (% of 27kW)
0	0	0	0
1000	0.06	8000	4.30
2000	0.50	9000	5.00
3000	1.40	10000	5.50
4000	2.10	11000	6.10
5000	2.70	12000	6.70
6000	3.10	13000	7.40
7000	3.60	14000	8.20

Table 3.2: Results from Idle Power Test

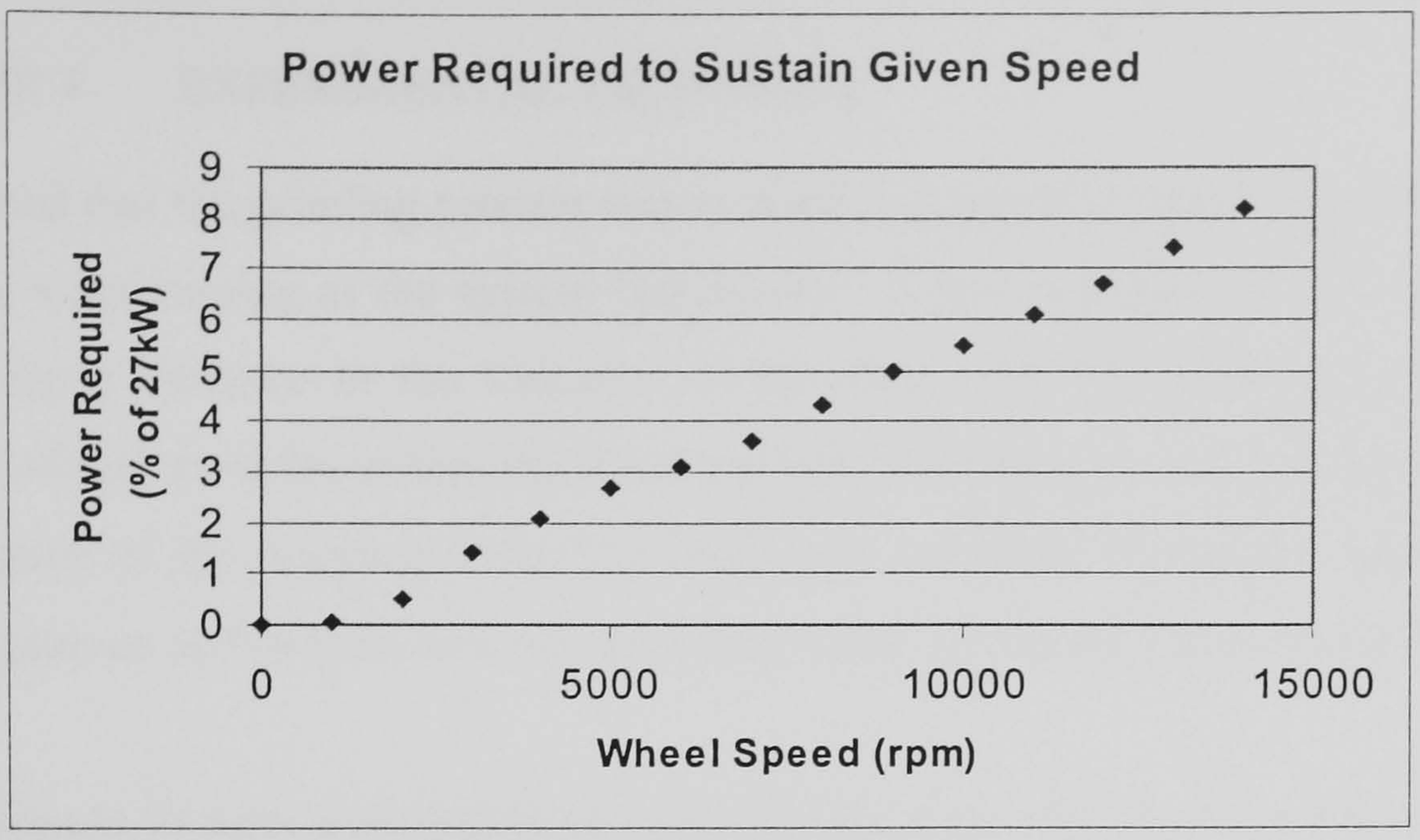

Figure 3.8: Plot of Idle Power to Speed Maintained.

3.7 Summary

Although these tests took up valuable time and resources, it was deemed important to ensure that the following experiments were based upon sound scientific facts. The next chapter sets out the grinding trials that investigated the HEDG grinding method in greater depth with a view on how the HEDG process performed with different materials.

CHAPTER 4 EXPERIMENTAL TECHNIQUE

It was noted that the grinding process was in itself a dynamic procedure, i.e. the system responses were varying as the system functioned. A few examples of these parameter changes are a variance in the viscosity of the fluid with the build up of heat, the inclusion of grit particles within the fluid and the formation of wear flats on the grits. The sponsors of the program wished to clarify the influence of various aspects of the grinding process and initially laid out predefined tasks which are shown in Appendix A.

All grinding tests were undertaken on M50 bearing steel and IN718 nickel superalloy using an Edgetek 5 axis superabrasive grinding centre. Electroplated CBN grinding wheels (B151) supplied by Winter were used for the various test conditions. The grinding fluid (a mineral oil Castrol Variocut 600SP) was applied in the form of a free jet using circular nozzles designed to provide laminar flow conditions. The range of grinding conditions used is summarised in Table 4.1.

Depth of cut (mm)	0.1 – 10
Work speed (mm/s)	0.5 – 125
Wheel speed (m/s)	50 – 135
Specific Material Removal Rate ($mm^3/mm.s$)	0.1 – 1250

Table 4.1: Range of conditions used for grinding trials

The initial grinding tests used blocks of both materials measuring 40 x 40 x 100 mm in the down grinding mode. Each test consisted of a series of cuts, between 3 and 15 mm wide. Grinding forces were measured using a 3 axis dynamometer and the total grinding power monitored using a Hall Effect probe. The net grinding power was estimated by measuring the power under spark-out conditions and subtracting this from the total power. For deep cuts, the "spark out" power was measured during an interrupted cut so that the additional power consumption due to the hydrodynamic effect of the grinding fluid over the full contact length could be quantified. The net grinding power was used to calculate the specific grinding energy.

Following grinding, the surface integrity of each test piece was evaluated for burn and residual stress. This included surface finish measurement using a Talysurf and visual observation of the ground surface to determine the extent of oxidation. Sections were also taken through the ground surface, normal to the grinding direction, to assess micro-structural changes and to measure micro hardness profiles. Residual stress was measured for selected workpieces using a Siemens D500 diffractometer with Brücker software.

The measured values of specific grinding energy were used to predict the finished workpiece surface temperature using the circular arc of contact model and the predicted temperatures were correlated with the micro-structural observations. In addition, the modelling results were also validated through a second series of grinding trials, using embedded thin foil thermocouples to estimate the workpiece surface temperatures. The K type thermocouples were 10μm thick and had a response time of 2ms. Both up and down grinding modes were used, at specific material removal rates of 50, 200 and 375mm^2/s with the grinding conditions chosen to provide relatively low values of specific grinding energy.

This chapter is laid out in three parts; parts one and two are intended to explain the methodologies used in both the experimental and workpiece characterisation portions of the research program. Therefore part one details the experimental designs carried out and part two explains the workpiece analysis techniques used, and finally part 4.3 summarises the chapter.

4.1 Experimental Methodologies

To investigate the process as a whole, various experiments were designed to take into account the influences of the many different aspects within the grinding process. The first three parts describe the use of the two initial systematic tests using M50 steel and the main screening tests used in both M50 steel and IN718 nickel superalloy. All used the Taguchi orthogonal designs of experiments, where two parameters are altered for each run and the software calculates the influence, or significance of these changes, regarding the individual parameters used. Part 4.1.4 is concerned with the high Q'_w

removal rate tests. These tests investigated the influence of up and down grinding with regard to the following responses; specific grinding energy, grinding forces and grinding damage. Also as part of this section the temperature modelling is described. The final section describes the methodology used to complete the component manufacturing phase of the initial tasks prescribed by the sponsors.

Section 4.2 outlines the procedures for the workpiece characterisation and analysis. Parts 4.2.1 to 4.2.6 gives explanations for techniques such as visual assessment, scanning electron microscopy, chemical etching techniques, surface microscopy, surface roughness and Vickers micro hardness. 4.2.7 describes the Barkhausen Noise Amplitude tests and section 4.2.8 explains the use of residual stress measurements.

4.1.1 Taguchi Style Design of Experiments

It was decided that Taguchi style design of experiments should be utilised to take into account as many of the prevalent factors as possible and view the indicated responses, while at the same time using the most efficient experimental design. The software package called Statistica was used to lay out and randomise the set of experiments.

The analysis sheet for the construction of Systematic Analysis One and the ultimate responses are shown in Table 4.2. The effects of these responses are derived by using the averages from each of the two different variables; one can calculate the probabilities of how each variable influences the other and therefore the significance of risk for each parameter.

The orthogonal Taguchi array works on the principle of maximum and minimum values. Where required, mid-point values can also be employed as references or repeatability tests. Therefore in Table 4.2 the minus one indicates where a minimum value would lie for that parameter and a plus indicates a maximum value.

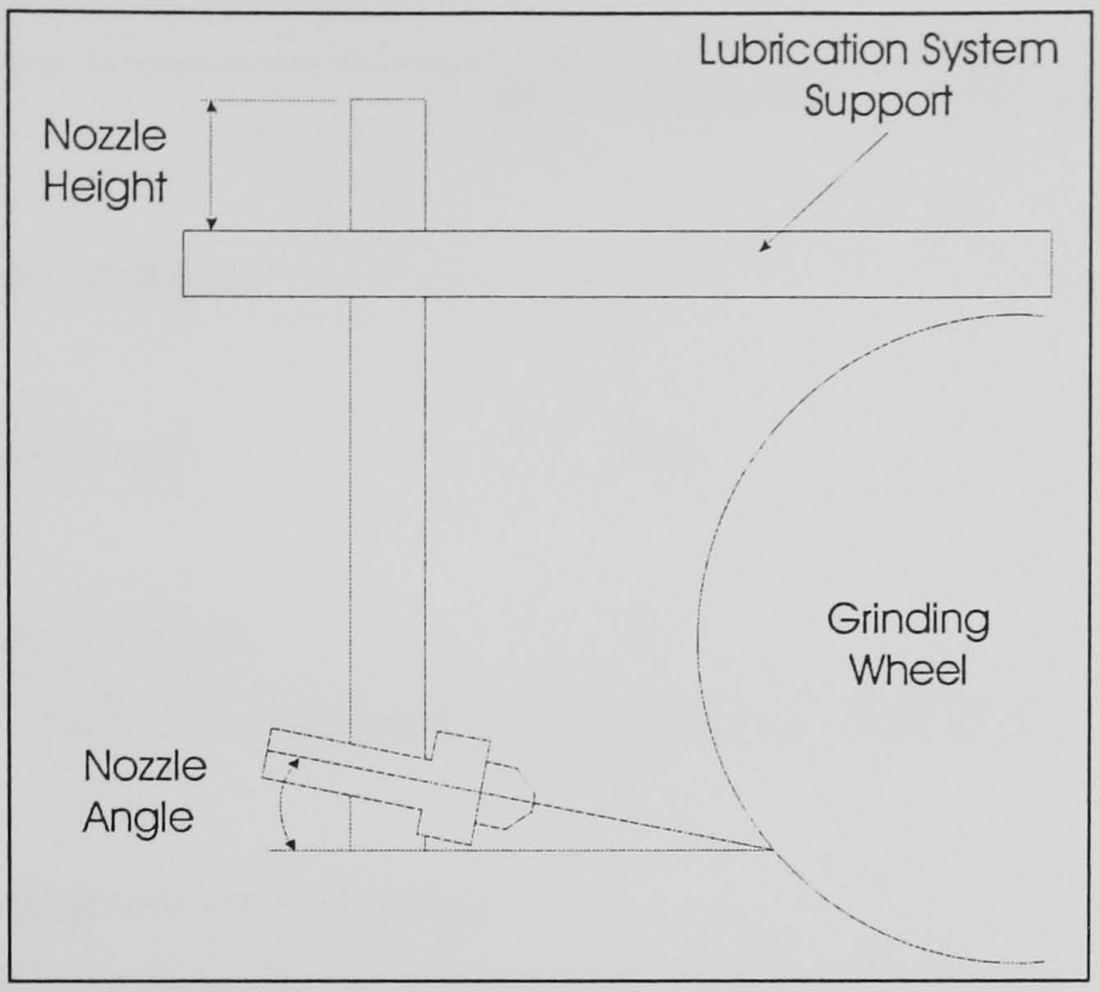

Figure 4.1: Explanation of Terms

Figure 4.1 shows the main terms with regard to the grinding fluid delivery system.

Basic Analysis Sheet					Completed Analysis Sheet				
Experiment Number	Nozzle Height (mm)	Angle Nozzle A (degrees)	Nozzle Diameter (mm)	Stiffness Range (N/micron)	Experiment Number	Nozzle Height (mm)	Angle Nozzle A (degrees)	Nozzle Diameter (mm)	Stiffness Range (N/micron)
1	-1	-1	1		1	110	5	7.5	10.7
2	1	-1	-1		2	120	5	6.7	13.14
3	-1	1	-1		3	110	10	6.7	8.82
4	1	1	1		4	120	10	7.5	1.02
5	-1	-1	-1		5	110	5	6.7	24.02
6	1	-1	1		6	120	5	7.5	11.84
7	-1	1	1		7	110	10	7.5	19.15
8	1	1	-1		8	120	10	6.7	16.41
Sum+					Sum+	42.41	45.40	42.71	
Sum-					Sum-	62.69	59.70	62.39	
Net Total					Net Total	-20.28	-14.30	-19.68	
Effect					Effect	-5.07	-3.58	-4.92	
1/2 Effect					1/2 Effect	-2.54	-1.79	-2.46	

Table 4.2: Response Sheets for Systematic Approach Number One

The parameters used in Systematic Experiment One are listed in Table 4.3.

Parameter	Minimum Level	Maximum Level
Nozzle Angle (degrees)	5	10
Nozzle Height (mm)	110	120
Nozzle Diameter (mm)	6.7	7.5

Table 4.3: Systematic Experiment One Parameters.

4.1.1.1 Experimental Procedure

The experimental procedure for systematic test one was as follows. Once a cut was taken a second spark out operation was performed and the same responses recorded. Outputs were also taken via a digital scope which logged normal force and spindle power against a common time scale and peak values of spindle power could be noted via a digital multi meter.

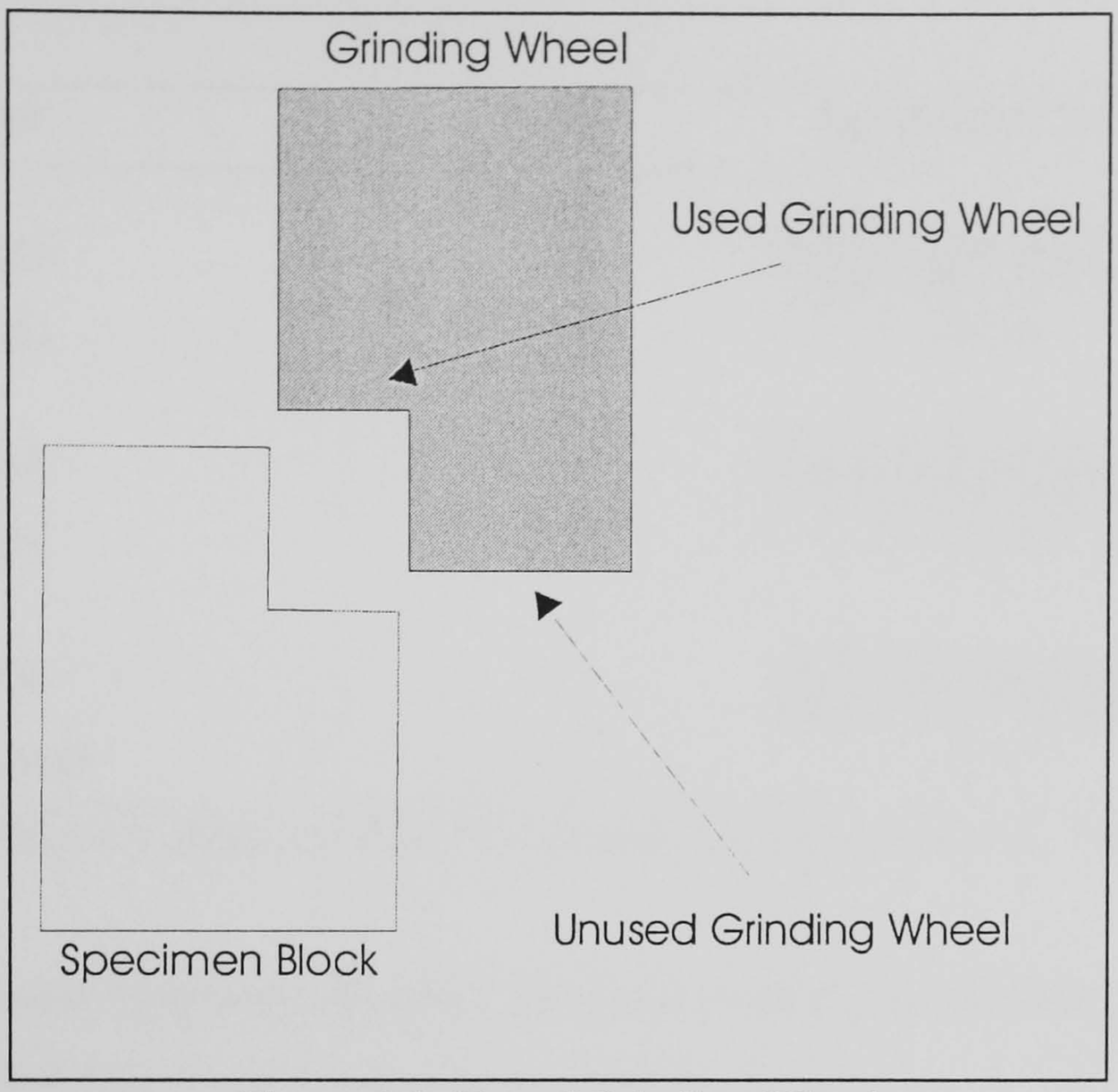

Figure 4.2: Use of Grinding Wheel

Figure 4.2 shows how only a portion of the wheel grinding edge was used for the tests. In this way, a measure of wheel wear could be calculated and subsequent grinding ratios determined, this being - volume of material ground / volume of wheel worn.

4.1.2 Systematic Experiment One Results

Quantitative measurements from the systematic test one were made except in the case of surface burn evaluation. This assessment was purely qualitative. The results from the systematic experiment one, which are summarised in Table 4.4, were used for determining the range of grinding parameters used for the systematic experiment two. As such the parameters which would give the greatest probability of an optimised process were reduced to include fewer options.

The resulting indications were; that a decrease in the height of the nozzle along with a smaller nozzle diameter and the smaller angle could result in a more optimum setting of the grinding fluid delivery system. The shaded areas show the higher averages of each pair, which indicate a possible increase in efficiency when that variable was set towards this value.

Factor	Level	Significance Factor
Nozzle Height	110	15.67
	120	10.60
Nozzle Angle	5	14.93
	10	11.35
Nozzle Diameter	6.7	15.60
	7.5	10.68

Table 4.4: Indicated Results Systematic Approach Number One

With this in mind Systematic Analysis Two was undertaken using the parameters as shown in Table 4.5.

Nozzle Height (mm)	Nozzle Angle (degrees)	Depth of Cut (mm)
110	5	2
120	5	2
110	10	2
120	10	2
110	5	3
120	5	3
110	10	3
120	10	3

Table 4.5: Parameters for Systematic Experiment Two

The results from this second set of experiments were not repeatable and this implies that there are other factors influencing the results. Clearly an understanding of how different

variables interact with each other would be of great benefit here. It was therefore decided to modify Task 2 and incorporate the original research plan into a more extensive and systematic factorial based design of experiments.

4.1.3 Screening Tests

Using the results from the previous two systematic tests, the parameters set out in Table 4.6 were used in a full factorial set of 16 runs with 6 centre points for both project materials. In this way the effects and influences of these intricate parameters could be evaluated at the same time. The main advantage of this type of testing is that the information obtained can be added to in the future to continually develop an understanding of the overall process. The series of tests outlined in Appendix E provided further information towards this understanding and contributed towards the final aim to develop predictive models for the HEDG process.

Parameter	Maximum Level	Mid-Point	Minimum Level
Parameters from Task Two			
Wheel Speed (m/s)	100	75	50
Grit Size (microns)	181	151	126
Depth Of Cut (mm)	1	0.55	0.1
Feed Rate (mm/s)	50	25.25	0.5
Other External Variables			
Nozzle Angle (degrees)	8	6.5	5
Nozzle Height (mm)	110	107.5	105
Nozzle Diameter (mm)	8	6.5	5
Grinding fluid Pressure (bar)	14	10	6

Table 4.6: List of the Parameters Investigated

Webster & Cui (1995) introduced a new design of nozzle which showed no degradation in the jet with a fluid cross section of over a 300mm length. This nozzle was manufactured and by precisely setting angles and heights it was incorporated so that the fluid jet could be delivered accurately where it was required.

4.1.4 Thermal Modelling

Theoretical temperature models were produced using the inclined heat source equations developed by Rowe & Jin (2001). Also published were the fluid convection factors for water based grinding fluids and oil; these being in the order of 100,000W/m^{2}K and 23,000W/m^{2}K respectively. Morgan et al (1998) published the thermal conductivity value for CBN grit to be 240W/mK, and Rolls Royce volunteered the thermal conductivity and specific heat capacity values which covered a wide range of temperatures for the M50 tool steel and both nickel super-alloys namely, MARM002 and IN718.

The above published values were used to construct a model for the burn thresholds for both IN718 nickel super-alloy and M50 tool steel. Rowe & Jin (2001) set out a number of equations which culminated in the calculation of the contact surface and finished surface temperatures which are shown in Appendix F in the case of M50 and Appendix G for IN718.

4.2 Workpiece Characterisation

As with any metallurgical study the post experiment analysis can be just as extensive as the experiential procedure. Samples were taken for two main streams of analyses, the first for polishing, followed by the production of sub surface micrographs, micro hardness profiles and surface roughness measurements. The second specimen was used for surface analysis and stress analysis.

These tests were carried out as standard post experiment analyses. Sub-surface microscopy was carried out using the procedure laid out by Field et al (1972). Samples were cut and mounted in Bakelite then polished through numerous grades of polishing media finishing with a 1 micron abrasive paste.

4.2.1 Visual Assessment

The samples were visually assessed for the onset of oxidation by viewing for any trace of a colour change on the surface of the sample.

4.2.2 Scanning Electron Microscopy

Samples were initially ultrasonically cleaned to remove all foreign bodies as well as any coatings which could have fluoresced under the electron beam of a scanning electron microscope.

Two microscopes were used, starting with an ABT 55 Scanning Electron Microscope; this was used to examine and record the surface defects of the sample. The required samples were coated with Gold-Palladium alloy and individual elements could be identified on the surface of the sample using the Cambridge Stereo-scan 250MK3.

4.2.3 Chemical Etching

Samples were etched to highlight the grain structure of the materials. Etchants were taken from Petzow (1978) and in the case of M50; the etchant used was Villelas Solution 10%. The ingredients are Methanol 90ml; Distilled Water 10ml; Picric Acid and Hydrochloric Acid 5ml. The etchant was applied via a cotton swab for 5 – 10 seconds and then the sample was washed off with water.

Both the nickel alloys used an Oxalic Acid/Distilled water mix. 100ml of water for 10g of acid was mixed together and applied via electrolytic action. The current was applied for less than a second at 6V DC and the sample was then washed with water.

4.2.4 Subsurface Microscopy

The polished and etched samples were analysed under various magnifications and relevant images recorded via digital camera equipment. The digital equipment also recorded the relevant magnification scale used.

4.2.5 Surface Roughness

The surface roughness was measured using a Talysurf 120L with a 2μm radius tip diamond stylus. Various measurements were taken simultaneously and the responses produced were examined via a print out of the surface trace. The main measurements examined were the arithmetical mean R_a and peak to valley maximum R_t.

4.2.6 Vickers Micro Hardness

The hardness profiling was carried out using a Vickers micro-hardness machine on the polished samples. A load was applied and an indent was measured using the sight glass. The size of the indentation was matched to hardness values using the Vickers Hardness tables.

4.2.7 Barkhausen Noise Amplitude

This comparative style of analysis required the user to become more familiar with the Barkhausen Noise Amplitude (BNA) responses to the specific characteristics of M50 tool steel. As steels have different constituents then the response to BNA analysis of one steel type will differ from other types of material. An experimental setup to test the BNA output against applied stress advocated by Shaw et al (1999) was unsuccessful due to the characteristics of M50 tool steel. The applied load was a bending stress and due to the hardness of the steel could not tolerate this type of stress. Therefore two calibration tests were designed; the first considered the static and the second the dynamic characteristics. The samples were simple 2mm deep slices 100mm long by 40mm high. Although the sample was fully annealed as per the manufacturer's instructions to produce in theory a totally stress free specimen, when the residual stress was measured a compressive stress of 200MPa was found to be present this could have been due to the fine grinding operation which was performed after the heat treatment process. Manufacturer's data sheets for M50 are shown in Appendix D.

4.2.7.1 Calibration Procedure

For analysis of the dynamic case, the two millimetre thick slice was cut from one of the parent blocks and finely ground. The use of a calibrated mechanical tension tester was enlisted to produce a known stress within the sample. The machine's grippers held the

sample, which applied a tensile load, a fifteen second time delay facilitated a steady state stress regime and a BNA reading was then taken. As the stress field produced was a simple bi-axial stress state and the sample was 2mm thick it was assumed that the stress was of a uniform nature throughout the sample. Figure 4.3 shows the profile of stress against BNA readings over a wide range of induced stresses. The zero in the compressive region in the figure can be explained due to the initial compressive residual stress within the sample.

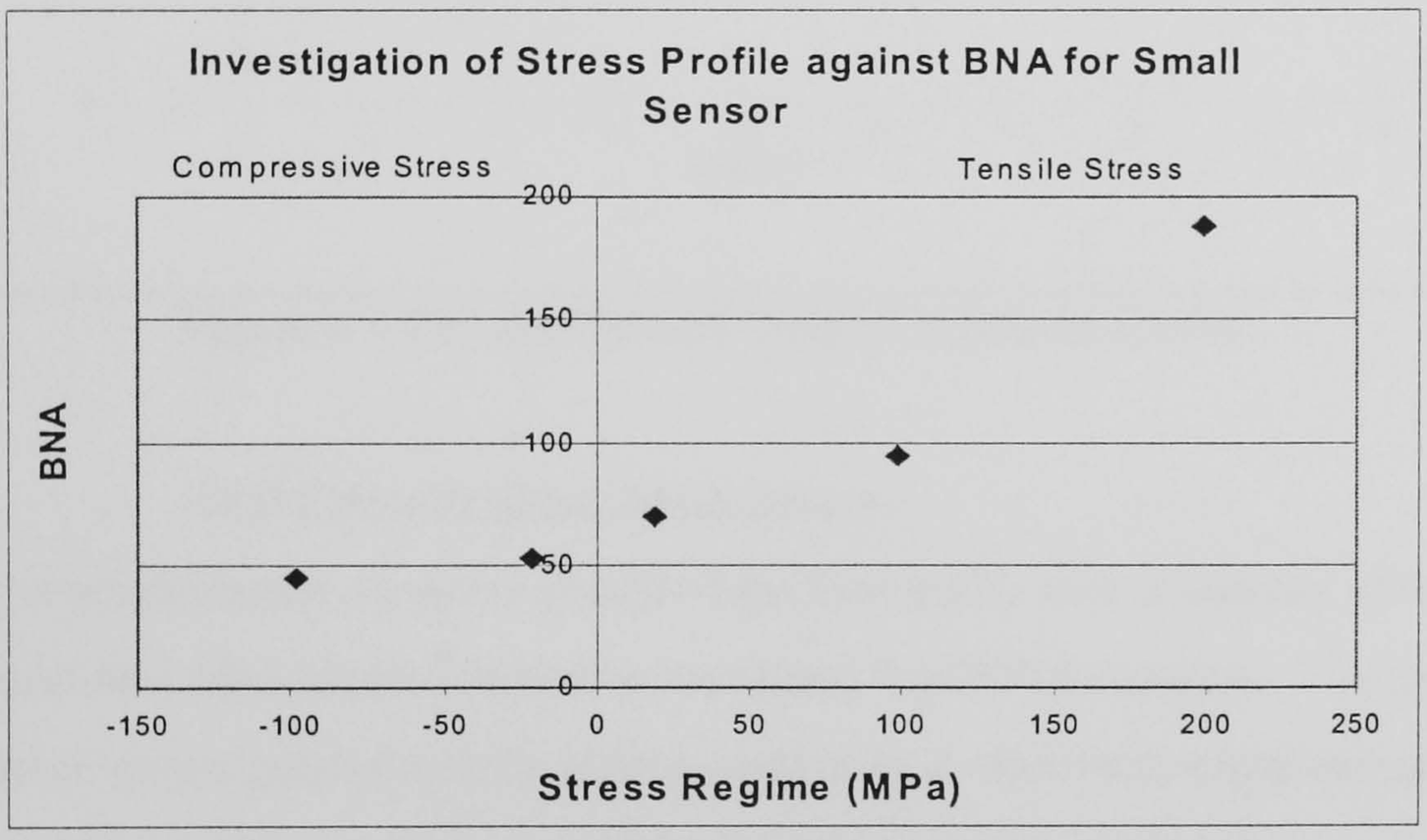

Figure 4.3: Comparison of Induced Stress to BNA

In the case of the static tests, samples were used on a "as is basis". As per the operator's manual, samples were measured at a Rollscan level of 50% and the magnification voltage which increases the amplification of the signal was stepped from 0 to 100% in 10% stages. Trend lines were then drawn and the point of calibration was to be taken at the largest distance between the maximum and minimum trend lines. This is shown in Figure 4.4 and was taken at a magnification level of 35%. All consequent measurements used the identical settings and so a direct comparison could be made with the virgin material.

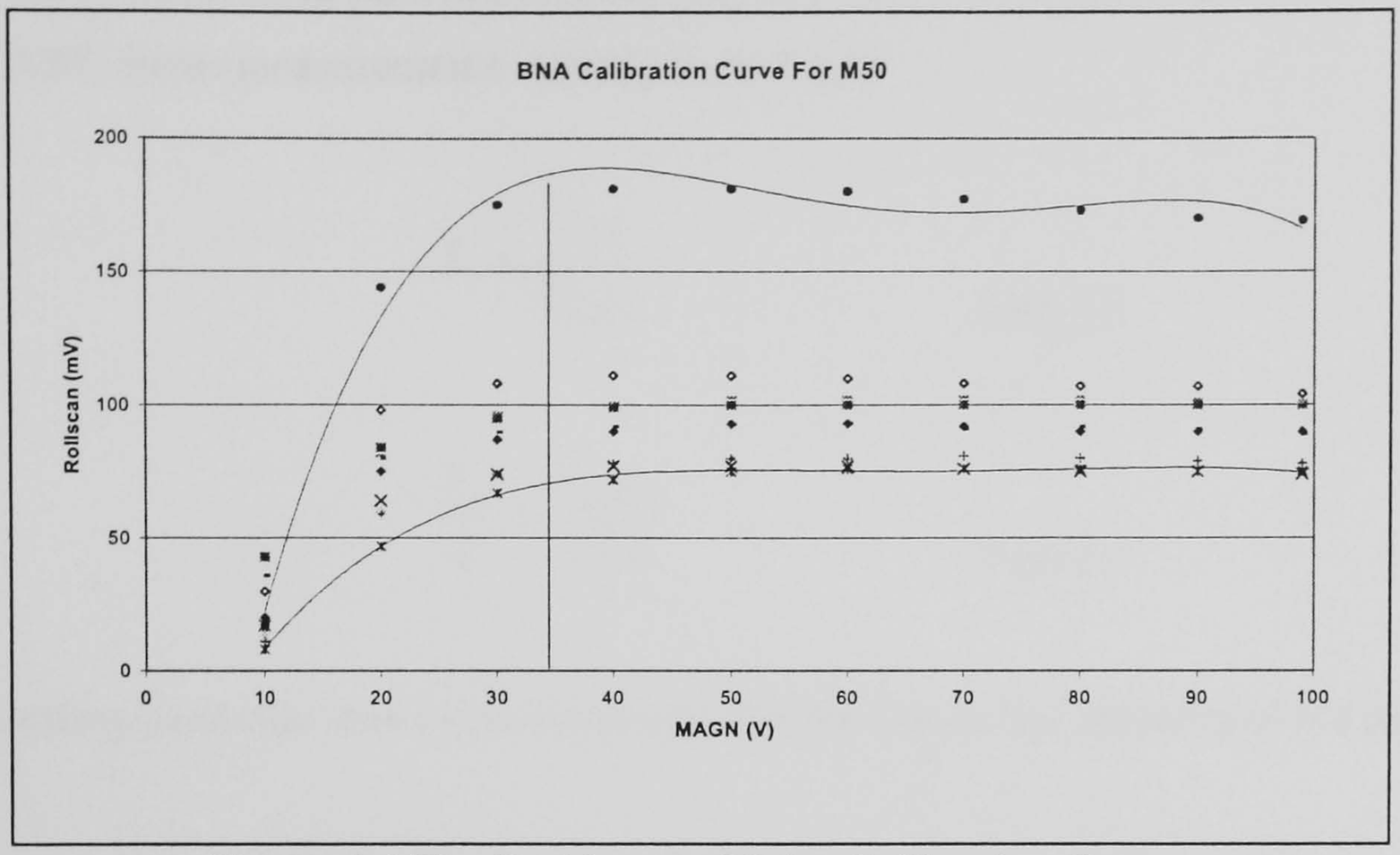

Figure 4.4 The Barkhausen Noise Calibration Curve.

4.2.8 XRD Stress Residual Measurement

A bearing manufacturing company provided the University with a number of test results on M50 steel and Manchester University measured the IN718 samples. The tests on the M50 samples were repeated and the results compared so that more experiments could be carried out with confidence using Cranfield University's own equipment.

4.2.8.1 Experimental Procedure

With any crystalline structure the basic elastic constants for the bulk material have to be known for any mechanical testing. However with XRD stress measurement one has to go further. One has to know the $E_{\{hkl\}}$ (Young's Modulus of Elasticity) and υ (Poissons Ratio) values. This {hkl} subscript denotes a plane within the crystal lattice which has shown to give the best diffraction of X-rays within the lattice for that specific material under examination. Prevey (1986) gives that {hkl} plane for M50 bearing steel and IN718 nickel based superalloy to be {211} and {311} respectively. Young's Modulus of Elasticity (E) for the bulk of the material is a different value to that of the {hkl} plane value due to the bulk having depth and in which imperfections are found within the structure. Therefore, the bulk E value can be taken as an average value of the {hkl} E value.

When these elastic constants are known, they are used to calculate the constants used within XRD stress measurements, namely S_1 and $S_2/2$.

$$S_1 = \frac{-\upsilon}{E_{\{HKL\}}} \qquad \text{Eqn 4.1}$$

$$\frac{S_2}{2} = \frac{E_{\{HKL\}}}{1+\upsilon} \qquad \text{Eqn 4.2}$$

The resulting parabolic curve was extremely shallow due to the hardness of the material.

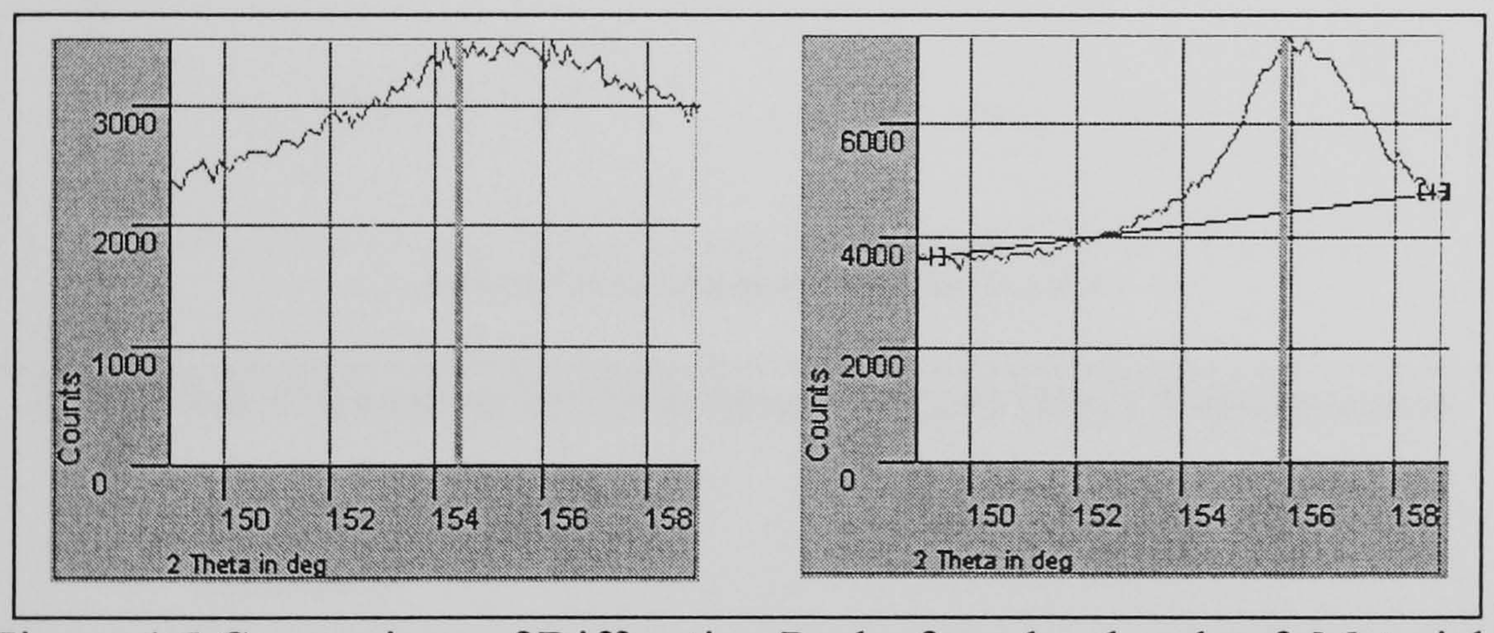

Figure 4.5 Comparison of Diffraction Peaks from hard and soft Materials

Figure 4.5 gives a comparison between a soft steel such as 51CrV4 and M50 tool steel. Both tests used identical parameters. Prevey (1986) gave the necessary constants for M50 steel and these are listed in Table 4.7.

Material	Radiation	Lattice Plane	Diffraction Angle 2θ	Young's Modulus of Elasticity GN/m^2	
				{hkl}	Bulk
M50	Cr Kα	(211)	154°	233	270

Table 4.7: M50 X-Ray Diffraction Constants

Also included is an indication that harder materials require longer step times. Because of this, a step size of 0.1° and a time period of 25 seconds per step were both used. The calibration tests were carried out using samples already measured for residual stress by a bearing company. The results of these initial tests plotted against Cranfield's in house measurements are shown in Figure 4.6.

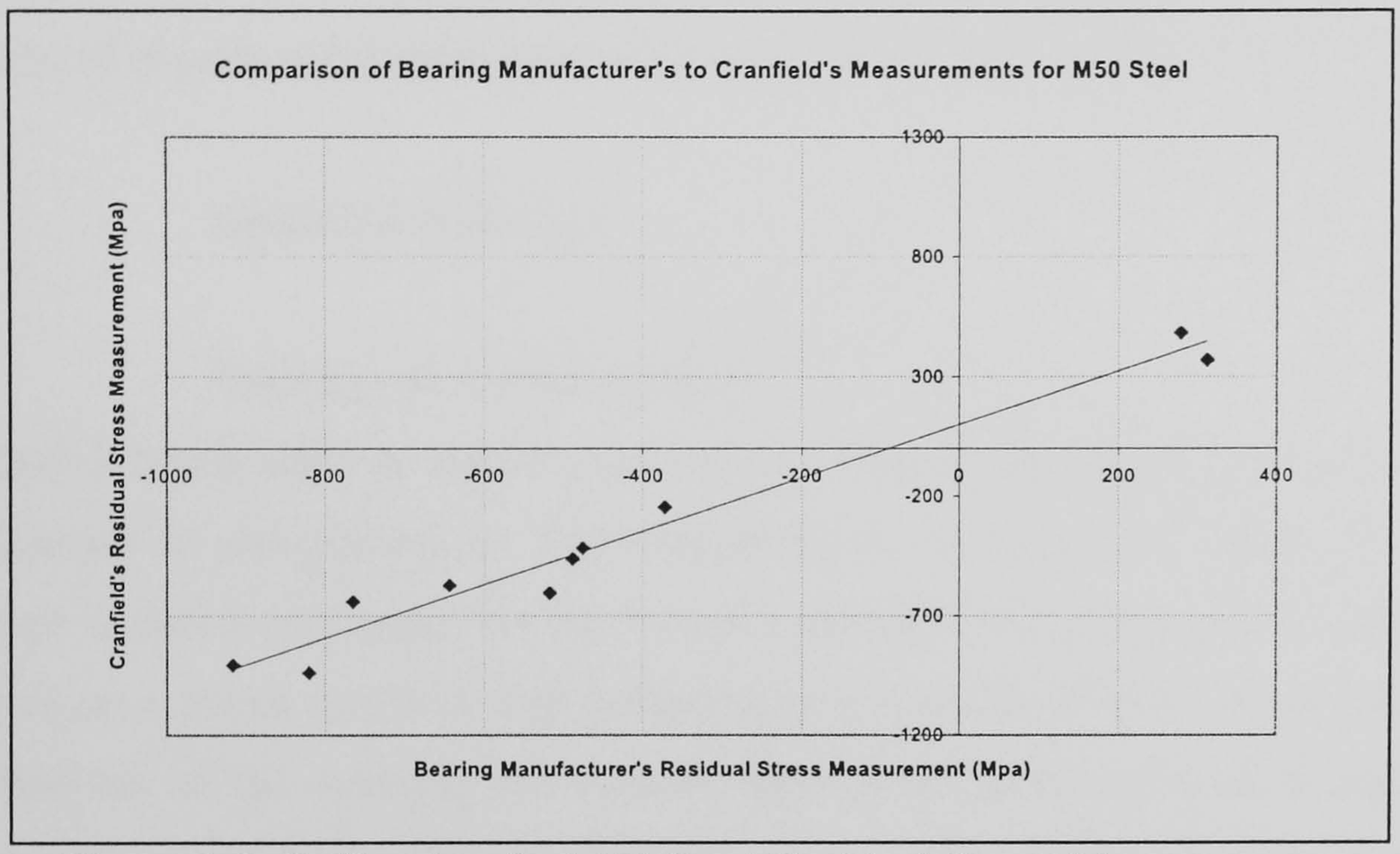

Figure 4.6: Calibration for M50 Steel Residual Stress Measurements

4.3 Summary

This Chapter has reviewed the main experimental procedures carried out during this research in order to investigate the HEDG process. The next chapter outlines the main results obtained highlighting the most significant aspects of the work.

CHAPTER 5 M50 BEARING STEEL

This chapter presents and discusses the experimental results from this research on the grinding of M50 bearing steel. Part one discusses the results relating to the Edgetek machine and the Taguchi analyses. Part two gives the salient points with regard to specific grinding energy and physical evidence such as sub-surface microscopy, Vickers hardness profiles and residual stress measurements. The final part contains the chapter summary; all experimental parameters used are shown in Appendix F.

5.1 Experimental Results

5.1.1 The Edgetek Grinding Centre

The Edgetek 5-axis machine has been put through vigorous testing and has exceeded all specifications as determined by the manufacturers as shown in Table 3.1. The maximum backlash was noted on the X-axis as being 0.37microns and the maximum overshoot on a 90mm travel of only 0.63microns was on the Z-axis. When taking the prescribed use of the machine into account these errors could be deemed negligible. Overall, with a static loop stiffness of 98N/μm measured at 210mm from the front face of the Z axis, the machine has been proven to be well within the prescribed limits of stiffness for a HEDG machining centre as discussed by Tawakoli (1993). As a comparison to this high value Shore (1995) investigated the static loop stiffness of a NION grinding centre used primarily in the field of brittle grinding, and he noted that it had a static loop stiffness value of only 60N/μm.

5.1.2 Screening Test Results

Where thousands of experimental runs would be required to investigate a process fully, Taguchi orthogonal arrays are designed to reduce the experimental runs required to make a derived conclusion on a process, with a view to optimisation.

Therefore the purpose of the results from the Taguchi Style Screening Tests was an attempt to recognise the significance of each parameter's use within an experimental environment. These probabilities are purely indicative in nature, but as these probabilities are calculated statistically the element of risk is a known factor and

therefore more confidence can be shown. Throughout the three initial Taguchi style experiments a robust fluid application setup was applied that was designated as a mid-point model i.e. nozzle height to be 107.5mm, nozzle diameter at 6.5mm and nozzle angle to be 6.5° below the horizontal. These parameters are described in Figure 4.1. To this end it was decided to utilise this set of parameters at least initially for each subsequent test.

Figure 5.1 below shows a Pareto chart produced using the results from the initial grinding trials on M50. As indicated by the P = 0.05 value, all columns in this chart have been chosen due to their significance value being greater than the prescribed minimum of 0.05. The magnitude of each effect is represented by a column, the greater the column length the greater the significance of that parameter. A vertical line is generated by the computer model and indicates how large a column must be to be deemed statistically significant.

The Pareto chart indicates that feed rate and depth of cut significantly affect the power used. Both these significant values are positive, which means that as these factors are increased from their lowest to highest levels the power will increase by the numbers shown to the right of each horizontal bar. If these values were negative then power consumption would decrease accordingly. This observed trend is logical in that a deeper cut would be expected to require more power. The experimental parameters used are shown in Appendix E, Table E.1.

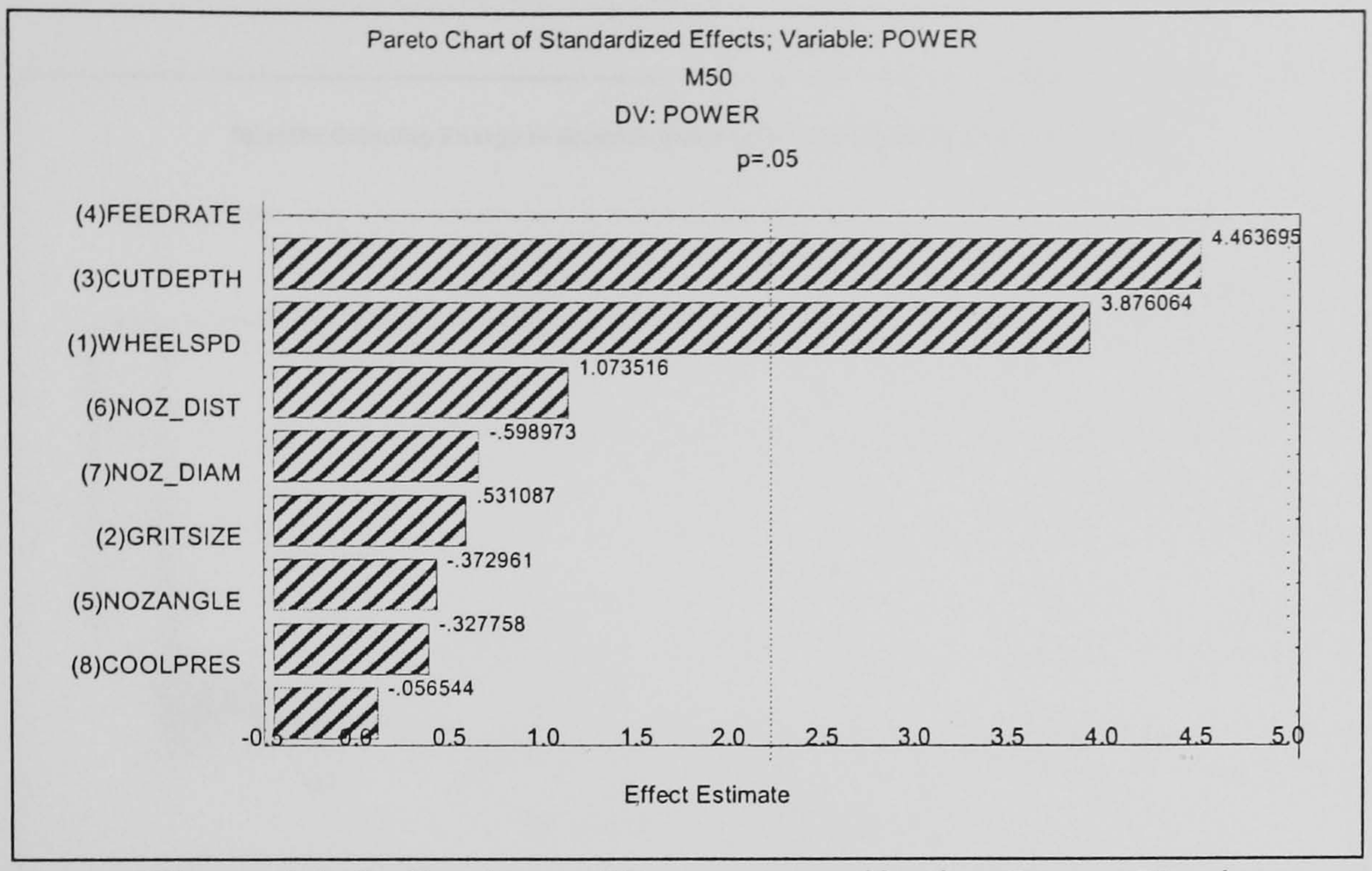

Figure 5.1: Indications of Parameters affecting Power Used

5.2 Analyses of Responses

5.2.1 Specific Grinding Energy

One of the main responses from a grinding process is Specific Grinding Energy. This is calculated by dividing the specific grinding power by the specific material removal rate and is a measure of how efficient the grinding process is.

Figure 5.2 illustrates the change in specific grinding energy with specific material removal rate for all grinding conditions. The general trend indicates a reduction in the upper limit of specific grinding energy as the specific stock removal rate is increased, although wide variations in specific grinding energy are observed, particularly at lower Q'_w values. Values of specific grinding energy show a trend to decrease to a minimum limit of around 10 to 13 J/mm^3 for M50 tool steel as Q'_w increases.

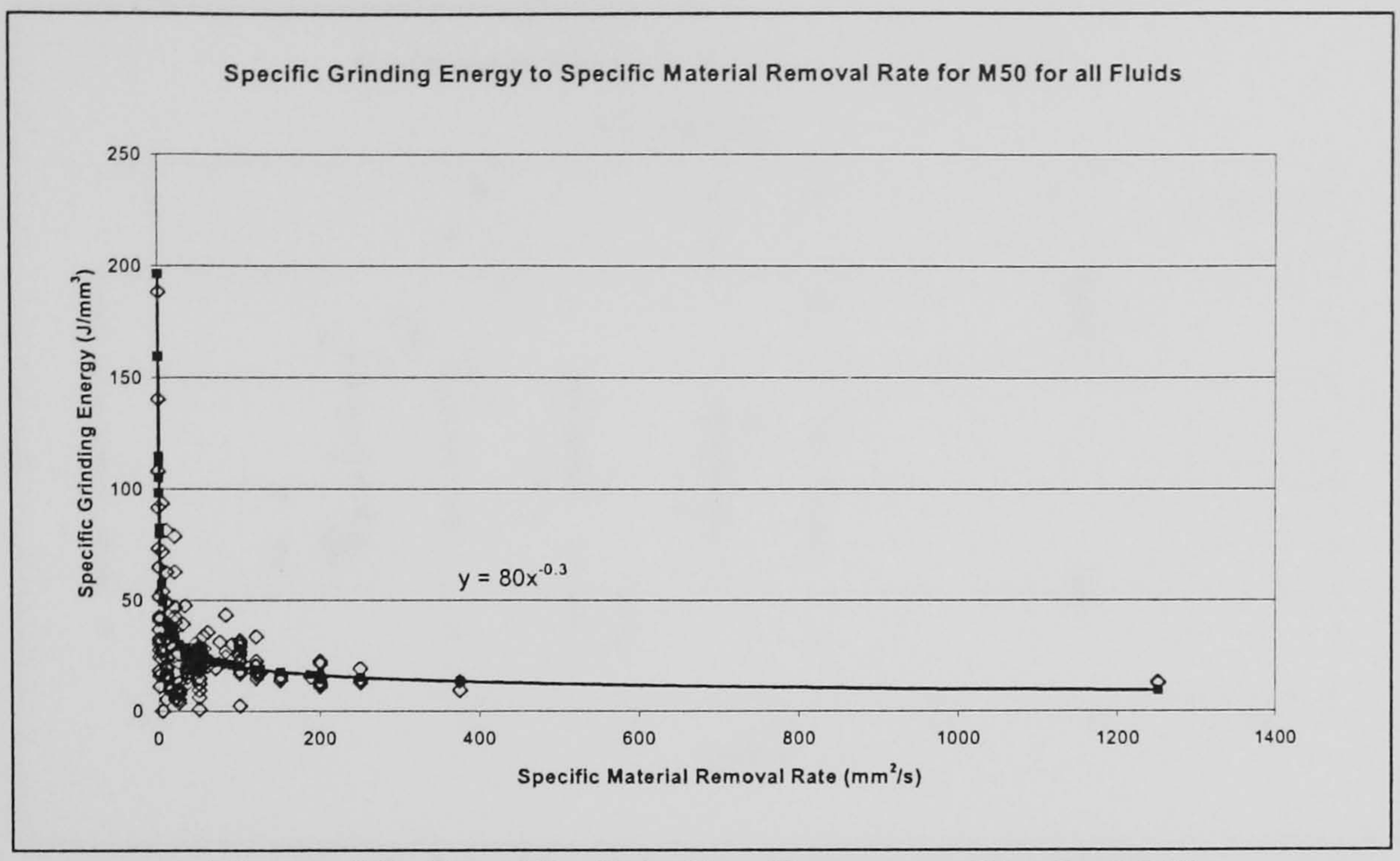

Figure 5.2: Specific Grinding Energy to Q'_w for M50

Illustrated in Figure 5.2 is the trend line which represents the average specific grinding energy throughout a wide range of energy values. Using these average specific grinding energy trend lines one can predict the range of possible temperatures within the grinding zone for theoretical Q'_w values for various permutations of feed rate and depth of cut. The mathematical expression for this average trend line is shown to be $y = 80Q'_w{}^{-0.3}$, where y represents the average specific grinding energy. Use will be made of this function when thermal modelling is discussed in Section 5.2.9.

As the specific grinding energy increases more energy is required to remove a given volume of material, which in turn increases the probability of higher grinding temperatures and the onset of oxidation. Figure 5.3 shows an example of a burn threshold diagram for M50, which takes into account wheel diameter, depth of cut and feed rate through the function $f(D^{1/4}a_c{}^{-3/4}V_w{}^{-1/2})$ as suggested by Malkin (1989). As wheel wear increases the grit flats have a greater rubbing component which increases the energy required for the operation, and this is observed through increases in the specific grinding energy.

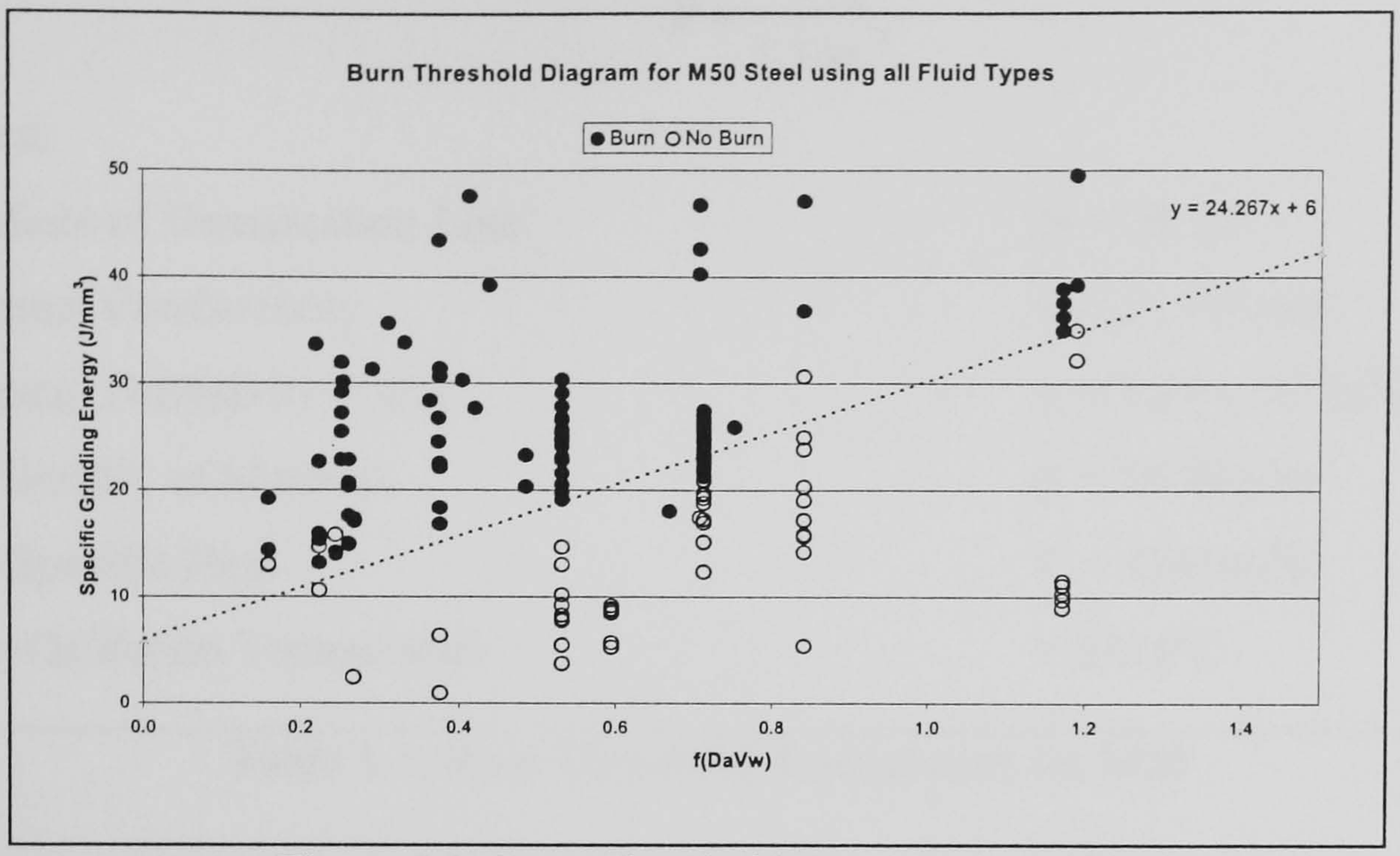

Figure 5.3: Burn Threshold Diagram for M50

A burn threshold diagram for M50 is shown in Figure 5.3. The criterion chosen to define grinding burn was visual signs of surface oxidation. The data generally fell within two well defined regimes separated by the dotted line which indicates a burn threshold boundary condition. Some scatter around the burn threshold boundary is evident and this may in part be due to the reliability of the visual assessment. However, the division between the burn and no burn regions is clear, with the intercept of 6J/mm^3 predicting a chip forming energy of around 13J/mm^3, a value typical for steels, Malkin (1989).

Malkin (1989) reported that the gradient of the burn threshold line was directly proportional to the burn threshold temperature. Table 5.1 shows the equation used to determine this temperature. As one can see the final oxidation temperature is shown as 2916ºC and is well above, in fact nearly double, the melting point of the material in question.

Malkin's Equation for Burn Threshold Oxidation Temperature

$$B = \frac{k\theta_m}{1.13\alpha^{0.5}}$$

When:

Gradient of Demarcation Line	B = 24.267
Thermal Conductivity	k = 25.7W/mK
Thermal Diffusivity = k/ρC	$\alpha = 7.47 \times 10^{-6} m^2 s^{-1}$
ρ = Density of Material	$\rho = 7870 kg/m^3$
C = Specific Heat	$C = 434 J/m^3 K$
θ_m = Oxidation Temperature	= 2916°C

Table 5.1: Burn Threshold Temperature for M50

As seen in Figure 5.2 for any given Q'_w value, especially low values, a wide range of specific grinding energies is possible. Experimental studies of a fixed Q'_w value suggested that the specific grinding energy gradually increases and this can be related to the change in grinding wheel characteristics during both the early conditioning period and normal use of the wheel. This is a major factor in the development of wear flats on active grits and the increase in active grit concentration as wheel wear proceeds. This results in a gradual increase in specific grinding energy as illustrated in Figure 5.9.

5.2.2 Workpiece Characterisation

5.2.3 Stress Measurement

As shown previously in section 4.3.8, the residual stress measurements undertaken on samples at Cranfield were in reasonable agreement with the samples measured by the bearing manufacturer and therefore the rest of the stress measurements on the M50 samples were measured using the same procedure.

Figure 5.4 shows the trend for residual stress to tend towards more tensile values as Q'_w increases for each of the three different fluid types used. For lower values of Q'_w ($<100 mm^2/s$) the surface residual stress tends to be compressive but at higher Q'_w

values tensile residual stresses may result. This suggests that the workpiece temperature is likely to increase as Q'_w increases.

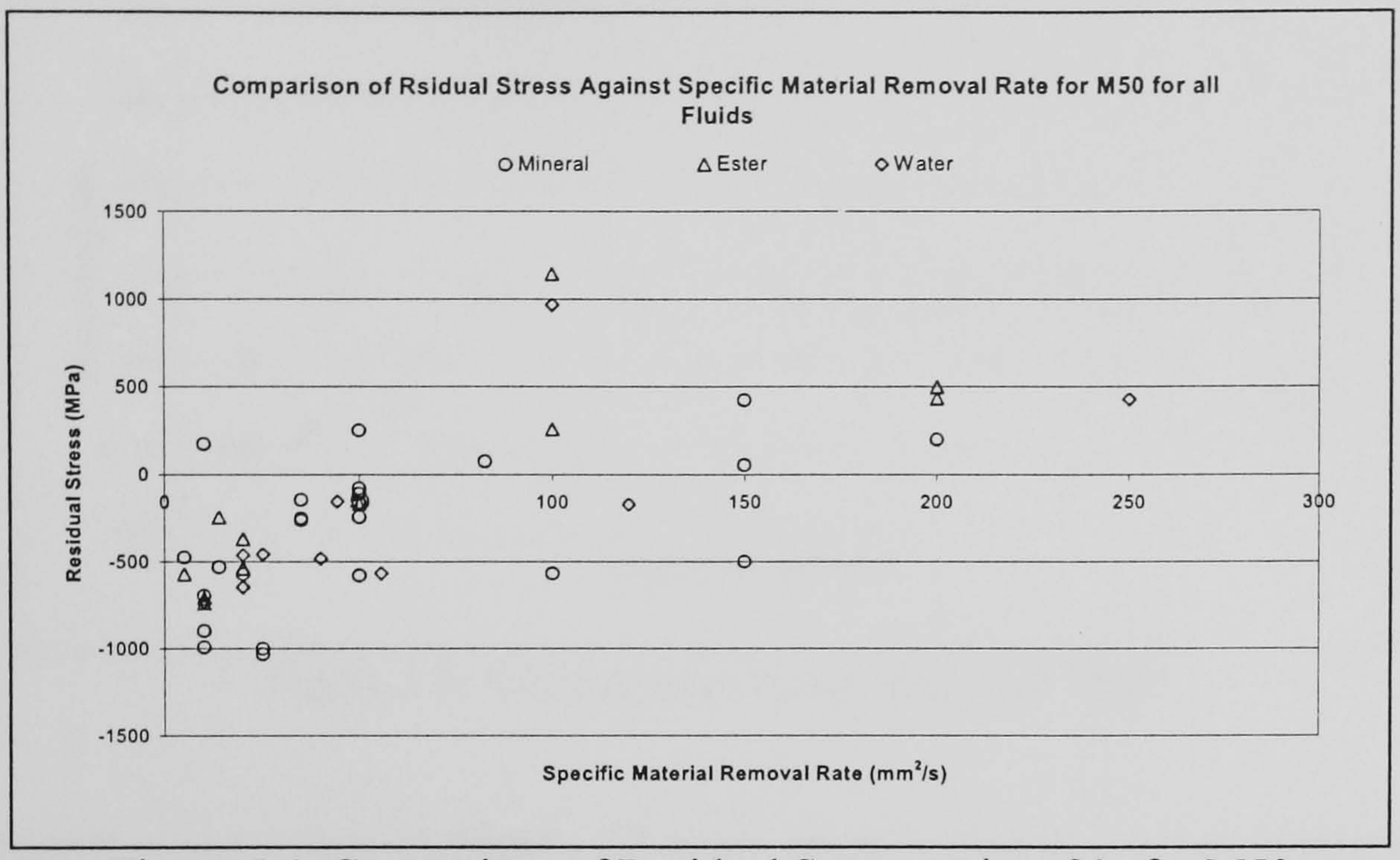

Figure 5.4: Comparison of Residual Stress against Q'_w for M50

Figure 5.5 views the same stress data set but against calculated temperatures with added information on the visual assessment of oxidation present. The burn threshold shown in Figure 5.2 is based only on visual signs of surface oxidation. Other burn threshold conditions could be envisaged, for example, a critical level of residual stress. To illustrate this, residual stress measurements were made by X-ray diffraction on selected workpieces. The level of the residual stress and the nature of the residual stress profile are a function of the magnitude of plastic deformation and the temperature reached within the grinding zone. In general there is a direct relationship between the level of residual tensile stress and temperature and it has been shown previously that the on-set of tensile residual stress occurs when a critical transition temperature is exceeded, M^{c}Cormack et al (2001). Thus, one might expect a correlation between the residual stress and temperature. Figure 5.5 illustrates the variation in measured residual stress with temperature and shows the distribution of burn and no burn data points based on visual observation.

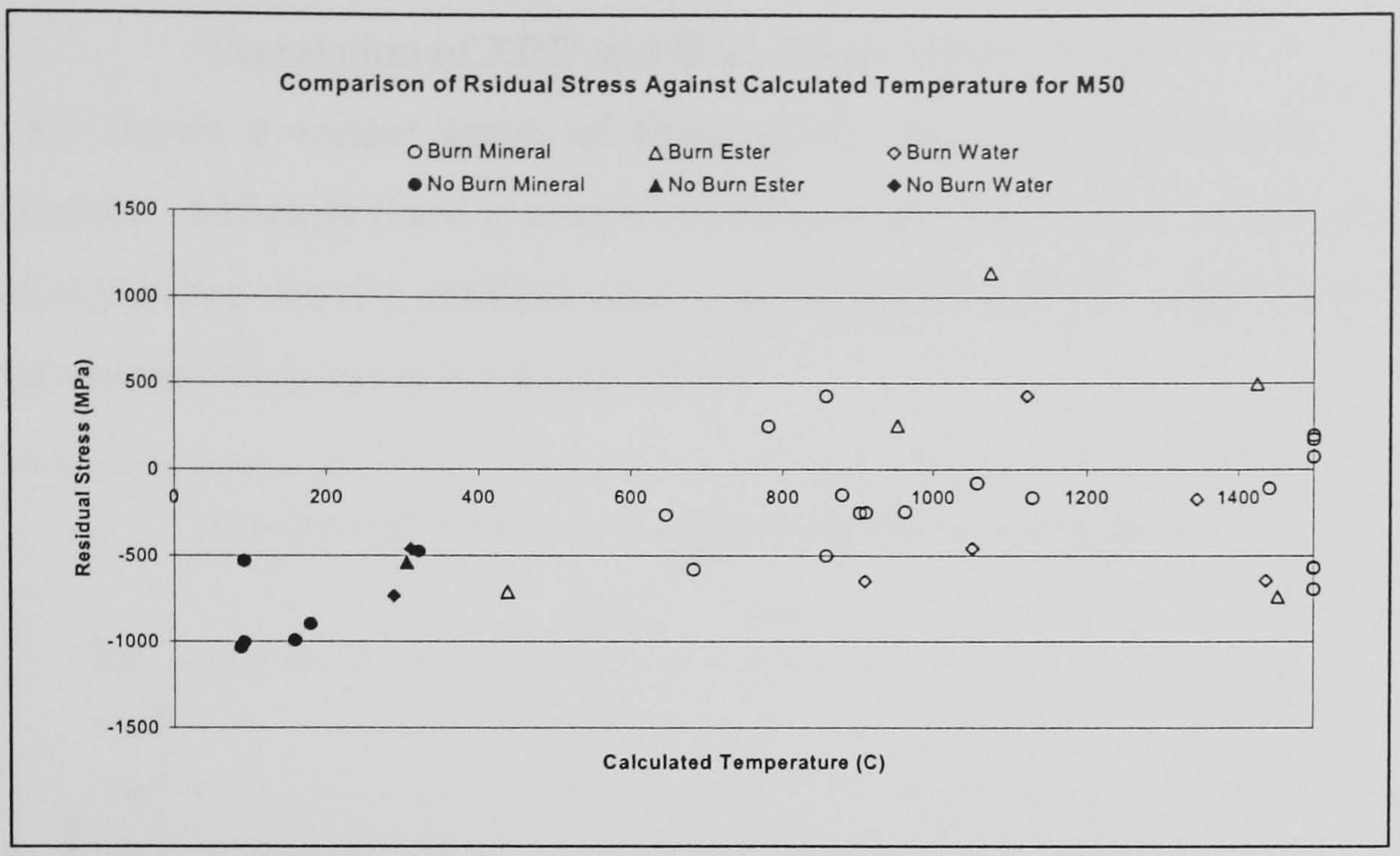

Figure 5.5: Stress against Temperature for M50

The residual stress values in Figure 5.5 show some scatter at a given temperature as might be expected for this type of measurement, but the general trend is clear. Low grinding temperatures promote the formation of compressive residual stress whilst high temperatures generate tensile stress. The transition between the visual burn and no burn observations is around – 400MPa. The transition to tensile stress occurs at around 600°C. From a practical viewpoint, the results suggest that satisfactory surface integrity should be obtained if the maximum grinding zone temperature is maintained below 400°C, i.e. fluid film boiling of the grinding fluid is prevented.

5.2.4 Barkhausen Noise Amplitude

Barkhausen noise amplitude (BNA) is a measure of changes in both stress regime and material hardness. When the workpiece surface stress characteristics become tensile the BNA signature increases. Also when a hard material is tested, the BNA is lower than for softer materials. Therefore BNA measurements are comparative and must be considered with respect to the calibrated standards and settings previously found in Section 4.2.7. for different hardness and micro-structural conditions.

5.2.4.1 Correlation of XRD and BNA Stress Measurements

Figure 5.6 shows a scatter graph of Barkhausen Noise results compared to XRD measurements. Although there is a some scatter present there seems to be a reasonable correlation between the two residual stress measurements and the correlations with the visual assessment of grinding burn is excellent.

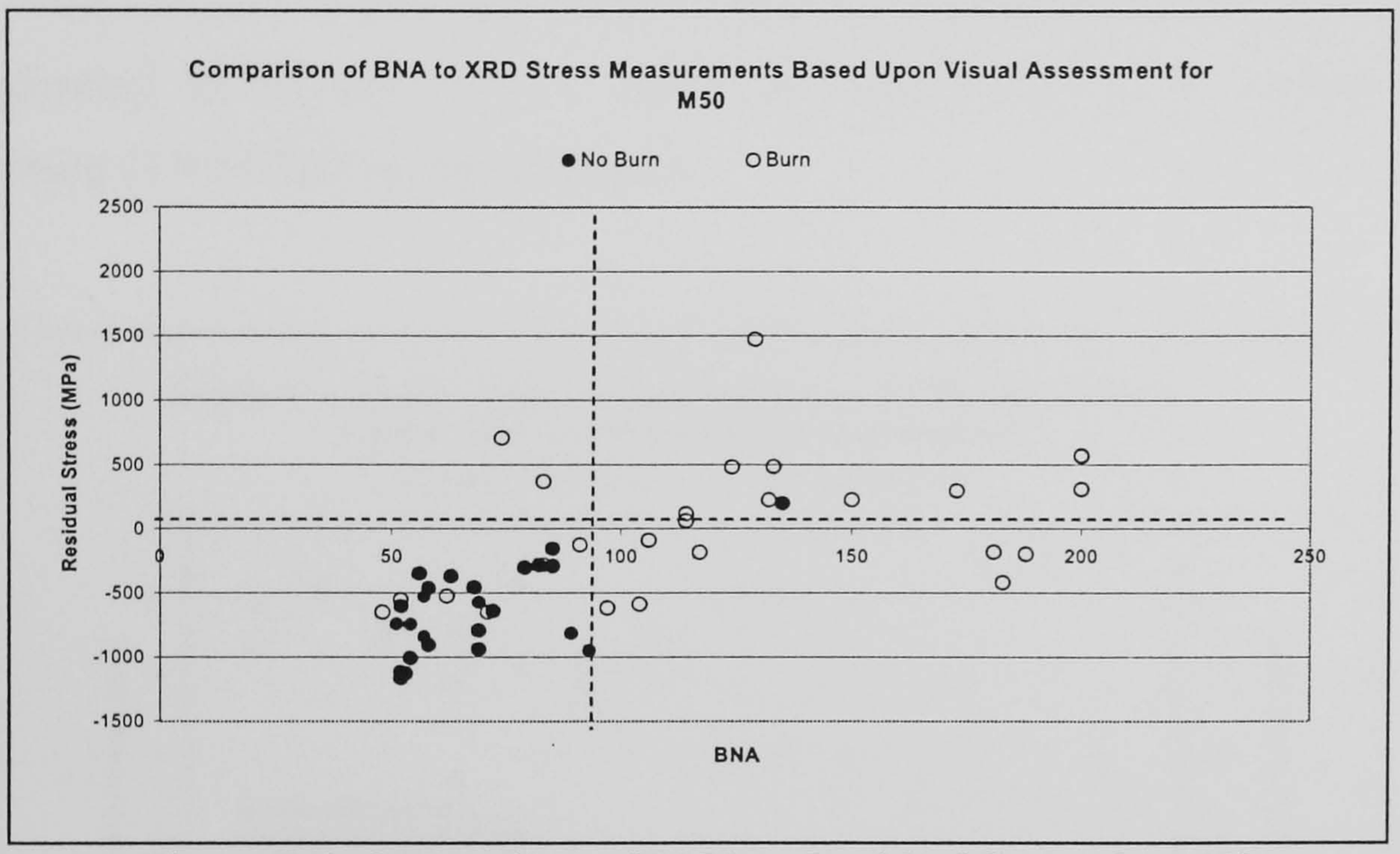

Figure 5.6: Comparison of BNA to Residual Stress for M50

From Shaw (1993) we see that the time required to formulate martensite via the grinding process is nanoseconds. Also Chen et al (2002) reported that when the thermally induced stresses overcome the yield stress then tensile stress regimes will occur on the surface layer. It is known from published datasheets from Stresstech that the magnetic domains change polarity and it is this change in polarity which is proportional to the amplitude of Barkhausen Noise measured. Tensile stress regimes give high Barkhausen Noise Amplitude measurements and compressive stresses low readings. When a material is magnetically hard then these domains find the polarity change inhibited therefore a hard material will reduce the BNA magnitude and a softer will give a higher reading. So a material may have a tensile core on its surface and have an overtempered region under this hard core. This could give rise to anomalous readings such as those burnt sample points which have given low BNA readings.

5.2.5 Surface Characterisation

The measure of surface roughness, R_a, was also monitored throughout the testing and the trend of decreasing R_a values with the rise in specific grinding energy during grinding operations carried out at one Q'_w value is clearly shown in figures 5.7 to 5.9. These figures clearly show that there is the same correlation between the gradual increase in specific grinding energy and the improvement in surface finish for all Q'_w values. This variation in measured energy values and surface finish was also observed when grinding IN718 and will be shown in section 6.2.3 to be related to the development of wear flats on the CBN grits.

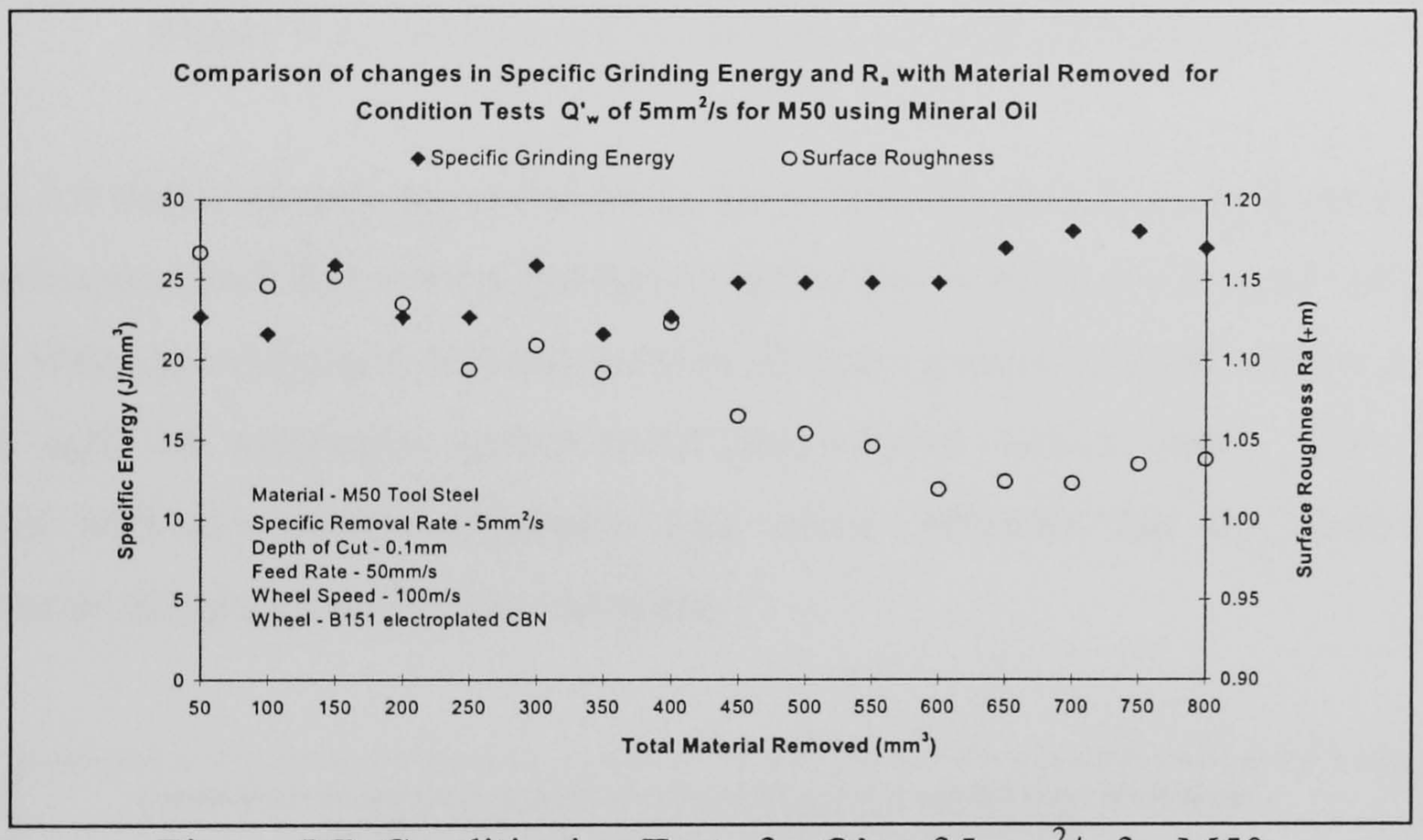

Figure 5.7: Conditioning Tests for Q'_w of $5mm^2/s$ for M50

Figure 5.7 shows the results from the conditioning tests when using a constant Q'_w of $5mm^2/s$. Although the specific energies were extremely low the same characteristics of rising specific grinding energy with decreasing surface roughness were evident in the plot.

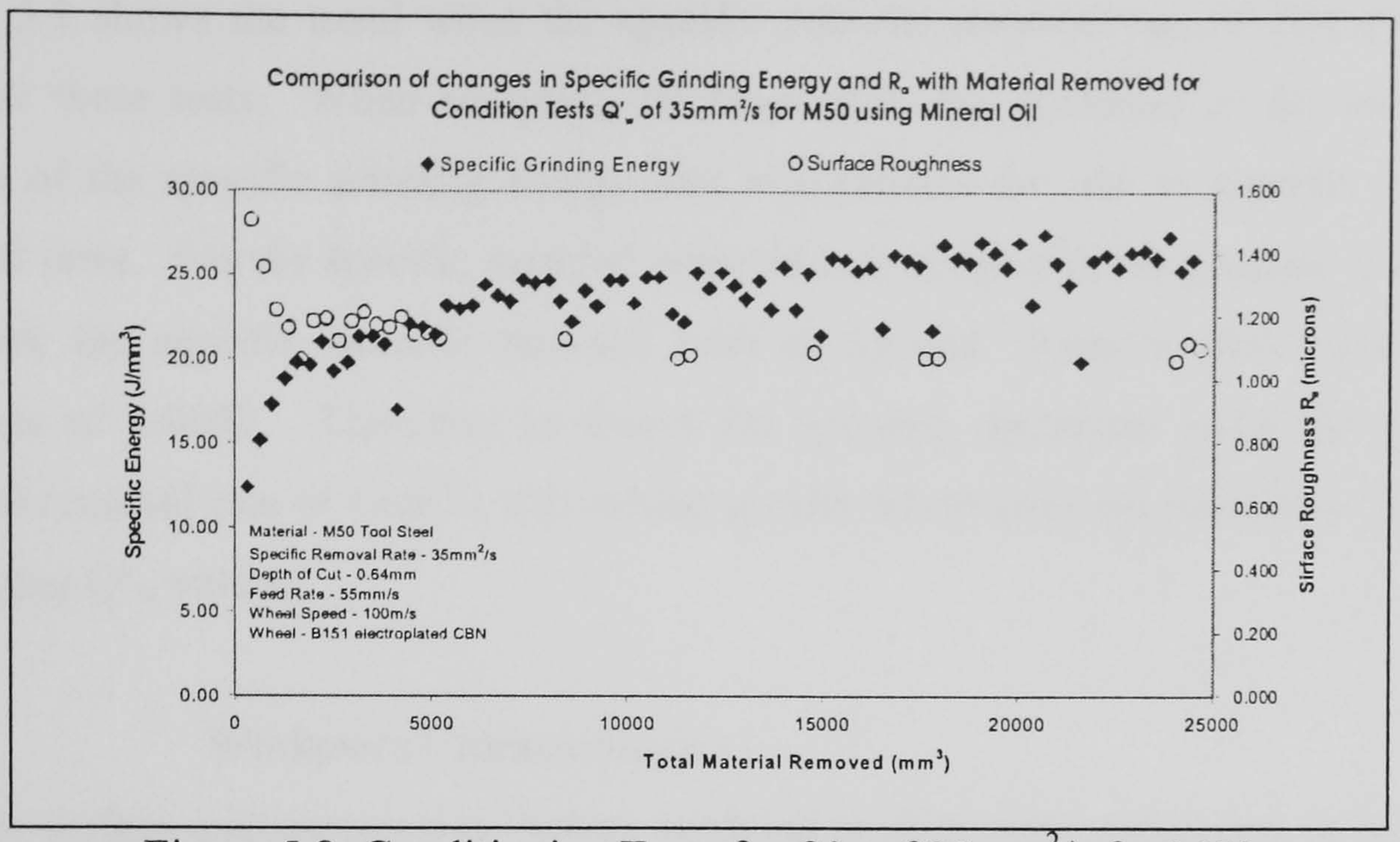

Figure 5.8: Conditioning Tests for Q'_w of $35mm^2/s$ for M50

Figures 5.8 shows clearly the initial steep rise in specific grinding energy as the grains are conditioned and then a more gradual increase due to more active grits coming into contact with the workpiece and also as wear flats are generated more surface area is in contact with the workpiece surface producing a better surface finish. This trend is mirrored with the surface roughness plot which indicates that the surface finish improves as the grit wear flat area increases.

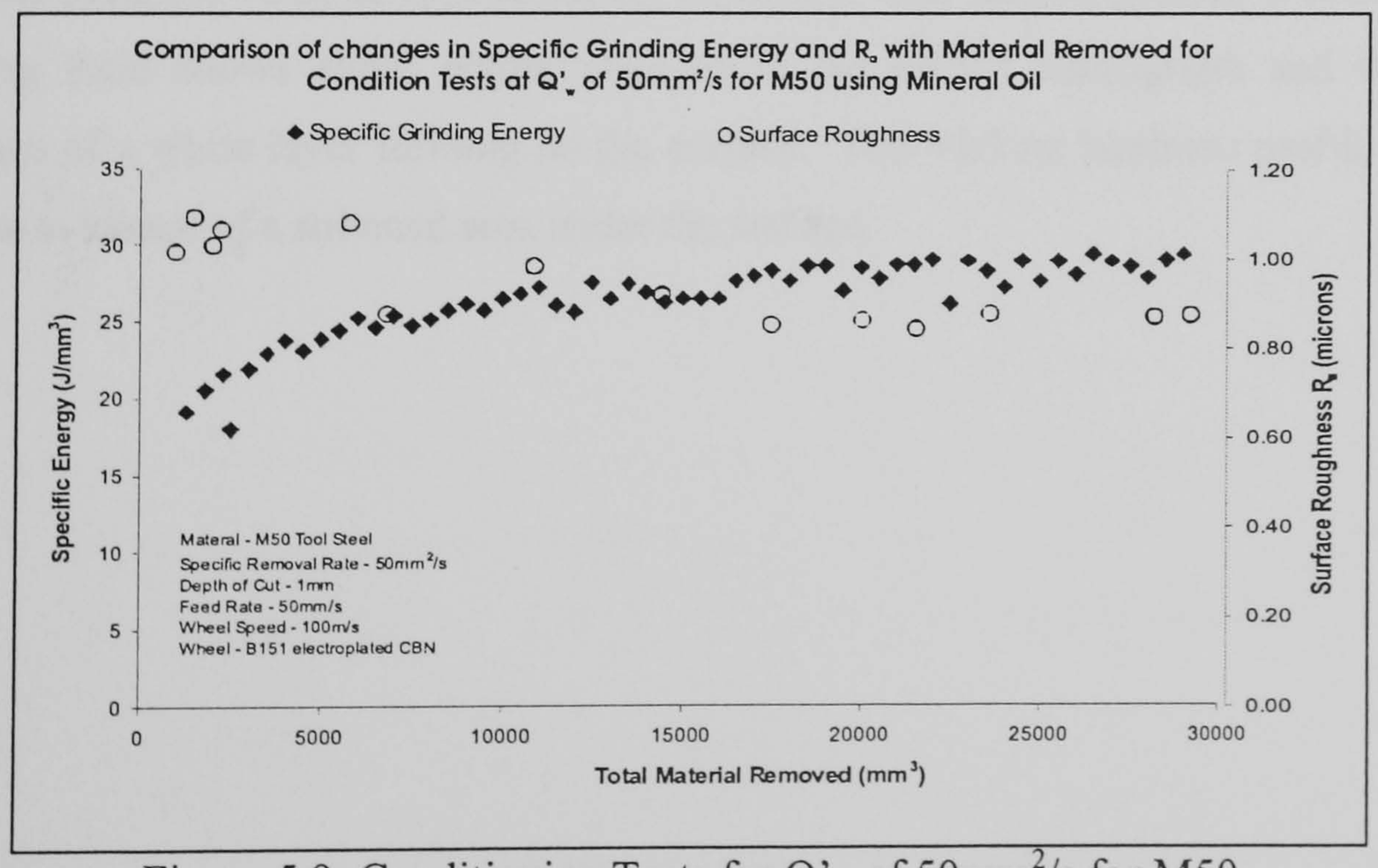

Figure 5.9: Conditioning Tests for Q'_w of $50mm^2/s$ for M50

Figure 5.9 shows the trend when the specific material removal rate of 50mm^2/s was used for these tests. When analysing the three plots the gradients of the secondary portion of the specific grinding energy plot also reflects the rise in specific material removal rates. For the specific material removal rate of 5mm^2/s the gradient is 0.0058 and both the specific material removal rates of 35 and 50mm^2/s plots have lower gradients of 0.0002. Therefore in theory the grinding operation using the specific material removal rate of 5mm^2/s will exhibit greater wheel wear characteristics than the two higher Q'_w values.

5.2.6 Workpiece Characterisation

The sub-surface microscopy and Vickers hardness profiles were undertaken to highlight any damage incurred during the grinding process. Any structural changes due to the ingress of substantial heat into the workpiece could alter the structure i.e. over temper the steel and in so doing soften the material, or there could be an extremely hard layer of untempered martensite at the surface.

Figure 5.10 shows the results from tests on a Q'_w value of 50mm^2/s. The micrograph of the sub-surface structure shows no darkened area or white layer at the surface. This is correlated by the Vickers hardness test results, which showed no deviation from the substrate hardness value of approximately 800$HV_{0.1}$. The sample ground in ester based grinding fluid shows slight colour changes in the etched micrograph and there is evidence of a white layer forming on the surface. The Vickers hardness profile shows definite evidence of a softened area under the surface.

Mineral Oil Grinding Fluid	Ester Based Oil Grinding Fluid
Test Number - 50-9	Test Number – 50-265

$Q'_w = 50mm^2/s$

Depth of Cut = 1mm

Feedrate = 50mm/s

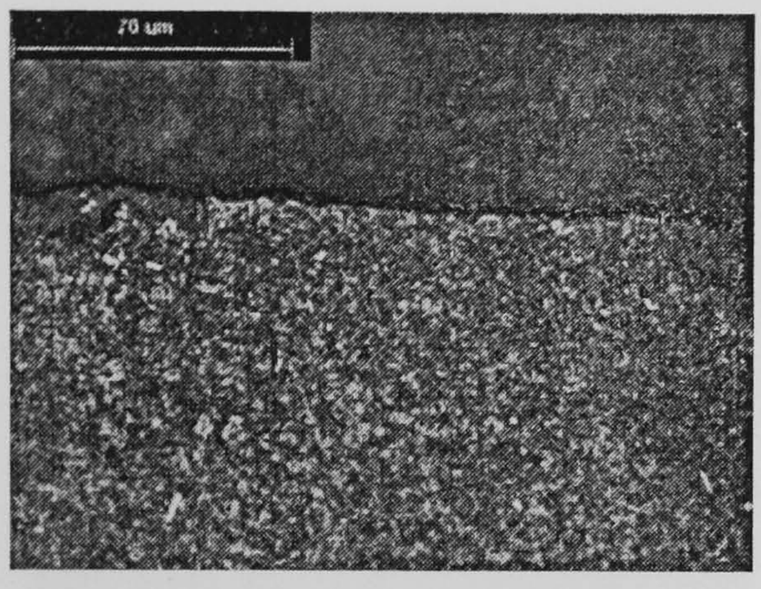

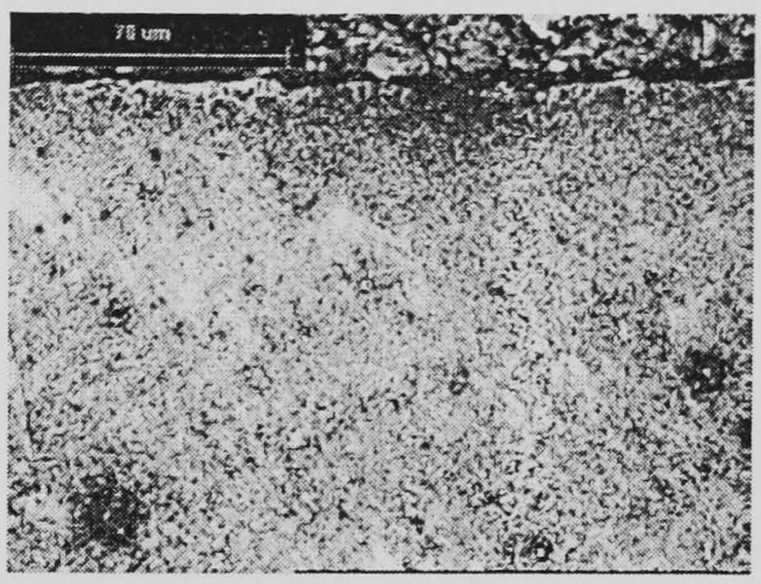

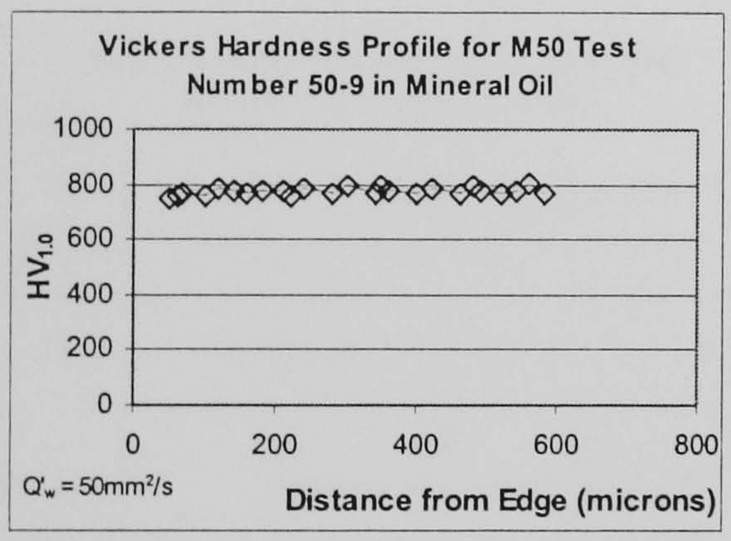

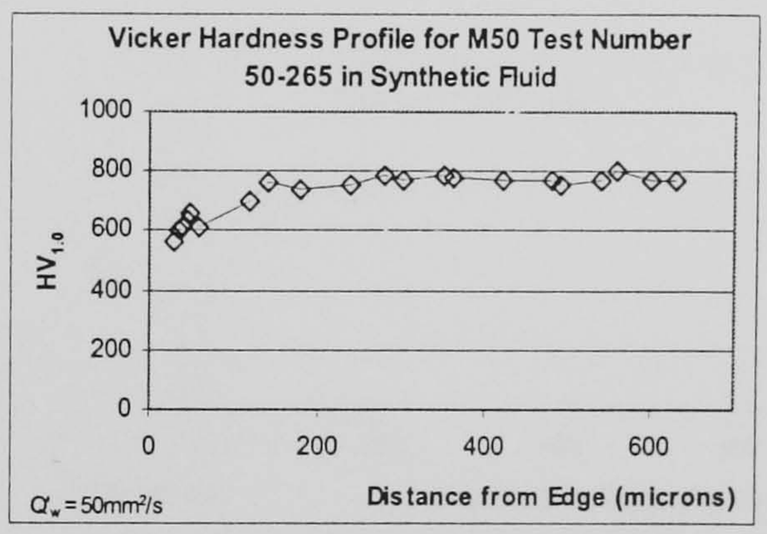

Residual Stress	-640MPa	371MPa
Calculated Temperature	682°C	839°C

Figure 5.10: Workpiece Characterisation for $Q'_w = 50mm^2/s$

The residual stress being negative for the mineral oil ground sample gives an indication that the predicted temperature is not accurate in this case. In the case of the ester based oil ground sample all measures used here corroborate the first impression that the finished surface has been damaged.

Mineral Oil Grinding Fluid	Ester Based Oil Grinding Fluid
Test Number - 50-3	Test Number – 50-266

$Q'_w = 14mm^2/s$

Depth of Cut = 0.55mm

Feedrate = 25.25mm/s

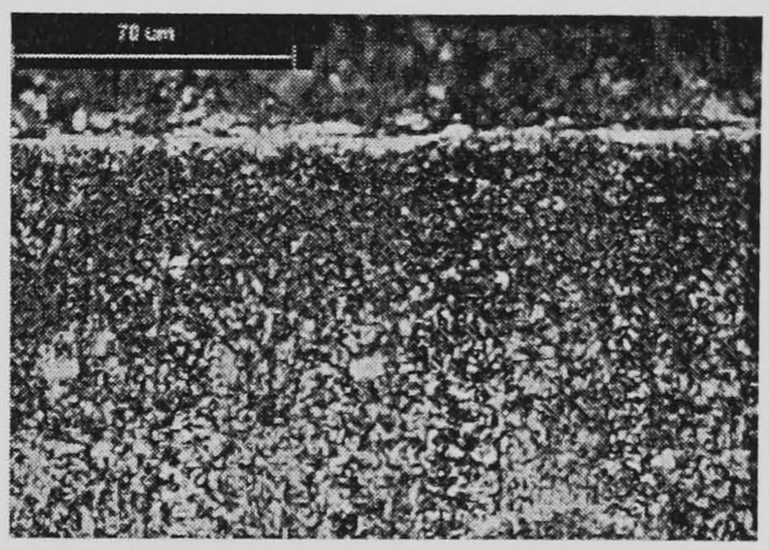

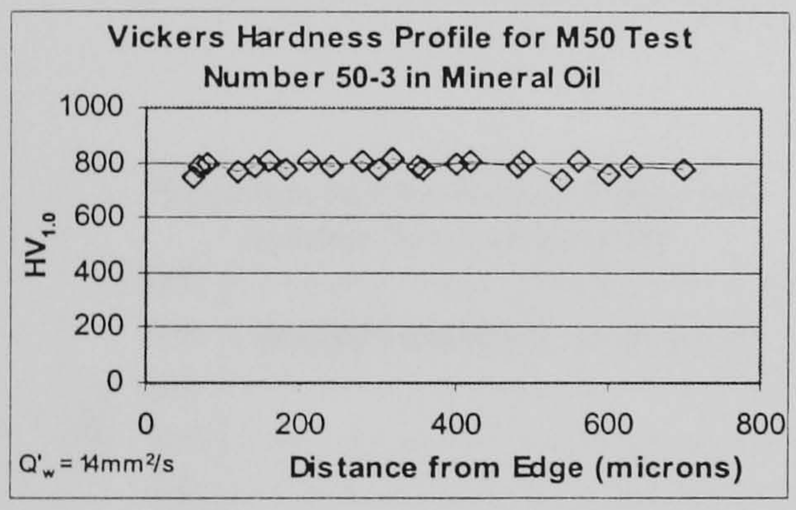

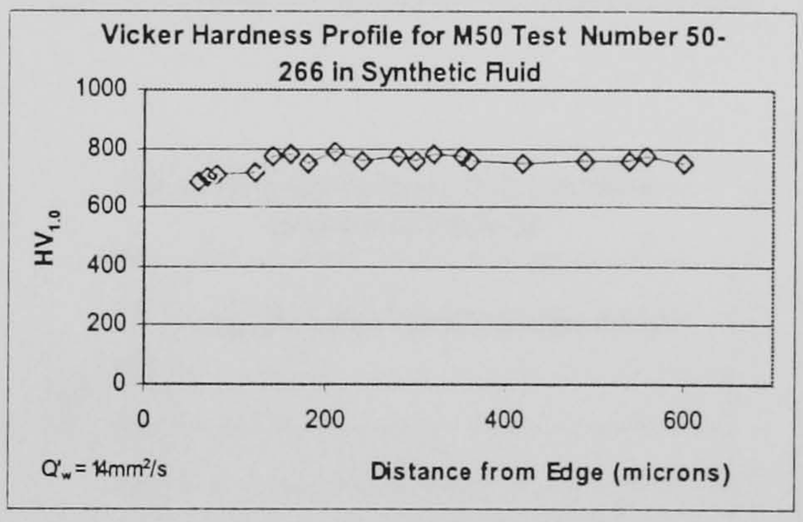

Residual Stress	-604MPa	309MPa
Calculated Temperature	112°C	529°C

Figure 5.11: Workpiece Characterisation for $Q'_w = 14mm^2/s$

Figure 5.11 shows a distinct difference in the two results for a Q'_w of $14mm^2/s$. The mineral oil grinding fluid ground surface exhibits no damage and there is no change to the Vickers hardness profile. The ester based grinding fluid ground surface shows a white layer present and a discolouration which is proven to be an overtempered zone by the Vickers hardness profile. Both the measured residual stress figures and predicted temperatures are consistent with these observations.

Mineral Oil Grinding Fluid	Ester Based Oil Grinding Fluid
Test Number - 50-11	Test Number – 50-264

$Q'_w = 5mm^2/s$

Depth of Cut = 0.1mm

Feedrate = 50mm/s

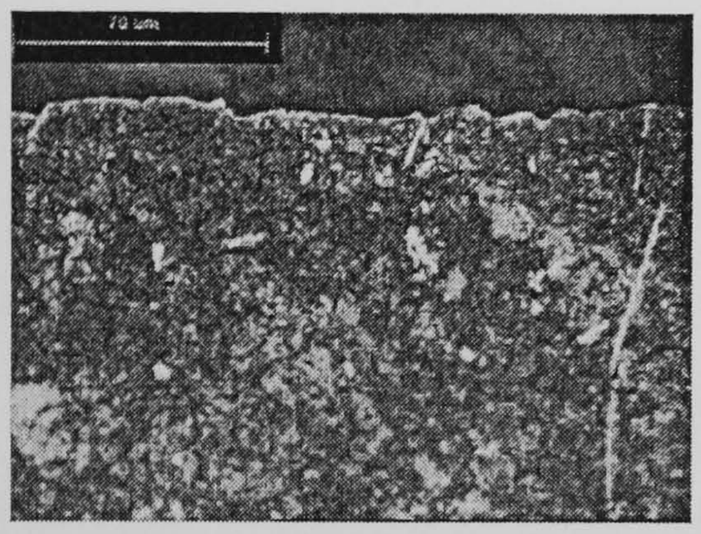

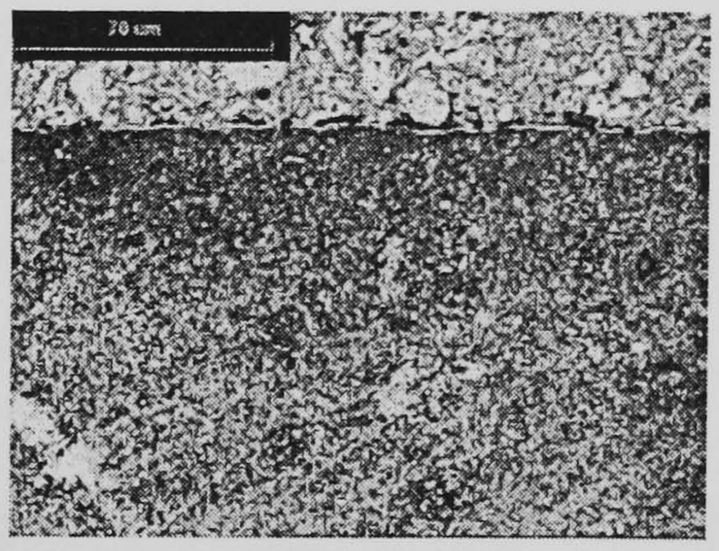

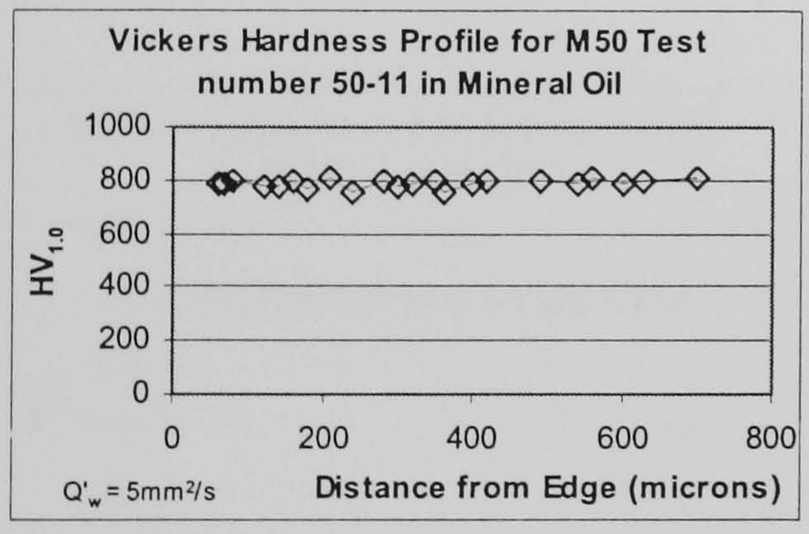

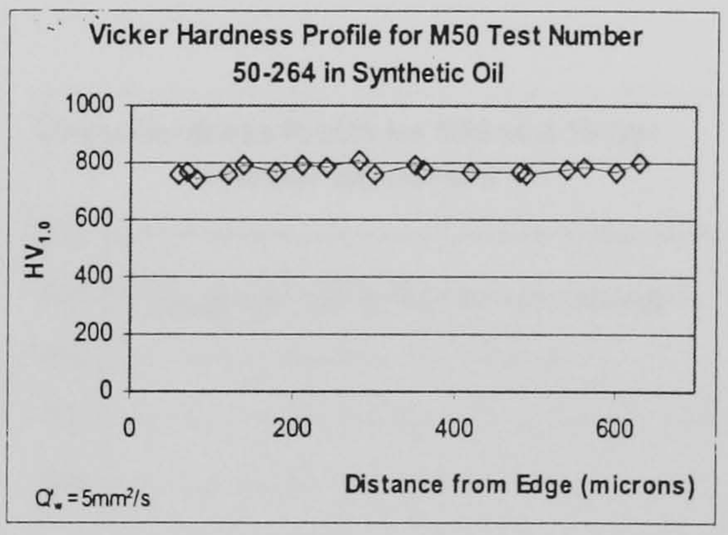

Residual Stress	-455MPa	-644MPa
Calculated Temperature	365°C	216°C

Figure 5.12: Workpiece Characterisation for $Q'_w = 5mm^2/s$

Figure 5.12 shows that for a Q'_w of $5mm^2/s$ there is no real damage to either sample at this rate of material removal. This is mirrored by both the measured residual stress values and predicted temperatures.

Water Based Grinding Fluid

Test Number - 50-297	Test Number – 50-301
$Q'_w = 120mm^2/s$	$Q'_w = 250mm^2/s$
Depth of Cut = 3mm	Depth of Cut = 5mm
Feedrate = 40mm/s	Feedrate = 50mm/s

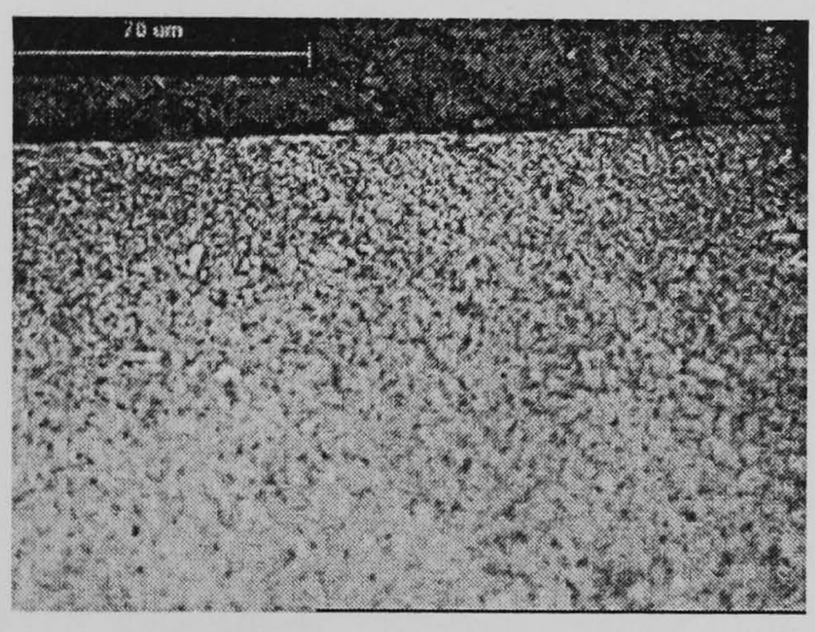

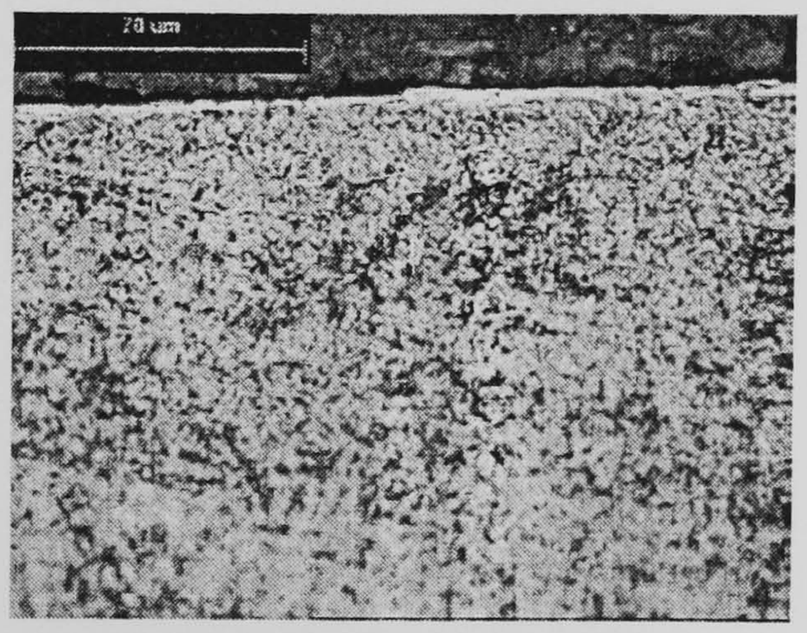

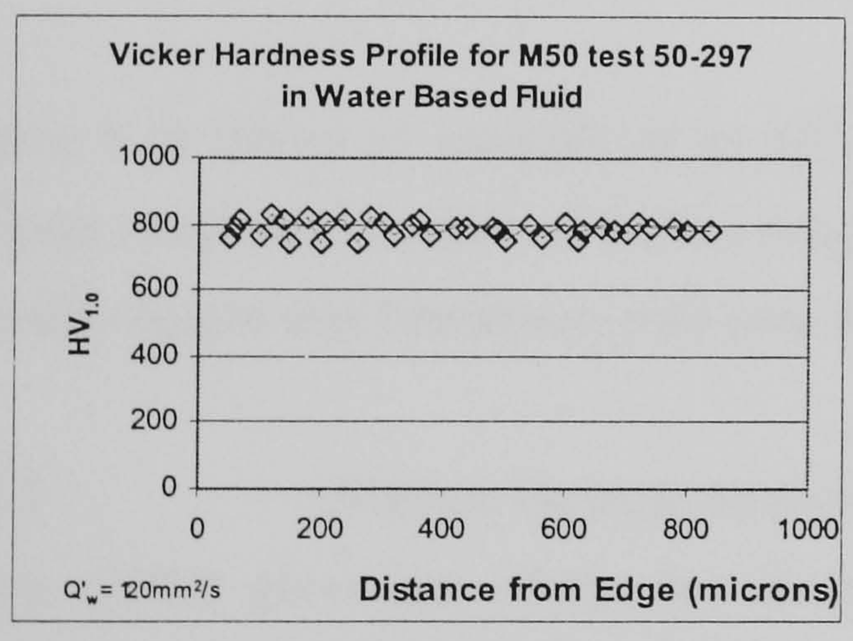

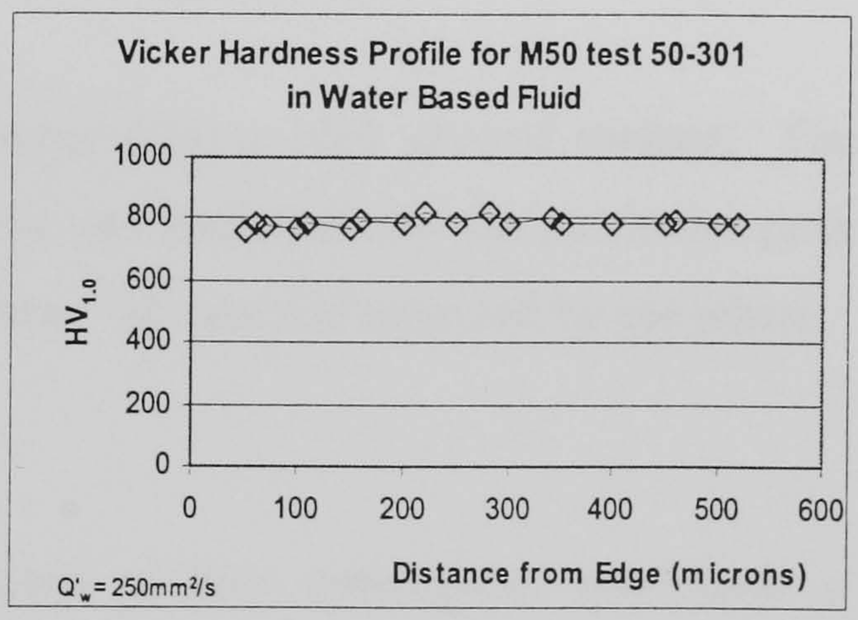

Residual Stress	-195MPa	481MPa
Calculated Temperature	917°C	1133°C

Figure 5.13: Workpiece Characterisation for Water Based Ground Samples

Figure 5.13 shows two samples ground using water based grinding fluid. The subsurface micrograph of test number 50-297 shows no white layer and the Vickers hardness profile substantiates this. The predicted temperature and measured residual stress values also correlate with this observation. One other example of water grinding

fluid is given by sample number 50-301. This sample used HEDG conditions and even though the micrograph shows a 0.7micron thick white layer with no overtempered zone a tensile stress of 481MPa was measured and a predicted temperature of 1133°C was calculated.

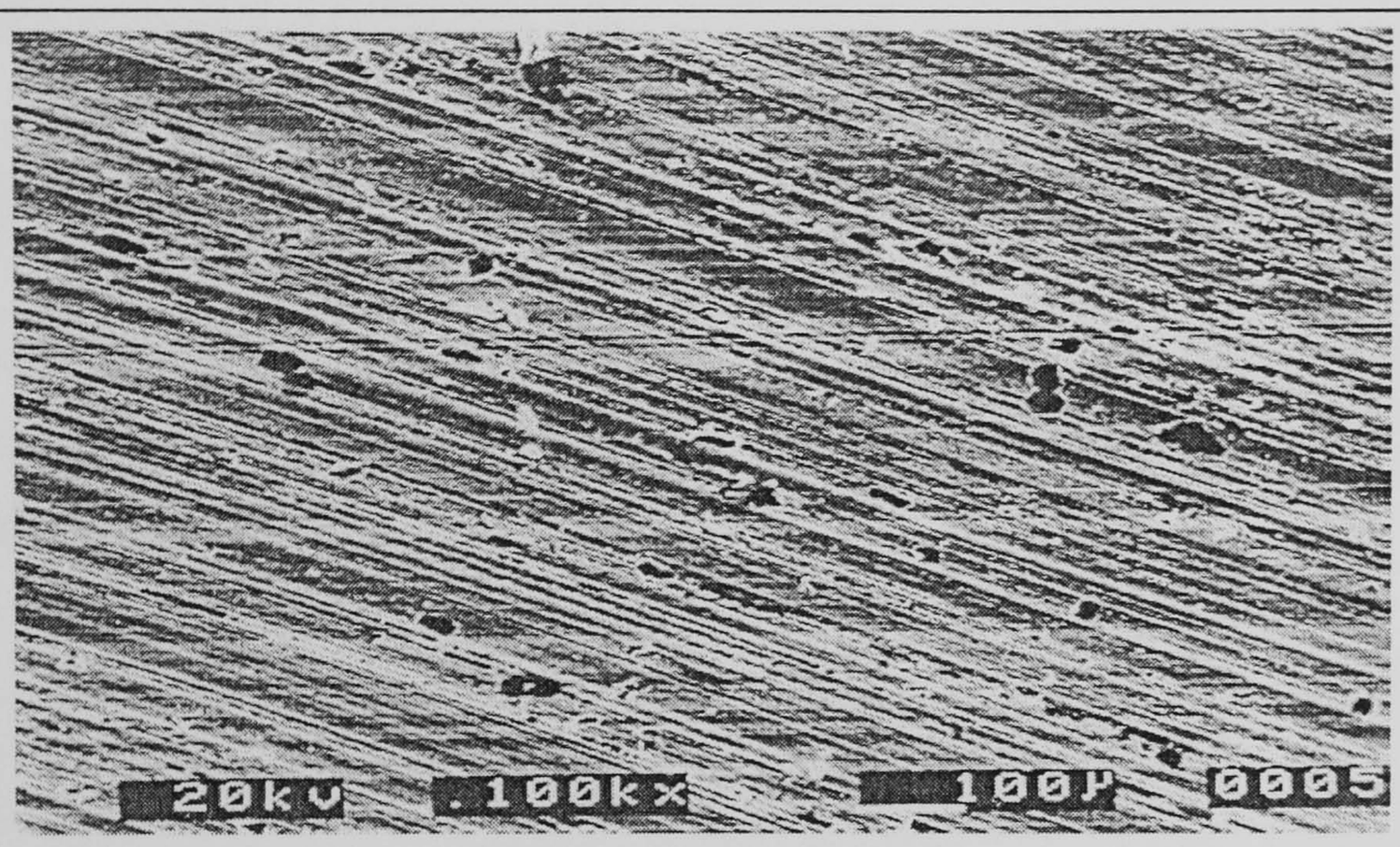

Figure 5.14: SEM Image of M50 Ground Surface

Figure 5.14 shows an example of an SEM image from a M50 ground surface. The average roughness measure of surface roughness was 2microns and the maximum peak to valley height was 19microns, with only 8100mm^3 of material removed by the wheel.

5.2.7 Grinding Damage Analysis

Shaw (1993) gives one of the few descriptions of how untempered martensite is produced. During normal heat treatment the material is heated and allowed to soak at around 50 to 100°C above the lower critical temperature, which is around 700°C. With the uniform structure formed this would allow the carbon atoms to be uniformly distributed in a body centred tetragonal (b.c.t.) structure. If the material is cooled quickly then this b.c.t. structure will remain forming a hard layer on the surface of the steel. Shaw states that the higher the concentration of alloying elements the lower the temperature required to initiate this process. This agrees with statements by McCormack et al (2001). When untempered martensite is produced by grinding, the time required is reduced through the ferocious grinding operation which releases a great

deal of energy via mechanical means. This energy release enhances the speed at which this micro-structural change occurs. So, untempered martensite is reported in this study to appear at 800°C and an over tempered zone is produced at around 780 to 800°C.

All sectioned samples which contained layers of over and untempered martensite had these layers measured and this data was corroborated using the Vickers micro-hardness profiles. Figure 5.15 shows the measured white layer formation against calculated temperature.

Also it is evident when using this temperature model that no formation of white layer has been predicated below 775-800°C. This in itself gives confidence in the temperature modelling used.

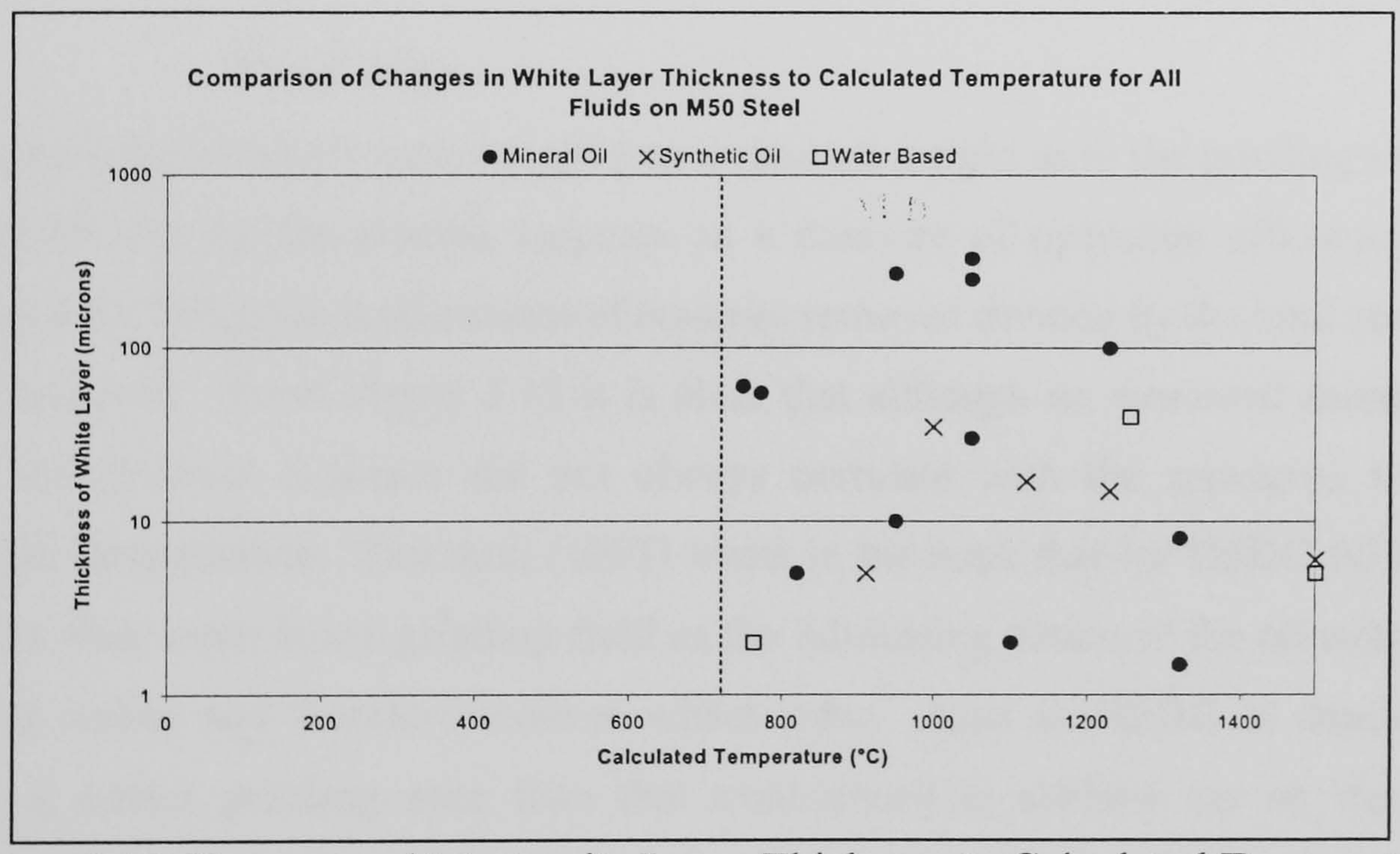

Figure 5.15: Untempered Martensite Layer Thickness to Calculated Temperature

Figure 5.16 shows that the trend for the onset of the formation of over tempered martensite on M50 steel is around 650°C and Figure 5.15 shows the trend for the formation of untempered martensite of around 800°C. Both these values correlate well with the findings from McCormack et al (2001).

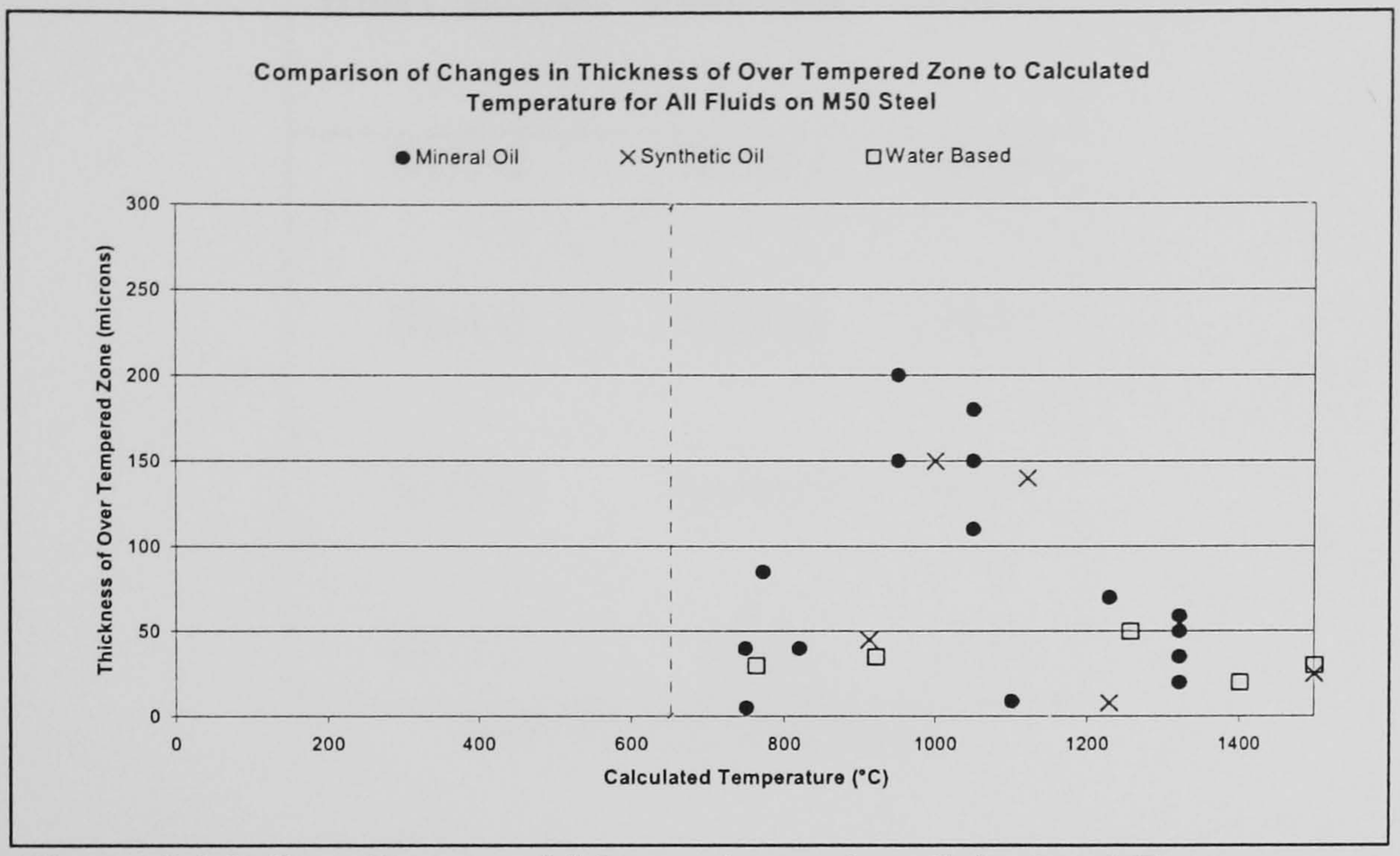

Figure 5.16: Over Tempered Martensite against Calculated Temperature

5.2.8 Wheel Wear

The monitoring of wheel wear can give an important insight as to the grinding ratio of a process for use by the process engineer as a measure of operation efficiency. The grinding ratio being the total amount of material removed divided by the total amount of wheel removed. From Figure 5.15 it is clear that although no structural damage was noted the physical evidence did not always correlate with the measured stress or predicted temperatures. Tawakoli (1993) wrote in his book that for HEDG oil is more effective than water based grinding fluid as the lubricating action of the oil reduces the grinding forces and therefore reduces wheel wear. Also as HEDG is described as having a cooler grinding zone than that experienced in shallow cut or creep feed grinding, the need for the attributes from a grinding fluid, i.e. heat dissipation, is not as high a priority as that required from a grinding fluid type, such as mineral oil.

As shown in Figure 4.2 only a portion of the wheel was used during a cut, therefore a part of the wheel was unused. The wheel was then used to cut a profile in graphite and the difference measured. This amount of wheel wear equated to the reduction per radius and the volume of wheel removed, which in reality was a cylinder, was calculated.

Wheel Number	Fluid Type	G-Ratio
B151-2	Mineral	126.02
B151-3	Mineral	129.83
B151-4	Synthetic	78.77
B151-5	Water	34.12

Table 5.2: Grinding Ratios

Table 5.2 shows the results from grinding M50 steel from the point of view of the grinding ratios. These ratios were calculated with respect to all conditions and so give an indication of the wheel wear characteristics. It can be seen that the worst grinding ratio calculated was when water based grinding fluid was used and the best was with mineral oil. This could give an indication that indeed the requirement for grinding fluid with cooling properties in the grinding zone is not as important as the need for a grinding fluid with lubrication properties.

5.2.9 Theoretical Modelling of Grinding Temperatures

The measured values of specific grinding energy were used to estimate the temperature of the finished workpiece surface through calculations based on the circular arc of contact model developed by Rowe & Jin (2001). The complete thermal modelling procedure is given in Appendix H. This thermal modelling approach is appropriate for deep grinding conditions and enables realistic energy partition coefficients to be determined. This is important since the burn threshold temperature estimated from the burn threshold diagram, based on the standard Jaeger sliding heat source model, considerably overestimates the temperature. Figure 5.17 shows the data from Figure 5.2 replotted in terms of temperature and illustrates the well defined regions between burn and no-burn data. The boundary for the burn threshold condition occurs at around

400°C which is consistent with the temperature at which the mineral oil is expected to boil.

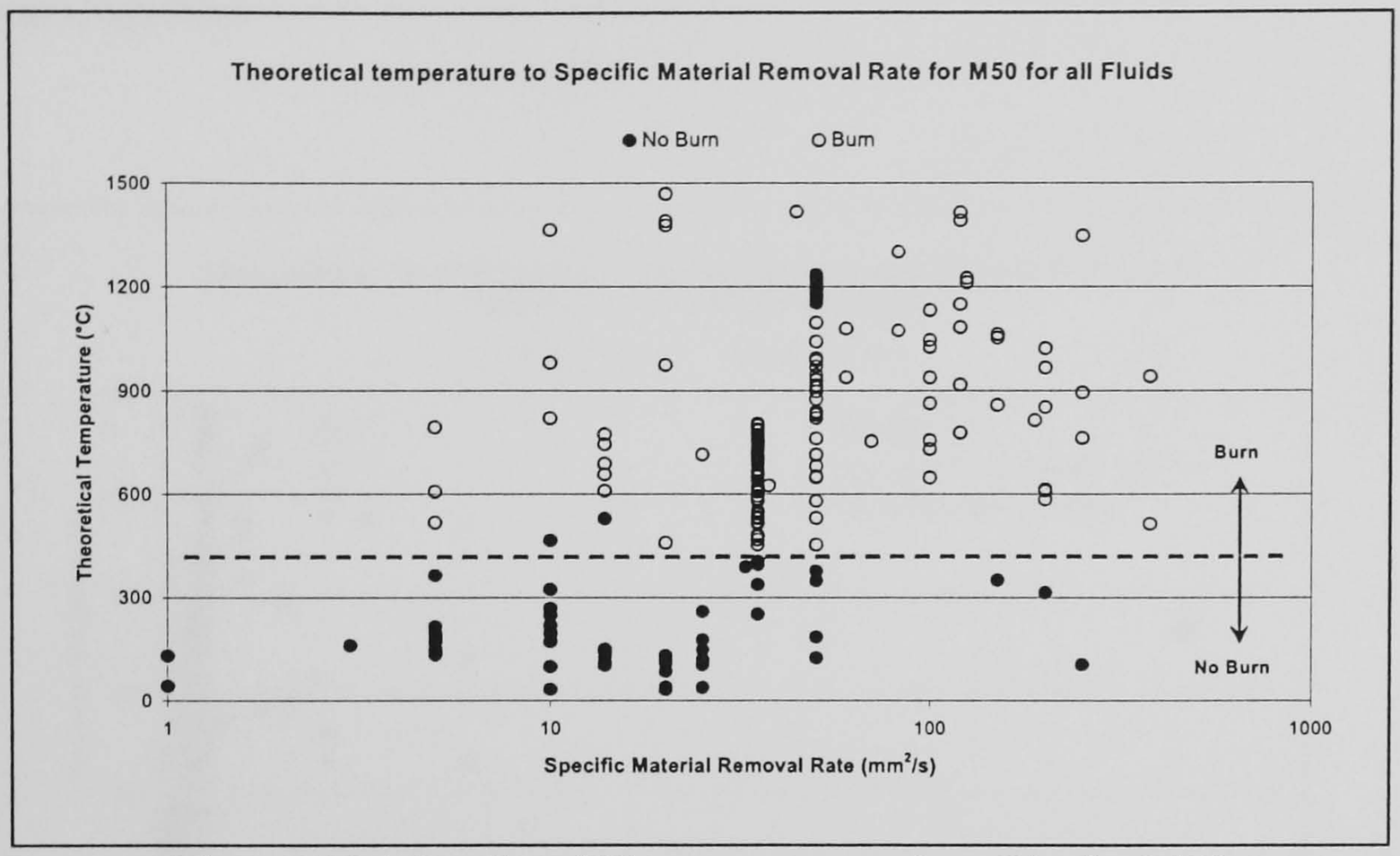

Figure 5.17: Predicted Temperature against Q'_w for M50

However, it should be noted that Figure 5.17 shows the resulting burn threshold temperature for all fluids concerned. The initial basis for this type of modelling is concerned with the visual assessment of burn on the sample surface, after which the specific grinding energy is taken into account specifically where the point lies in Figure 5.3. Therefore Figure 5.17 is related to the actual burn threshold for the material and not the boiling of the specific grinding fluids used throughout these trials.

5.2.10 Specific Energy Band

With such a wide variety of specific grinding energies being produced from an even wider range of conditions and parameters it was decided that it would be beneficial if the data could be viewed in such a way as to isolate unknown factors such as wheel wear. Therefore, the data were sorted to only show a narrow band of specific grinding energies; these energies could only be produced where the same grinding wheel conditions had been experienced and a true representation of the HEDG effect could be viewed.

Figure 5.18 shows the resulting plot after analysing a band of specific grinding energies such as 0.1 – 25J/mm^3. One can view the spread of possible contact and finished surface temperatures over a wide range of Q'_w which are all influenced by similar wheel wear characteristics.

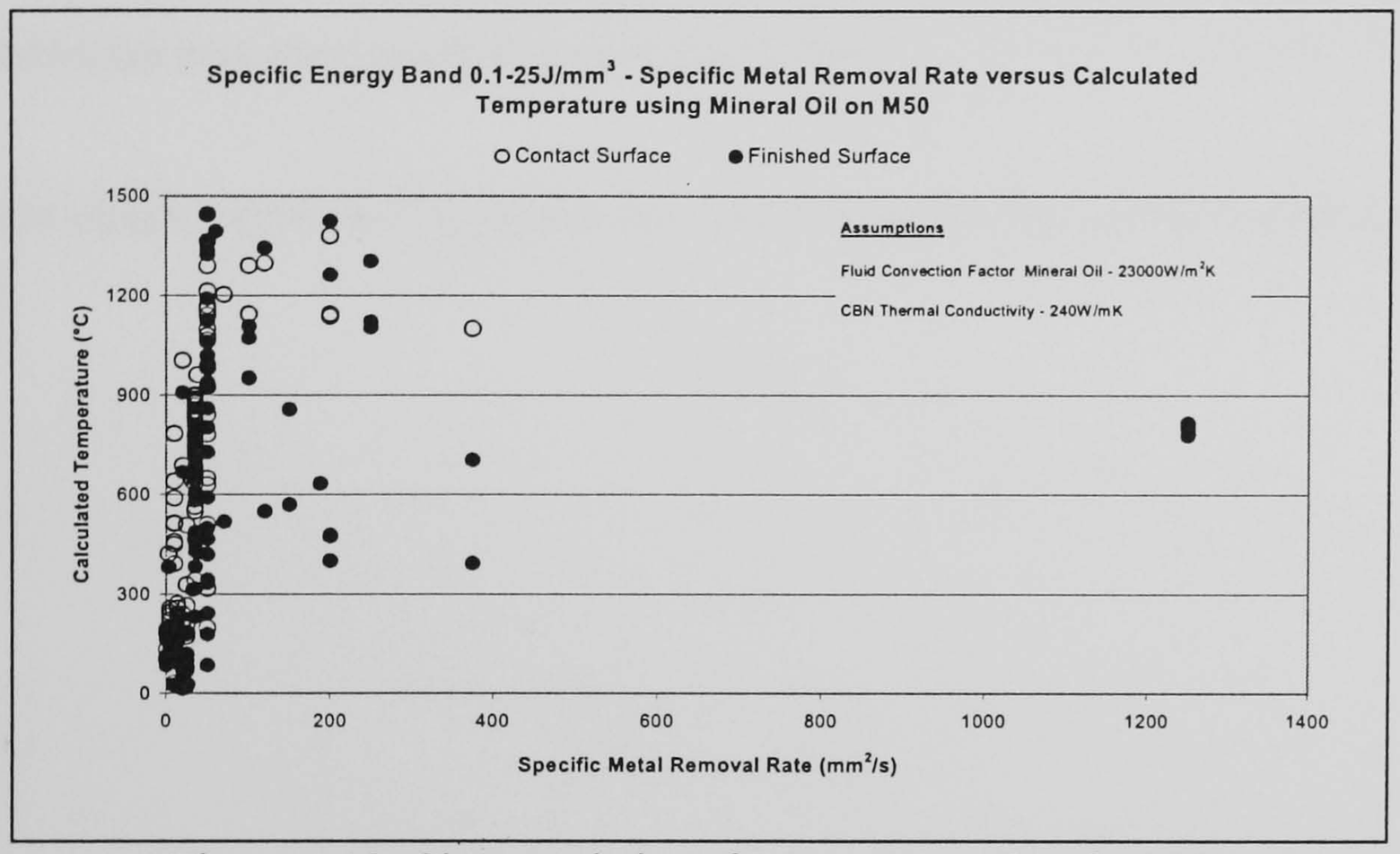

Figure 5.18: Characteristics of Temperature Q'_w for M50

From Figure 5.18 it can be seen how the characteristics of the finished surface temperatures rise sharply, reach a maximum then begin to decrease as specific material removal rate increases. As this decrease begins the scatter is quite apparent, as if the specific grinding energy becomes extremely sensitive to any changes in the grinding parameters.

5.3 Summary

The work presented, shows that a good all round understanding of the HEDG process using the Edgetek 5-axis machine to grind M50 tool steel has been achieved. The variety of experiments undertaken has encompassed various feed rates, depths of cut, wheel speeds and grinding fluid strategies and has shown that there are fundamental trends within this process. These trends and results correlate well with conventional measures such as residual stress measurements and new procedures such as BNA.

Also the evidence that mineral oil was the more efficient fluid of the three fluid types used answers one of the questions asked by the sponsors. The physical evidence is quite overwhelming by way of sub-surface microscopy, SEM images and grinding ratio. The grinding fluid qualities of the mineral oil used were excellent even without the addition of operation enhancing additives such as sulphur and chlorine. These were omitted due to requirements from the sponsors as aviation parts were manufactured, and these additives may have resulted in corrosion issues.

The next chapter views and discusses the results from the first nickel based superalloy IN718.

CHAPTER 6 IN718 NICKEL BASED SUPERALLOY

Although a large number of experiments have taken place concerning this 'tough' nickel based superalloy during this research, the salient points relating to experimental results are given in part 6.1, and 6.2 describes the procedures followed to carry out the workpiece analysis. Part 6.3 summarises the chapter. The experimental results have been used to give overall depth and enhance confidence in the results. All experimental parameters when grinding with the three types of grinding fluid are shown in Appendix G.

6.1 Experimental Results

6.1.1 Taguchi Design of Experiments

The screening test was carried out so that the maximum amount of data would be derived from the minimum number of test runs. With this in mind a 16 run orthogonal array with 6 centre points was undertaken with a width of cut of 15mm.

Test Number	Wheel Speed (m/s)	Grit Size (micron)	Depth of Cut (mm)	Nozzle Angle (degrees)	Nozzle Height (mm)	Feed Rate (mm/s)	Nozzle Diameter (mm)	Fluid Pressure (bar)
718-1	75	252	0.55	6.5	107.5	25.25	6.5	10.75
718-2	100	301	0.1	5	110	0.5	8	14
718-3	50	301	0.1	5	105	0.5	5	7.5
718-4	100	301	1	8	105	0.5	5	14
718-5	50	301	1	8	110	0.5	8	7.5
718-6	100	301	1	5	110	50	5	7.5
718-7	50	301	1	5	105	50	8	14
718-8	50	301	0.1	8	110	50	5	14
718-9	100	301	0.1	8	105	50	8	7.5
718-10	75	252	0.55	6.5	107.5	25.25	6.5	10.75
718-11	75	252	0.55	6.5	107.5	25.25	6.5	10.75
718-12	75	252	0.55	6.5	107.5	25.25	6.5	10.75
718-13	75	252	0.55	6.5	107.5	25.25	6.5	10.75
718-14	50	181	1	5	110	0.5	5	14
718-15	100	181	1	5	105	0.5	8	7.5
718-16	50	181	0.1	8	105	0.5	8	14
718-17	100	181	0.1	8	110	0.5	5	7.5
718-18	100	181	1	8	110	50	8	14
718-19	50	181	1	8	105	50	5	7.5
718-20	100	181	0.1	5	105	50	5	14
718-21	50	181	0.1	5	110	50	8	7.5
718-22	75	252	0.55	6.5	107.5	25.25	6.5	10.75

Table 6.1: IN718 Screening Test Parameters in Order of Testing

This took into account 8 parameters which are shown in Table 6.1. The trends produced duplicated results found when the procedure was carried out with M50 steel.

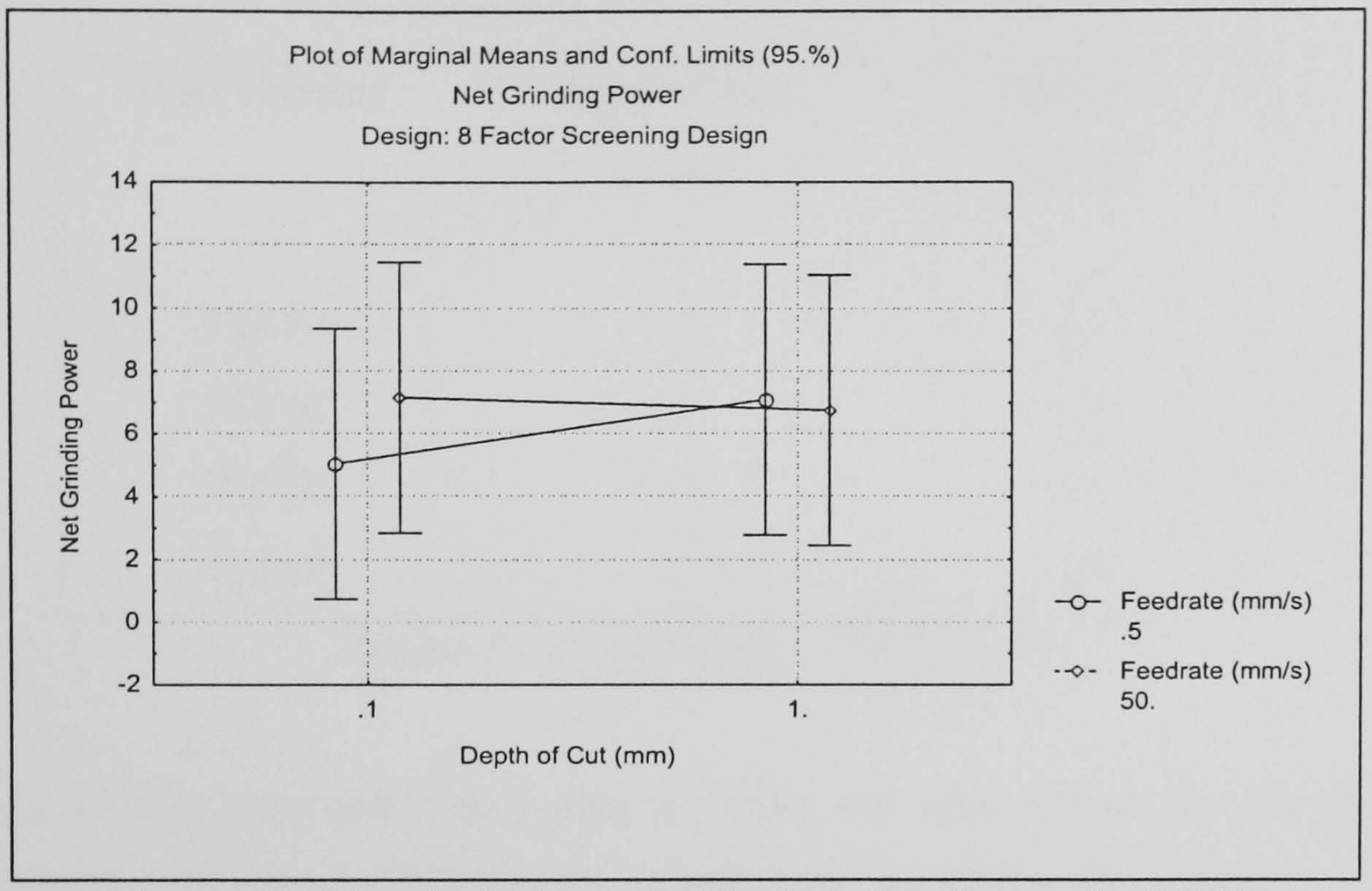

Figure 6.1: Marginal Means for Net Grinding Power for IN718

Work by Tawakoli (1993) reported that HEDG is characterised by increases in all the following parameters: wheel speed, depth of cut and work feed-rate, thus permitting extremely high stock removal rates. Figure 6.1 illustrates that although the main effects are from depth of cut and feedrate there is an indication of an interaction between the two parameters when considering their effect on net grinding power. The diagram shows that when the depth of cut is increased from its lowest value of 0.1mm to its highest level of 1mm with the lowest feedrate value of 5mm/s the net grinding power increases. The second graphic correlates with modern theory by showing that at the higher feedrate of 50mm/s and going from the lower 0.1mm depth of cut to the higher depth of cut of 1mm the tendency is for the grinding power to decrease. This indicates that feedrate has a higher significance than depth of cut and the interaction is characterised by the crossing lines.

6.1.2 High Q'_w Removal Rates

Four high specific material removal rate experiments were undertaken, which were designed to investigate the effects of high Q'_w values on such a tough material.

Test Number	Depth of Cut (mm)	Feedrate (mm/s)
718-92	2.5	125
718-93	3	125
718-94	3.5	125
718-95	4	125

Table 6.2: IN718 Deep Cut Parameters

The set of four parameters as shown in Table 6.2 were chosen for the grinding experiments. These conditions were selected to investigate the influence of high specific material removal rates on this type of material.

After the first cut, numbered 718-92, was completed the surface was assessed visually for signs of oxidation and in this instance there was no sign of burn. The three subsequent cuts had oxidisation on the surface. Figure 6.2 shows that the specific grinding energy increased for each subsequent cut, which is a result of excessive grit wear.

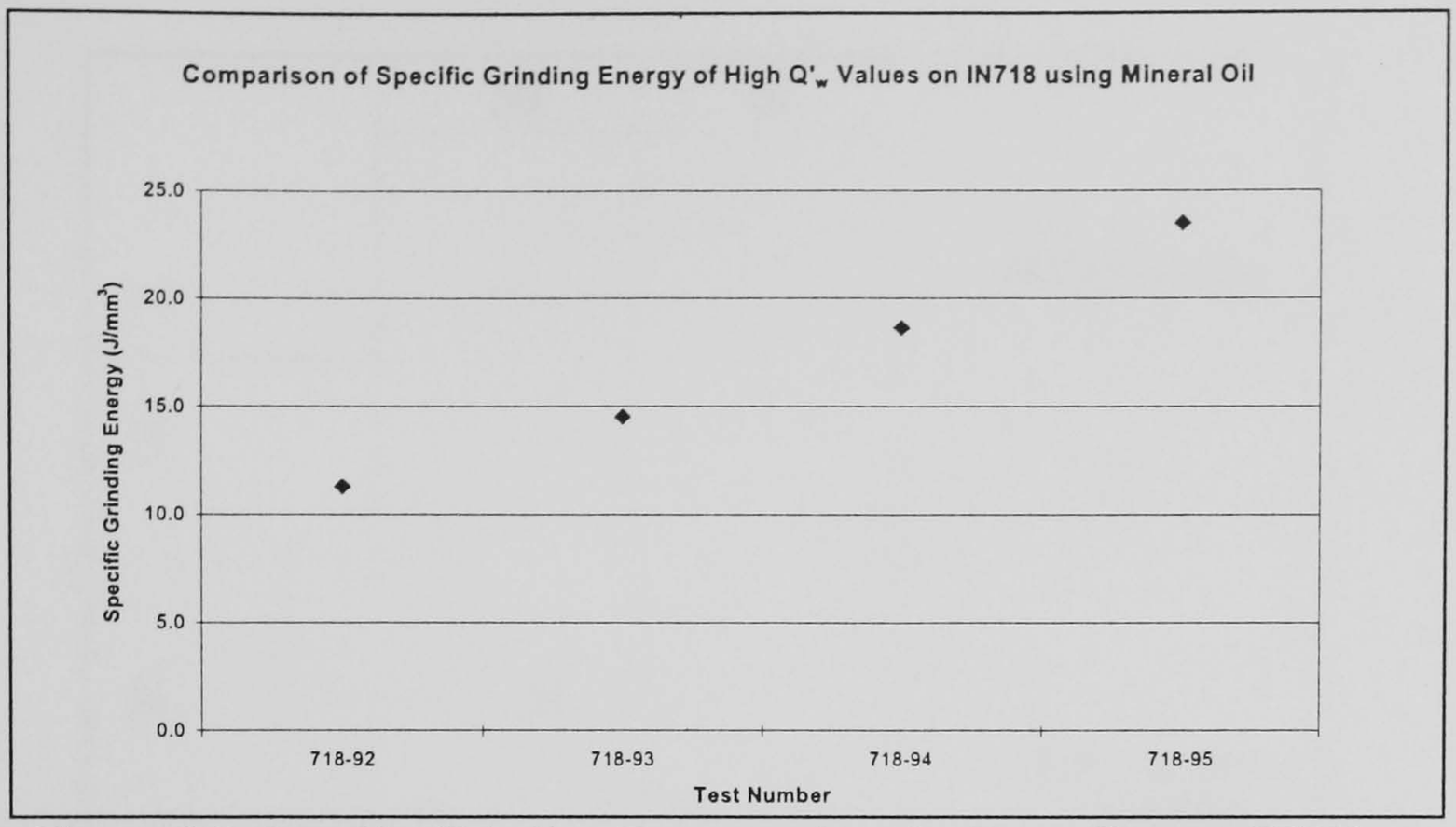

Figure 6.2: Specific Grinding Energy values for Deep Cuts on IN718

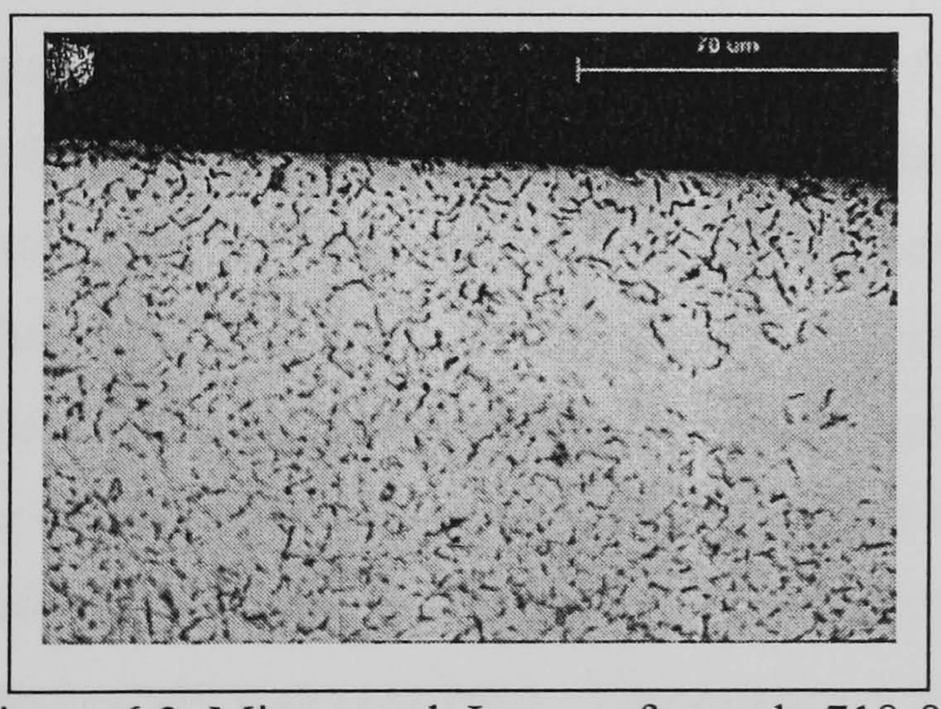

Figure 6.3: Micrograph Image of sample 718-92

Figure 6.3 shows a typical IN718 grain structure with no evidence of grain drag or redeposition of material after grinding.

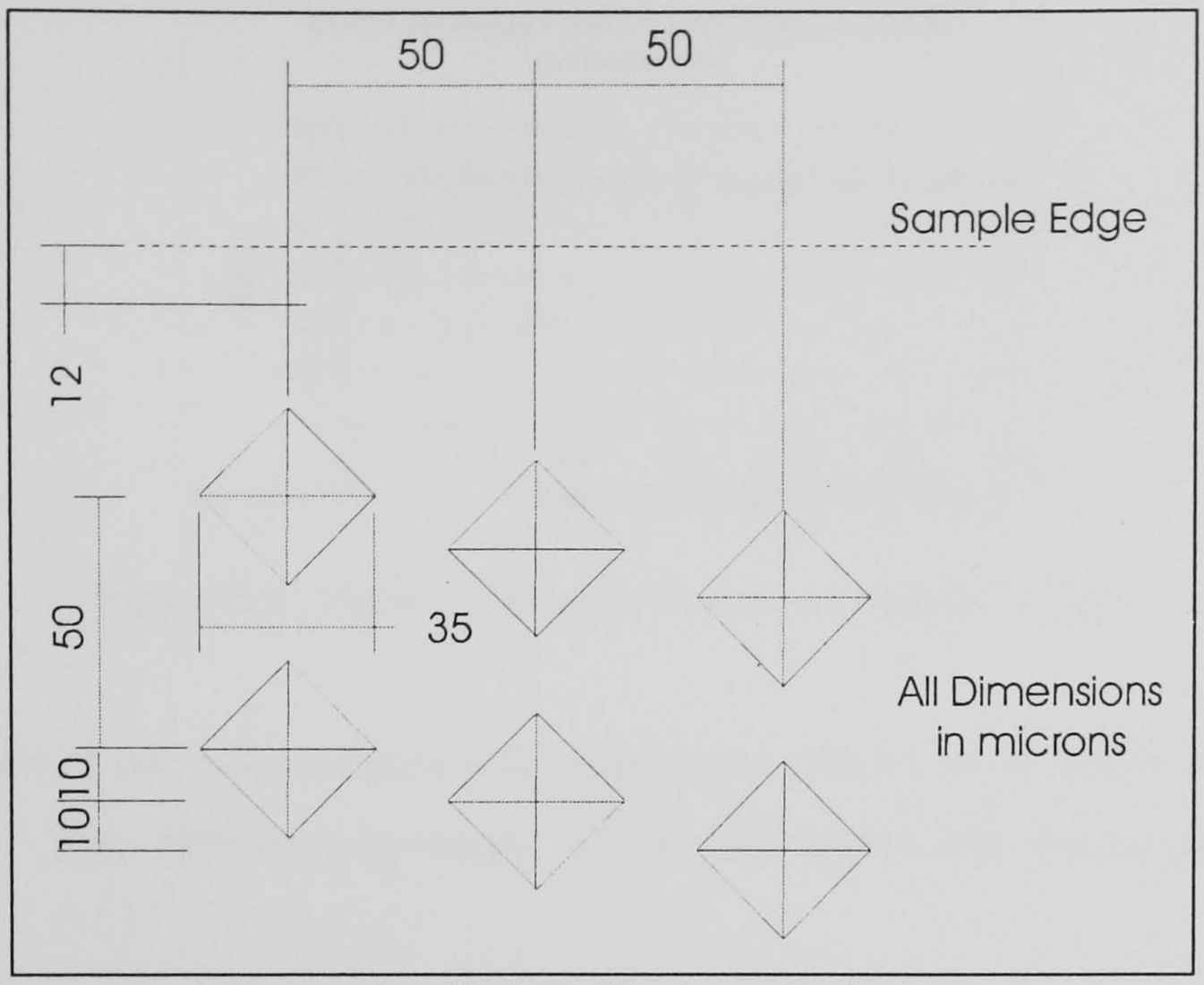

Figure 6.4: Vickers Hardness Technique

Figure 6.4 shows the general technique followed to acquire the Vickers hardness profiles for all samples. For IN718 a load of 300grammes force was used for a duration of 15 seconds. At this load and time setting nominal indentation sizes were 35microns. Tests were taken at 50micron intervals; this reduced the possibility of indentations interfering with each other to produce ambiguous results. Tests were then taken 50microns measured laterally along the sample and the first test being performed 60microns longitudinally into the sample subsurface and each subsequent test taken using 50 micron intervals. The width in two directions of the indentations were measured and an average was calculated. This average was used in the Vickers tables to produce a hardness value. This procedure was repeated until a nominal substrate hardness had been found, then the testing was moved along another 50microns with the first test being taken 70microns from the edge. With the sample being tested in this manner, and assuming that the hardness was reasonably uniform throughout the sample, an accurate test profile could be acquired.

The Vickers Hardness profile for sample 718-92 is shown in Figure 6.5. From this figure, it is possible that the first two points may have been compromised due to inconsistencies within the material or weaknesses close to the edge of the sample.

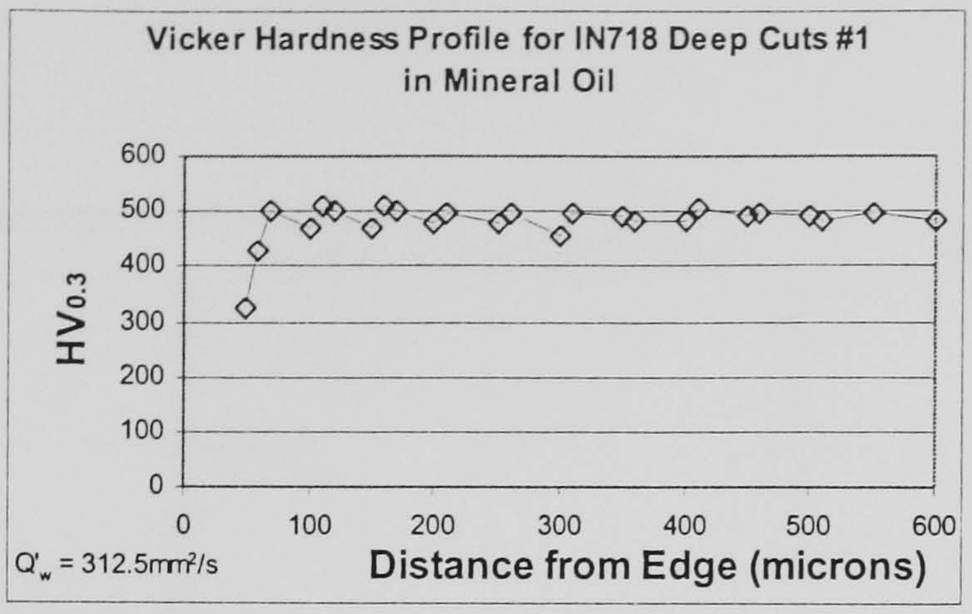

Figure 6.5: Vickers Hardness Profile for sample 718-92

After the set of cuts was completed the wheel was used to cut a profile in a graphite test piece. The difference in height of the two levels was measured using the Talysurf.

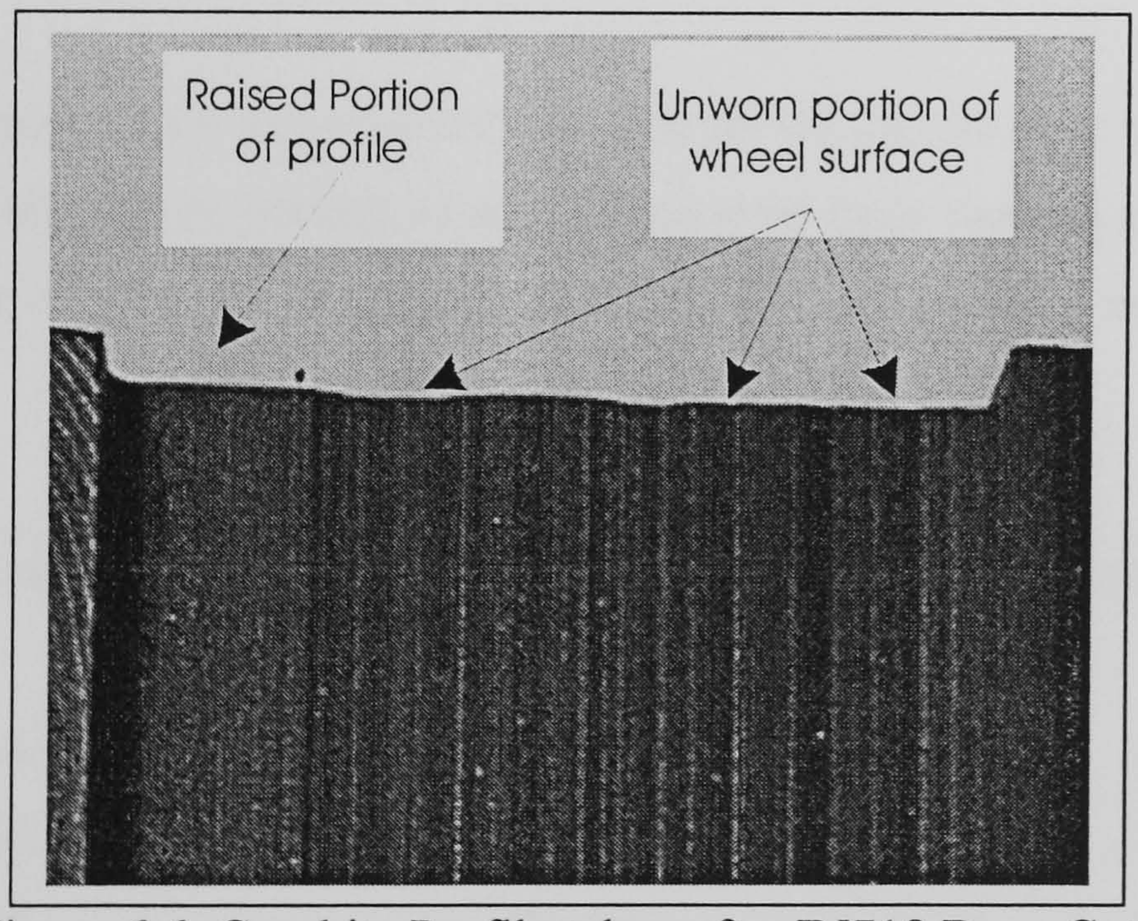

Figure 6.6: Graphite Profile taken after IN718 Deep Cuts

Figure 6.6 shows the surface of the actual graphite block used to calculate the wheel wear after the deep cut experiments were completed.

An example of a worn portion in Figure 6.7 is indicative of the surface of the wheel after conditioning of the active grits and grinding wear. The trace shows two levels of CBN grain heights, the difference in these heights is indicative of the volume of

wheel worn away during the set of tests, and from this figure the grinding ratio can be calculated.

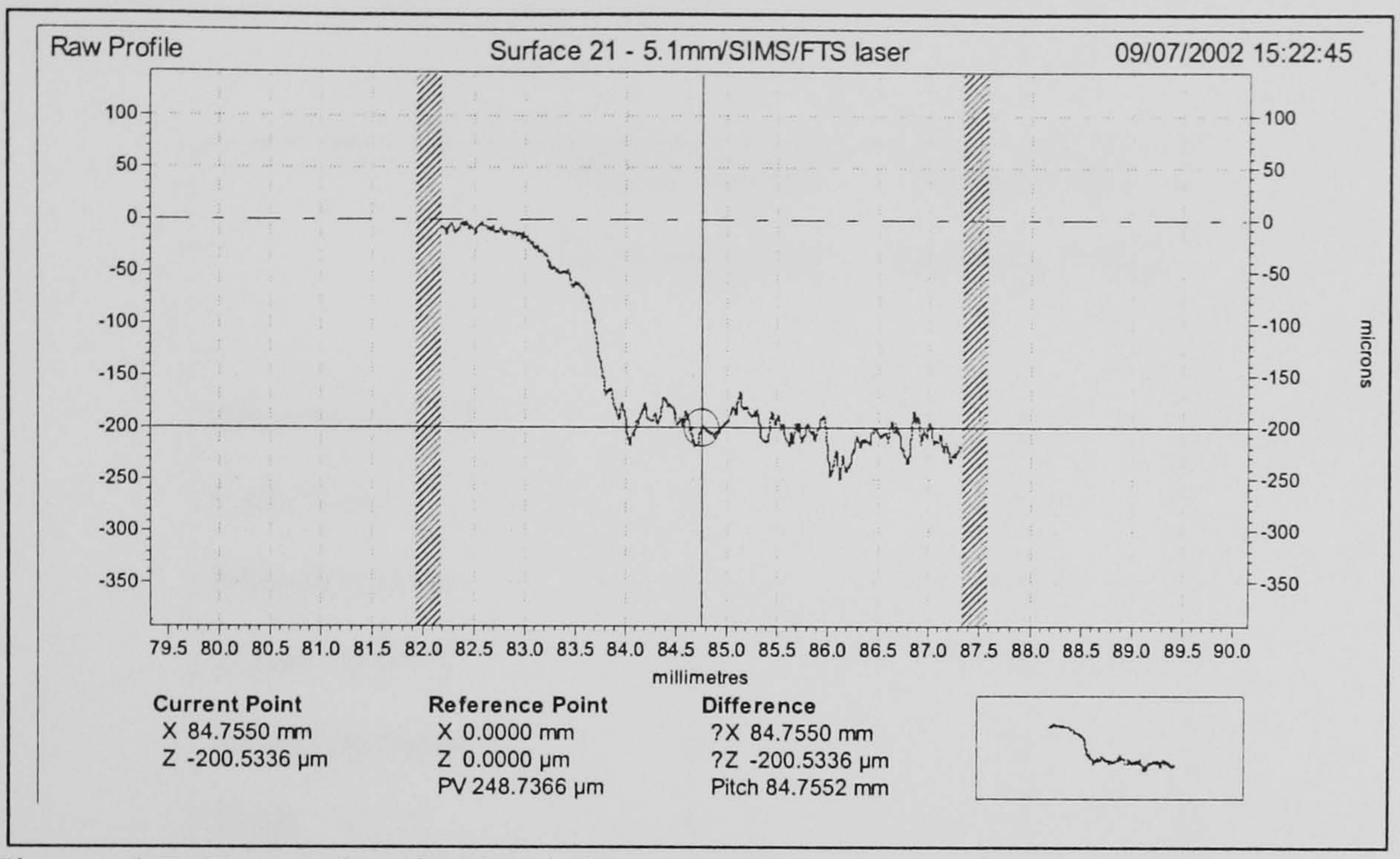

Figure 6.7: Example of Wheel Wear Profiles taken after Grinding Operation

The highest grinding ratio recorded for this material during the deep cut tests was 20, which is relatively low in relation to what is required from modern grinding wheels, but at this stage of experimentation the operating parameters were in no way finally optimised.

Wheel Number	Grinding Fluid Type	Grinding Ratio
B252-4	Mineral Oil	39.18
B252-6	Mineral Oil	19.63
B252-5	Water	18.18

Table 6.3: IN718 Grinding Ratios

Table 6.3 shows the three grinding ratios calculated using B252 wheels for this material. Carius (1989) reported that when grinding IN718 with CBN using mineral oil as a grinding fluid, this outperformed grinding with water based grinding fluid by 1.5 to 9 times. This was due to CBN being broken down to boric acid in the presence of high temperature steam when using water based fluids.

Table 6.4 shows the results of a study carried out by Abrasive Technology Inc. (1989) where 1 indicates the poorest and 4 the best response. It can be seen that the straight mineral oil has virtually the opposite set of results to that of the water based grinding fluid.

	Water Based Grinding fluid	Straight Oil Grinding Fluid
Heat Removal	4	1
Lubricity	1	4
Maintenance	3	4
Filter Ability	4	1
Environmental	4	1
Cost	4	1
Wheel Life	1	4

Table 6.4: Grinding Fluid Characteristics

6.2 Analysis of Responses

6.2.1 Specific Grinding Energy

Figure 6.8 shows that the specific grinding energy reduces with an increase in specific material removal rate. For this material the values of specific grinding energy seem to be around 13 J/mm^3 to 21J/mm^3 for the highest removal rate tried in these tests. Also included in this figure is the best fit of the average specific grinding energy trend line, which is $y = 85Q'_w{}^{-0.3}$, where y represents the calculated average specific grinding energy of the experimental set. This expression will be used to calculate predictive temperatures using Rowe & Jin's thermal modelling approach in Part 6.2.4 of this chapter, Rowe & Jin (2001).

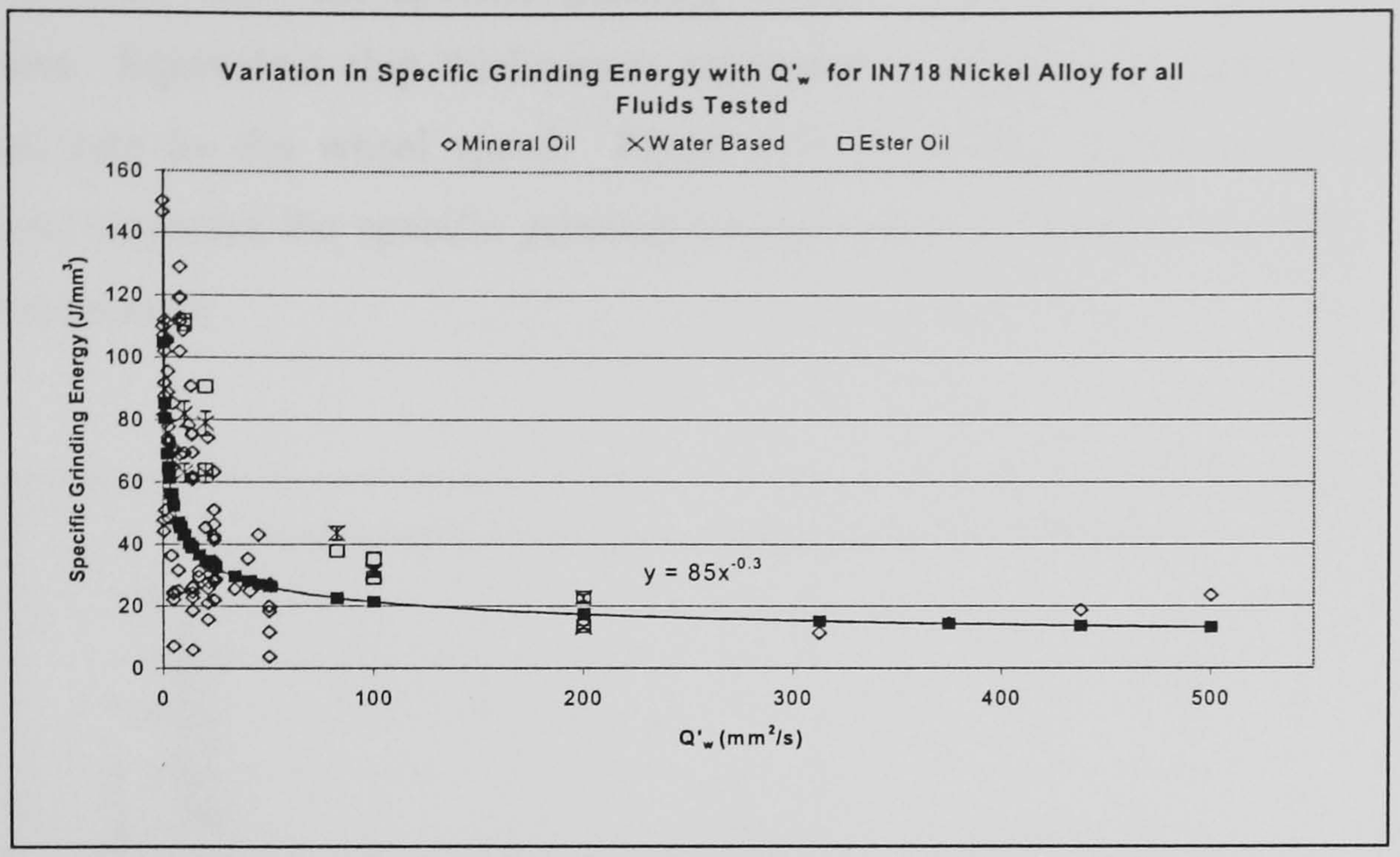

Figure 6.8: Specific Grinding Energy to Q'_w for IN718

Figure 6.8 shows the complete dataset for IN718 for all conditions and fluid types used throughout these tests. The three fluids were a mineral oil; ester based synthetic oil and a water based fluid. Throughout these tests water based fluid and ester based fluid produced the least efficient results with the highest wheel wear characteristics. It can be seen in Figure 6.8 that both the crosses and boxes, which denote these fluids respectively, are consistently at the upper edges of the dataset. Howes (1987) tested water based fluid and found that in a shallow cut environment fluid boiling limits cooling effectiveness and lubricating properties. He also found that grinding conditions were reasonably stable until the 130°C fluid temperature was surpassed, when the water based fluid boiled away and the energy partition ratio to the workpiece increased. The boiling of the fluid would increase wheel wear and finished workpiece temperatures through the production of flats on the grits due to lack of grinding fluid and higher frictional forces. For this reason, the mineral oil based fluid produced the lowest specific grinding energy and the best wheel wear characteristics.

One can also view the specific grinding energy with regard to equivalent chip thickness. Equivalent chip thickness is calculated by dividing the specific material removal rate by the wheel speed. Figure 6.9 shows that as the equivalent chip thickness increases the specific grinding energy reduces, thereby indicating a more efficient process.

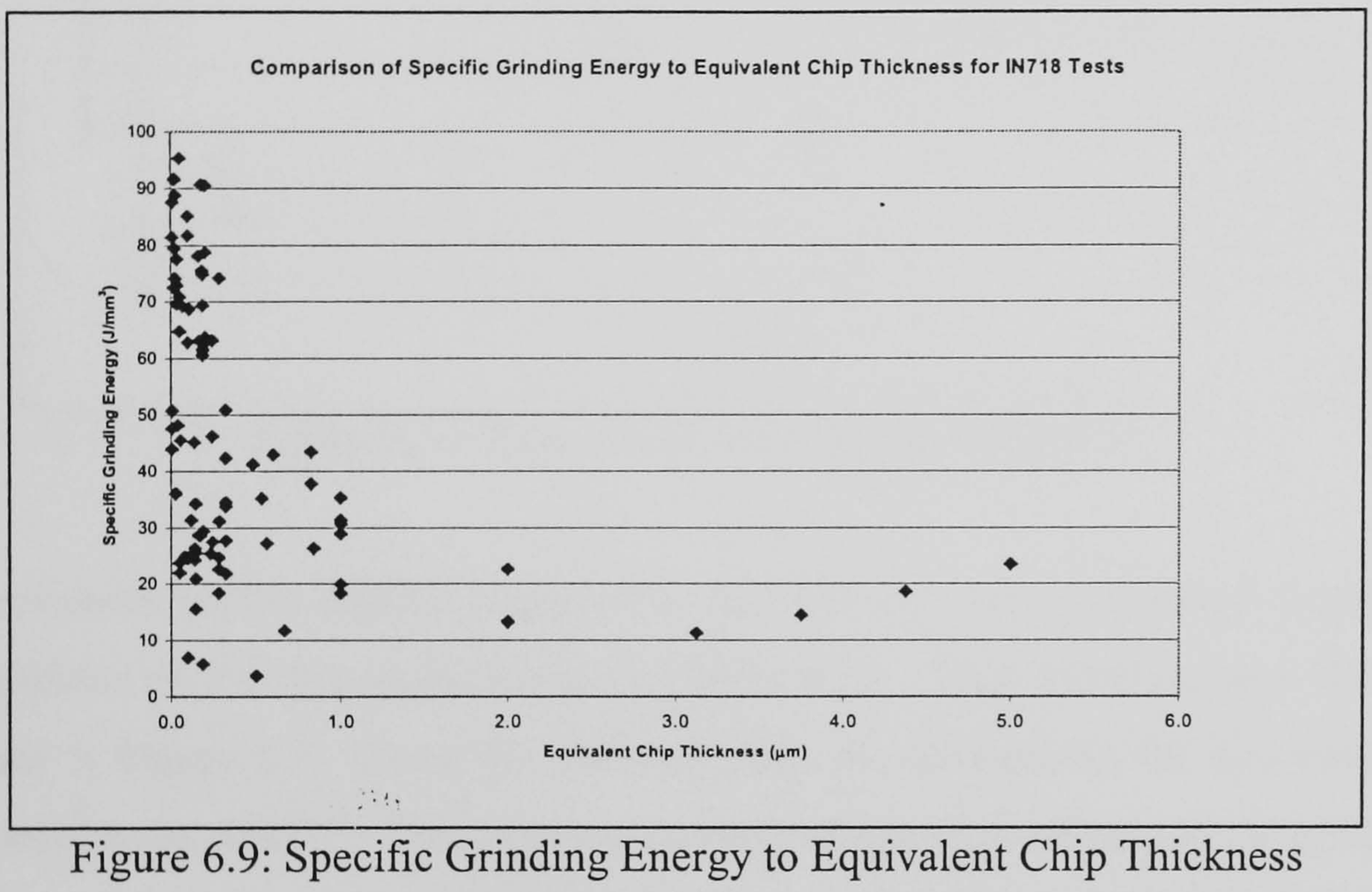

Figure 6.9: Specific Grinding Energy to Equivalent Chip Thickness

Figure 6.10 shows the burn threshold diagram for the complete data set for IN718. The dotted line denotes a nominal boundary between burn and no burn samples. This diagram shows the whole range of results where the surface was assessed visually for the onset of burn, and it can be seen that the demarcation line is quite distinct even at higher $f(D^{1/4}a_e^{-3/4}V_w^{-1/2})$ values.

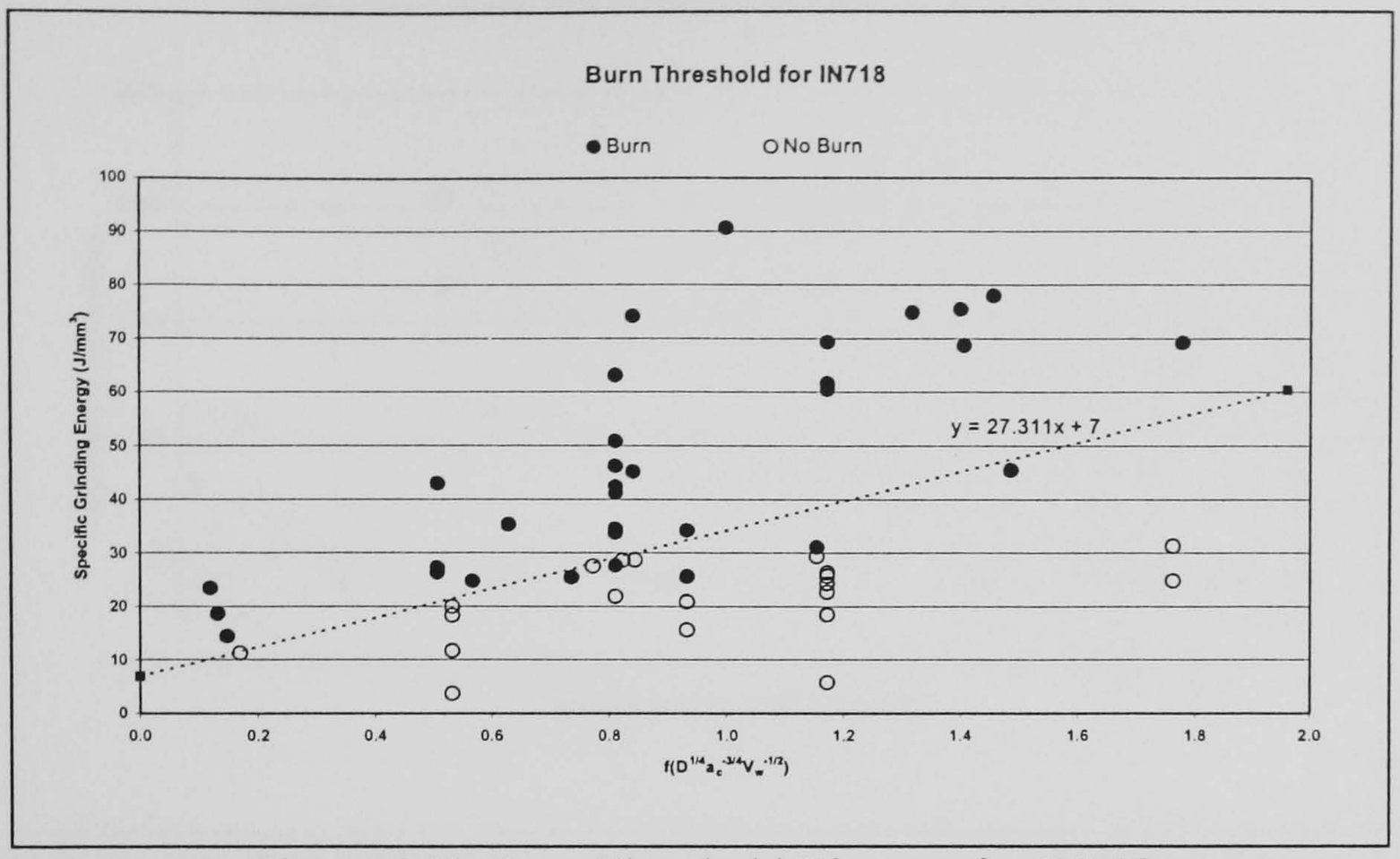

Figure 6.10: Burn Threshold Diagram for IN718

As previously shown, Malkin's equations calculate the burn temperature based upon the gradient of the demarcation line in Figure 6.10. This technique was shown in Chapter 5, Figure 5.3. Using the same equation the temperature for this material is calculated to be 4782°C. This figure is virtually double that calculated for M50 steel. This is probably due to the thermal conductivity of IN718 being less than half of that for M50.

6.2.2 Stress Measurement

Cullity (1967) states the plastic deformation of a material can be induced through thermal or mechanical means. An added concern when grinding IN718 is the thermal conductivity which has a value of 11.4W/mK. This indicates that the material retains much of the heat generated at the surface further enhancing the probability of high temperatures being retained at the surface and subsequent tensile stress profiles being formed.

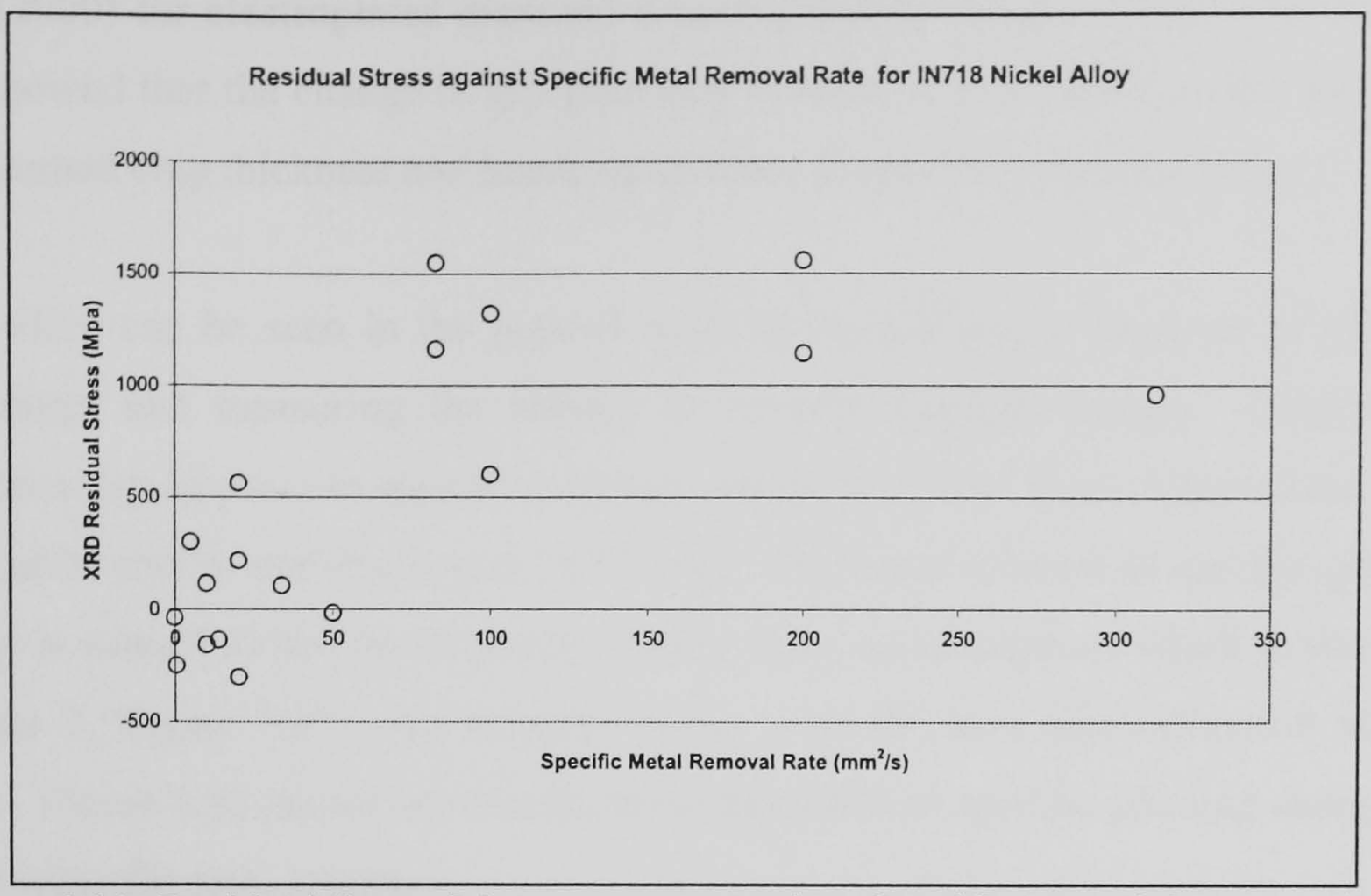

Figure 6.11: Residual Stress Measurements against Specific Material Removal Rate

Due to the need to use a Manganese K alpha radiation as prescribed by Prevey (1986), stress measurements were carried out at the University of Manchester Institute of Science and Technology (UMIST) in Manchester. Figure 6.11 shows the change in measured surface residual stress with specific material removal rate and demonstrates how compressive stresses can be generated at lower Q'_w values. However these quickly become tensile as the material removal rate is increased which suggests that the surface temperature also increases. It should be noted that it is common for this type of alloy to exhibit tensile residual stress profiles after grinding. Figure 6.11 also indicates that at the highest value of Q'_w the tensile residual stress is levelling off or even decreasing, as might be expected if the HEDG effect (Chapter 2, Figure 2.6) occurs.

6.2.3 Surface Characterisation

The specific grinding energy is determined by components associated with cutting, ploughing and sliding. Stock removal is primarily associated with the cutting component. Thus, this suggests that for a given value of equivalent chip thickness, the ploughing and sliding components must change. This should be expected as the abrasive grit geometry changes as a result of wheel wear. The development of wear flats and an increase in the total grit/workpiece contact area will result in an increase in specific grinding energy. Similar observations have been made recently by Hwang

et al (2000) for electroplated diamond wheels grinding silicon nitride. Hwang et al also showed that the change in grit geometry resulted in a reduction in the maximum undeformed chip thickness and hence an increase in specific grinding energy.

This effect can be seen in the present work by considering a fixed set of grinding parameters and measuring the change in specific grinding energy. Figure 6.12 illustrates the increase in specific grinding energy with total stock removed for a Q'_w value of 24 mm^2/s and wheel speed of 75 m/s. The linear increase in specific grinding energy is related to the development of wear flats, an example of which is shown in Chapter 7, Figure 7.25. An increase in the wear flat area also influences surface finish. Figure 6.12 shows how the R_a value decreases as specific grinding energy and hence wear flat area, increase.

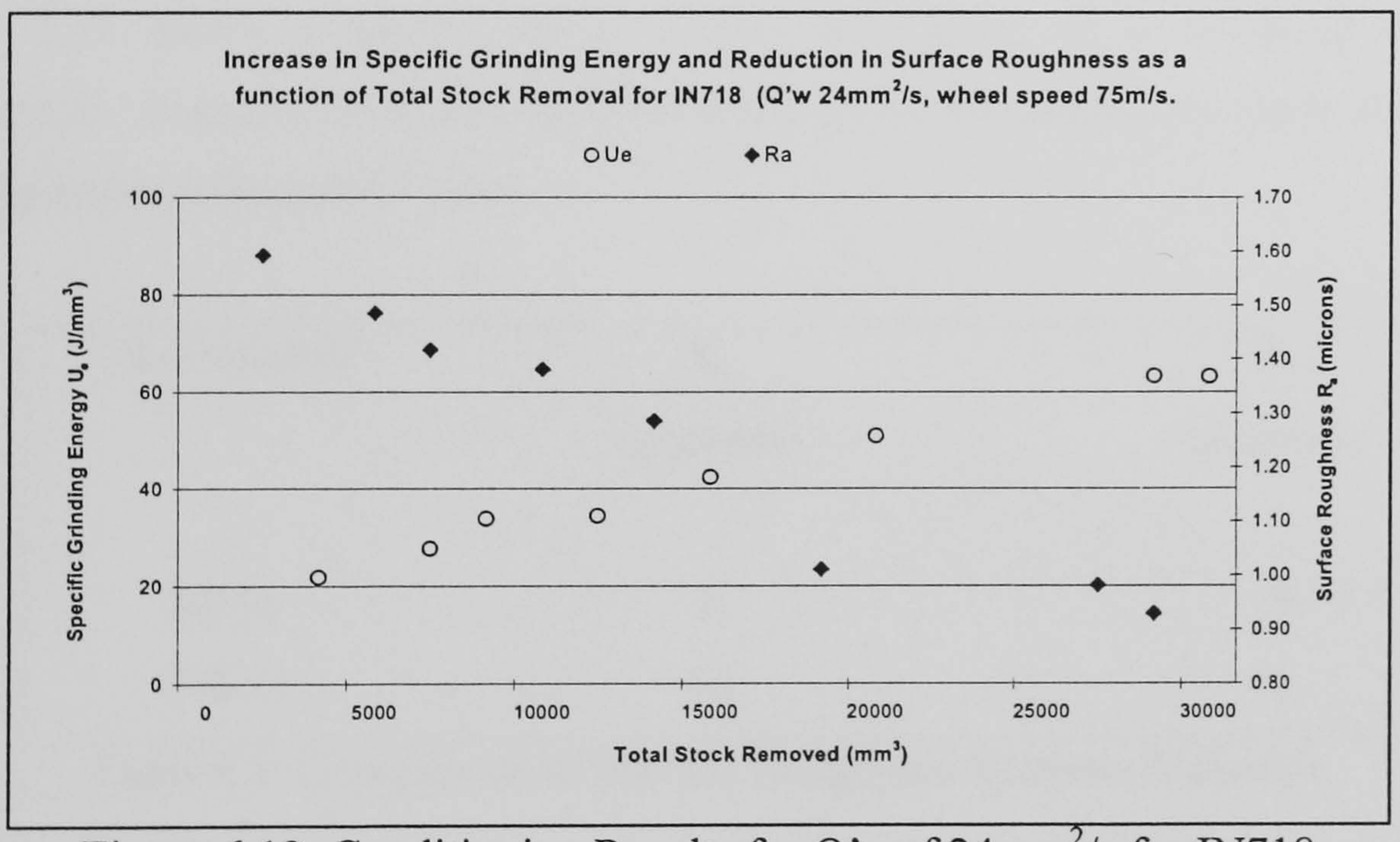

Figure 6.12: Conditioning Results for Q'_w of 24mm^2/s for IN718

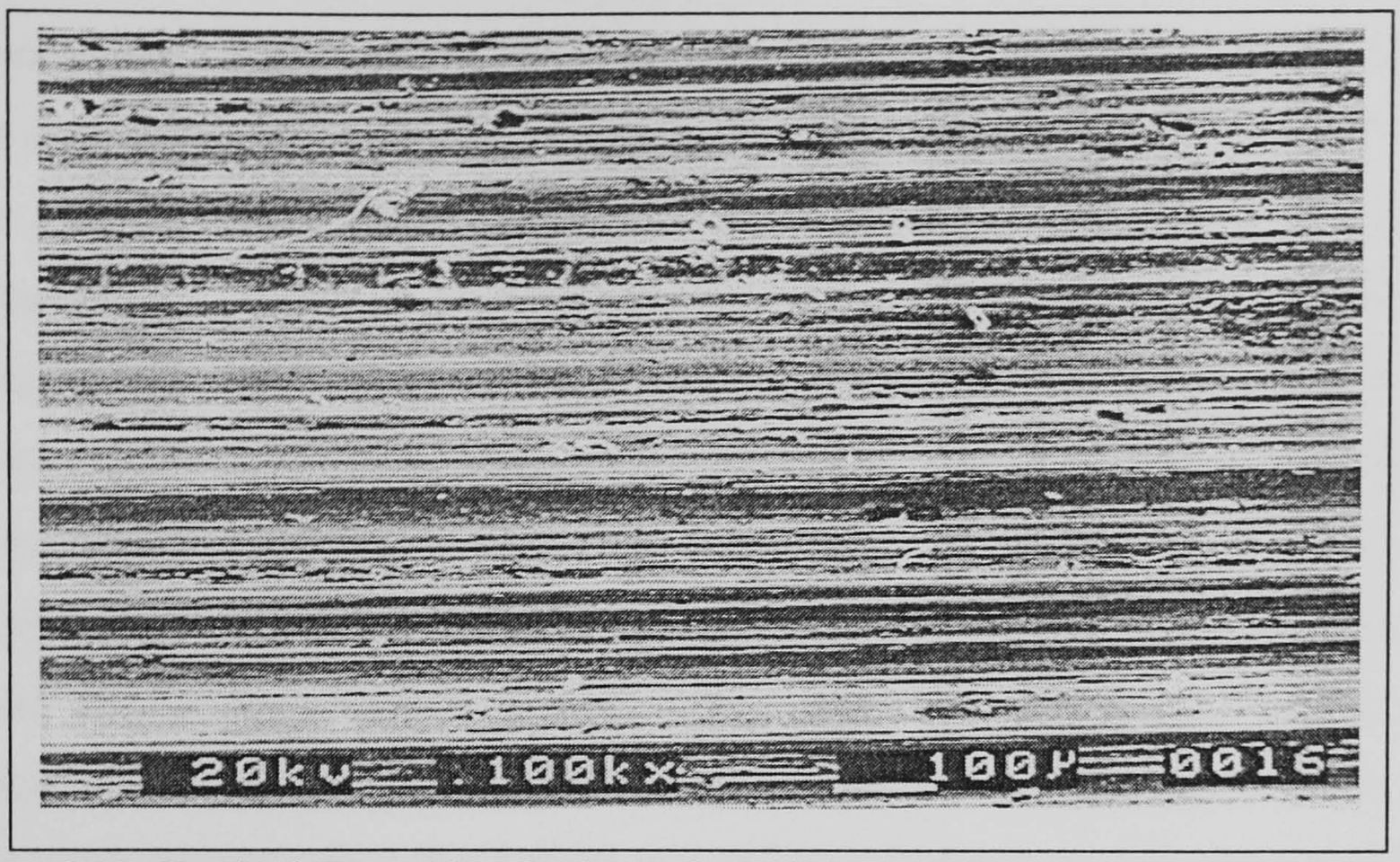

Figure 6.13: Typical Example of a Scanning Electron Micrograph of IN718 Surface

Figure 6.13 shows a typical IN718 surface as viewed by a scanning electron microscope. Figure 5.14 shows an SEM image of a comparable cut taken using the same parameters from M50 steel.

Test Number	R_a (microns)	R_t (microns)
50-11	2	19
718-13	7.1	41

Table 6.5: Comparison of Surface Roughness between Materials

Table 6.5 highlights that the surface for IN718 is a poorer surface finish and has been subjected to higher proportions of grit rubbing, sliding and ploughing actions. If these components of the total specific grinding energy are increased then the temperature experienced by the sample is increased and therefore the requirement of an efficient grinding fluid strategy is of paramount importance especially with this type of material.

6.2.4 Theoretical Modelling

The responses of each of the individual grinding operations have been noted and visual assessment of the level of oxidation has been carried out and cross referenced to the predicted temperature that this oxidation occurred in relation to the specific grinding energy. Rowe & Jin's analysis has been applied to the measured specific grinding energy levels to produce a plot which is designed to predict the temperature at which oxidation will occur during grinding IN718. The plot replaces the measured specific grinding energy values with calculated temperatures for the finished workpiece surface. This diagram is shown in Figure 6.14 and the process engineer can use this type of diagram to predict the onset of oxidation/grinding burn with regard to specific grinding energy for any given variation of depth of cut and feedrate. Figure 6.14 indicates that the boundary line between burn and no burn regions for IN718 is around 550°C.

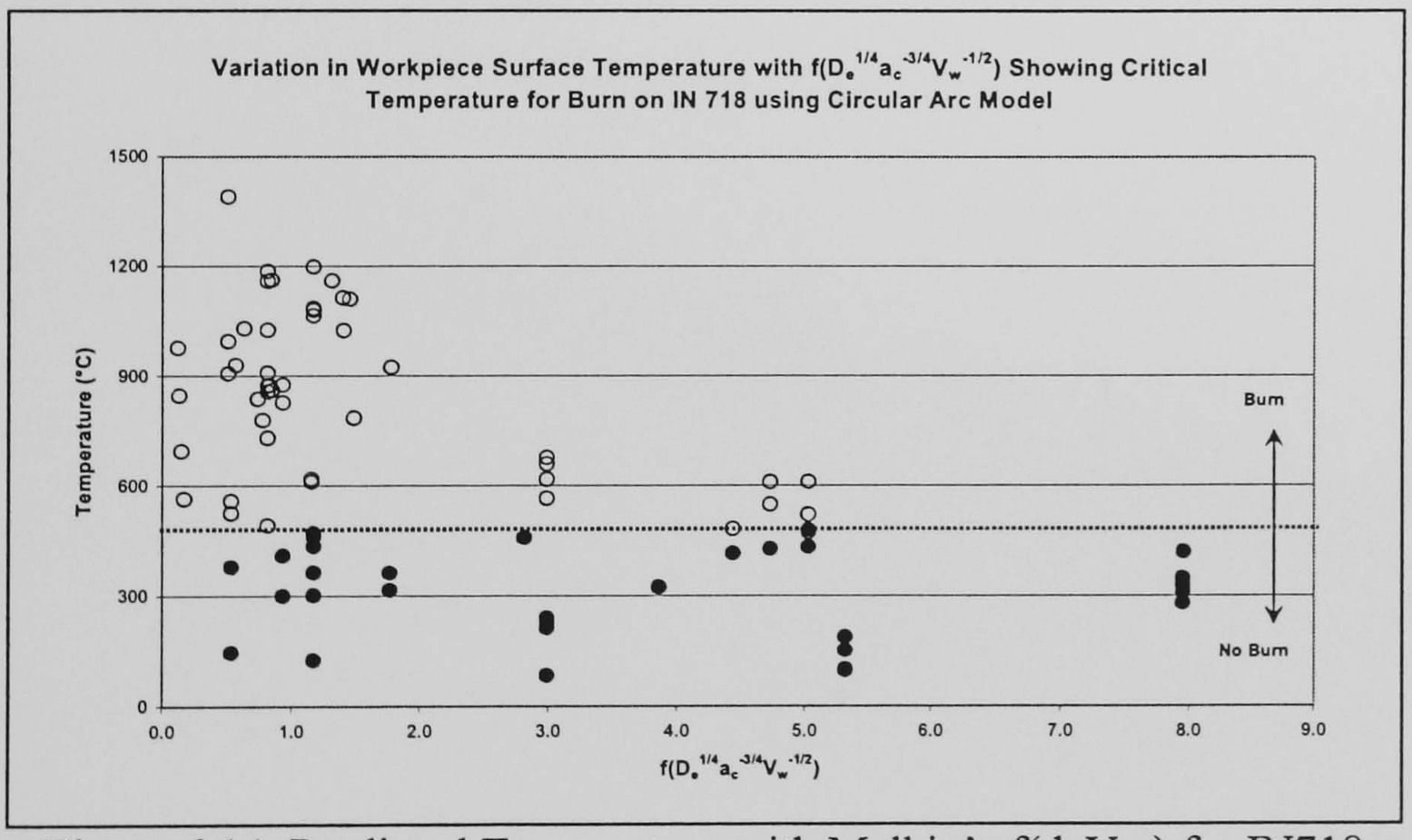

Figure 6.14: Predicted Temperature with Malkin's f(daVw) for IN718

6.3 Summary

This Chapter has highlighted and discussed the difficulties associated with grinding the nickel based superalloy IN718. The results for IN718 have correlated well with results found in Chapter 5 for M50 steel. This implies that the trends are common within this type of grinding to all materials and so heightened the importance of this fundamental study. Taking these findings as a reference, the research has been taken forward to be implemented in the component manufacturing phase which is described in Chapter 7.

CHAPTER 7 VALIDATION EXPERIMENTS

The previous chapters investigated the HEDG effect with regard to various experimental outputs and theoretical predictions concerning M50 steel and IN718 nickel based superalloy. This chapter investigates two basic areas of grinding both regarding M50 steel;

- influence of ultra high specific material removal rates upon the finished workpiece surface for M50 steel concerning both up and down grinding

- thermal characteristics within the grinding zone

Therefore part one investigates the high specific material removal rates, part two presents experimental temperature measurements and the chapter summary is given in part 7.3.

7.1 High Q'_w Removal Rates

These experiments were designed to investigate the influence of wheel direction and depth of cut at one specific material removal rate.

7.1.1 Experimental Procedure

It was calculated by graphical means that when using a 100mm long specimen it would take a 200mm diameter wheel 43mm from point of initial contact to actually experience a full 10mm depth of cut. This is shown in Figure 7.1.

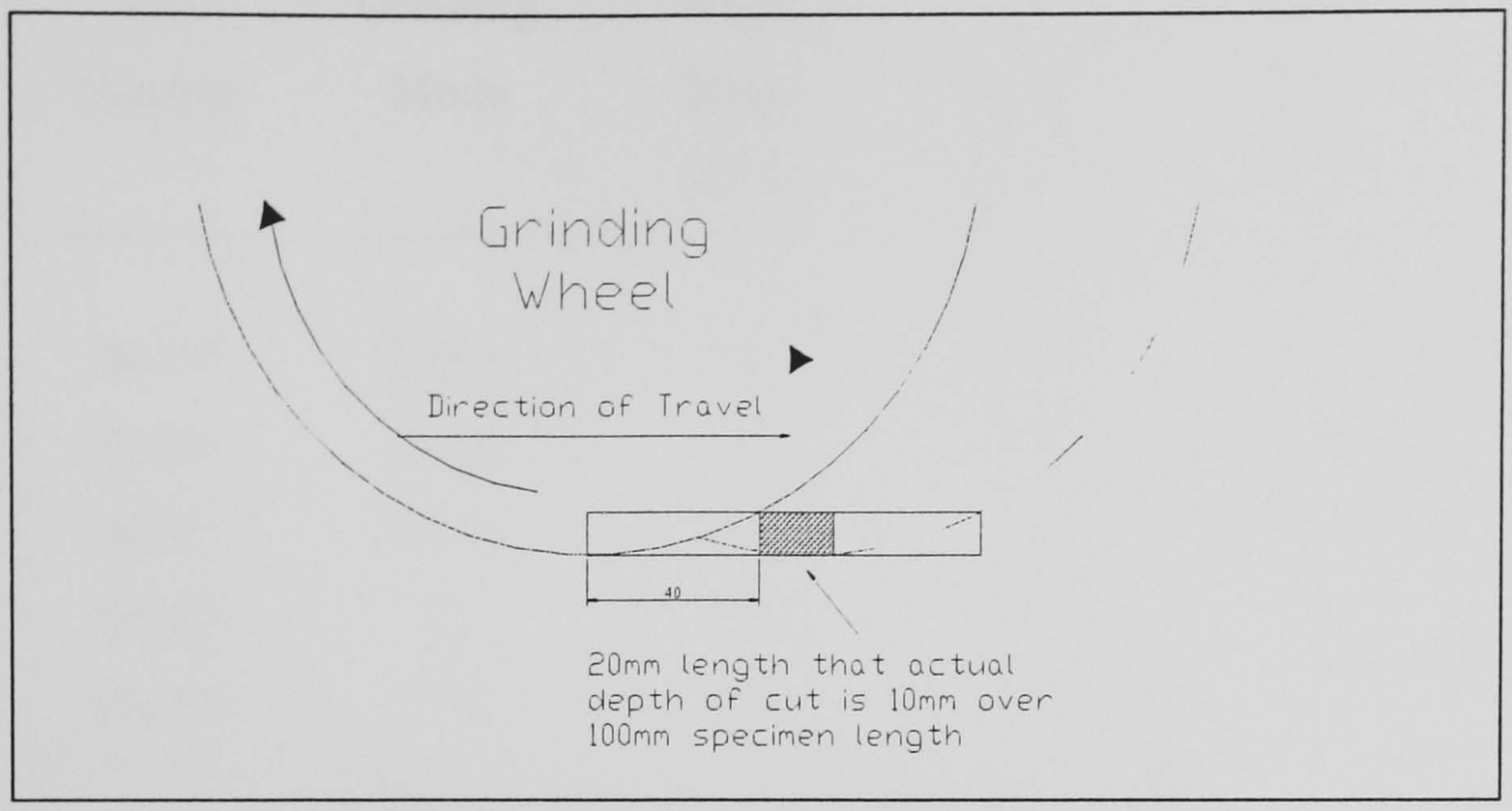

Figure 7.1: Position of the True10mm Depth of Cut

In addition, this true depth of cut would be experienced for only 20mm of the cut length after which point the depth of cut decreases for each test. Two samples were taken from each of the 20mm full depth of cut lengths for analysis purposes. At all times the spindle power was measured by the Hall Effect Probe and the grinding forces were measured via the Kistler Dynamometer.

With the sample fixed to the Kistler Dynamometer a 'touch on' cut was performed and then a full 10mm depth of cut was taken at a feed rate of 125mm/s giving a Q'_w value of $1250mm^2/s$. The series of tests, outlined in Table 7.1, were designed to investigate the influence of up and down grinding and wheel speed on the finished surface.

The initial cut was taken in a down grinding mode using the nozzles designed by Webster et al (1995), who advocated that the impinging fluid velocity should match the peripheral wheel speed and that the nozzle diameter should be that of the width of cut undertaken. A 2mm diameter nozzle was first used with a fluid velocity of 100m/s. Extreme oxidation of the surface deemed this cut to be unsuccessful, and so the cut was repeated but with a 3mm nozzle with the fluid pressure increased to maintain the 100m/s wheel velocity. When using the 3mm diameter nozzle the maximum fluid velocity was calculated as being 126m/s, which was the closest match to the 146m/s wheel speed used in the later experiments.

Test Number	Grinding Mode	Wheel Speed (m/s)	Fluid Velocity (m/s)	Nozzle Diameter (mm)
50-249	Down	100	100	2
50-250	Down	100	100	3
50-251	Down	146	126	3
50-252	Up	100	100	3
50-253	Up	146	126	3

Table 7.1: Parameters used for Deep Cuts

In order to measure the values for spark out power and forces a partial cut at 10mm deep was taken and stopped 45mm from the end of the specimen. In this way it was known that the actual depth of cut was 10mm. The parameters were then repeated, moving the workpiece at the prescribed feedrate until a forward cut of approximately 0.5mm was taken. The feedrate was stopped and the rotating wheel dwelled in that position. Spindle power and forces were recorded and subtracted from the total values taken during the cut. Figure 7.2 shows the samples in position after the spark out operations were carried out.

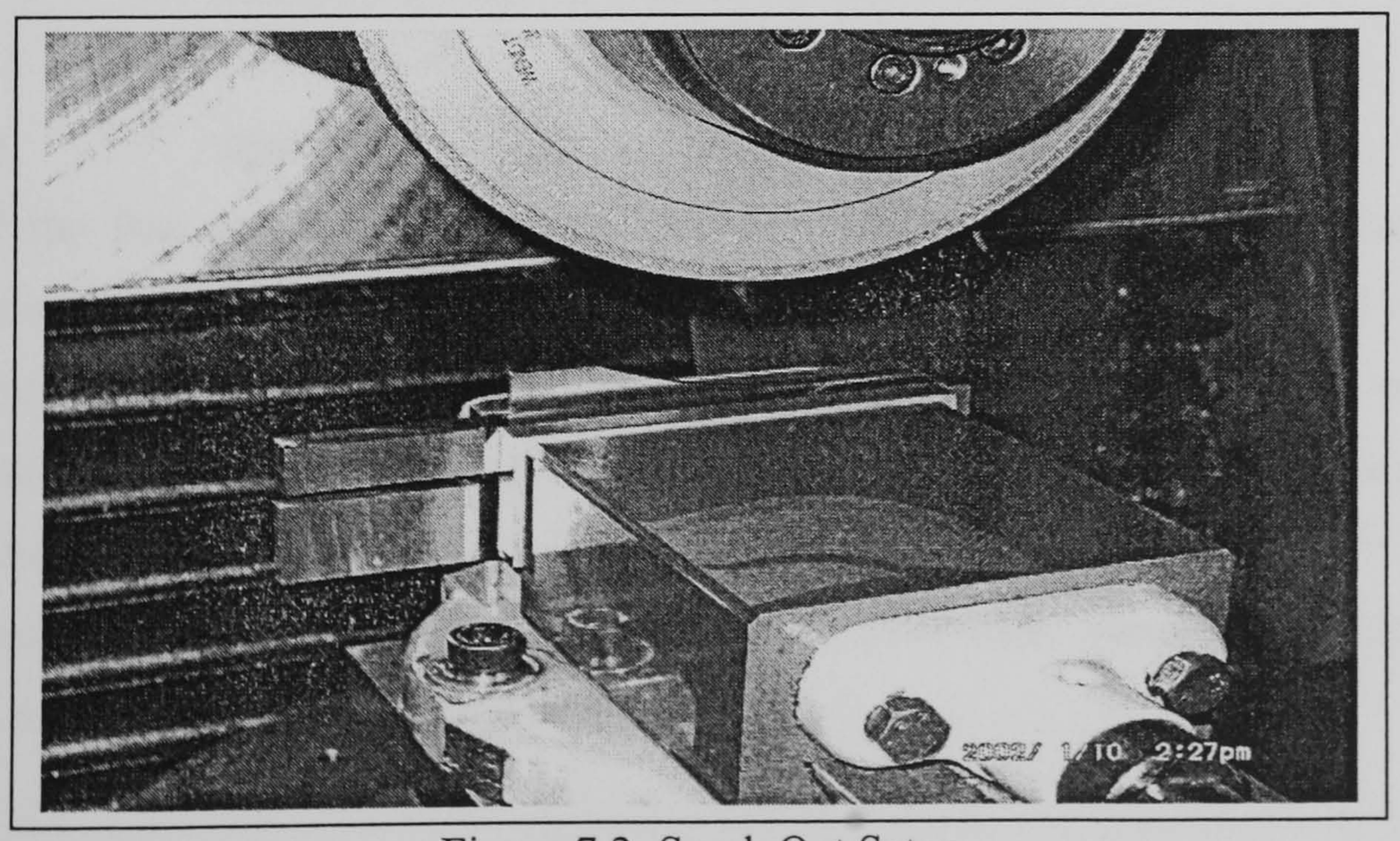

Figure 7.2: Spark Out Setup

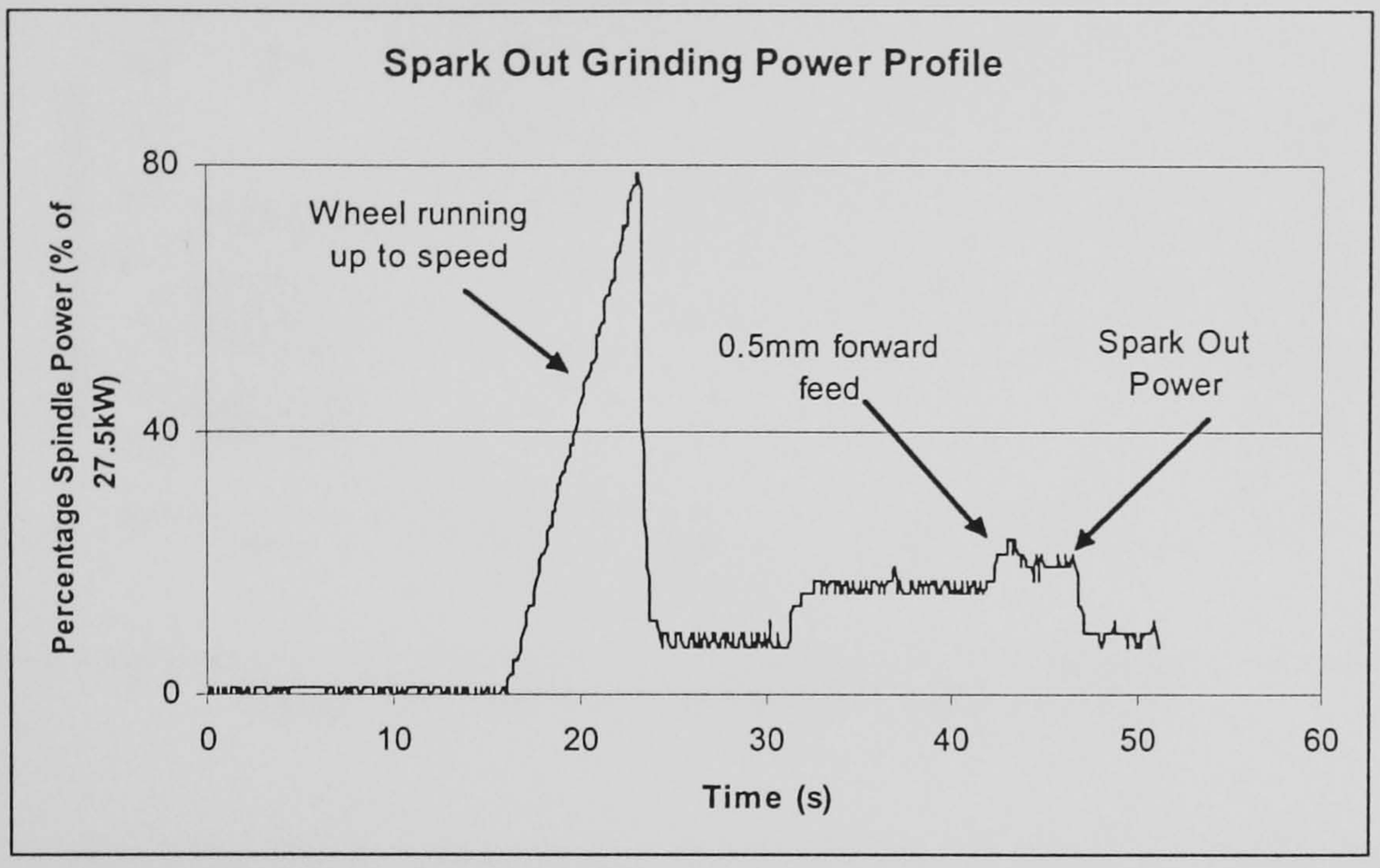

Figure 7.3: Spark Out Power Trace

The spark out power trace shown in Figure 7.3 indicates how the information logged was interpreted. The actual value of spark out power was taken to be the value just after the 0.5mm forward cut power. Using this technique, for each deep cut condition, retained a consistency throughout the deep cut tests and therefore minimised any error.

7.1.2 Analyses of High Q'_w Removal Rate Results

7.1.2.1 Specific Grinding Energy

All of the five conditions tested showed visual evidence of oxidation, although as shown in Figure 7.4, the values of specific grinding energy varied which could indicate that the higher wheel speeds were more successful at these high specific material removal rates. Figure 7.4 shows that the 100m/s wheel speed produced a higher surface roughness measure and specific grinding energies than those recorded for the 146m/s peripheral wheel speed. One could speculate that for these conditions, up grinding seems to produce a more favourable result.

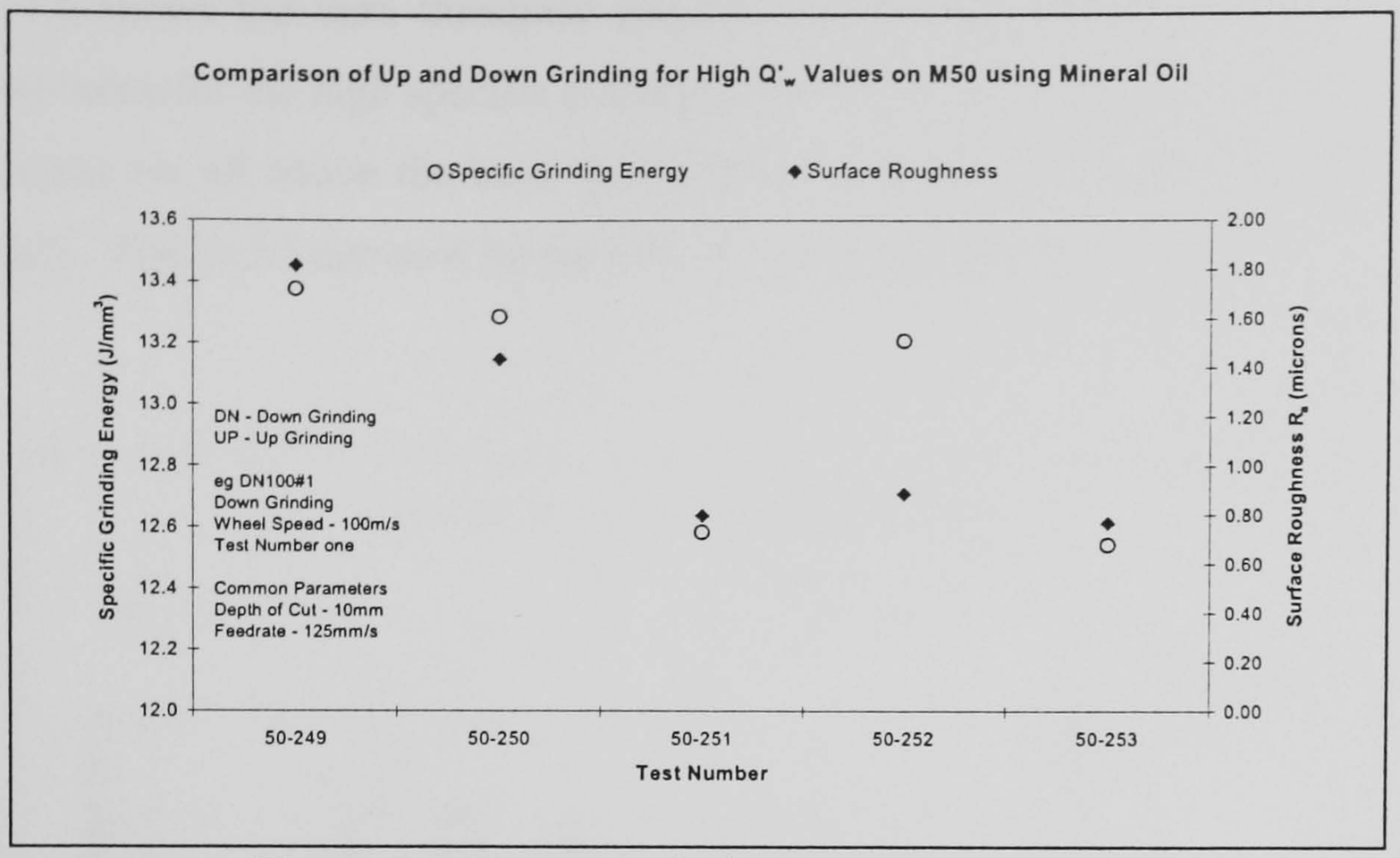

Figure 7.4: Response during Deep Cuts on M50

Figure 7.5 shows the power usage during the deep cuts on M50. It can be seen that at the higher peripheral wheel speeds the net grinding power required for the cut decreases but the spark out power increases. This concurs with the theory put forward by Tawakoli (1993) that with increased wheel speed the temperature decreases. When the wheel speed increases the amount of active grits increase during a cut which would reduce the wear on each individual grit, reducing the production of flats on the grits and thereby reducing specific grinding energy.

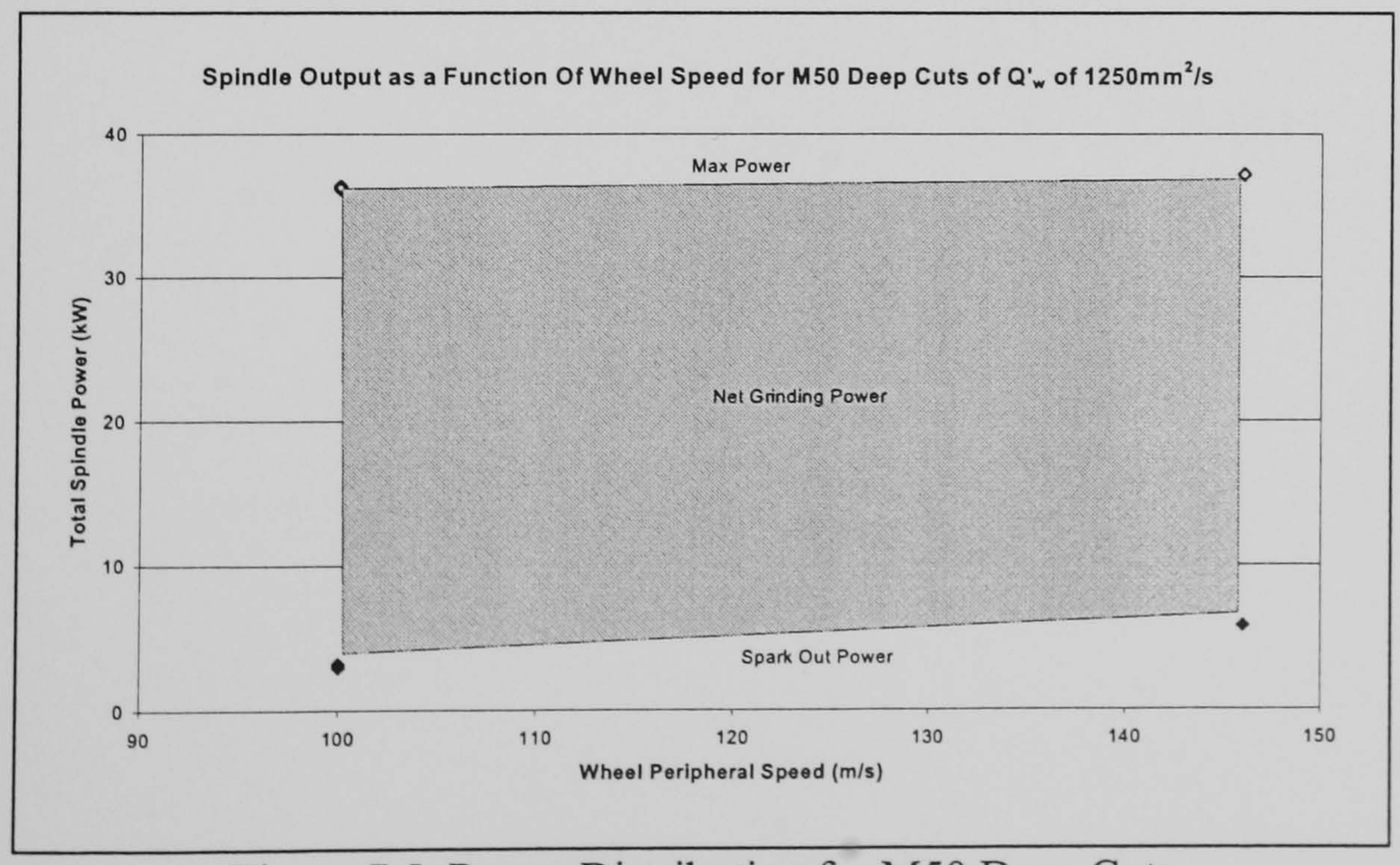

Figure 7.5: Power Distribution for M50 Deep Cuts

Figure 7.6 shows the burn threshold diagram for all tests carried out on M50. The f(DaVw) value for the high specific material removal rates was 0.06. It can be seen that these points are all above the burn threshold line, thereby following the trend shown previously. Figure 5.3 can now be replotted to include the deep cut results.

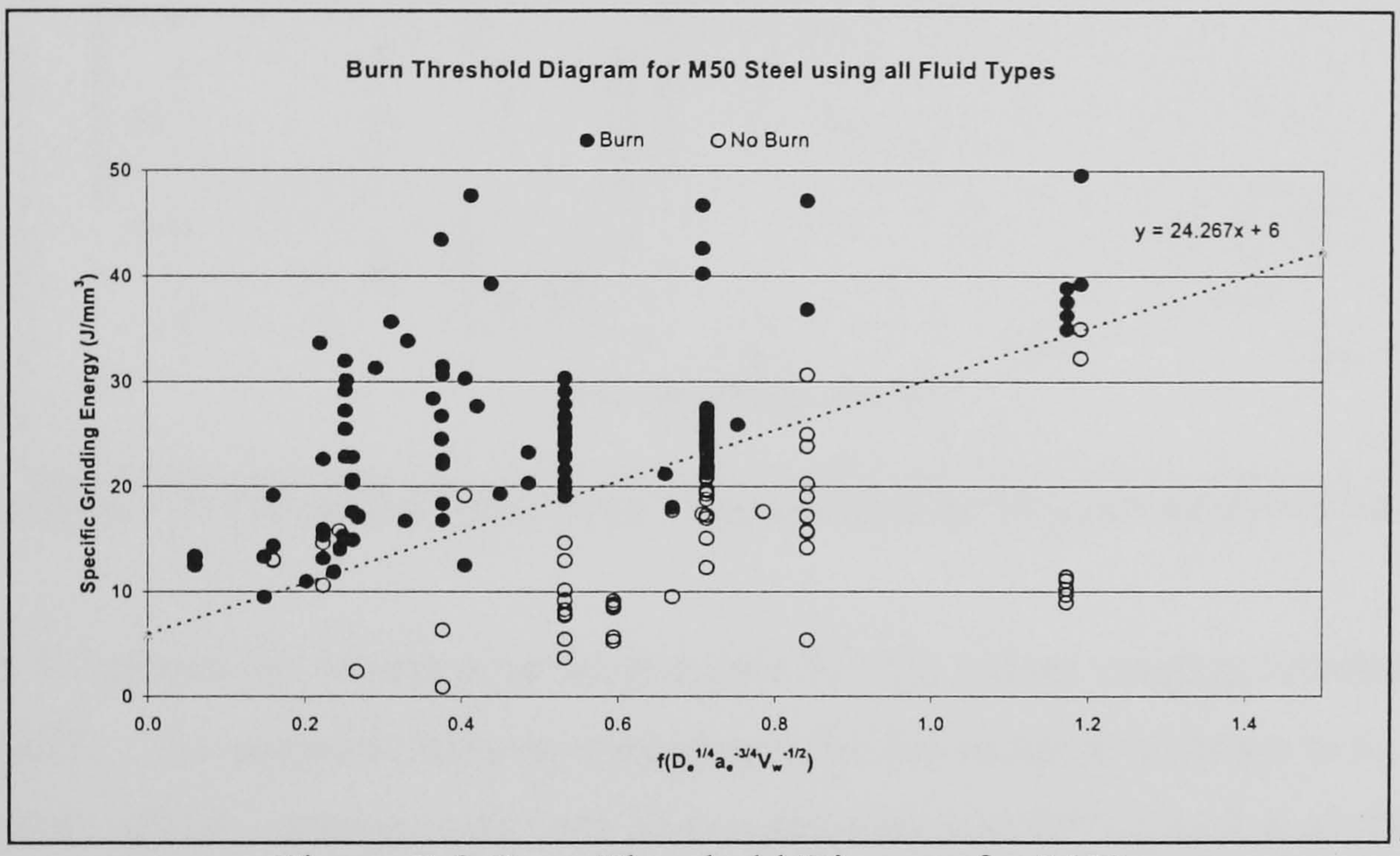

Figure 7.6: Burn Threshold Diagram for M50

The results in Figure 7.6 can be re-plotted to illustrate the variation in predicted workpiece temperature with specific stock removal rate.

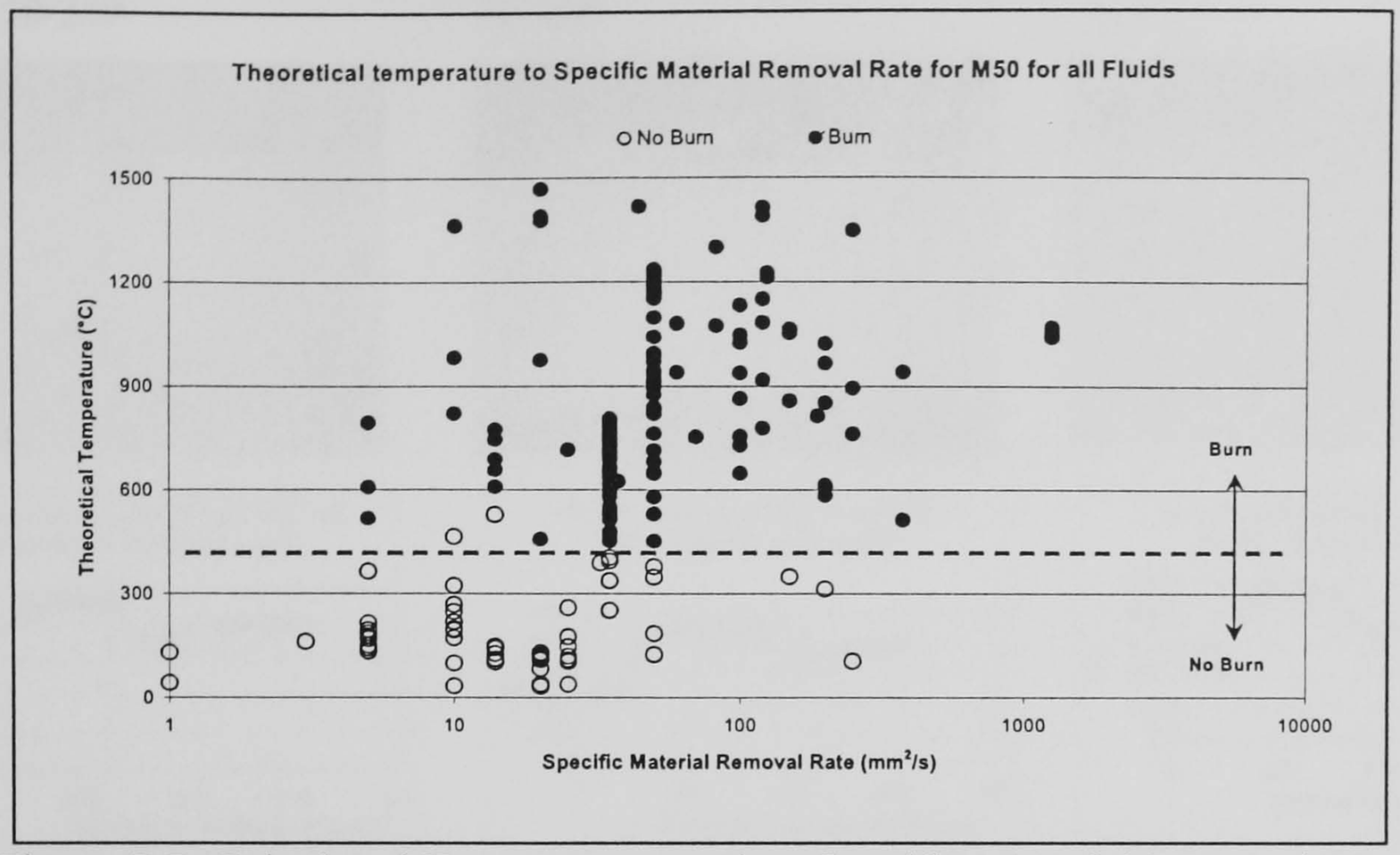

Figure 7.7: Calculated Temperature against Specific Material Removal Rate

Figure 7.7 shows the variation in temperature for Q'_w values ranging between 1 and 1250mm^2/s. The predicted burning temperature for this material is shown to be around 400-450°C, which correlates well with other authors such as M^{c}Cormack et al (2001).

7.1.2.2 Surface Characterisation

The sub surface microscopy results shown in Figure 7.8 illustrates severe grinding damage was evident in all the down grinding operations carried out. Also the micrograph results matched reasonably well with the Vickers hardness profiles. These correlated well with the specific grinding energy results and the burn threshold diagram plots.

Sample 50-249	50-250	50-251
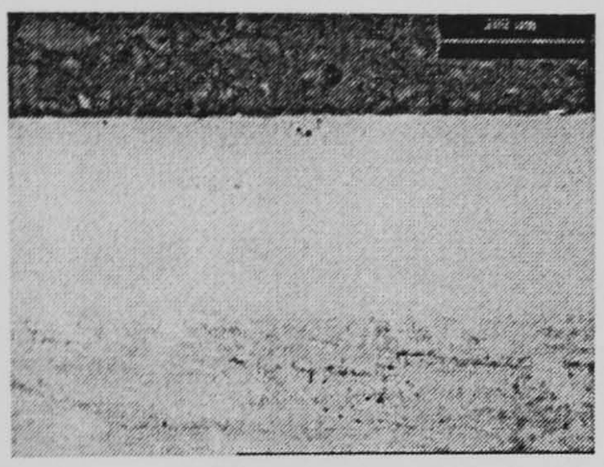	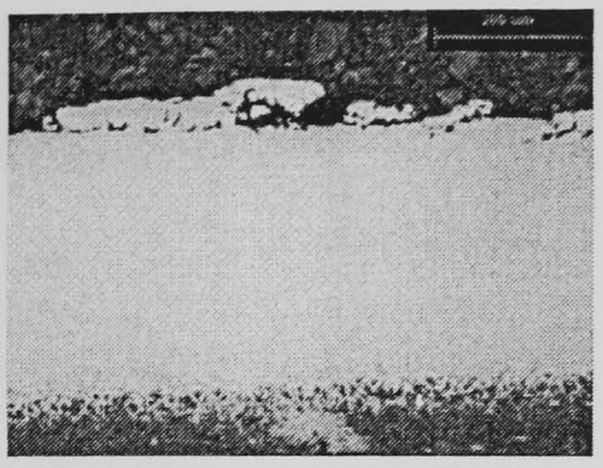	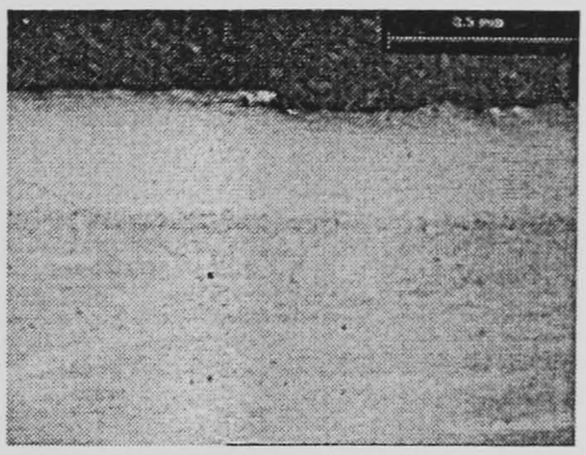
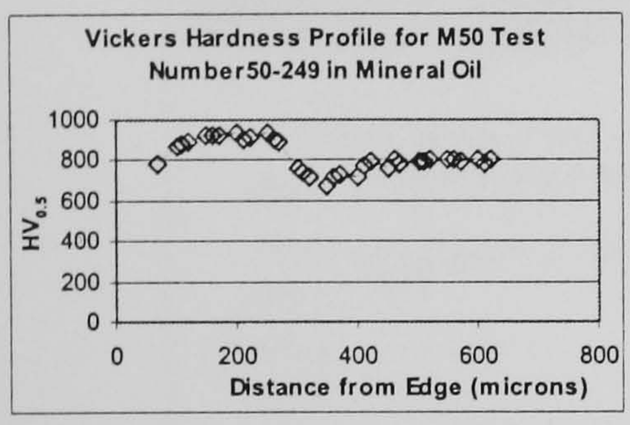	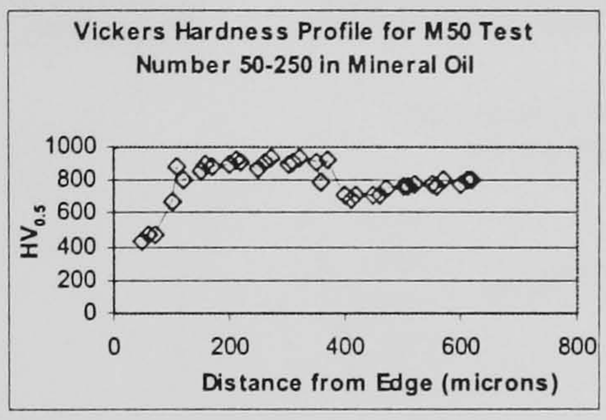	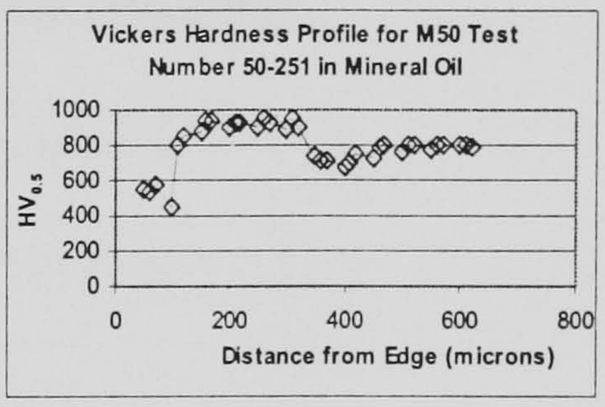
White Layer – 250μm	330μm	270μm
Over-tempered Region - 180μm	110μm	150μm
Predicted Temperature		
Circular Arc Model 1069°C	1058°C	1047°C
Heat Transfer Equations 875°C	902°C	882°C

Figure 7.8: Workpiece analysis Result for Down Grinding Deep Cuts

As well as excessive grinding damage the down grinding mode sample showed evidence of surface cracking and surface oxidation damage.

Sample 50-252	50-253
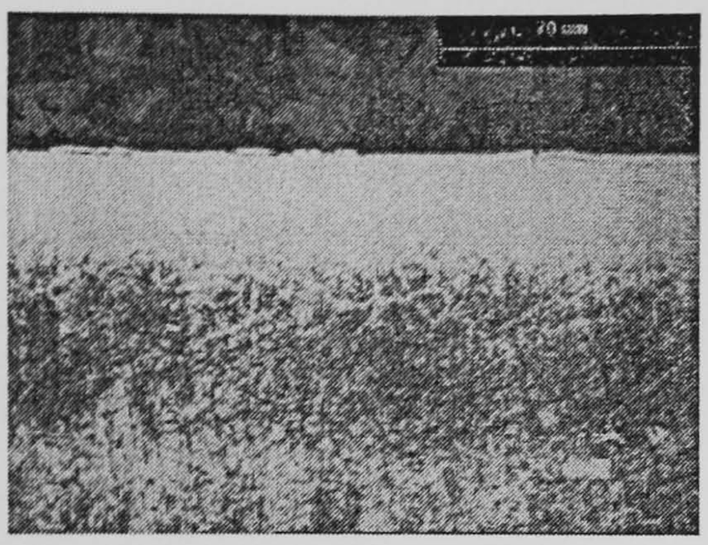	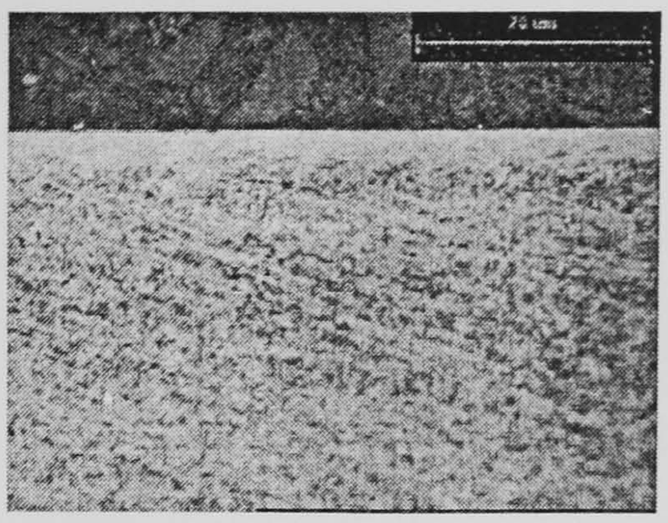
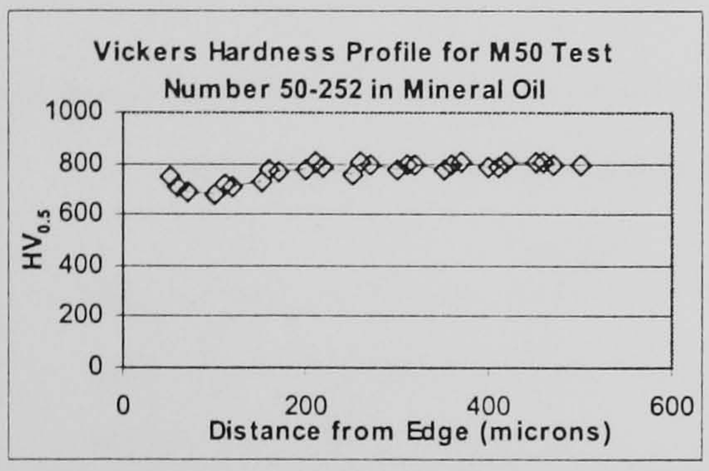	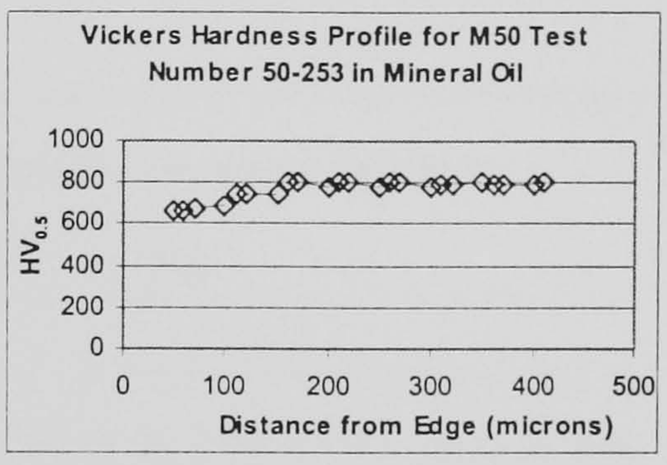
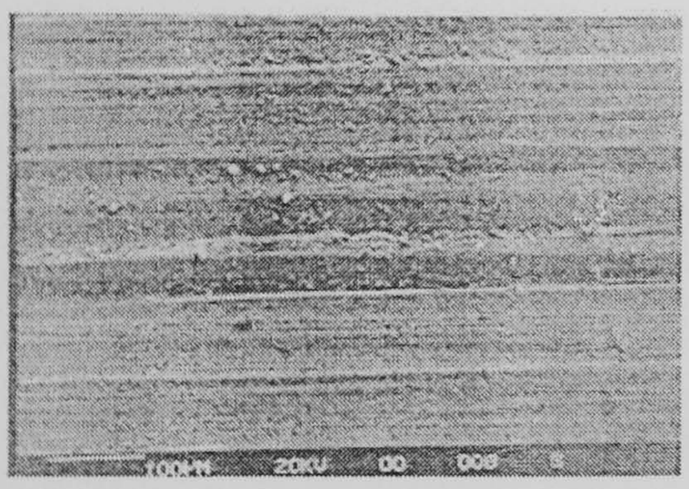	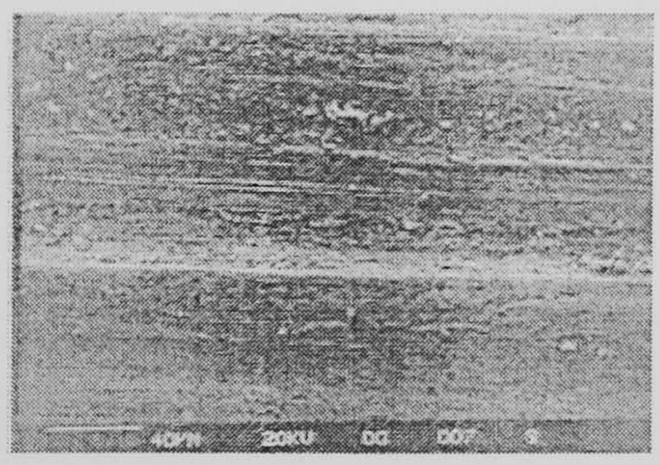
White Layer – 30μm	10μm
Over-tempered Region – 150μm	200μm
Predicted Temperature	
Circular Arc Model 1047°C	1042°C
Heat Transfer Equations 808°C	802°C

Figure 7.9: Workpiece analysis for Test Numbers 50-252 and 50-253

Figure 7.9 illustrates the sub-surface microscopy, SEM images and Vickers hardness profiles for the "up grinding" mode operations. The depth of both the overtempered and untempered martensite layers is lower than that of the 'down grinding' results. One can only surmise that when comparing Figures 7.8 and 7.9 in these circumstances up grinding is more efficient than down grinding. Even though the surface of test number

50-253 shows slight damage one should recall that the process used here is for stock removal purposes and that a finishing cut would be required.

7.1.2.3 Stress Measurement

The M50 deep cut test's residual stress measurements carried on the trend seen in Chapter 5. Figure 7.10 shows the complete M50 experimental dataset for all M50 tests and even taking into account that these tests have used a host of depths of cut, feedrates and wheel speeds the same general trend can be seen.

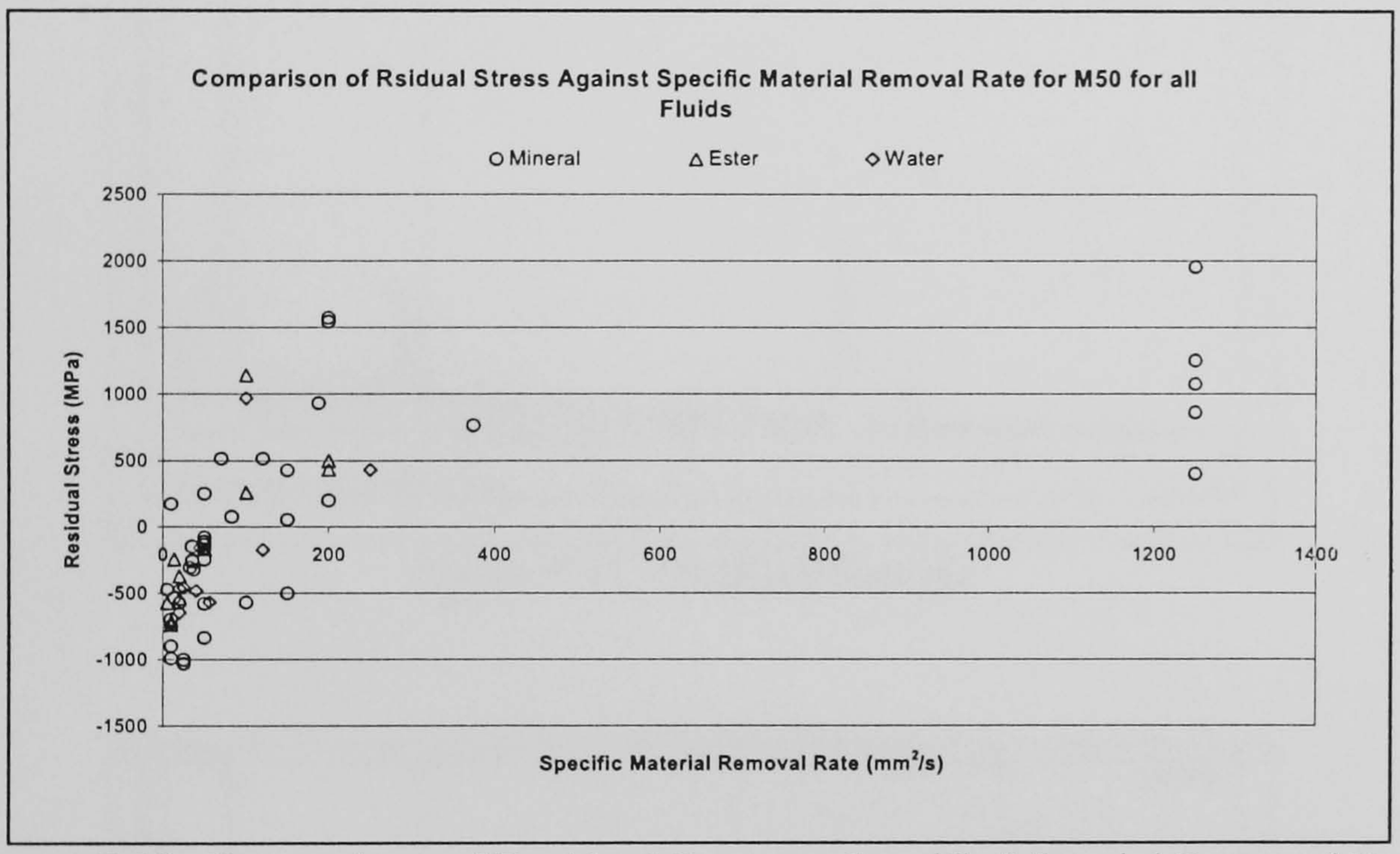

Figure 7.10: Comparison of Residual Stress to Specific Material Removal Rate

7.1.2.4 M50 Burn Analysis

Questions arose during this research as to when the browning upon the finished surface was oxidation or due to some other effect. To answer this query three samples were prepared, one from a known oxidised sample, one clean M50 sample which had oil heated until the surface was dry and a control sample free from oil and oxidation.

The samples were analysed using a Scanning Electron Microscope (SEM), and the three results are shown in Figures 7.11 to 7.13. Taking the background noise into account the only discernable difference is the large Carbon peak which is prevalent in the burned sample shown in Figure 7.11, but not in the other two plots.

The results would indicate that because there was no evidence of a large O_2 peak and hence no real evidence of oxidation, we could be seeing the effects of excess carbon deposited from the breakdown of the oil during the ultra high pressures and temperatures experienced in the grinding zone where oxidation occurred. This could indicate that the burn threshold results which are based on a visual assessment of the surface, could be residual effects from the breakdown of the grinding fluid and not in fact oxidation of the material.

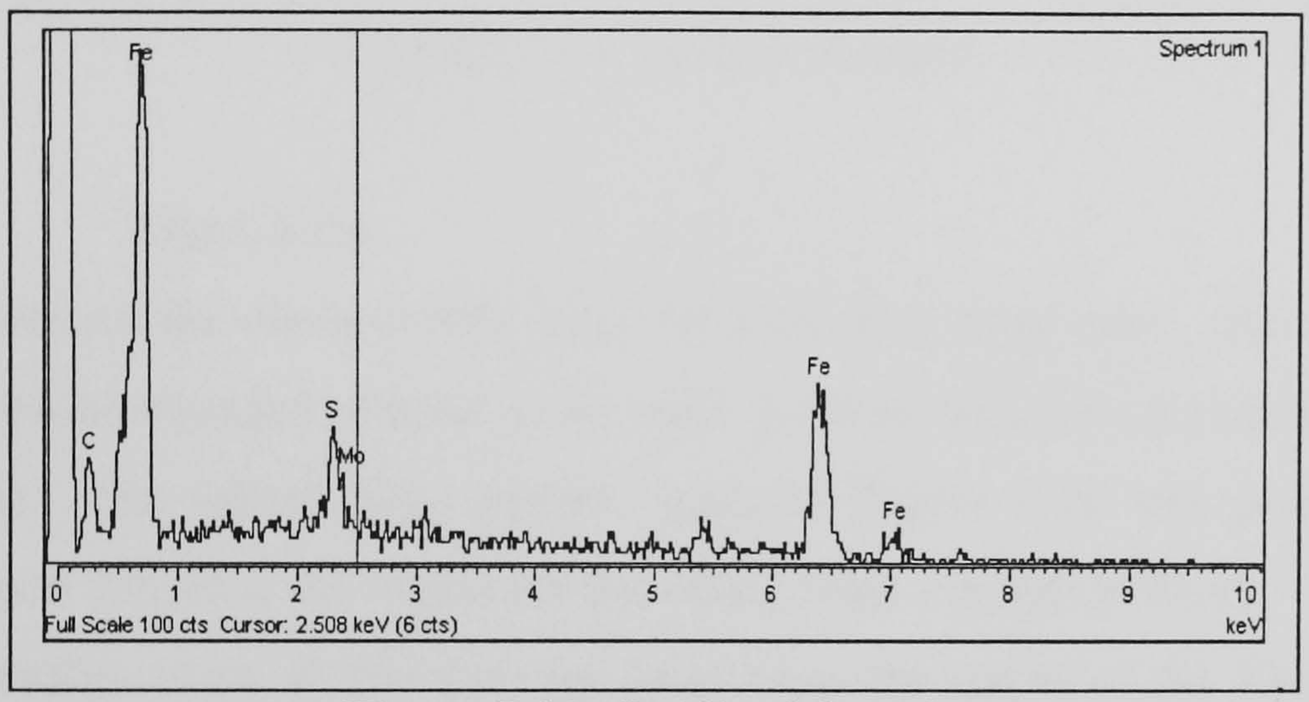

Figure 7.11: Oxidised Sample

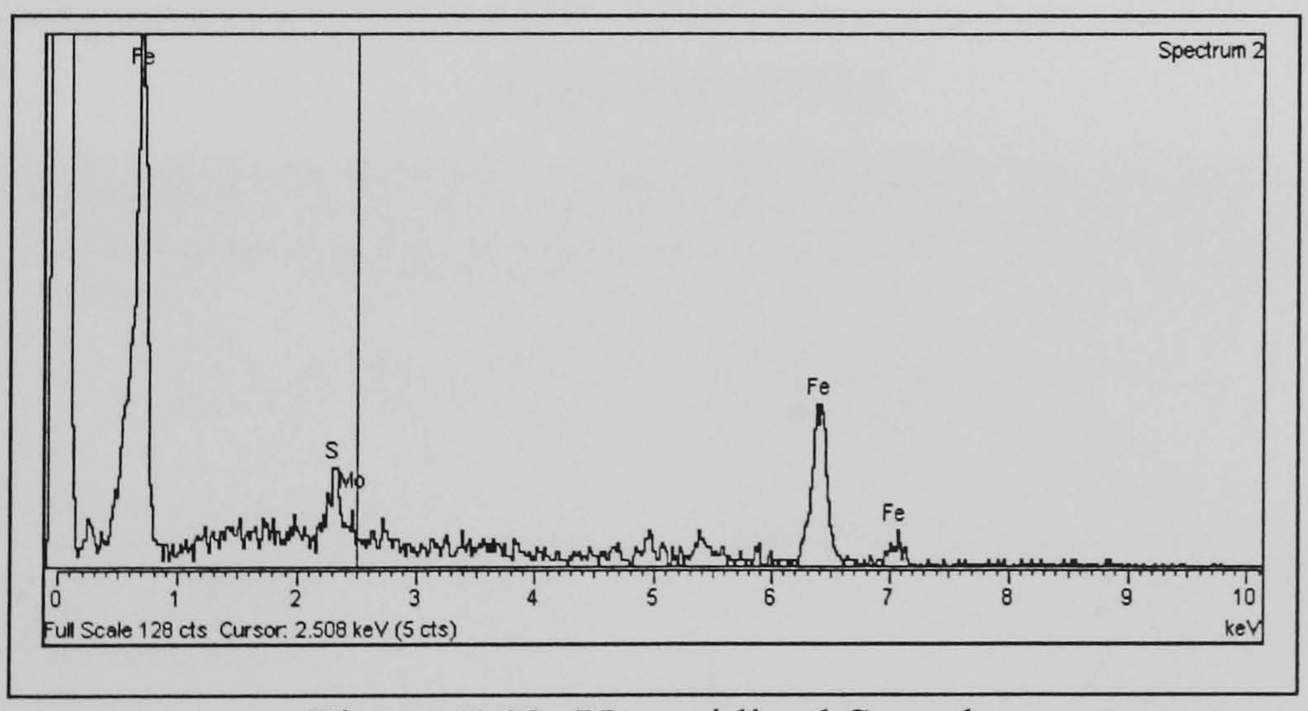

Figure 7.12: Un-oxidised Sample

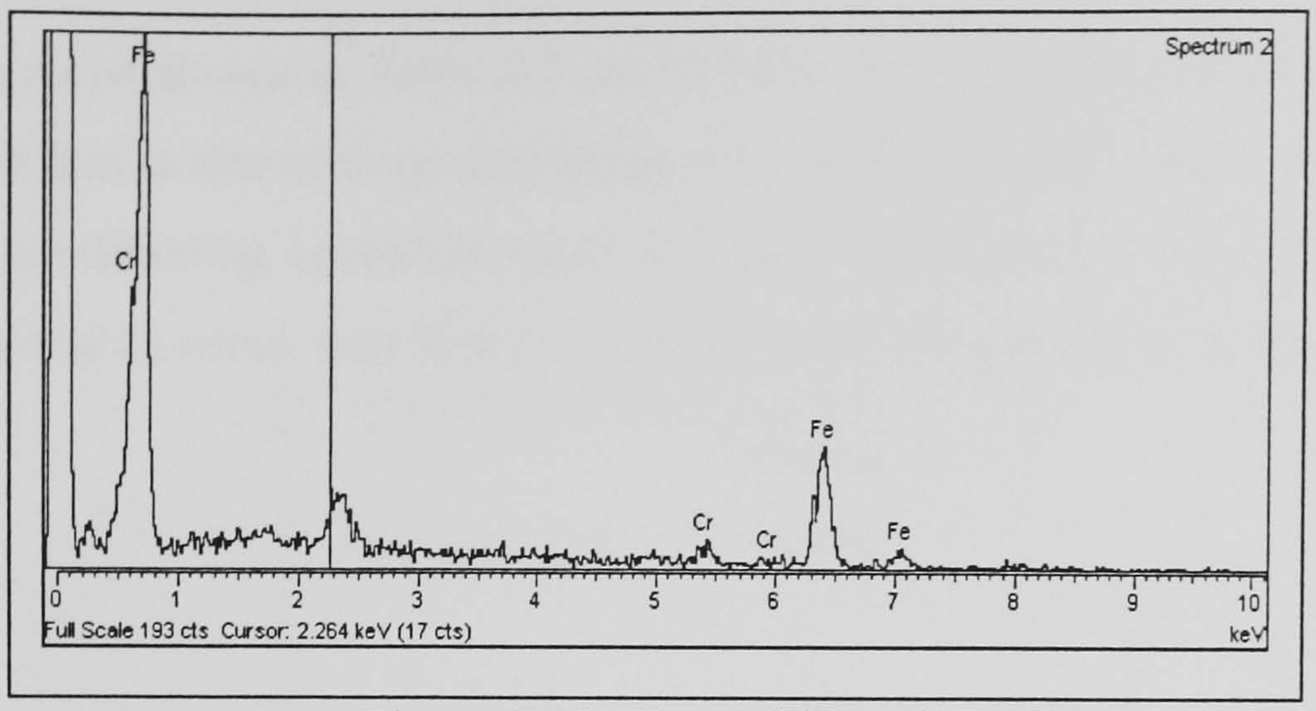

Figure 7.13: Control Sample

7.1.2.5 Wheel Wear

Figure 7.14 shows the wheel profile from the M50 steel deep cuts. After each sample was cut the wheel was moved 4mm to the right and therefore each cut used a "new" part of the wheel. The wheel wear profile shown in Figure 7.14 was produced by the Talysurf which followed the wheel profile taken from a graphite block. The numbers below the profiles relate to the wear recorded from the radius of the wheel after each initial cut.

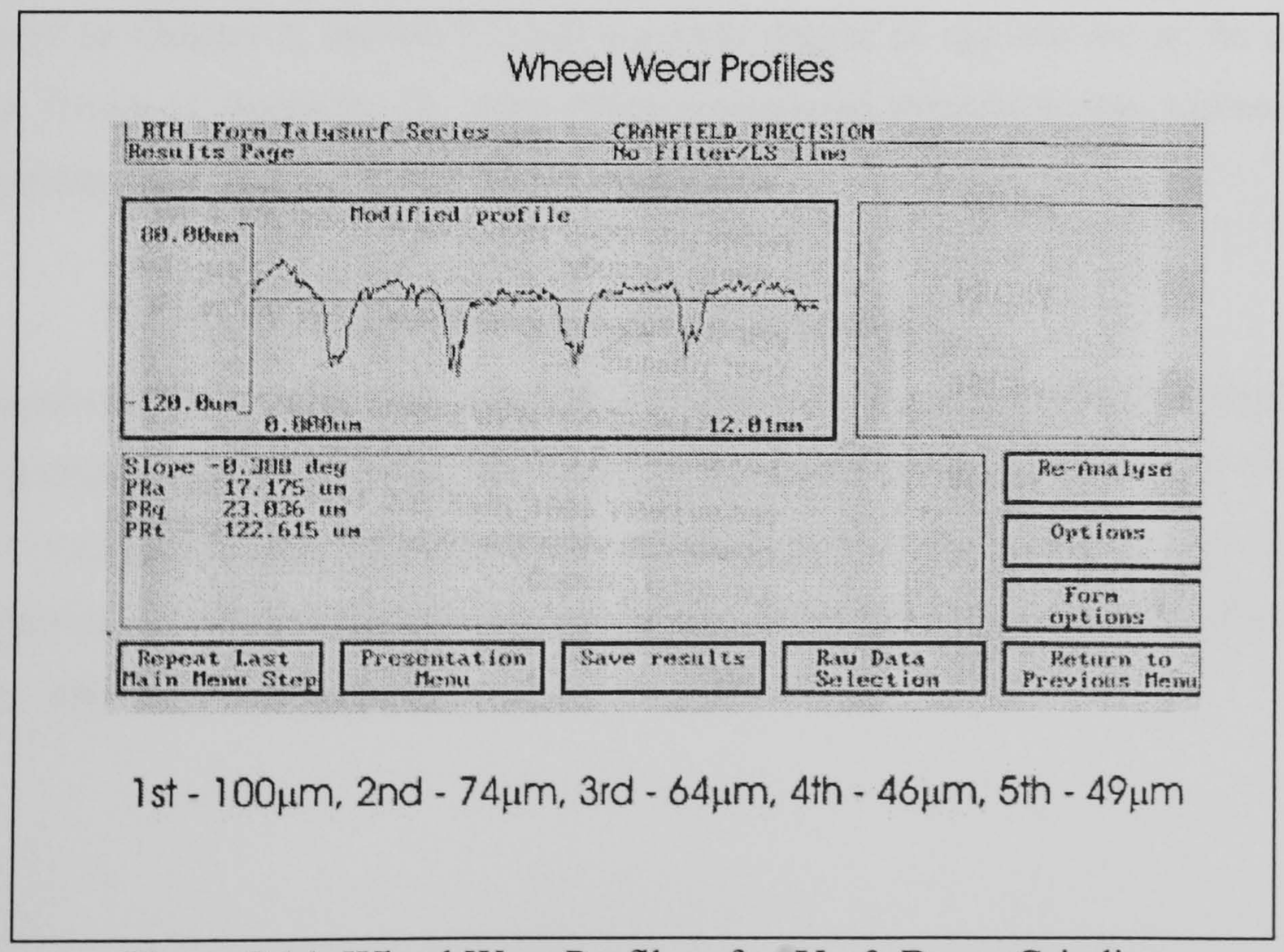

Figure 7.14: Wheel Wear Profiles after Up & Down Grinding

The grinding ratios shown in Table 7.2 are all relatively low, and so could give a false impression, as this is due to these cuts being the first from a new wheel. A new wheel undergoes a conditioning operation when first used which removes all the high points from the grits and so wheel wear from this early part of the wheel life is relatively high.

Test Number	Grinding Ratio
50-249	15.92
50-250	21.51
50-251	24.87
50-252	34.59
50-253	32.48

Table 7.2: Grinding Ratios from Deep Cut Experiments

7.1.2.6 Thermal Modelling

The theoretical thermal modeling used in this research was based on the circular arc model of Rowe & Jin (2001). The background to the thermal modeling work is presented in Chapter 2, section 2.7 and a greater degree of explanation of the process used is shown in Appendix H. Also when untempered martensite was witnessed the heat transfer equations were used as a comparison.

7.2 Experimental Temperature Measurements

This aspect of the research was undertaken to correlate the predicted temperatures with experimentally measured values for both up and down grinding modes. In this way greater confidence can be shown in the predictive tools produced by previous experimental trends and theoretical calculations using techniques published by Rowe (2001). This section describes the procedure followed.

7.2.1 Experimental Procedure

A series of tests to investigate the influence of feed rate and depth of cut were designed. The parameters chosen are shown in Table 7.3 and were repeated for both modes of grinding.

Depth of Cut (mm)	Feed Rate (mm/s)	Specific Material Removal Rate (mm^2/s)
0.4	125	50
1.6	125	200
3	125	375
3	66.67	200
3	16.67	50

Table 7.3: Temperature Measurement Parameters

Four samples were manufactured to make 2 pairs, one sample from each pair had a slot spark eroded along the centre line to accommodate the thermocouple wires. Figure 7.15 shows an illustration of the M50 blocks used for temperature measurement.

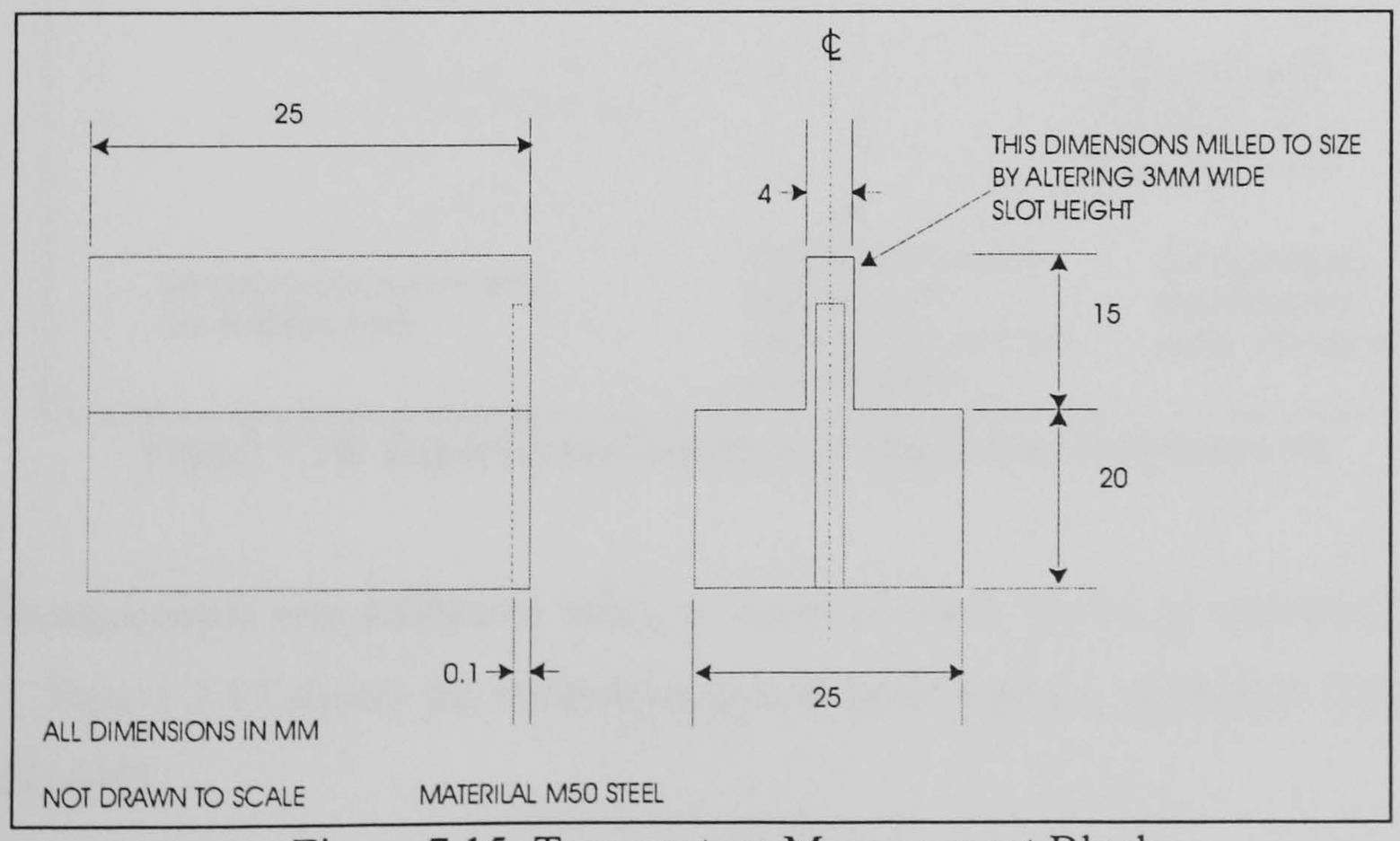

Figure 7.15: Temperature Measurement Blocks

The slot was coated with high temperature cement (OMEGA TYPE CC High Temperature Cement) and a standard K-Type foil thermocouple (Type CO-2) was bonded to this face. A protective layer of cement was applied upon the thermocouple, allowed to cure and the two halves of the specimen were clamped together in a fixture which in turn was bolted upon the Kistler Dynamometer.

With the thermocouple bonded on to the high temperature cemented surface the distance between the end of the thermocouple and the sample edge was measured using a calibrated eyepiece fitted to a CNC milling machine. The two halves were then positioned and assembled together, as shown in Figure 7.16. Due to the 25μm thickness of the thermocouple cables continuity tests were carried out to ensure electrical continuity of the system. The in-house written software which logged the data, was then run to ensure the system was working satisfactorily.

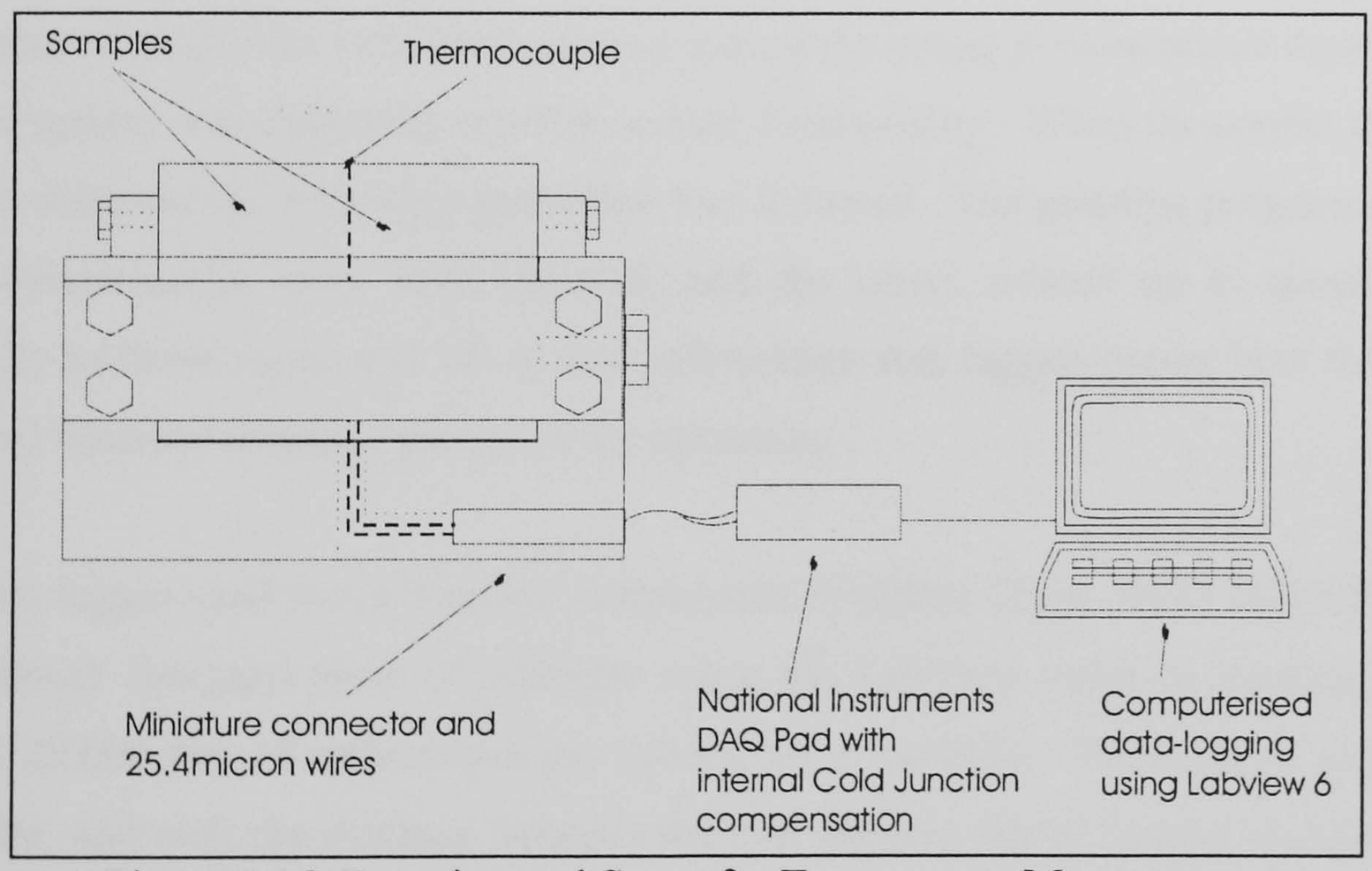

Figure 7.16: Experimental Setup for Temperature Measurement

The thermocouple was calibrated using a vessel of water heated to between 29°C and 90°C. Figure 7.17 shows the calibration points taken using a calibrated thermometer RS(650-419).

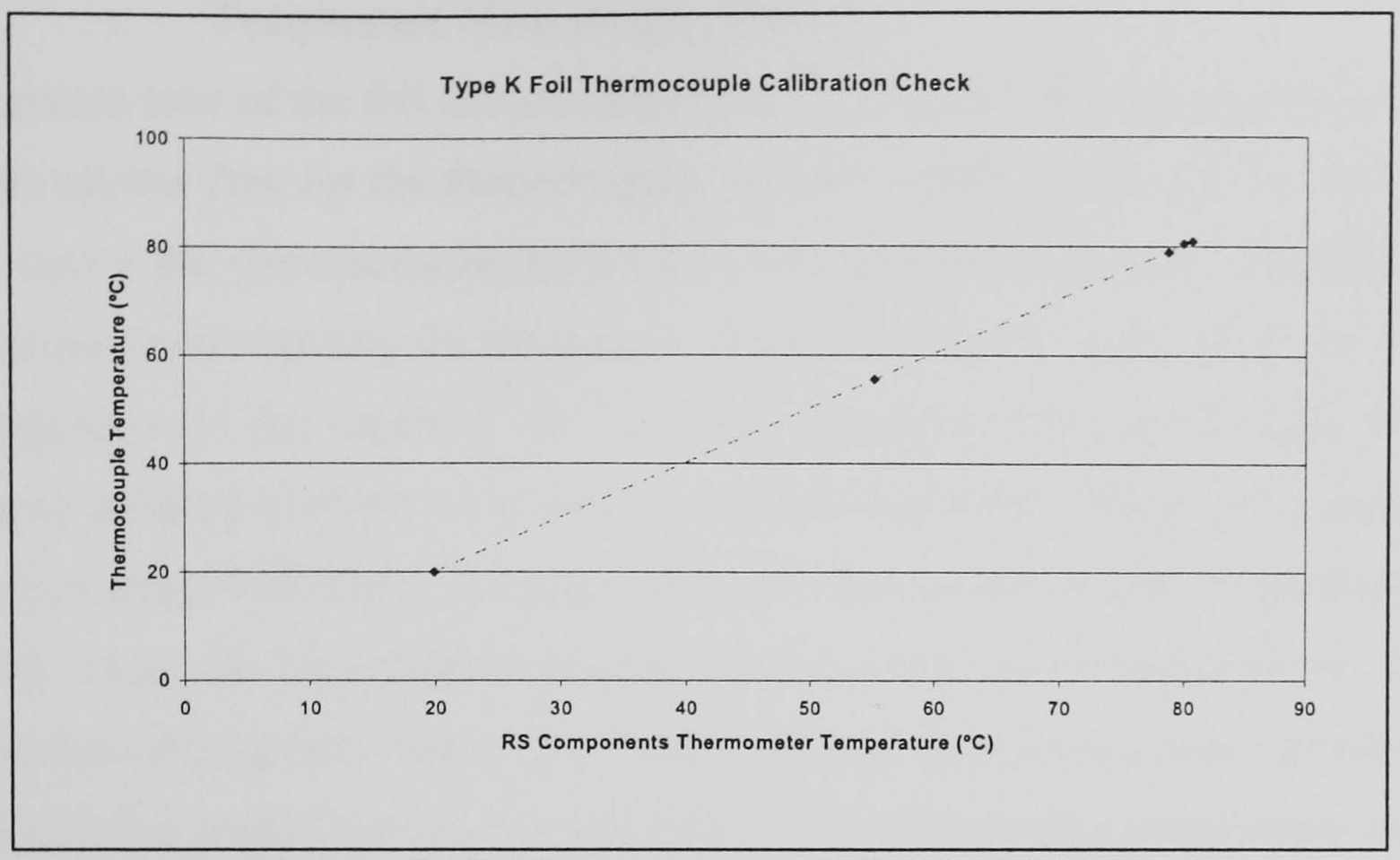

Figure 7.17: Thermocouple Calibration Check

The distance between the edge of the thermocouple and the sample edge was measured. A number of small cuts were then taken to control the actual predetermined depth of cut and the system was constantly tested to ensure functionality. When the correct depth of cut was achieved the following procedure was followed. The grinding program and the force dynamometer were both initiated, and the wheel rotated up to speed. The manually initiated signal was set so that information was logged during both the initial and final transient response phases of the operation.

The data logger used was a National Instruments DAQPad (Type -MIO-16XE-50). and an in house designed piece of software using the LabView software package. This logged 20,000 bits of information per second for 6 seconds. Therefore at maximum feed rate, and with the distance between the two samples which housed thermocouple being around 150 microns, the software would log 24 bits of information in 1.2ms during this period.

The most important issue in this experiment was not to touch the thermocouple assembly in any way. If contact was made between the wheel and the thermocouple assembly the circuit would be broken and would cause wild fluctuations due to noise. Therefore 50μm was left between the surface and the thermocouple tip.

7.2.2 Temperature Measurement Results

The response time of the foil thermocouple used is 2ms and, this measure indicates that it would require 2ms for the thermocouple to react to 66% of the signal. This meant that in theory the thermocouples may not be fast enough to show the maximum peak temperature experienced by the workpiece. Figure 7.18 shows a comparison of the raw data responses for test numbers 50-254 which represents the down grinding example and the up grinding comparison shown is test number 50-259. Wager (1991) noted that the contact length was higher for up grinding and that the subsequent temperatures were relatively equal for both modes of grinding; this temperature characteristic was not mirrored here during these higher Q'_w values. As each experimental run was carried out the net grinding power was used to calculate the finished surface temperature using the circular arc contact model.

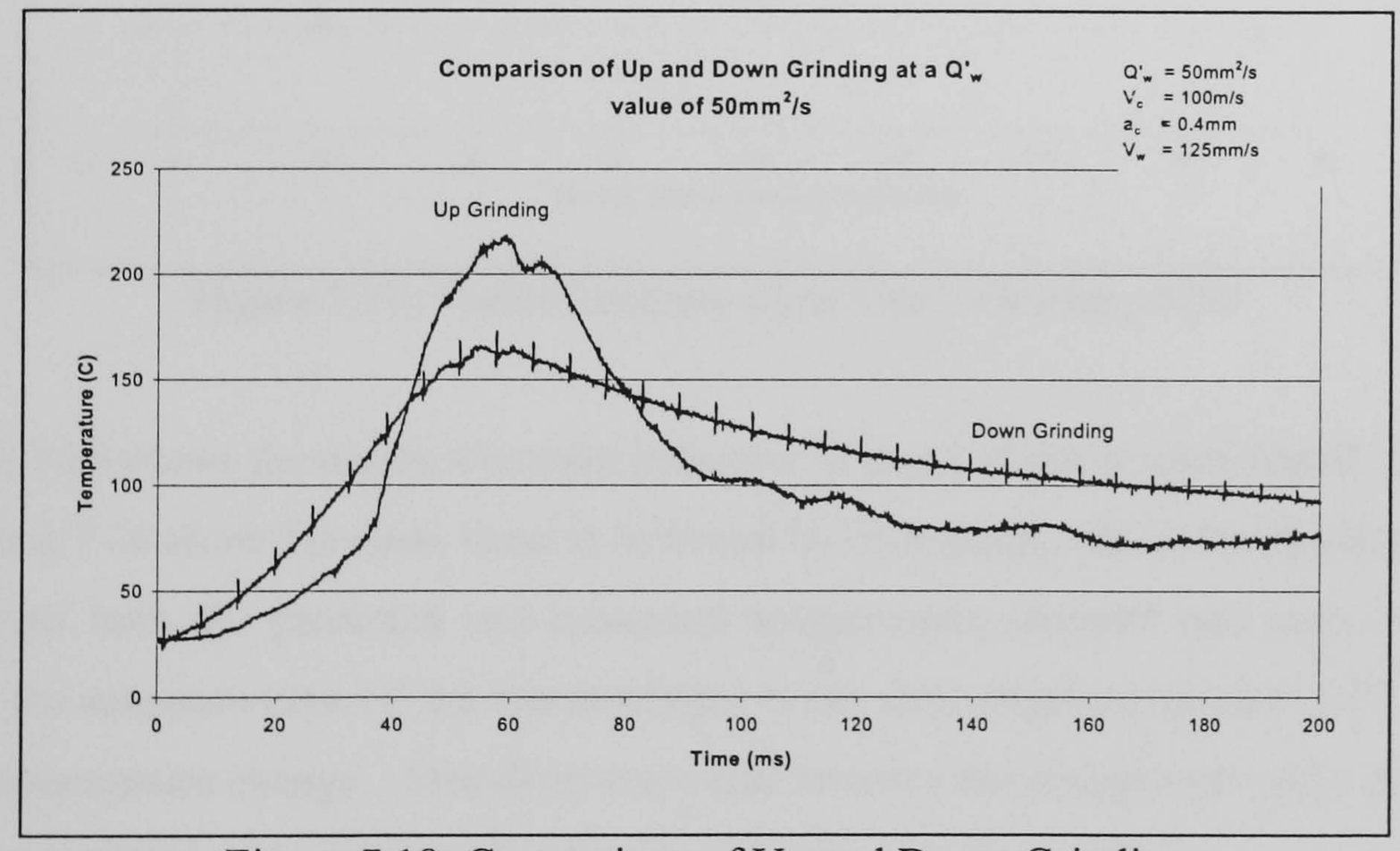

Figure 7.18: Comparison of Up and Down Grinding

Figure 7.18 has been graphed using the raw data logged at 2000 bits per second. There is evidence of a constant frequency noise signal in the down grinding example which had a lower peak temperature value but still had a high signal to noise ratio. From the curves one can see that the heat distribution in both cases is relatively equal albeit at different temperature levels.

The experimental results shown in Figure 7.19 investigate the influence of feedrate when using the three feedrates involved, which were 16.66, 66.67 and 125mm/s. It is quite obvious that the thermocouples slow response time is responsible for the constant disparity but the general trend of increasing then decreasing temperature is followed by both measures.

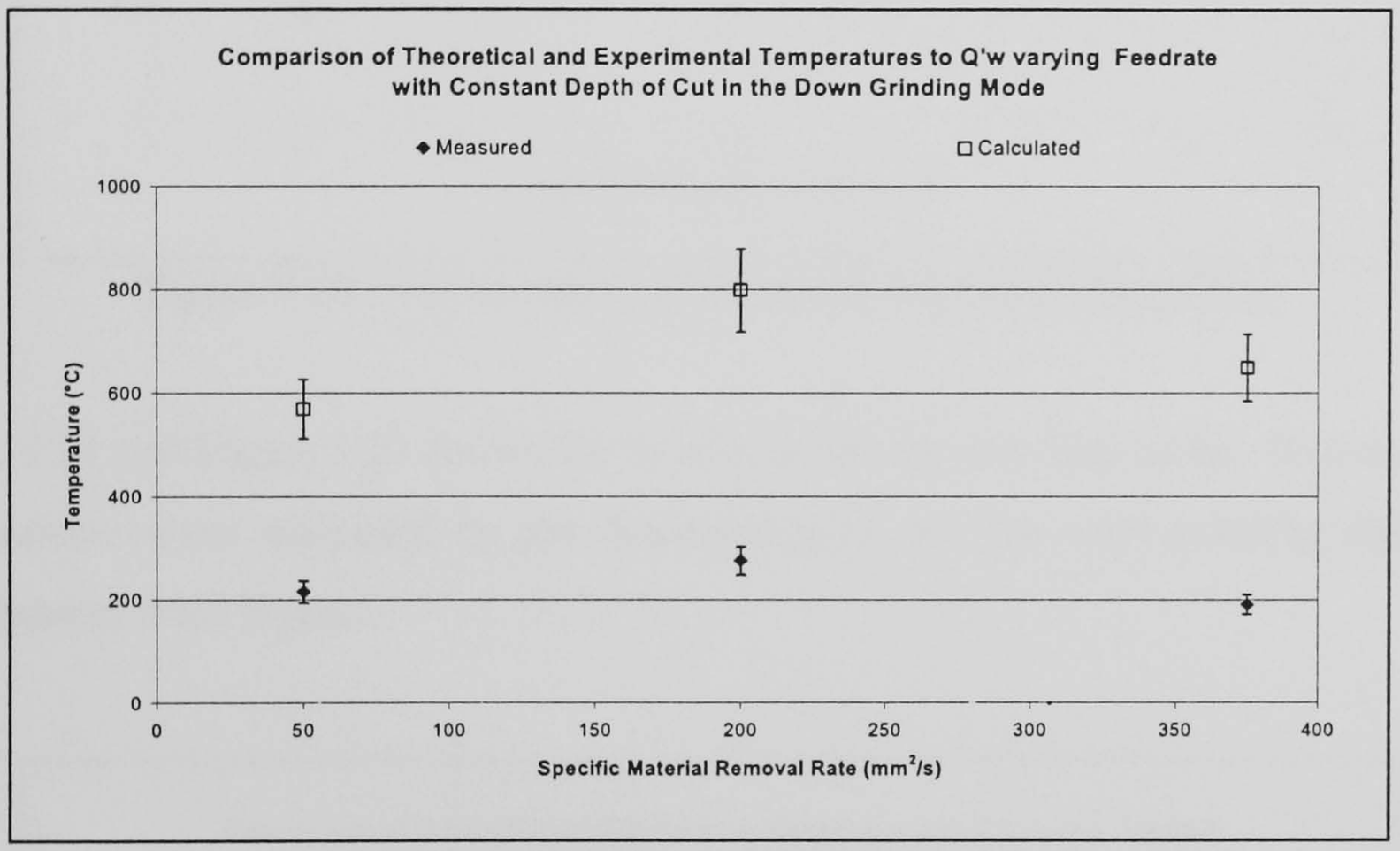

Figure 7.19: Varied Feedrate when Down Grinding M50

Figure 7.20 shows the results when the influence of depth of cut is investigated. Figures 7.19 and 7.20 show the same trend is followed by both plots, and as the depth of cut is increased both the predicted and measured temperatures increase and then decrease. Also, the response time of the thermocouple is the time required to reach 66% of the total temperature change. Therefore one could increase the temperature plots by a half which would bring the measured and predicted values closer together.

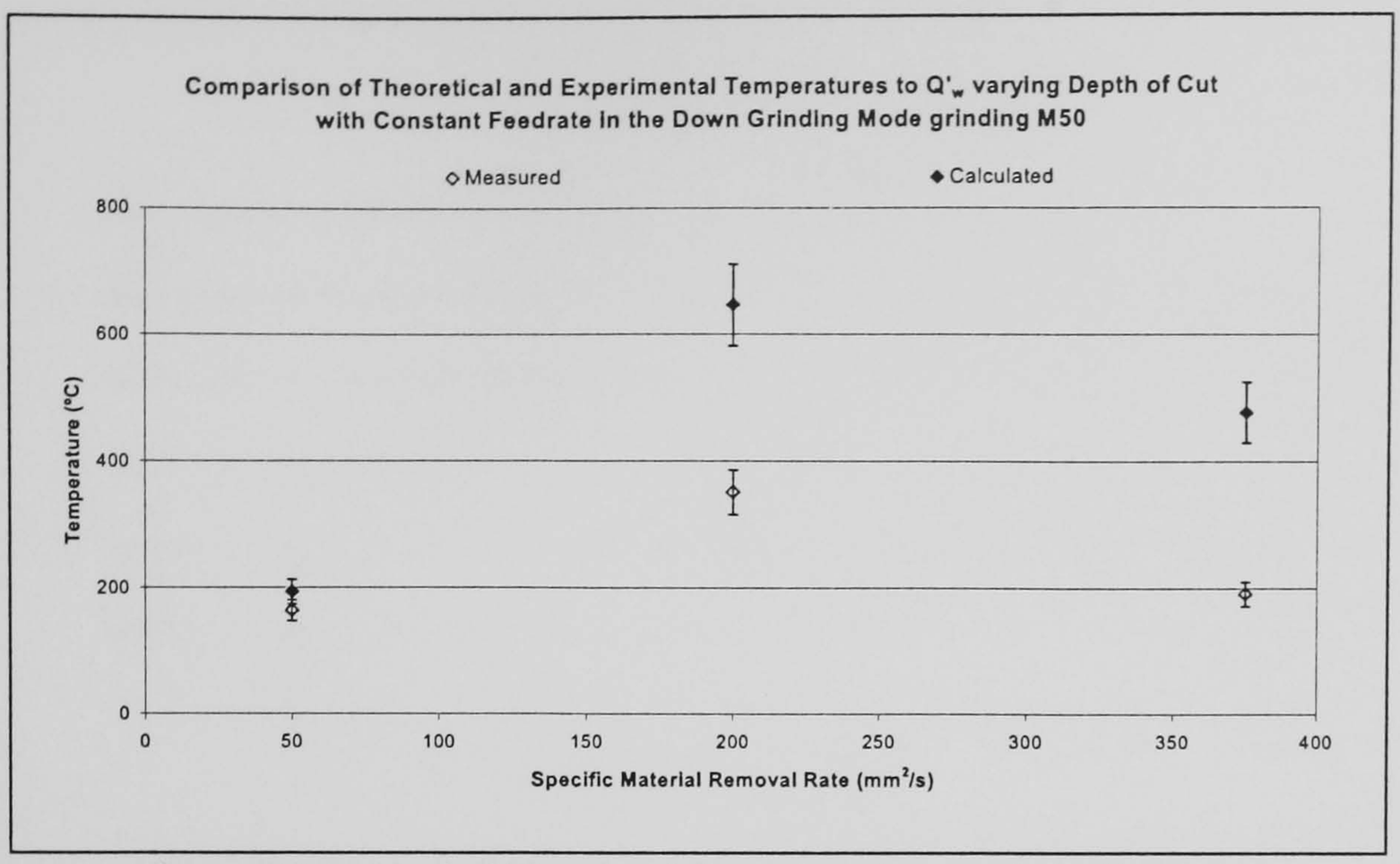

Figure 7.20: Varied Depth of Cut when Down Grinding M50

Figure 7.21 and Figure 7.22 shows the results for the up grinding mode. Overall higher temperatures were measured by the thermocouples and the corresponding calculated temperatures were higher.

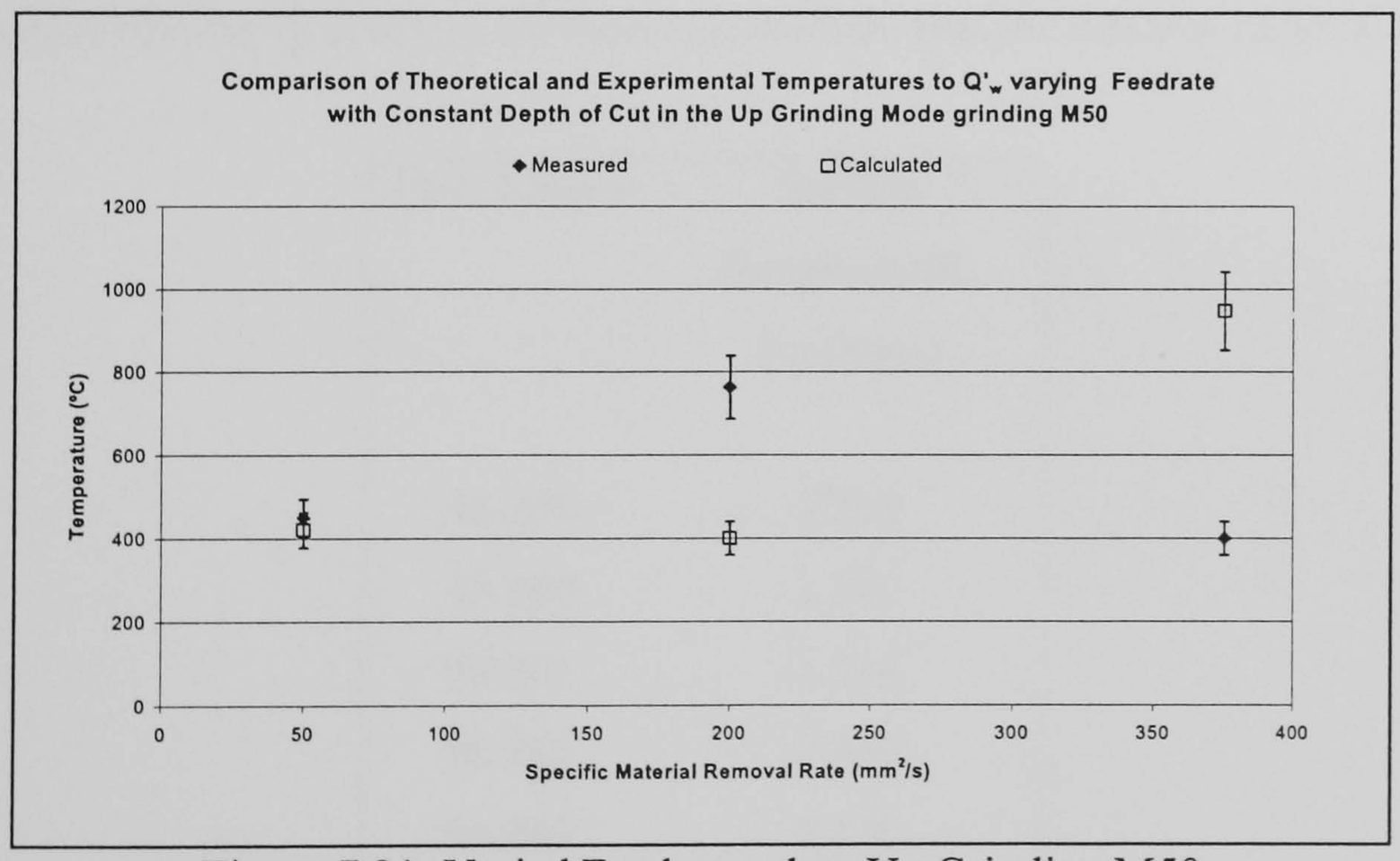

Figure 7.21: Varied Feedrate when Up Grinding M50

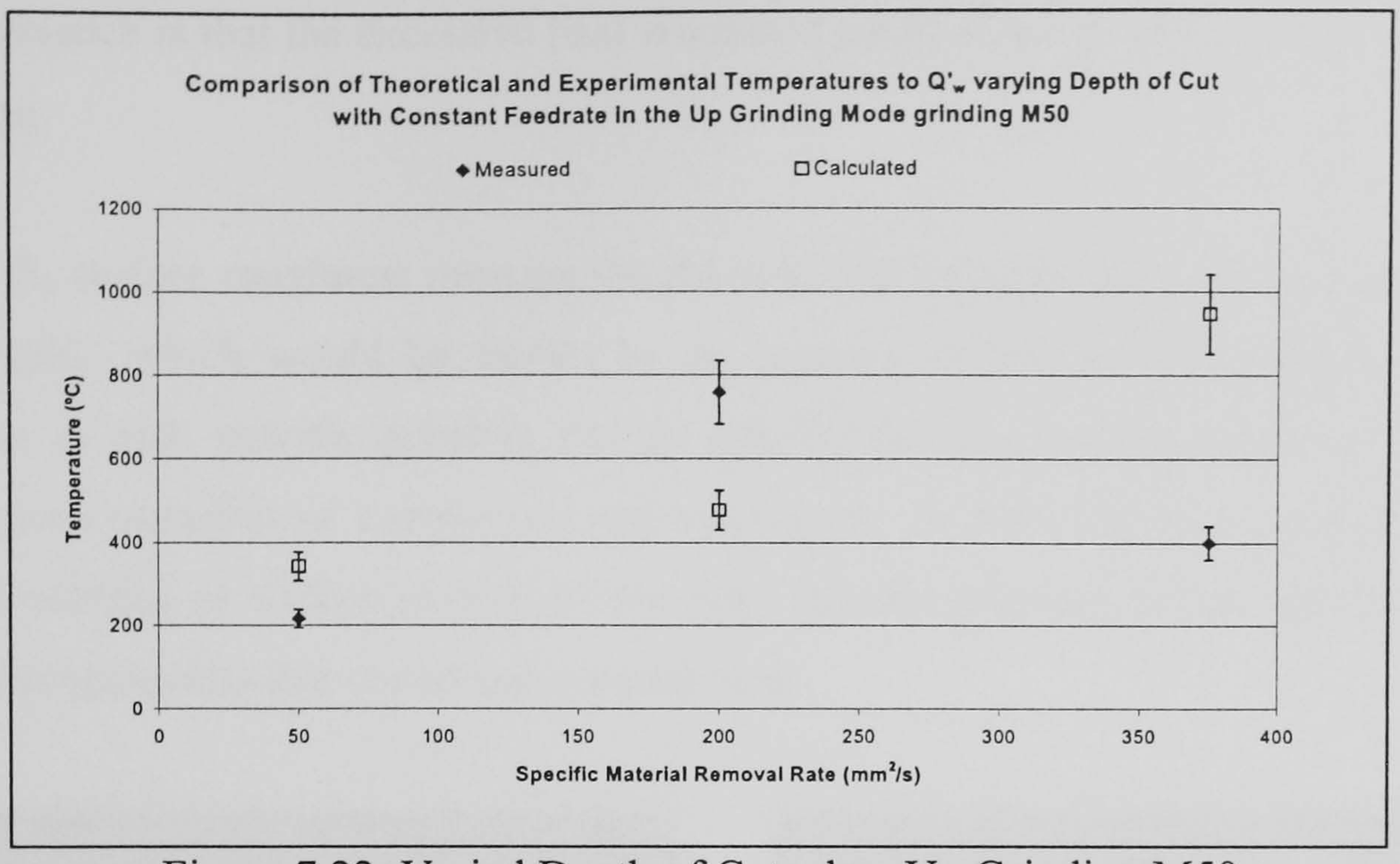

Figure 7.22: Varied Depth of Cut when Up Grinding M50

Comparing Figures 7.19 to 7.22 with a view to mode of grinding there have been a number of discussions as to the efficiency of the two modes. Tawakoli (1993) advocated an up grinding mode for Q'_w values between 20 to 70mm^2/s and down grinding for values above 70mm^2/s. It can be seen that the general trend is for higher temperatures during up grinding for these intermediate specific material removal rates.

Test Number	Surface Roughness R_a (microns)
50-259	1.328
50-260	1.341
50-261	1.415
50-262	1.360
50-263	1.109

Table 7.4: Surface Roughness after Up Grinding Operations

Table 7.4 gives the surface roughness measure R_a results which indicates that the wheel used in these experiments has merely been conditioned by these grinding operations.

The inference is that the excessive heat witnessed could actually be due to the mode of grinding.

A low R_a surface roughness measure would infer that the grits had worn to a more flat topography, which would be shown by an increase in the rubbing portion and an increase in both specific grinding energy and finished surface temperatures. Figure 7.23: gives examples of conditioned and worn grits. A worn flat area would create a greater rubbing or sliding portion of the total specific grinding energy and therefore higher temperatures due to excessive wheel wear.

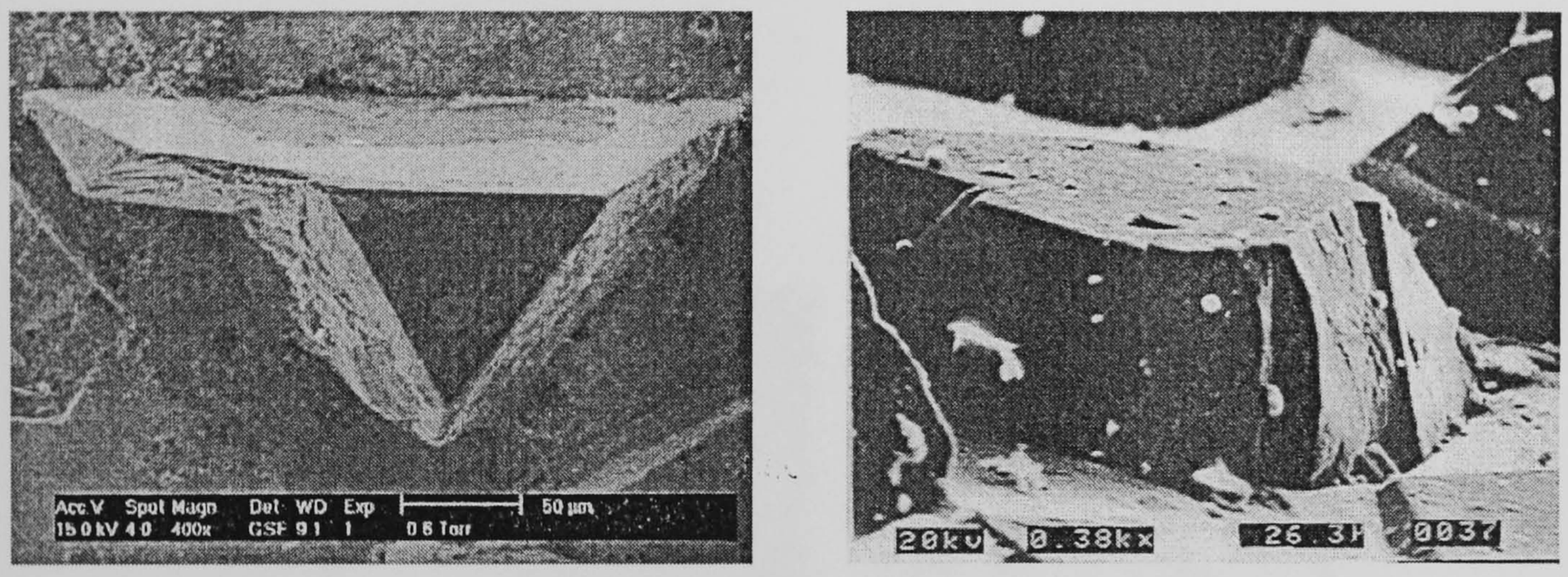

Conditioned Grit Worn Grit

Figure 7.23: Examples of grit wear

7.2.3 Up Grinding Workpiece Analysis

Figure 7.24 gives details of parameters used, sub-surface micrographs at the area of material adjacent to the thermocouple position and Vickers hardness profiles for the up-grinding tests. From Figure 7.24 it can be seen that all samples received no real grinding damage other than the sample 50-262 for which it could be construed that the surface had been slightly overtempered.

Q'_w = 50mm²/s	200mm²/s	375mm²/s	200mm²/s	50mm²/s
Feedrate = 125mm/s	125mm/s	125mm/s	66.67mm/s	16.67mm/s
Depth of Cut = 0.4mm	1.6mm	3mm	3mm	3mm
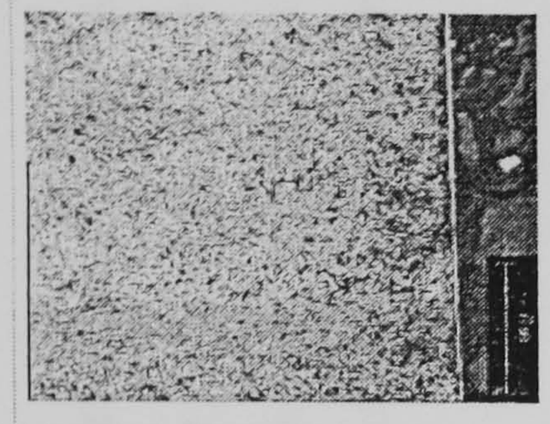		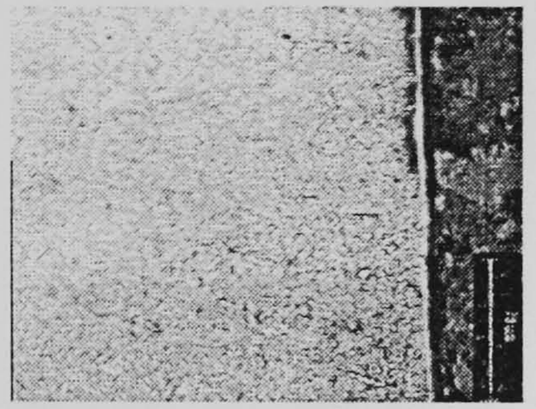	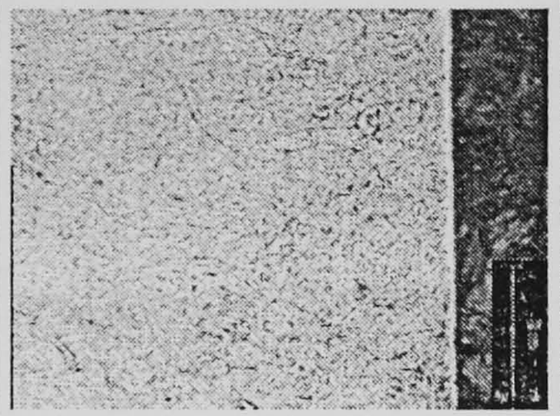	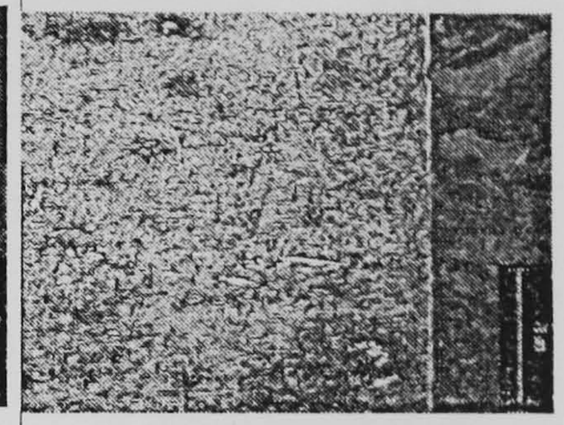
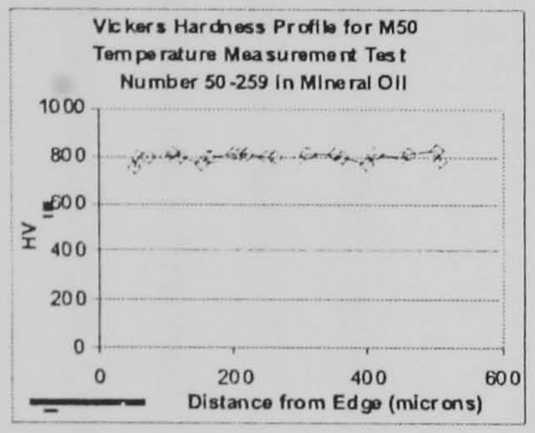	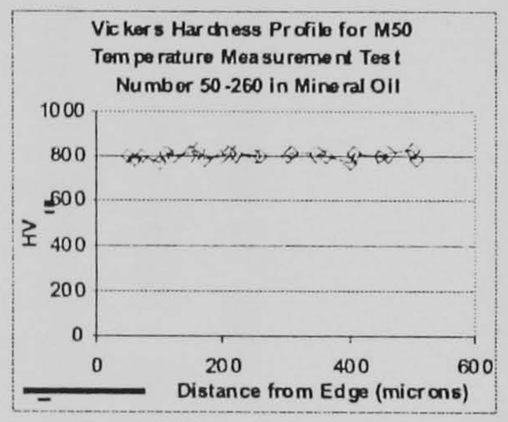	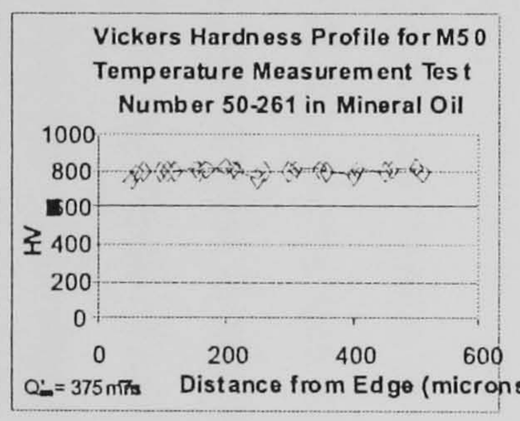	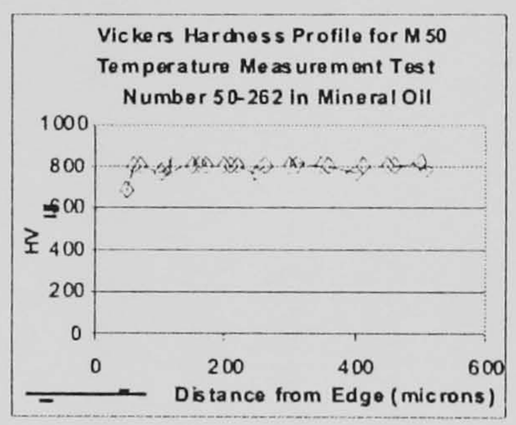	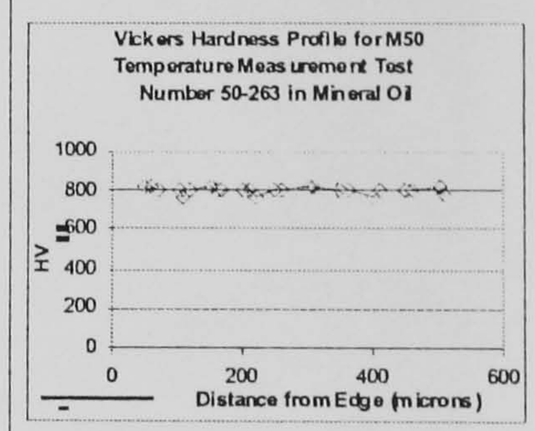

Figure 7.24: Overall results from Subsurface and Vickers Hardness Analysis

Figure 7.25 shows details of grinding damage prior to the thermocouple position.

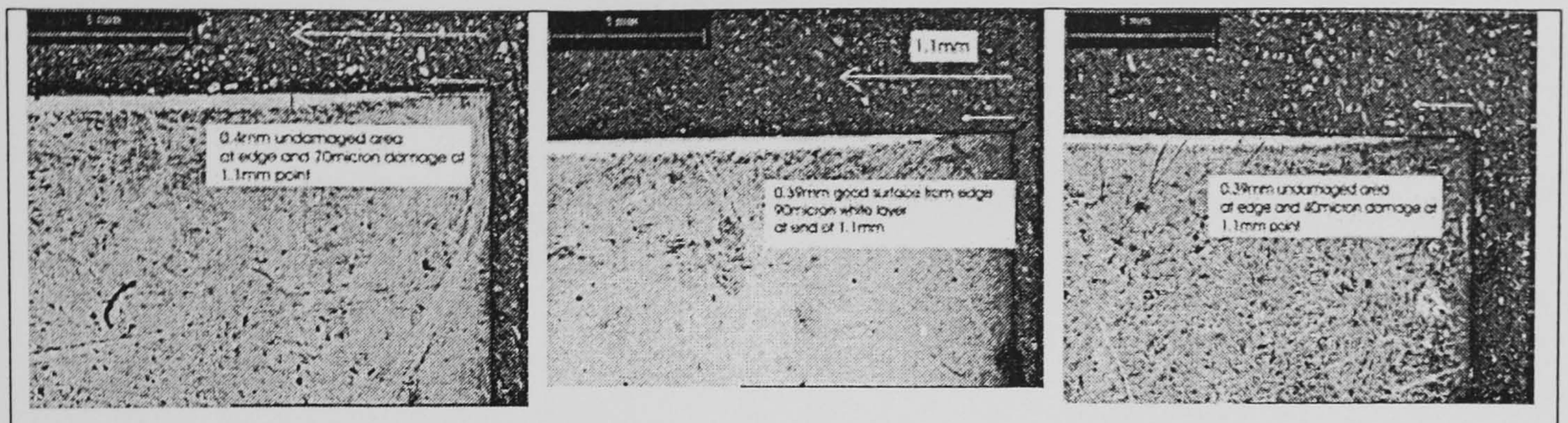

50-262		50-263	50-264
Q'_w	$= 200mm^2/s$	$375mm^2/s$	$200mm^2/s$
Feedrate	= 66.67mm/s	125mm/s	125mm/s
Depth of Cut	= 3mm	3mm	1.6mm

Figure 7.25: Evidence of Tapering Grinding Damage

The total length of samples used was 60mm, and it should be noted that the maximum depth of cut is only achieved midway through the cut when the contact length has increased to its maximum value. For a 3mm depth of cut this occurs after 29.9mm. Figure 7.25 shows that as the specific material removal rate is increased through the cut the temperature increases then decreases and as the full depth of cut is experienced there seems to be a lag time for the grinding damage to cease. The depth of grinding damage varies for each test, 50-262 – 70microns, 50-263 – 90microns and finally 50-264 – 40microns.

Using the heat transfer equations we can use the depth of white layer penetration to calculate the temperature experienced by the finished surface. A worked example for 50-263, parameters are depth of cut – 3mm, feedrate 125mm/s and 100m/s wheel speed, is shown in Appendix H, Figure H.3.

Figure 7.26 gives an illustration of the sample's finished surface. The first triangle represents the white layer grinding damage which is measured 1.1mm from the end of the cut. This point is when the true depth of cut had been reached. The second triangle represents the true grinding depth when using a depth of cut of 1.6mm. For reasons of

comparison the grinding damage was measured for both instances at the same distance from the end of the grind.

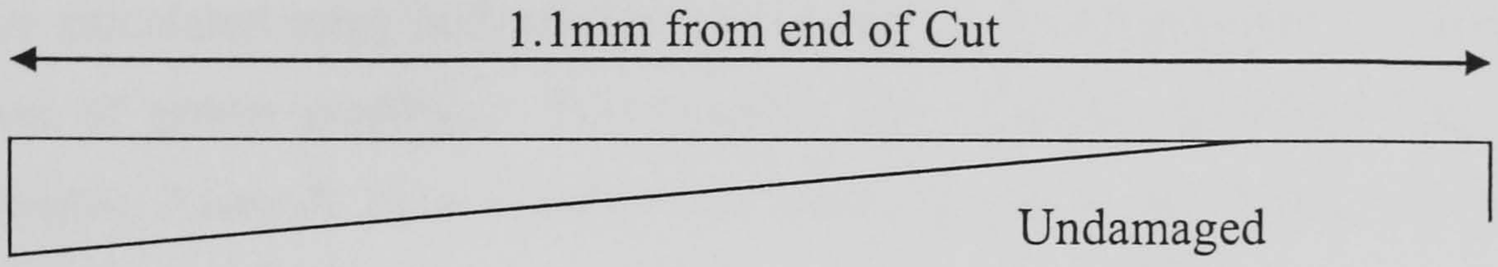

$Q'_w = 375mm^2/s$	Depth of Cut – 3mm	Feedrate – 125mm/s
Circular Arc Model	762 - 824	882 - 1025
Heat Transfer Method	835	
$Q'_w = 200mm^2/s$	Depth of Cut – 3mm	Feedrate – 66.67mm/s
Circular Arc Model	532 - 758	569 - 865
Heat Transfer Method	815	

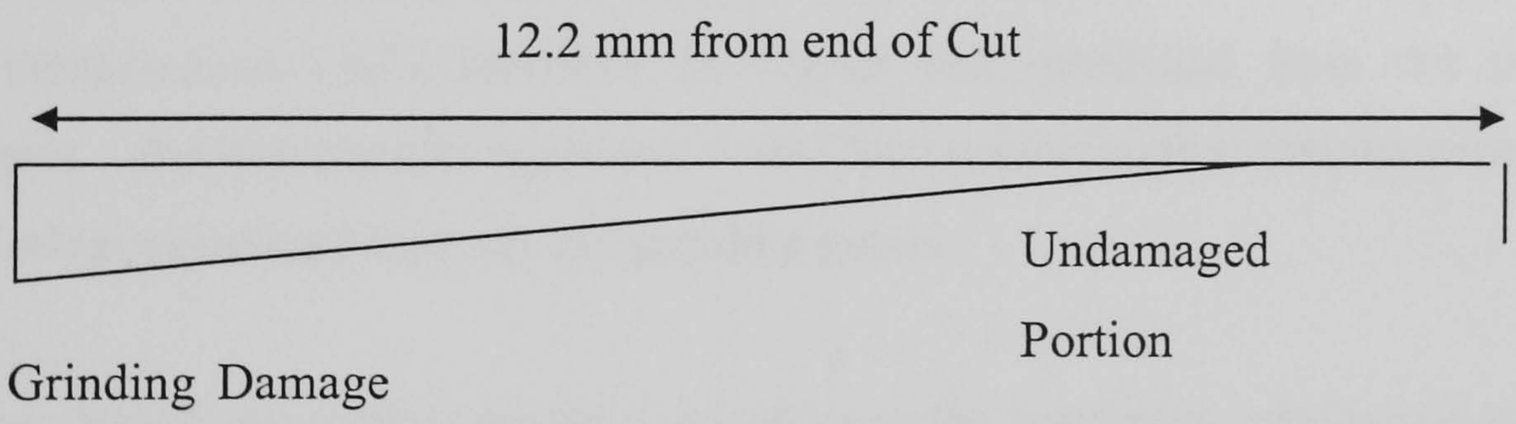

$Q'_w = 200mm^2/s$	Depth of Cut – 1.6mm	Feedrate – 125mm/s
Circular Arc Model	589 - 865	625 - 854
Heat Transfer Method	827	

Figure 7.26: Calculated Temperatures

It was noted that even after the maximum specific material removal rate had been reached the power usage increased to a peak which correlated with the mid-point of the samples, then the power decreased. Therefore the predicted temperatures shown in Figure 7.26 were calculated using both net and total power to investigate the use of the maximum spread of power readings. Two models were used to calculate finished surface temperatures; Rowe & Jin's Circular Arc Model Rowe & Jin (2001) and the heat transfer equations. M^{c}Cormack et al (2001) stated that tempering of the surface begins at approximately 450°C and untempered martensite begins to form at around 800°C. It can be seen that there is reasonable correlation between the contact model and the heat transfer equations. However it could be unfair to compare these two sets of results, as all the heat transfer equation results lean toward the maximum power readings.

One theory as to why this has occurred could be due to the surface temperature at this point being extremely high and the workpiece partition ratio would also be high. Any heat conducted into the workpiece prior to the 1.1mm point would still be present and even as the finished surface temperature decreases due to HEDG principles after this point the thermal flux could diffuse further into the workpiece so that a thermal lag occurs. Temperatures could therefore be higher than predicted from the power measurements. The heat transfer equations would then predict higher temperatures than is possible when calculated from the net grinding power.

Also, as the circular arc contact model is based upon the maximum grinding angle for each temperature calculated and Jin et al (2002) assumed that for HEDG conditions the temperature of the chip (T_{CH}) varies linearly with a maximum workpiece surface temperature T_{max}, in the range 1000°C ~1500°C, the temperatures calculated would be slightly higher overall in comparison to the inclined plane model.

7.3 Summary

Figure 7.27 shows the general shape of response that has been noted throughout this research when investigating responses such as predicted temperature, measured residual stress and specific grinding energy. This type of curve illustrates reasonably well what has been noted in Chapter 5, Figure 5.21 when plotting the specific grinding energy band of 0.1 – 25J/mm^3.

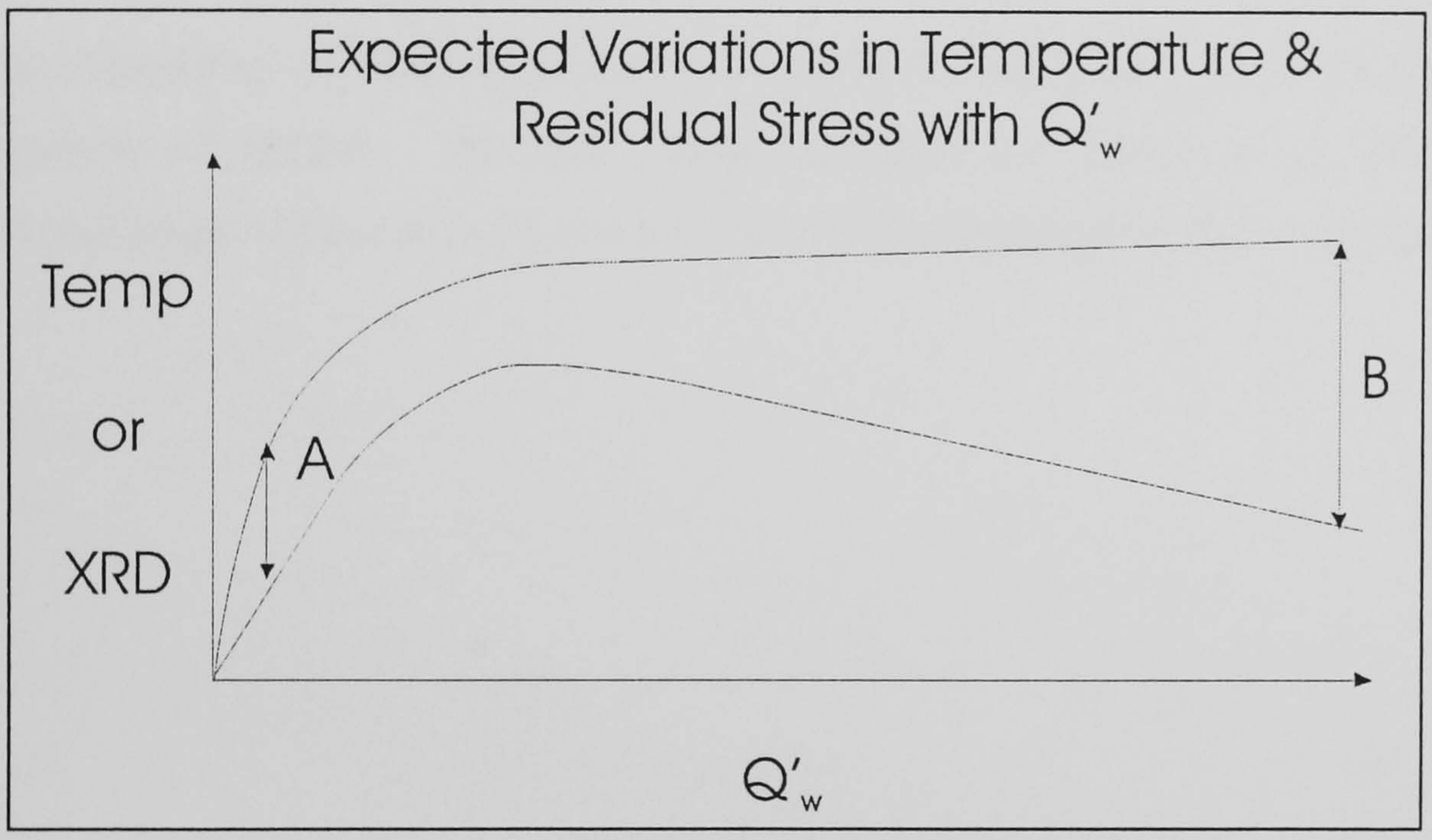

Figure 7.27: Expected Trends for HEDG

Here it was seen that when the specific material removal rate is increased from zero at the point marked "A" in Figure 7.27, the specific grinding energy levels rises quickly with large oscillations in values resulting in relatively small changes in the calculated temperatures. Point B indicates an area where small changes in specific grinding energy result in extreme changes in calculated temperature. Also the small variations in specific grinding energy at point B could indicate a limitation of the HEDG process. Therefore methodologies should be devised and utilised in a bid to control these variations in specific grinding energy during the grinding process. These trends are mirrored when looking at residual stress measurements, as shown in, Figure 7.10.

The results from this chapter have correlated well with the overall trends noted throughout this research. The circular arc contact model predicts temperatures which can be correlated with the sub-surface microstructure and residual stress measurements.

The temperature measuring experiments showed that the thermocouple response time was inadequate for both the high feedrates and depths of cut employed. Also, the temperature measurement experiments highlighted a possible finished surface integrity problem at the start and finish of cuts which could be unique to the HEDG process.

With the completion of these experiments a more complete picture is now available of the principles of HEDG. The next chapter presents and discusses the component manufacture stage of this research to which these HEDG principles have been applied.

CHAPTER 8 COMPONENT MANUFACTURE

The following chapter presents examples of components ground using HEDG principles. The grinding conditions were chosen based on the previous experimental findings and have been used to demonstrate the potential of the HEDG process. The grinding trials on components also provided a further means of validating the grinding models proposed for HEDG. For each component the aim was to remove material at rates that were substantially higher than currently achieved whilst achieving the required level of surface integrity.

This chapter is presented in five parts. Part 8.1 describes the procedures followed in the experimental stage when producing M50 bearings. Part 8.2 discusses and summarises the results found. Part 8.3 explains the MARM-M-002 turbine blade experimental procedure, 8.4 discusses the results found and the turbine manufacture stage and results is summarised in Part 8.5.

8.1 M50 Bearing Manufacture Experimental Procedure

At present the bearings are produced by a combination of milling and finish grinding operations to achieve the surface finish requirement. Aluminium oxide wheels are used for the finish grinding and as such are prone to generate grinding burn of the workpiece. This is primarily due to the low thermal conductivity of this type of wheel. Shaw (1993) states that the thermal conductivity of alumina is around 50W/mK, and this also contributes to a high workpiece partition ratios when using a shallow cut grinding procedure.

This experiment required the grinding of four slots 50mm wide by 4mm deep into a M50 bearing ring. The machining parameters were decided using the information obtained during the project and from published literature as reviewed in Chapter 2.

The objectives of the grinding tasks were as follows:

- carry out the prescribed grinding operation on each component in a grinding time of less than 60 minutes

- achieve a Ra surface roughness target of better than 2μm

- ensure that the grinding procedures produced only compressive residual stress characteristics

Thirty two component manufacturing tasks were carried out using the rotary axis fixture on the B-axis of the Edgetek machine along with a shoe nozzle and associated tooling which were designed and manufactured at Cranfield University. The first two numbers of the numbering system used, describe the material, in this case 50 as in M50, then two more digits designate the tests in numbered order. The machining set up is shown in Figure 8.1 where a component is being held in place before the start of a grinding test. The tests used mineral oil (Castrol Ilogrind 600SP) that was supplied at a rate of 110l/min via a shoe nozzle with a maximum grinding fluid output velocity from the shoe nozzle of 350mm/s. Saint-Gobain supplied the B151 CBN electroplated grinding wheels which were 50mm wide by 200mm diameter.

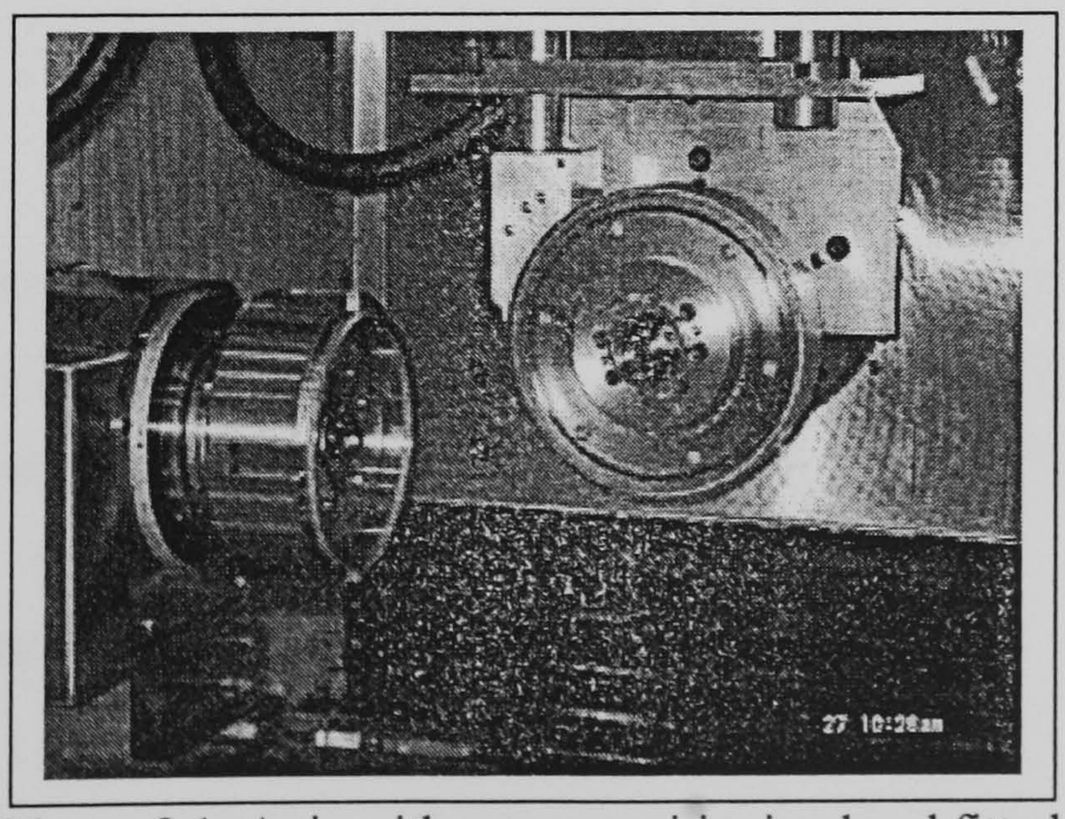

Figure 8.1: Axis with rotary positioning head fitted

The experimental procedure was divided into several stages as follows:

- design and manufacture of tooling and associated equipment
- grinding trials
- initial Q'_w testing
- evaluation of surface integrity

8.1.1 Design and Manufacture of Tooling and Associated Equipment

The fixture to hold the bearing in a rigid manner is of critical importance as any free movement may give rise to vibration and/or chatter. A shoe nozzle also was designed to take into account the following requirements:

- deliver adequate grinding fluid along the whole width of the wheel
- give adequate clearance to facilitate ease of finished component removal and the fitment of a new component

8.1.2 Bearing Grinding Trials

Five rings were delivered for grinding trials and these were divided into three categories:

Initial Q'_w Testing	– Test Numbers 50-58 to 50-65
Conditioning Tests	– Test Numbers 50-66 to 50-81
Final Grinding Operations	– Test Numbers 50-82 to 50-89

The test results are summarised in Appendix I.

8.1.2.1 Initial Q'_w Testing

As the slots would be produced in one operational run with a constant 4mm depth of cut, four different feedrates were used initially to investigate four Q'_w values; these were 1, 20, 50 and 100mm^2/s. The machining process used two different wheel speeds, 3000 and 14000rpm which are equivalent to a peripheral speed of 30 and 146 m/s respectively. Using these broad grinding parameters enabled the component surface integrity to be correlated with the grinding conditions.

At specific times the pallet holding the bearing fixture was replaced with one holding a graphite block. When using a new wheel an initial datum cut was taken, and any discrepancy between the initial and any subsequent cuts of the same nominal depth were compared using the Edgetek's control system. The set depth of cut could be compared with the actual depth of cut and any discrepancy would represent a measure of any wheel wear. Figure 8.2 shows an illustration of the set up.

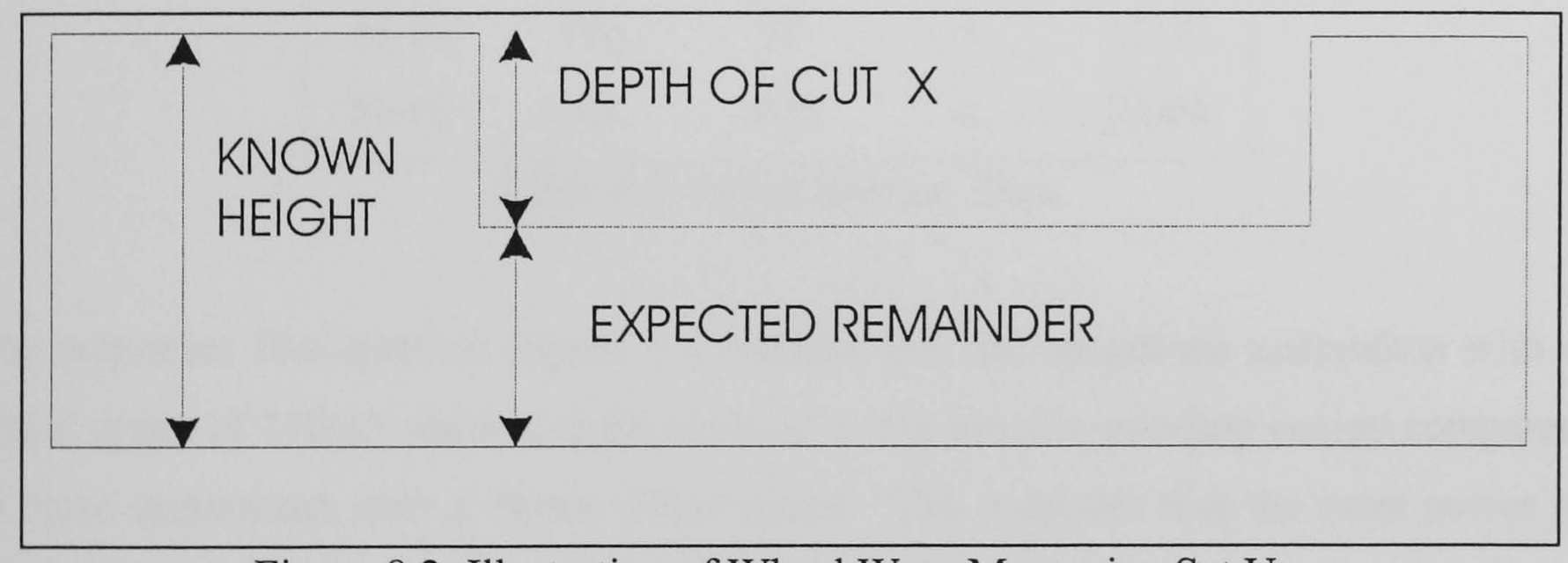

Figure 8.2: Illustration of Wheel Wear Measuring Set Up

During all cuts the Hall Effect device monitored the spindle power which was displayed via a calibrated multi meter. From these calibrated readings the total, spark-out and net power used for each cut could be ascertained.

8.1.2.2 Evaluation of Surface Integrity

From the onset it was noted that due to the wheel being 50mm wide and with a maximum depth of cut of 4mm, the feedrate would need to be restricted in order to keep within the machine's maximum power capacity. This restricted the maximum

attainable material removal rate. The first ring was used to investigate the influence of wheel speed and specific material removal rate. Table 8.1 shows the initial parameters used.

Test Number	Wheel Speed (m/s)	Q'_w (mm^2/s)	Depth Of Cut (mm)	Feed Rate (mm/s)
50-58	30	1	4	0.25
50-59	30	20	4	5.00
50-60	30	50	4	12.50
50-61	30	100	4	25.00
50-62	146	1	4	0.25
50-63	146	20	4	5.00
50-64	146	50	4	12.50
50-65	146	100	4	25.00

Table 8.1: Initial Bearing Tests

The responses illustrated in Figure 8.3 confirm that the operations undertaken with a wheel speed of 146m/s show a slight increase in the specific grinding energy compared to those undertaken with a 30m/s wheel speed. This indicates that the extra power is required to rotate the wheel at this higher peripheral speed and also, as the surface roughness shows, more grits are sharing the load, producing a finer surface finish. Also, the chip thickness will be smaller at the higher wheel speed.

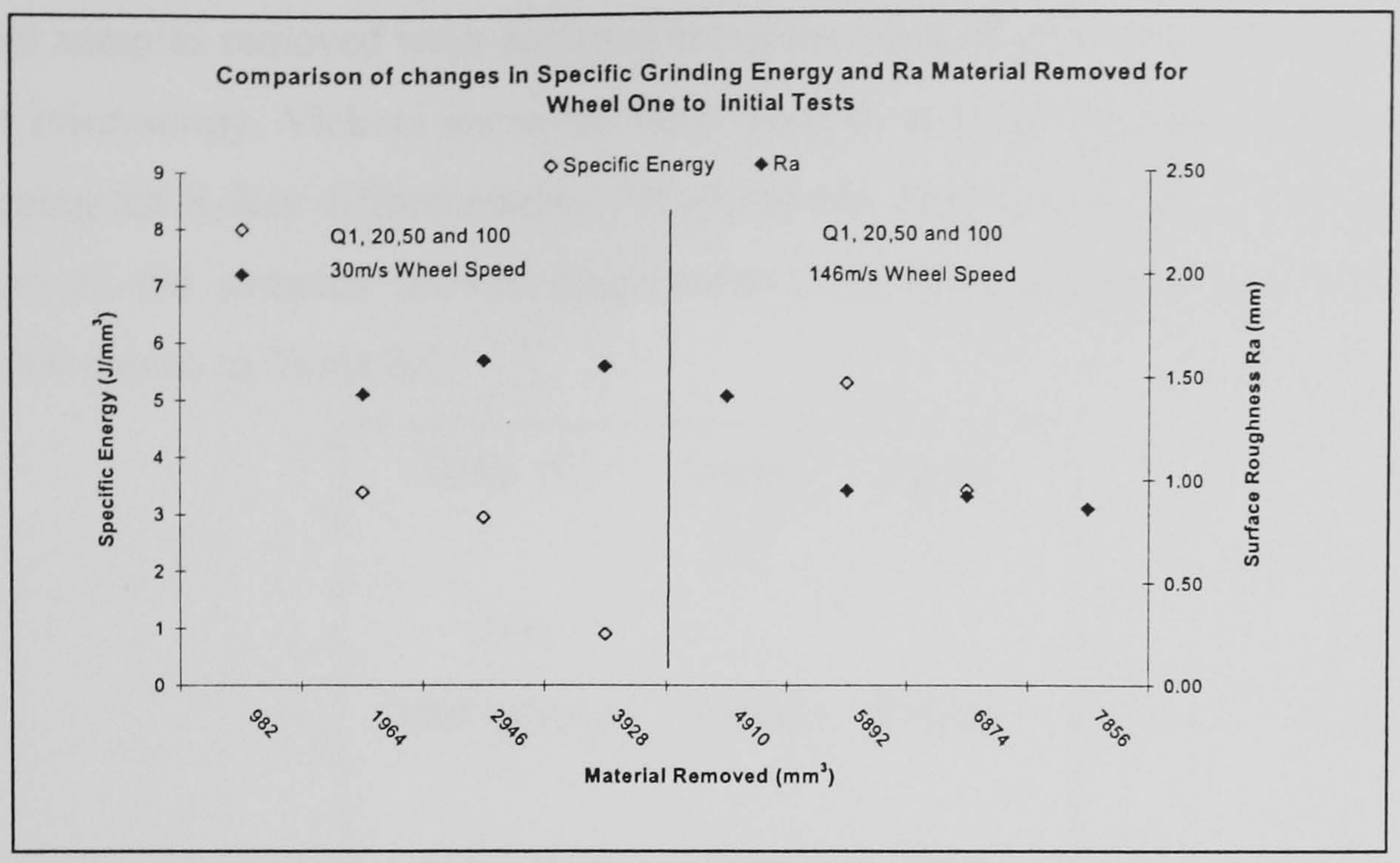

Figure 8.3: Initial Test Results

Further tests were performed using the maximum wheel speed of 146m/s and two specific material removal rates; a maximum of $25mm^2/s$ and for reasons of comparison $10mm^2/s$. In these tests one ring was used a total of sixteen times. Test numbers 50-66 to 50-73 were taken on one side at a Q'_w of $25mm^2/s$ and test numbers 50-74 to 50-81 were taken on the other side at a Q'_w of $10mm^2/s$. This gave a greater understanding of the wheel wear characteristics in relation to this type of grinding process, in relation to this type of wheel with different removal rates using this type of grinding fluid delivery strategy.

For test numbers 50-66 and 50-74, samples were removed from the $10mm^2/s$ edge and 50-75 and 50-77 from the $Q'_w = 25mm^2/s$ tests. The resulting residual stress measurements were taken using the Siemens XRD Diffractometer.

8.2 M50 Bearing Results

The analysis of the sectioned bearing rings utilised a number of procedures varying from surface, sub-surface analysis to XRD residual stress measurements. A Talysurf profilometer was used to quantify the R_a and R_t surface roughness measurements and these proved to be consistently below the stipulated roughness of $2\mu m$ R_a.

The four samples removed were analysed using the Scanning Electron Microscope, sub-surface microscopy, Vickers micro-hardness profiles and residual stress measurements taken using the X-Ray diffractometer. Of all the test results the most interesting feature was that all the samples showed characteristics of high compressive stresses. The results are shown in Table 8.2.

Ring 103 Test Designation	Sigma X (MPa)	Sigma Y (MPa)
50-66	-1032	-826
50-74	-1001	-801
50-75	-897	-979
50-77	-992	-959

Table 8.2: XRD Residual Stress Measurements

Sub-surface micrographs were taken from the four specimens chosen. For all four samples no sub-surface damage was noted, which correlates well with the residual stress measurements listed in Table 8.2, sub-surface microscopy and Vickers hardness profiles.

Test Number 50-66

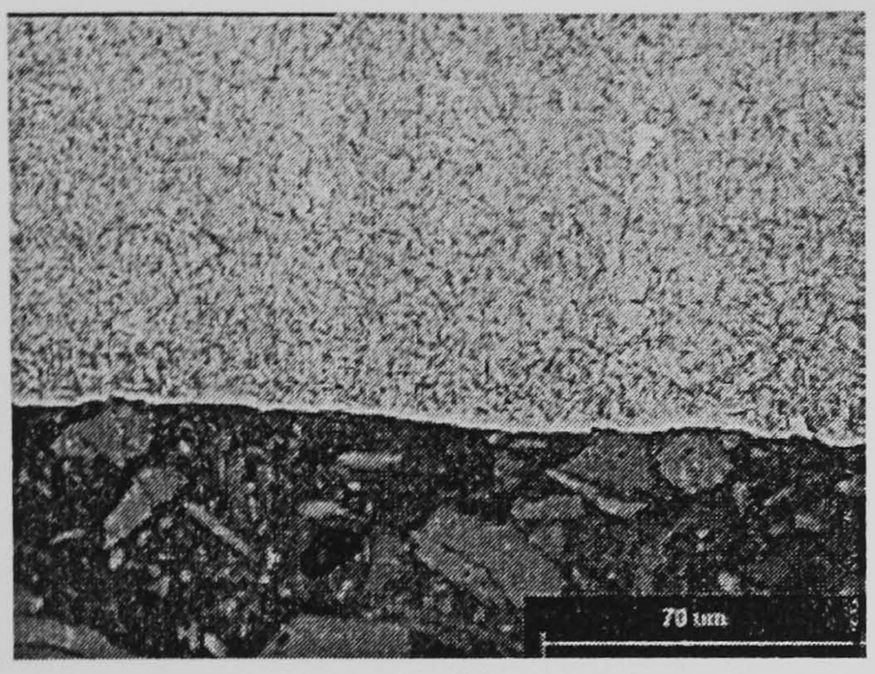

Sub surface Microscopy

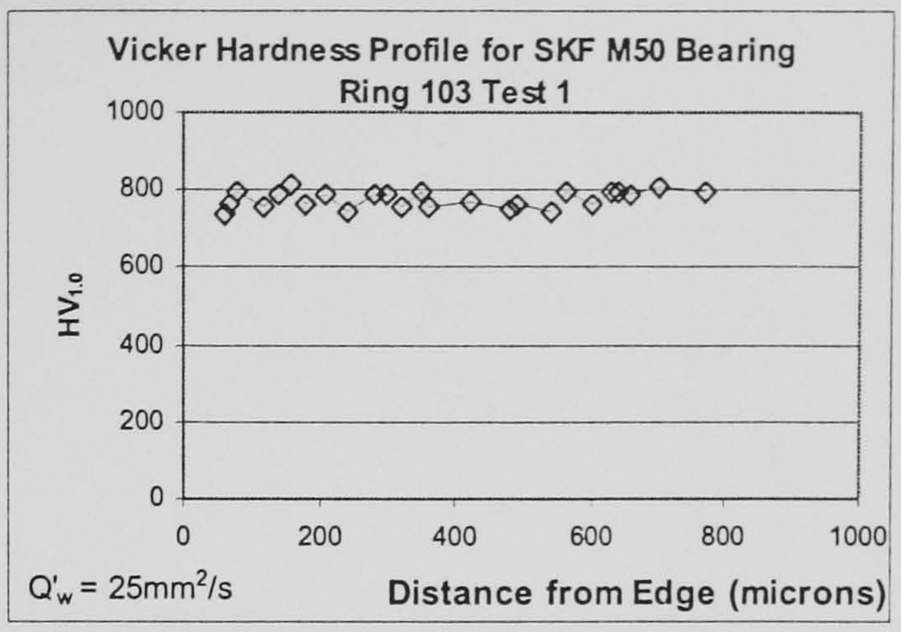

Vickers Hardness Profile

Figure 8.4: Example of Bearing Test Number 50-66

Figure 8.4 shows no damage was evident and the Vickers hardness profile is consistent with this result.

Due to the various Q'_w values and wheel speeds tested, one way in which this array of parameters can be analysed is by the measure of specific grinding energy against Q'_w. Figure 8:5 shows that as the chip thickness increases in size the specific energy required for the process decreases showing that indeed, when Q'_w is increased a more efficient process is produced, as expected for HEDG.

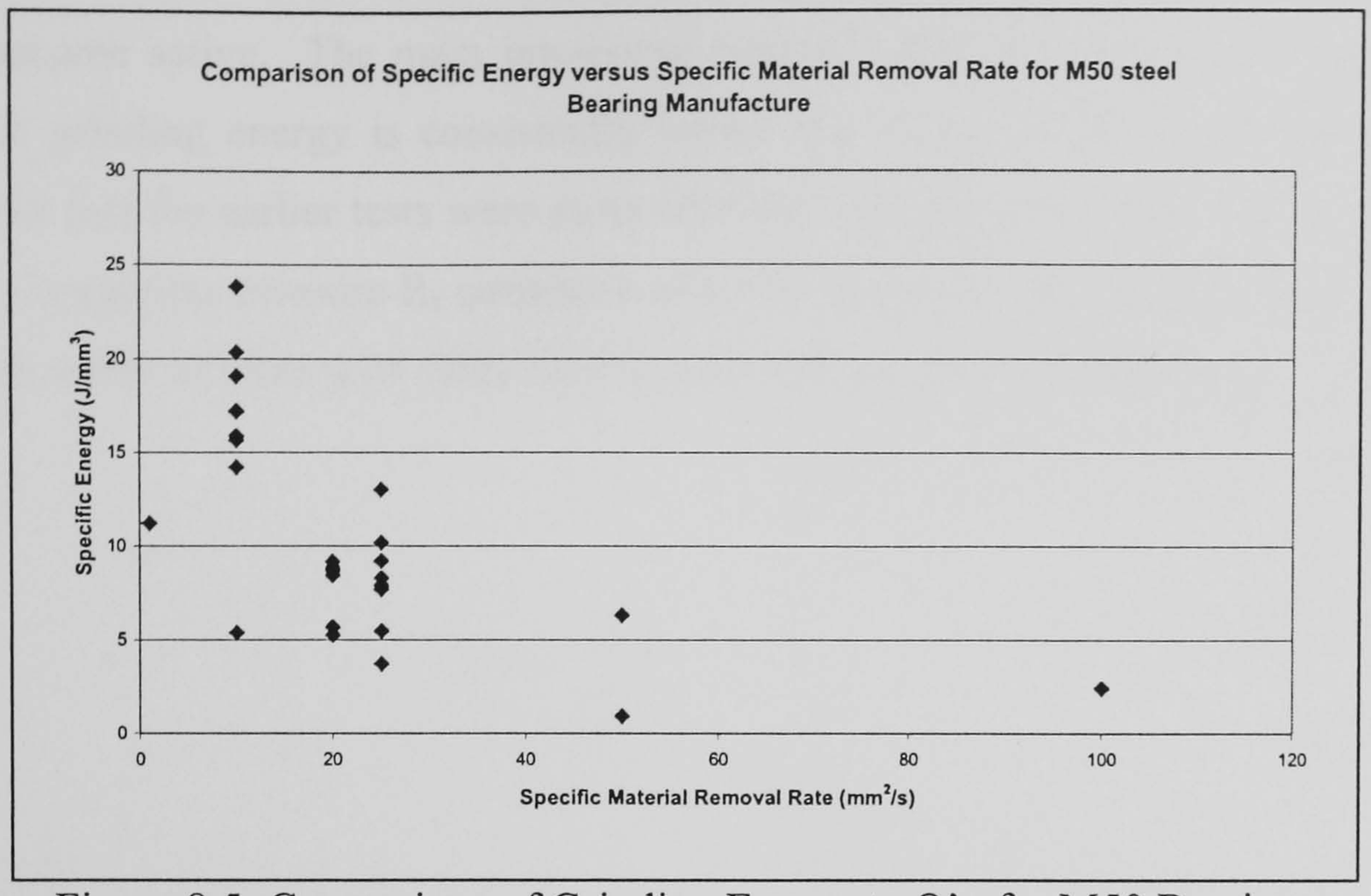

Figure 8.5: Comparison of Grinding Energy to Q'_w for M50 Bearings

Figure 8.6 illustrates the results obtained from tests 50-82 to 50-89, which were used for the final testing of two specific material removal rates with four tests being undertaken at each rate. Firstly a Q'_w value of 25mm²/s was used, then one of 10mm²/s for four tests.

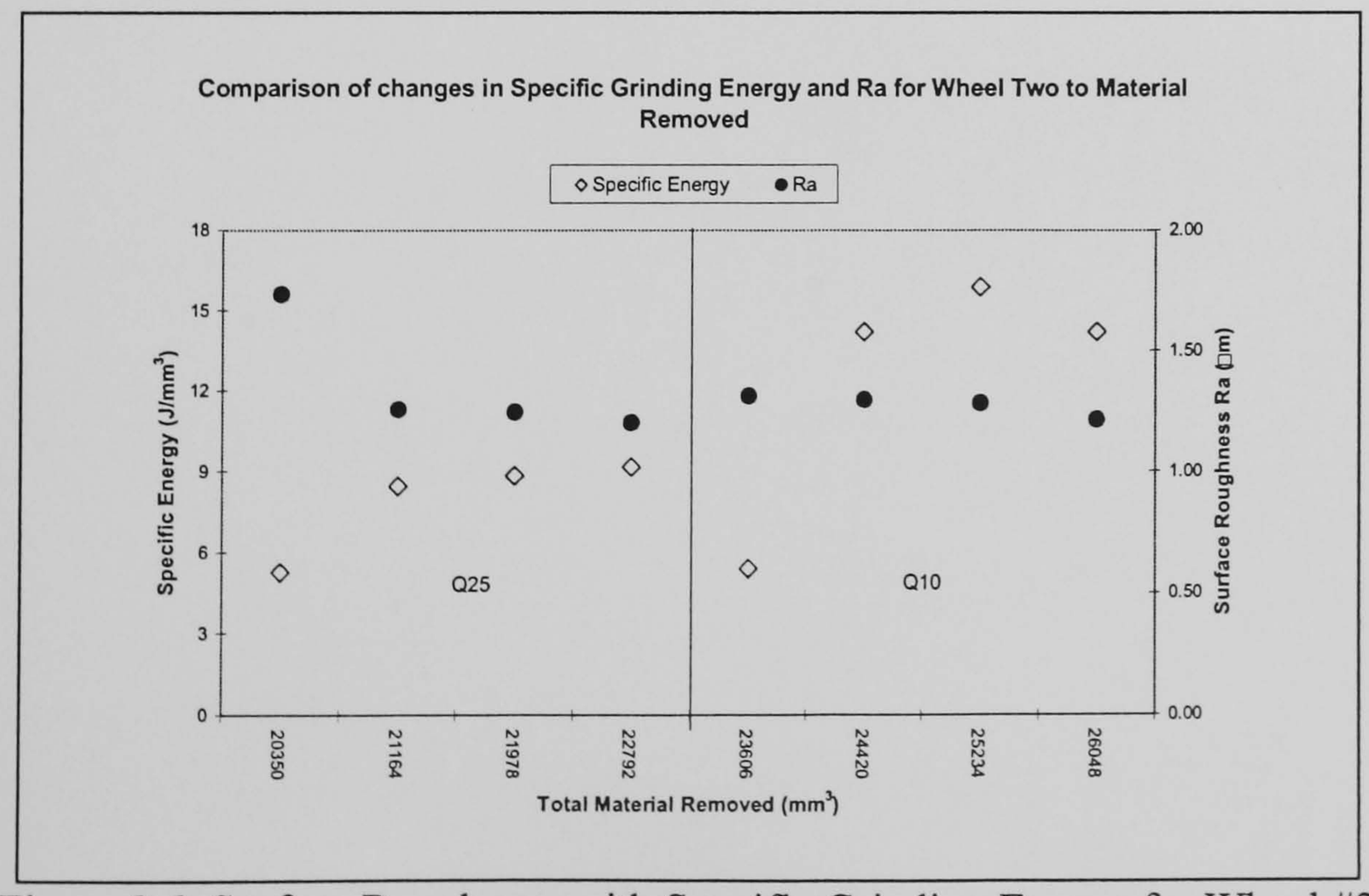

Figure 8.6: Surface Roughness with Specific Grinding Energy for Wheel #2

Figure 8.6 shows a rise in specific grinding energy as the wheel is conditioned and more grits become active. The main interesting feature is that with a Q'_w of $25mm^2/s$ the specific grinding energy is consistently lower than when the Q'_w is $10mm^2/s$. This indicates that the earlier tests were more efficient with regard to wheel wear. Also the surface roughness measure R_a correlates with this theory because the R_a value seems to be more stable as more grits come into contact with the workpiece surface.

Test Number 50-75

M50 Ground with mineral oil – Q' = 10 mm^2/s

Wheel Speed = 100m/s

Feed Rate = 2.5mm/s

Depth of Cut = 4mm

Grit Size = B151

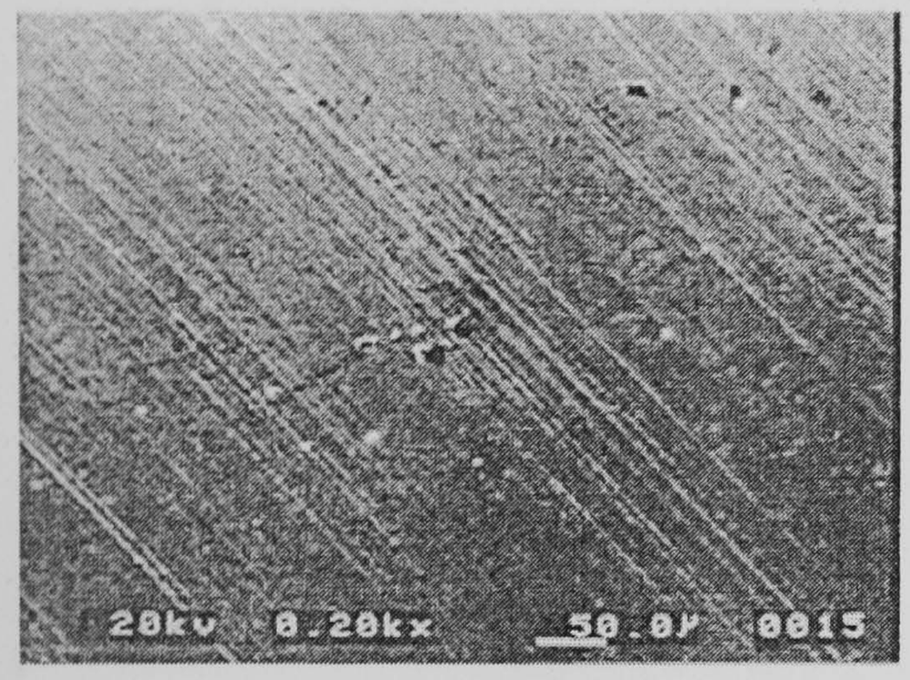

Scanning Electron Microscope Image

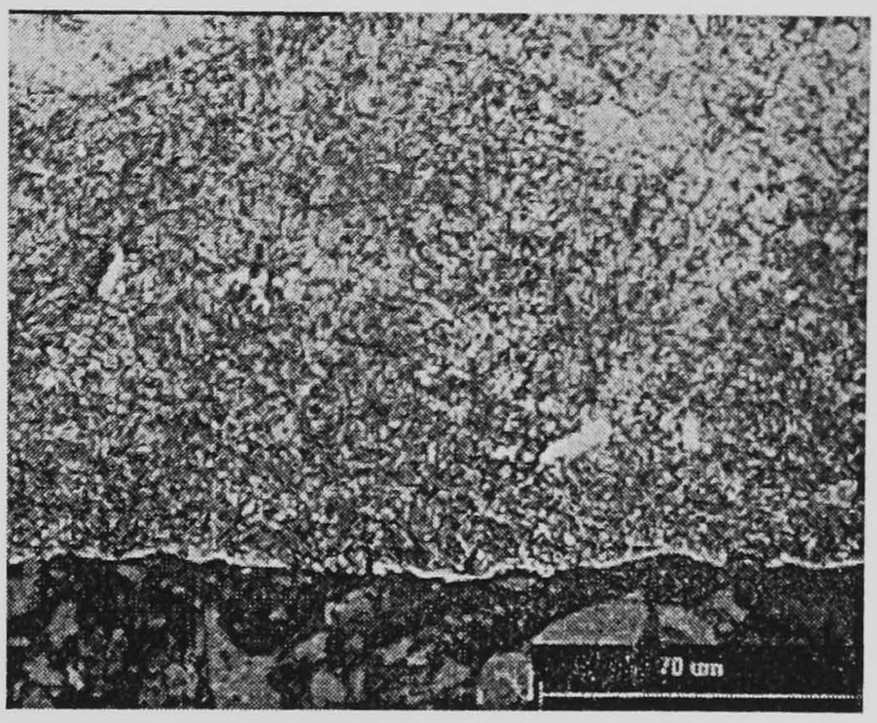

Sub-Surface Micrograph

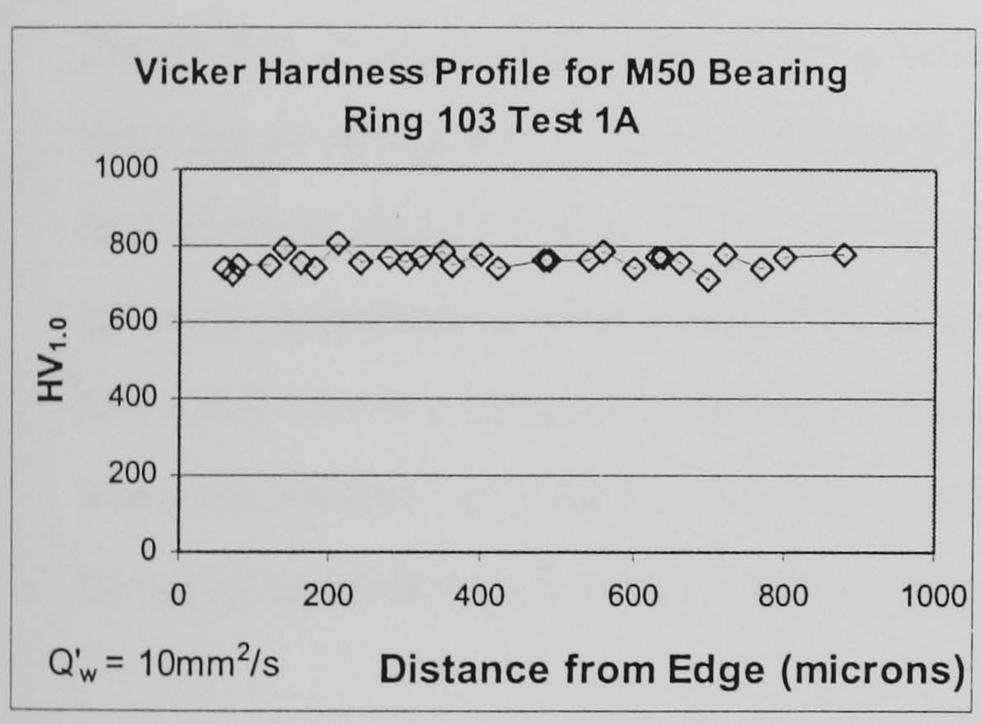

Vickers micro-hardness

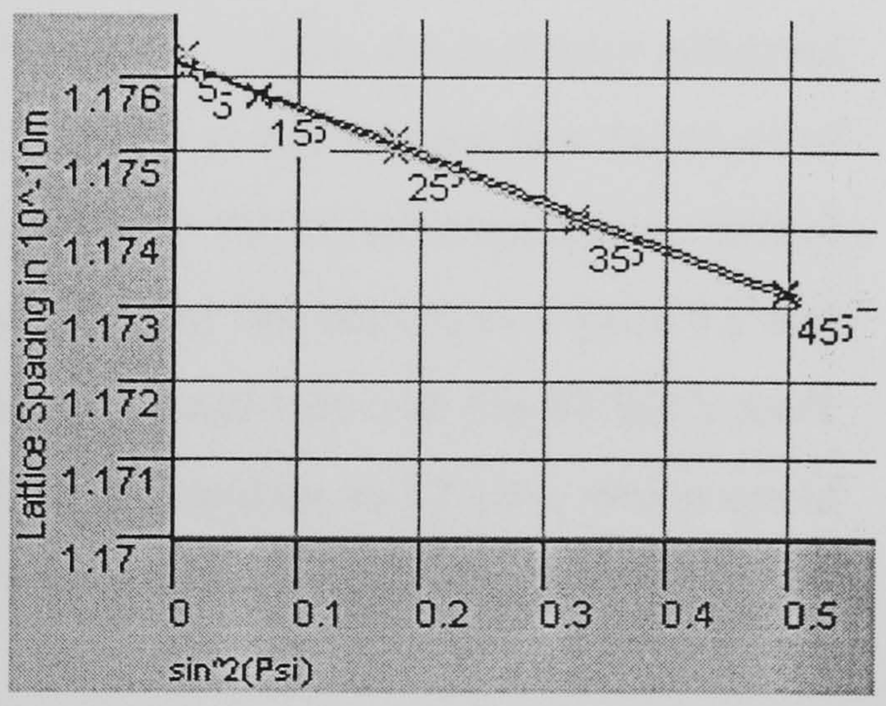

XRD Stress Trace

Responses	Outputs
R_a	0.858 microns
R_t	6.884 microns
Specific Energy	19.07 J/mm^3

Figure 8.7: Test Number 50-75

Figure 8.7 shows an example of a test summary for test number 50-75

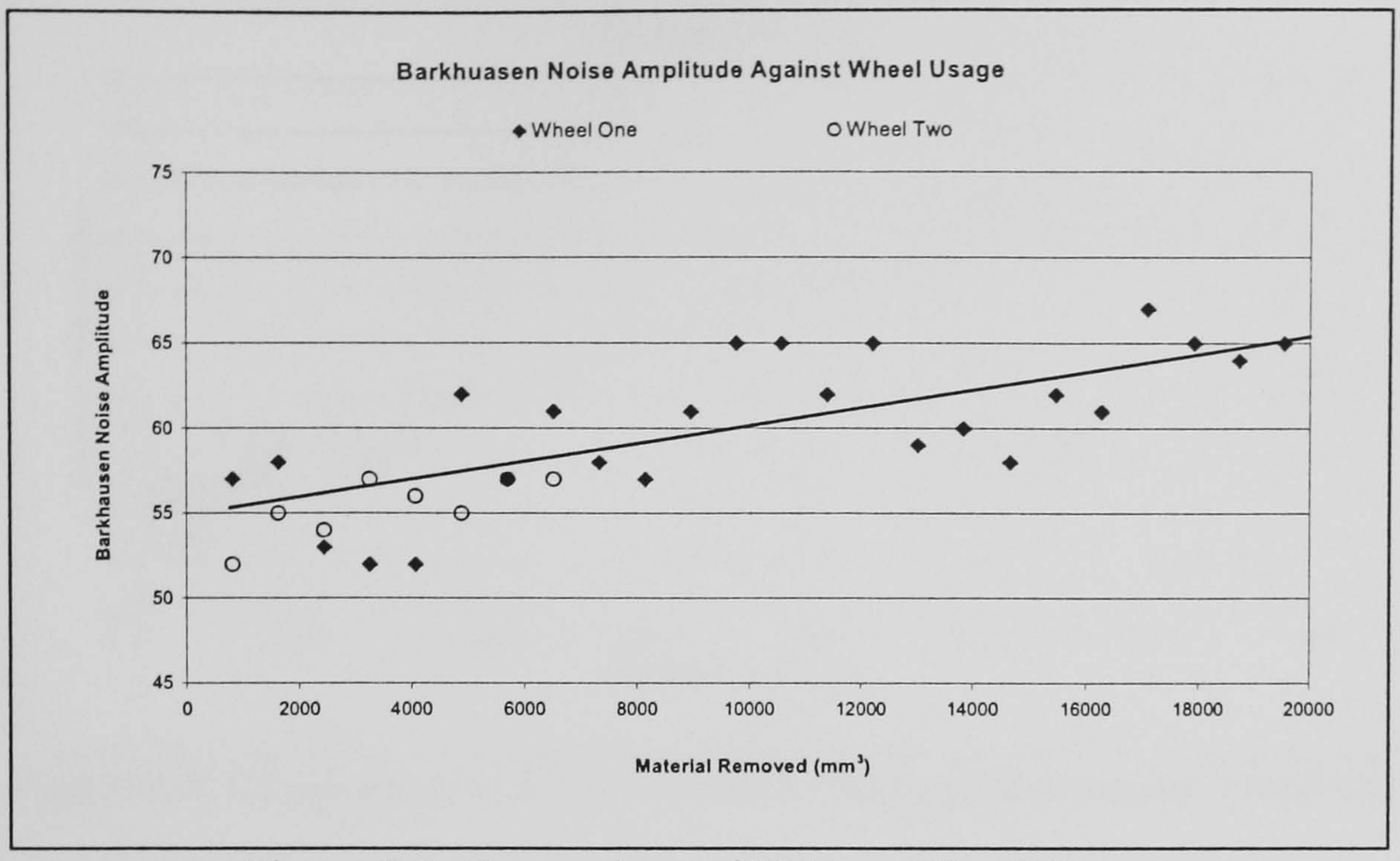

Figure 8.8: Comparison of BNA to Wheel Usage

Figure 8.8 shows a slight rise in BNA with wheel usage. Using the evidence collected from the grinding tests shown in Figure 5.7 of Chapter 5, it can be seen that the onset of tensile stress occurs with a BNA number of around 85 to 90. If the responses to further grinding operations follow a linear trend such as the trend line shown in Figure 8.9 and this trend line is extended as shown in Figure 8.9, the trend line cuts the 90 BNA mark when 66,500mm^3 of material has been removed. This equates to 82 cuts, which could be easily exceeded with a more optimised grinding fluid delivery strategy.

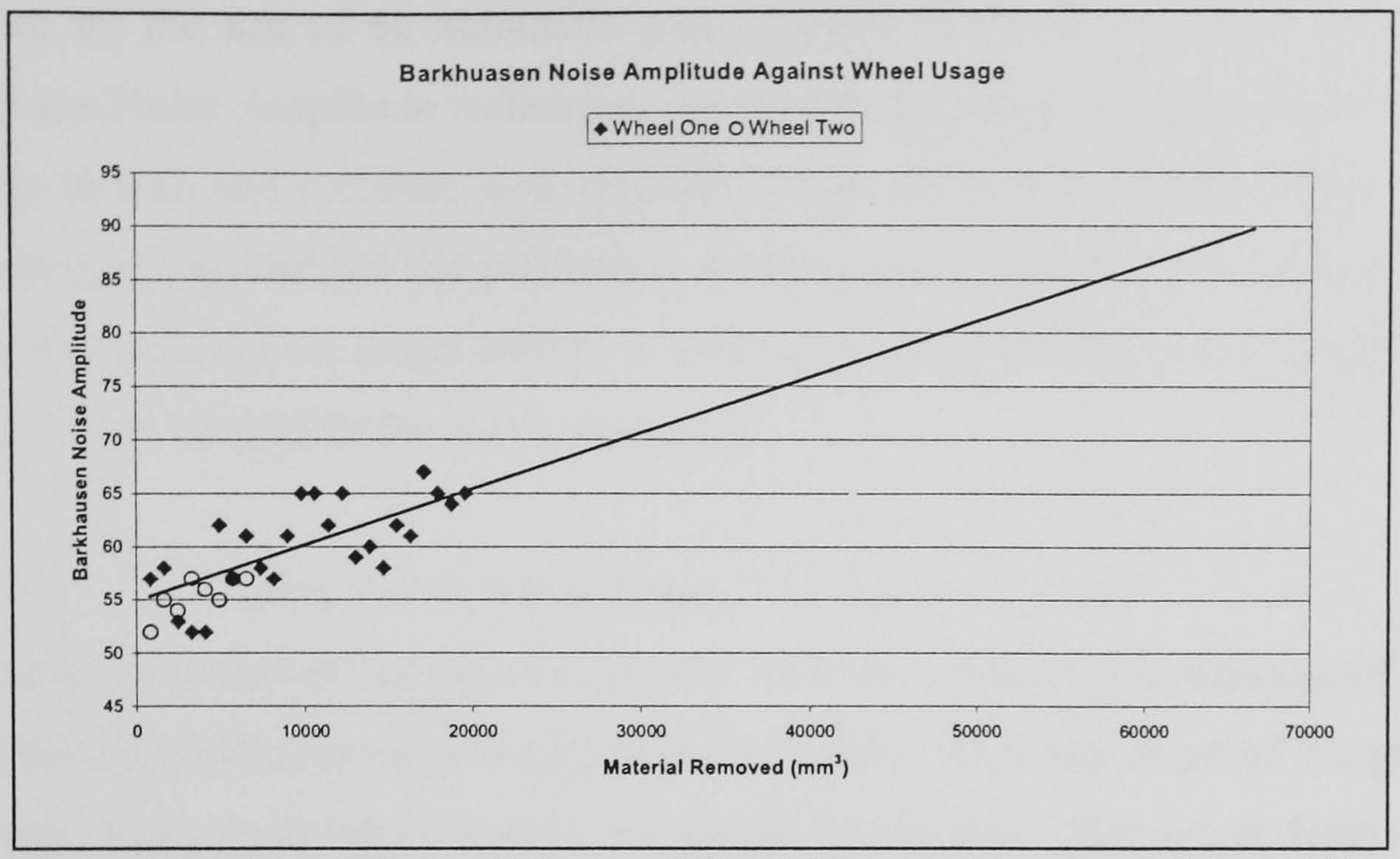

Figure 8.9: Comparison of BNA to Wheel Usage with extended Trend line

8.2.1 Summary

The main objectives laid down by the sponsoring bearing company have been consistently equaled and surpassed. The timescale was easily surpassed from the 60 minutes prescribed to approximately 7 seconds at the maximum specific metal removal rate attempted. At present a number of passes are required for the completion of a bearing whereas only one was used during these tests. Conventional abrasives are currently used and these are not as tough as CBN grits and the thermal characteristics of the grits are less efficient than those of CBN. Therefore the depths of cut taken have to be lower which in turn means higher specific grinding energies and subsequent higher temperatures being experienced by the workpiece. The HEDG concept of high depths of cut and high feed rates enabled, through the excellent mechanical and thermal properties of CBN grits, the attainment of higher efficiencies which can be of major benefit to industry.

Even when using the highest specific metal removal rate no grinding damage was witnessed. The benefits of this process over the original manufacturer's process are considerable. By using a grinding centre such as the Edgetek, the operator's skill requirement can be reduced due to the process being totally automated. Because the time required for the completion of the process is cut so dramatically the economical benefits of an increase in production levels will be substantial. This could be further

enhanced by the use of an automatic part changer within the system. The use of Barkhausen Noise Amplitude techniques has shown that these measurements are quick and easy to take and correlate well with the X-Ray diffraction measurements. Using this technique has enabled the prediction of when the onset of tensile stresses occur. This in itself could be a major benefit to aviation bearing manufacturers where tensile stresses are not acceptable for safety reasons.

8.3 Turbine Blade Manufacture

This section summarises the final assignment with respect to the manufacture of MAR-M-002 turbine blades for an aero-engine manufacturer. This task required the grinding of 'fir tree' blade roots which were to be ground in one pass. The actual depths of cut experienced by the wheel varied from 1.2mm to a maximum of 7.8mm using the Edgetek 5-axis superabrasive-grinding machine. The parameters used and experimental responses are shown in Appendix J.

The objectives of the programme of work were as follows:

- achieve an R_a surface roughness target value of better than 1.6μm
- ensure that the grinding procedures produced samples with only compressive residual stress characteristics
- compare CBN HEDG grinding with the current Viper process

With both the final dimensions of the finished blades and the depth of cut to be used already decided, the only other variables were feed rate and wheel speed. The Viper process cuts the material using Aluminium Oxide wheels at a peripheral wheel speed of 30m/s, at a feed rate of 1m/min with a depth of cut of 1mm. This equates to a Q'_w value of 16mm^2/s, and one of the aims of this project was to surpass this figure.

8.3.1 Experimental Procedure

The manufacturing tasks on the component were carried out using an in house designed fixture as shown in Figure 8.10 which illustrates how each blade was held in place during the test runs.

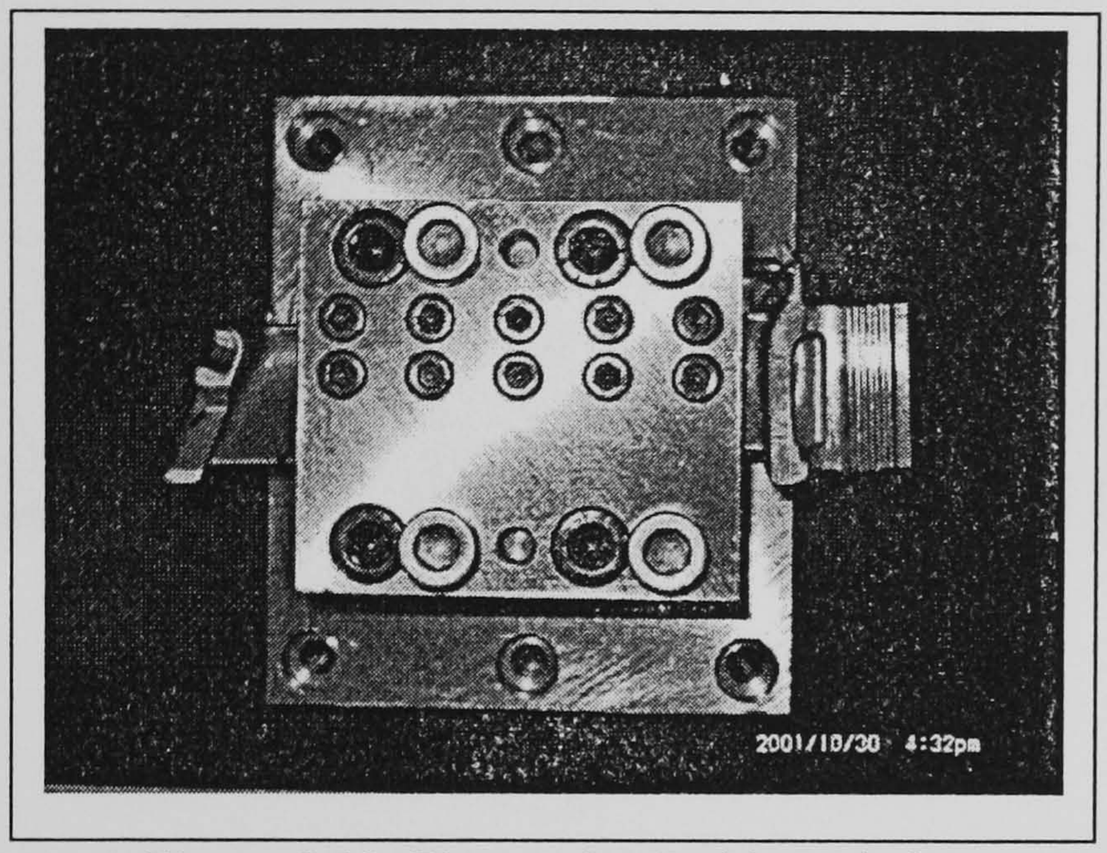

Figure 8.10: Fixture for Turbine Blades

The tests used mineral oil (Castrol Ilogrind 600SP) that was supplied at a rate of 110l/min via a 6.7mm diameter jet nozzle at a pressure of 15bar which was the mid-point set up previously found in Chapter 5, section 5.1.2. The grinding wheels were supplied as a pre-conditioned and balanced set which were pre-profiled for the task. The roughing outer wheel was 270mm in diameter and was B252 type grit, and the finishing B126 grit wheel was 200mm in diameter. Figure 8.11 shows a wheel and the grinding fluid nozzles fitted to the Edgetek.

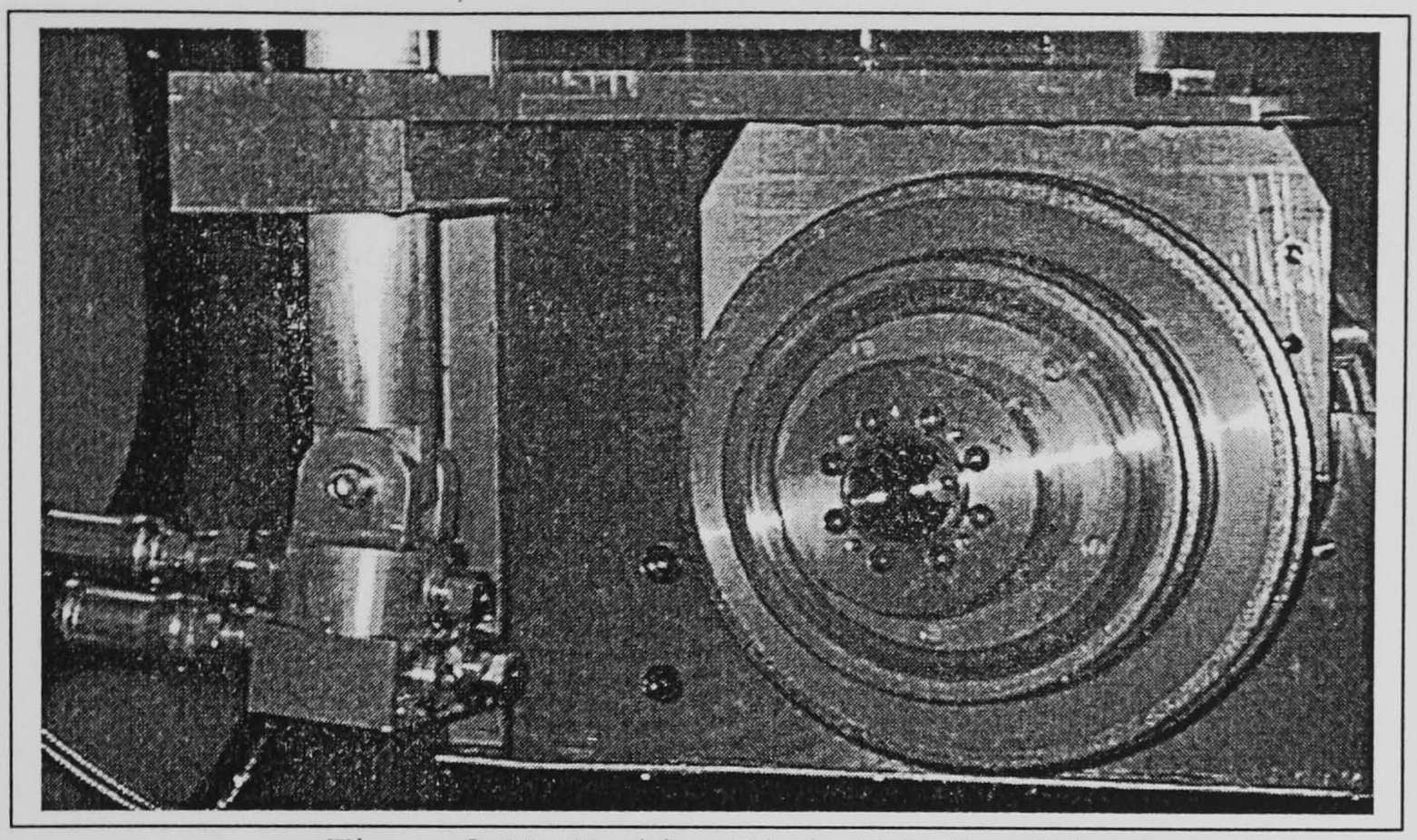

Figure 8.11: Turbine Blade Grinding Wheel

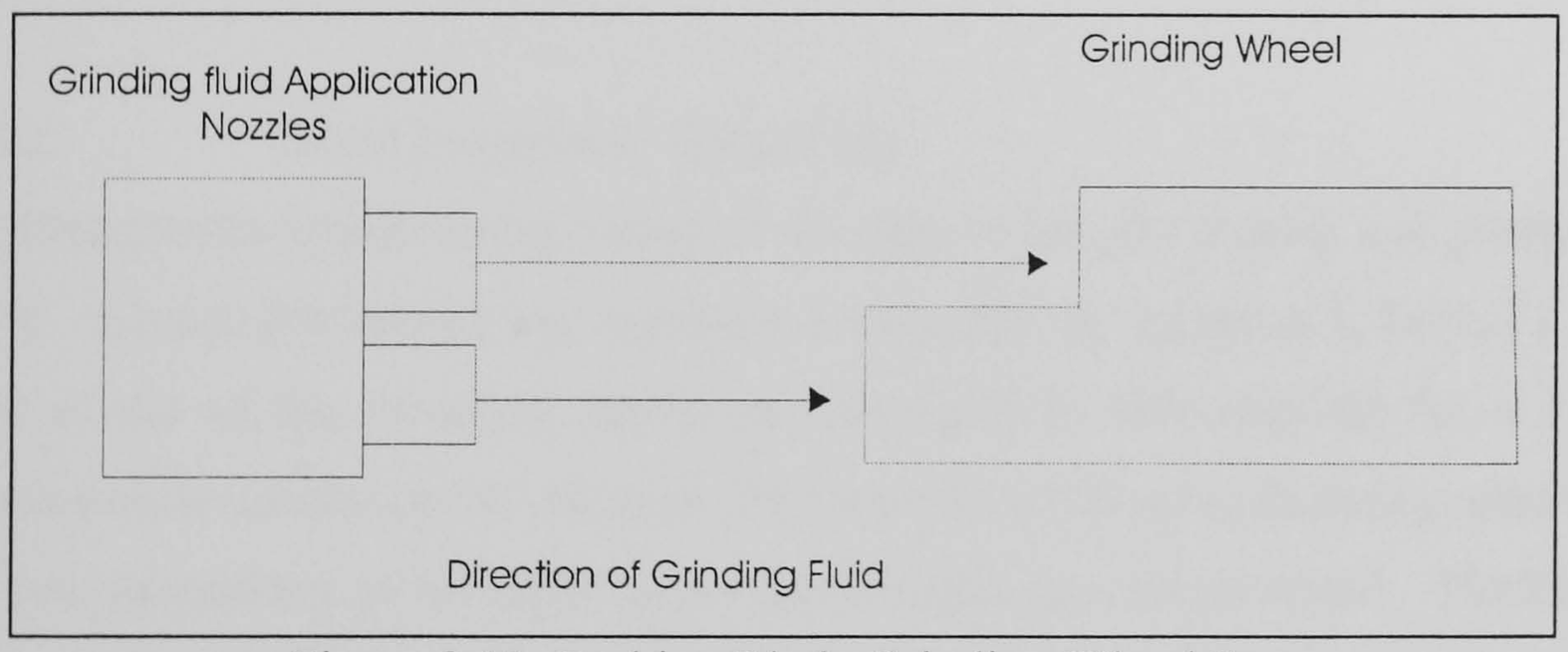

Figure 8.12: Turbine Blade Grinding Wheel Setup

Figure 8.12 shows an illustration of the grinding wheel- grinding fluid setup.

The experimental procedure was divided into several stages as follows:

- tool design and manufacture
- initial exploratory blade cuts
- flat surface grinding
- workpiece analysis
- finished blade analysis

8.3.1.1 Tool Design and Manufacture

The fixture to hold the blades in a rigid manner was of critical importance as any free movement would give rise to vibration and/or chatter and distortion. The design specification of the wheel and the tooling used are given in Appendix J, Figures J.1 to J.3.

8.3.1.2 Initial Exploratory Blade Cuts

Five blades were ground using various feed rates to test the tooling and grinding fluid supply. The test parameters and responses are detailed in Appendix J, Table J.1. As the depth of cut of the roughing operation was fixed to that required for a complete operation to be carried out in one pass, followed by a 50micron finishing operation, the only two parameters to be altered were the feed rate and wheel speed. The feed rates used were 2, 4, 8 and 12.5m/min with the wheel speed being rated to a maximum safe wheel speed of 130m/s. The aero engine manufacturer arranged for the ground blade specimens to be analysed by an independent laboratory. This independent analysis was carried out and the results are presented in Appendix K. Although the conclusions were related to a non-optimised scenario the initial indications were that the CBN HEDG grinding process produced less localised deformation on the surface and it was noted that "the CBN process resulted in a cleaner cut".

8.3.1.3 Flat Surface Grinding

Three flat samples of equi-axed MAR-M-002 material were produced to make a direct comparison with a current state-of-the-art industrial process and the HEDG process. A sample had already been prepared by the company and so this was included as an example of a surface ground under conventional industrial conditions.

As the profiled wheels used in the grinding of the MAR M 002 blades were of specific grit size, the same sized grits were used in the flat surface grinding operations. Thus, roughing cuts were taken by B252 CBN grit wheels and the finishing cuts were taken using a B126 grit wheel. All wheels were 15mm wide with a diameter of 200mm.

Six separate cuts were undertaken and were numbered 1 to 6. The first set of three were purely exploratory in terms of setting up suitable grinding fluid parameters. Three further cuts were then performed. The first (cut 4) was a direct comparison with the competing process but using a CBN electroplated wheel rather than an aluminium oxide wheel. Cuts 5 and 6 investigated the influence between two wheel speeds, these being 100m/s and 146m/s. The depths of cut and feed rates were 2mm and 25mm/s respectively.

8.3.1.4 Workpiece Analysis

The analysis of the final blades utilised a number of procedures varying from surface, sub-surface analysis to XRD residual stress measurements. A Talysurf profilometer was used to quantify the R_a and R_t surface roughness measurements and residual stresses were measured at University of Manchester Institute of Science and Technology (UMIST).

8.3.1.5 Final Grinding Operations

Utilising the knowledge gained from the initial series of experiments, the final grinding operations were carried out on MAR-M-002 blades. As the depth of cut was essentially fixed to the full amount, the main parameters which were varied were wheel speed and feed rate.

It became clear that as the geometry of the cut was quite complex the normal calculation for specific grinding energy would not be appropriate under these conditions. The depth of cut varied from 2.2mm to 7.8mm, therefore as the maximum depth of cut could not be used to calculate the specific grinding energy, it was decided that a calculated mean specific grinding energy would be used based upon the mean depth of cut of 4mm and width of cut of 10.5mm. To this end all calculations, assumptions and conclusions have been based on this measure.

8.4 Blade Analysis

The analysis of the final blades utilised a number of procedures varying from surface, sub-surface analysis to XRD residual stress measurements. A Talysurf profilometer was used to quantify the R_a and R_t surface roughness measurements and these proved to be consistently below the stipulated maximum surface finish requirement of 1.6μm. Also the residual stress measurements were consistently compressive in nature.

Two blades were sectioned and the end 4mm wide parts of the blade roots were dispatched to UMIST for XRD residual stress analysis. The remaining samples were used for surface analysis using the Scanning Electron Microscope, sub-surface examination and Vickers micro-hardness profiles. The measured residual stresses are listed in Table 8.4.

Test Number	Residual Stress (MPa)	Process Used
002-04	-651	HEDG
002-06	-707	HEDG
002-07	-1894	HEDG
002-10	+905	VIPER
002-46	-916	HEDG
002-48	-805	HEDG
002-54	-468	HEDG
002-56	-219	HEDG

Table 8.3: MAR-M-002 XRD Residual Stress Measurements

Test number 002-04 used a feedrate of 17mm/s with a wheel speed of 39m/s. These relatively low parameters were used to compare the influence of CBN directly with the flat cut sample produced by the turbine blade manufacturer's process. The manufacturer's sample had a residual stress of +905MPa and the CBN sample was -651MPa. This can probably be attributable to the thermal characteristics and toughness of the grit in comparison to Aluminium Oxide grit. Sample 002-06 used a feedrate of 25mm/s with a wheel speed of 100m/s. Again this sample produced a compressive stress which is a mandatory requirement for an aviation turbine blade. One could argue that it is an added advantage of HEDG that no post process such as shot-peening was required to produce these stresses. Sample 002-07 used the same parameters as 002-06 but the wheel speed was increased to the maximum value of 146m/s. The residual stress was found to be compressive with a value of -1894MPa.

These results indicated that grinding operations using CBN grits would be more efficient than those using aluminium oxide wheels. Taking into account the radical

levels of compressive stress it was deduced that a wheel speed of 100m/s was the most efficient for this type of procedure which on the evidence seen here would produce mid-range compressive stresses.

The micro hardness profiles which are shown in Figure 8.13 gave some evidence of hardening at the surface of flat sample 002-04 which could be due to the extremely slow feed rate used. The remainder had similar characteristics of relatively undamaged material.

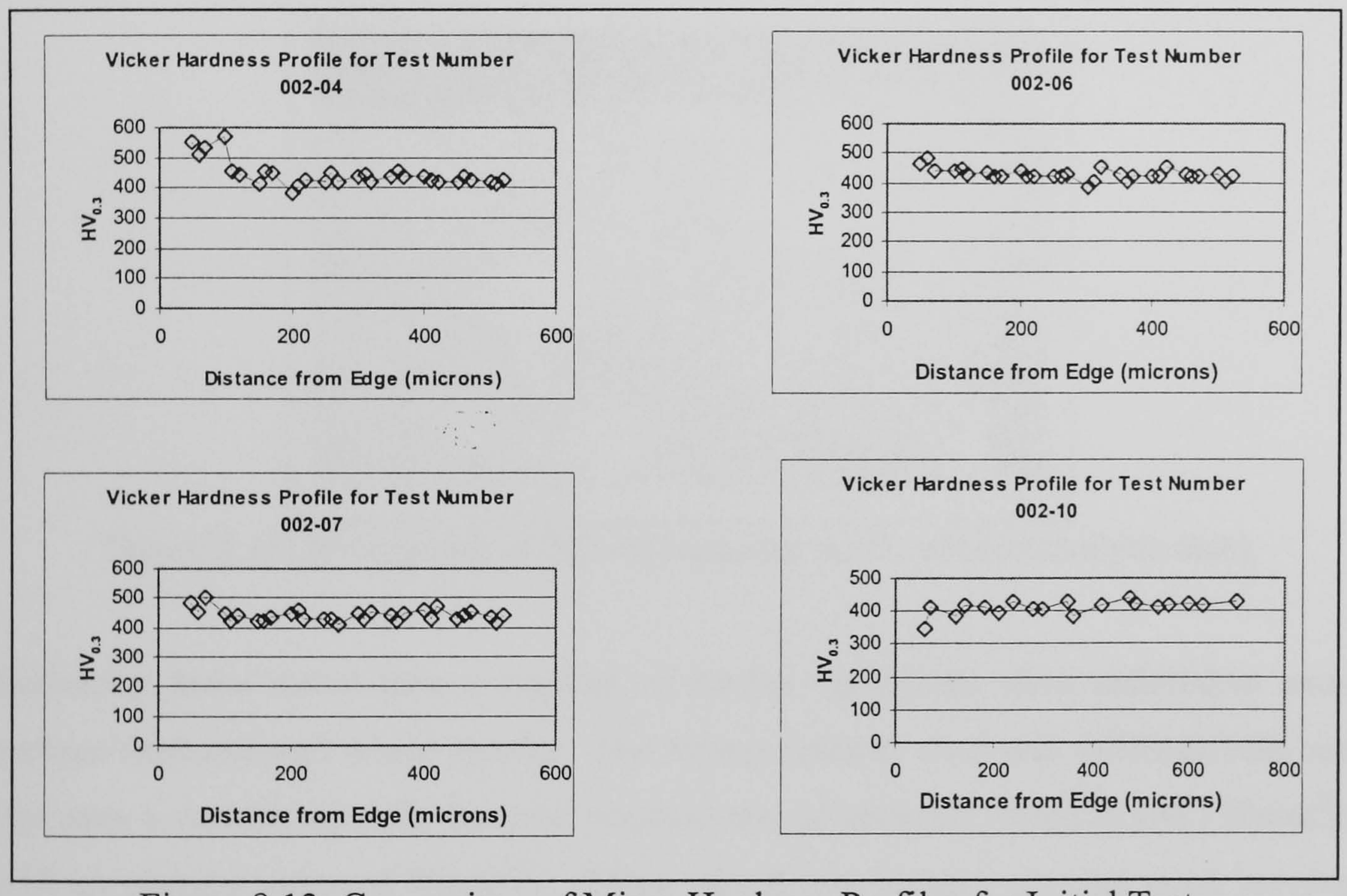

Figure 8.13: Comparison of Micro Hardness Profiles for Initial Tests

Figures 8:14 and 8:15 show micrograph comparisons of the Viper process with a cut using similar parameters but with CBN grit. The same dendritic structure with large carbides can easily be seen in both figures, and in the case of Figure 8.14 it can be seen that the wheel used was in an unconditioned state and the cut edge of Figure 8.15 has been performed using an extremely well conditioned aluminium oxide wheel. Even taking this into account both surfaces seem quite jagged in appearance.

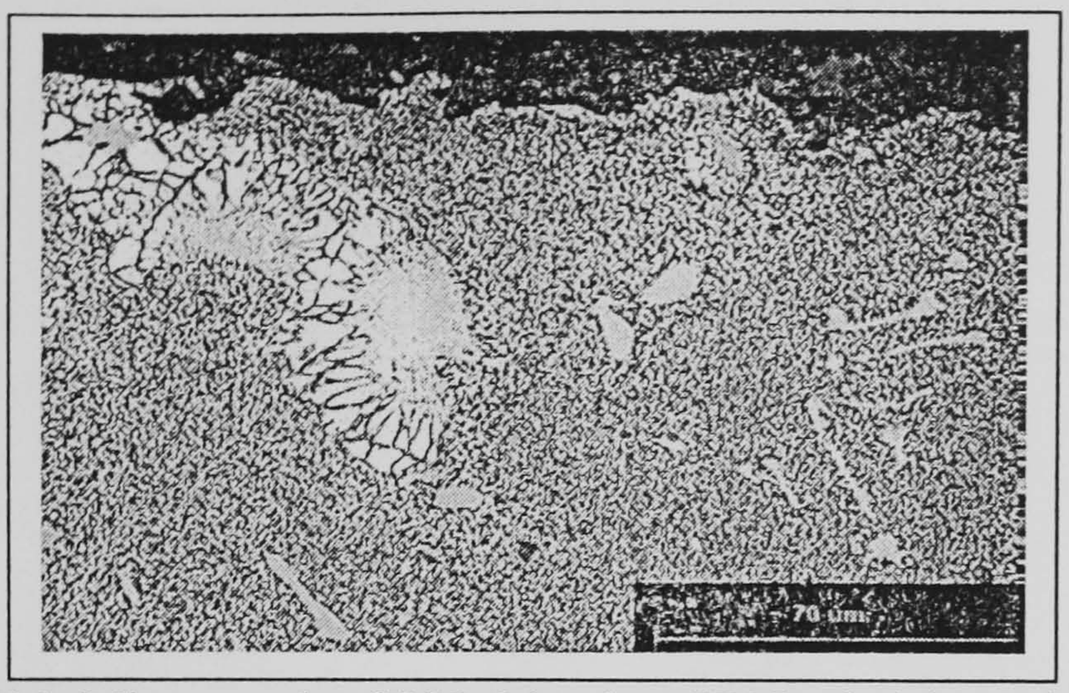

Figure 8.14: Micrograph of 002-04 using CBN grit (electrolytic etch)

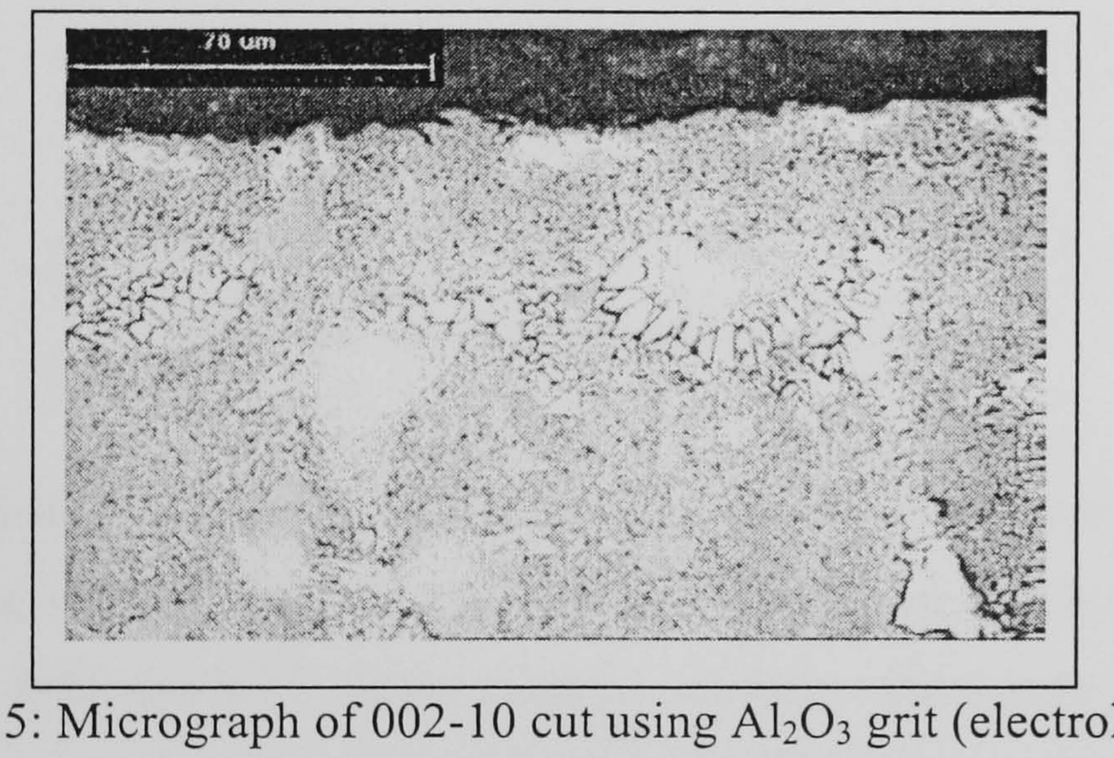

Figure 8.15: Micrograph of 002-10 cut using Al_2O_3 grit (electrolytic etch)

Following these initial tests a number of further operations were undertaken using various feedrates and wheel speeds. The fastest feedrate used was 1000mm/min, and this gave a variable specific material removal rate of between 19mm^2/s and 130mm^2/s, with an average value of 75mm^2/s. When taking into account that the stock removal was performed with one cut at these high feedrates on this tough material, it is quite impressive in comparison to the specific material removal rate of the Viper process. The finish grinding operation was performed using the same feedrates but the depth of cut was reduced to 50microns.

Test Number	Feed Rate (mm/min)	R_a (microns)	R_t (microns)
002-47	400	0.749	4.478
002-49	400	0.694	5.215
002-51	1000	0.604	4.754
002-53	1000	0.118	1.563
002-55	1000	0.125	1.485
002-57	1000	0.112	1.554
002-61	1000	0.111	0.865
002-65	1000	0.120	0.875

Table 8.4: Surface Roughness Results

With the wheel quickly conditioned, the surface roughness R_a measure was consistently around 0.1micron, which again was an excellent achievement for this type of grinding centre. Figures 8.16 and 8.17 show scanning electron microscope images and sub-surface microscopy images of sample 002-55 respectively, which demonstrate the very high quality surface.

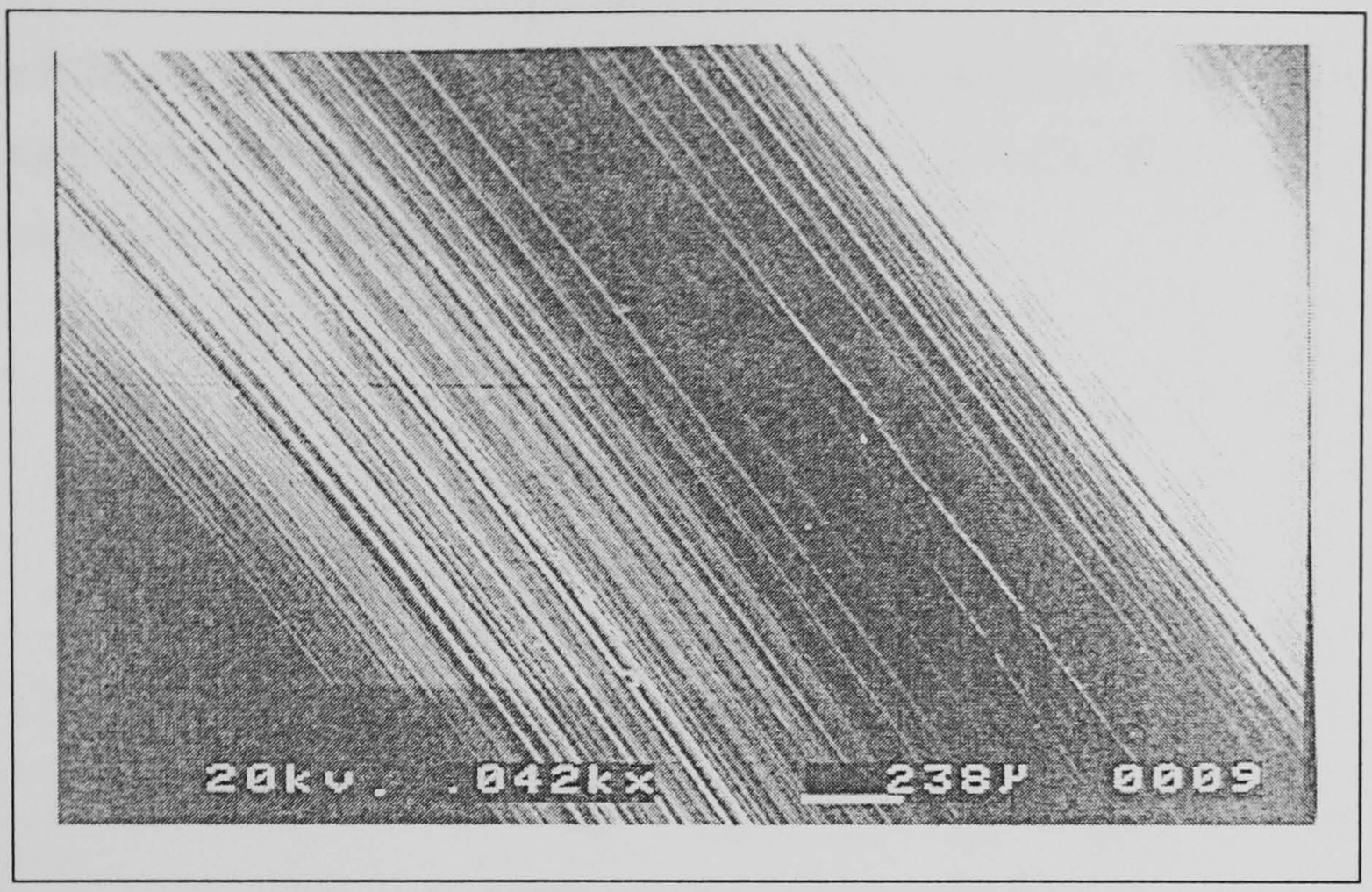

Figure 8.16: SEM micro graph of 002-55 Root

Figure 8.17 shows no evidence of a redeposited or damaged layer and one can also see the smooth surface finish which could be due to the higher wheel speeds used than those employed during the Viper process.

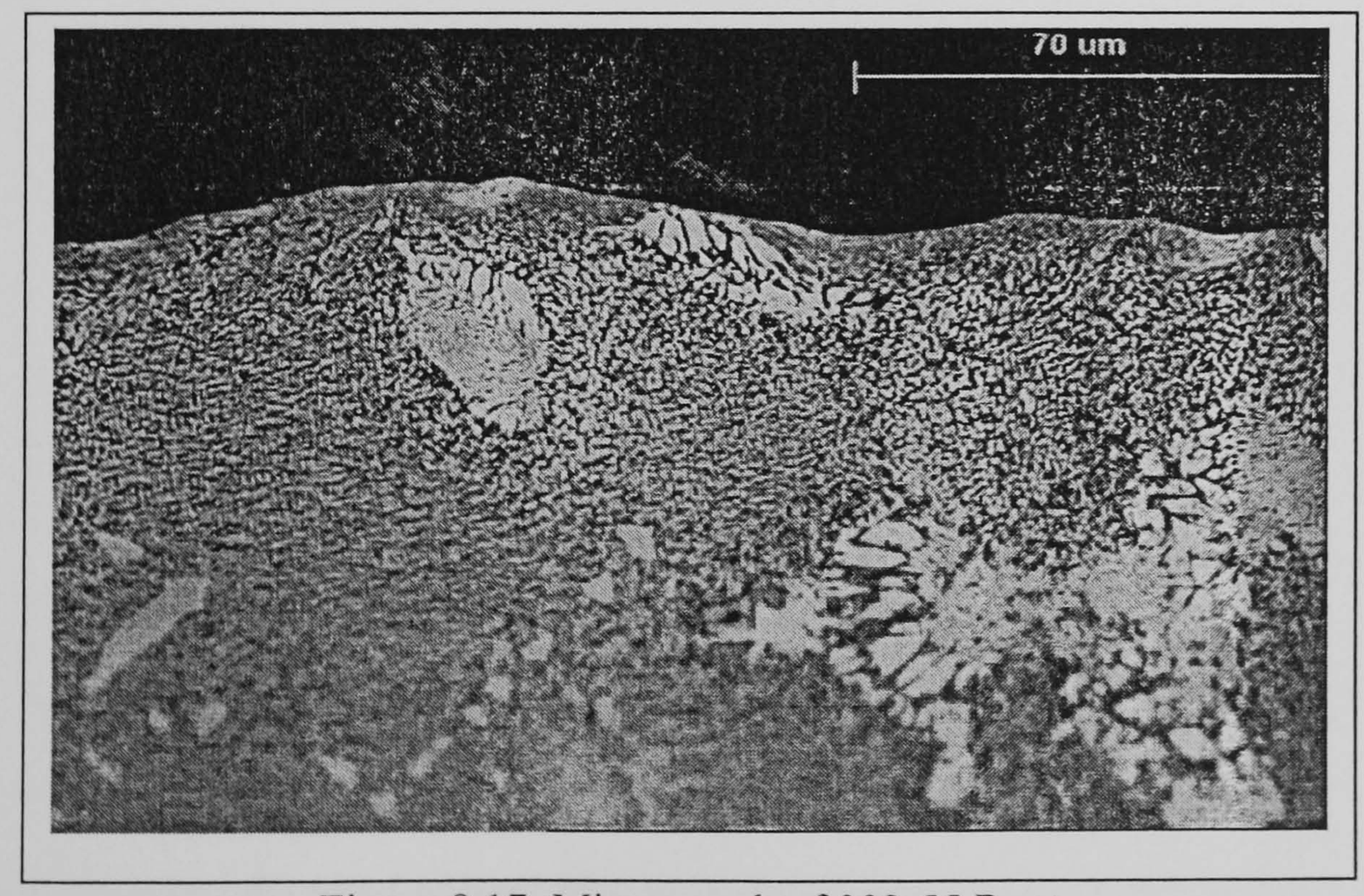

Figure 8.17: Micro graph of 002-55 Root

Figure 8.18 shows the Vickers micro hardness results associated with sample 002-55. Although there seems to be an increase of hardness close to the surface one could associate this with the diamond impacting upon carbide.

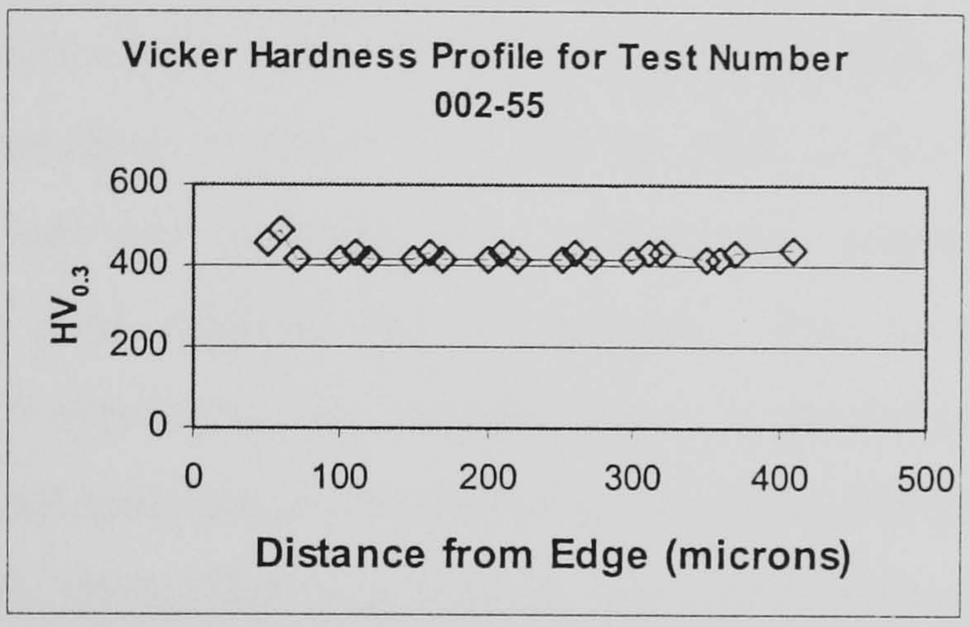

Figure 8.18: Micro hardness profile of 002-55

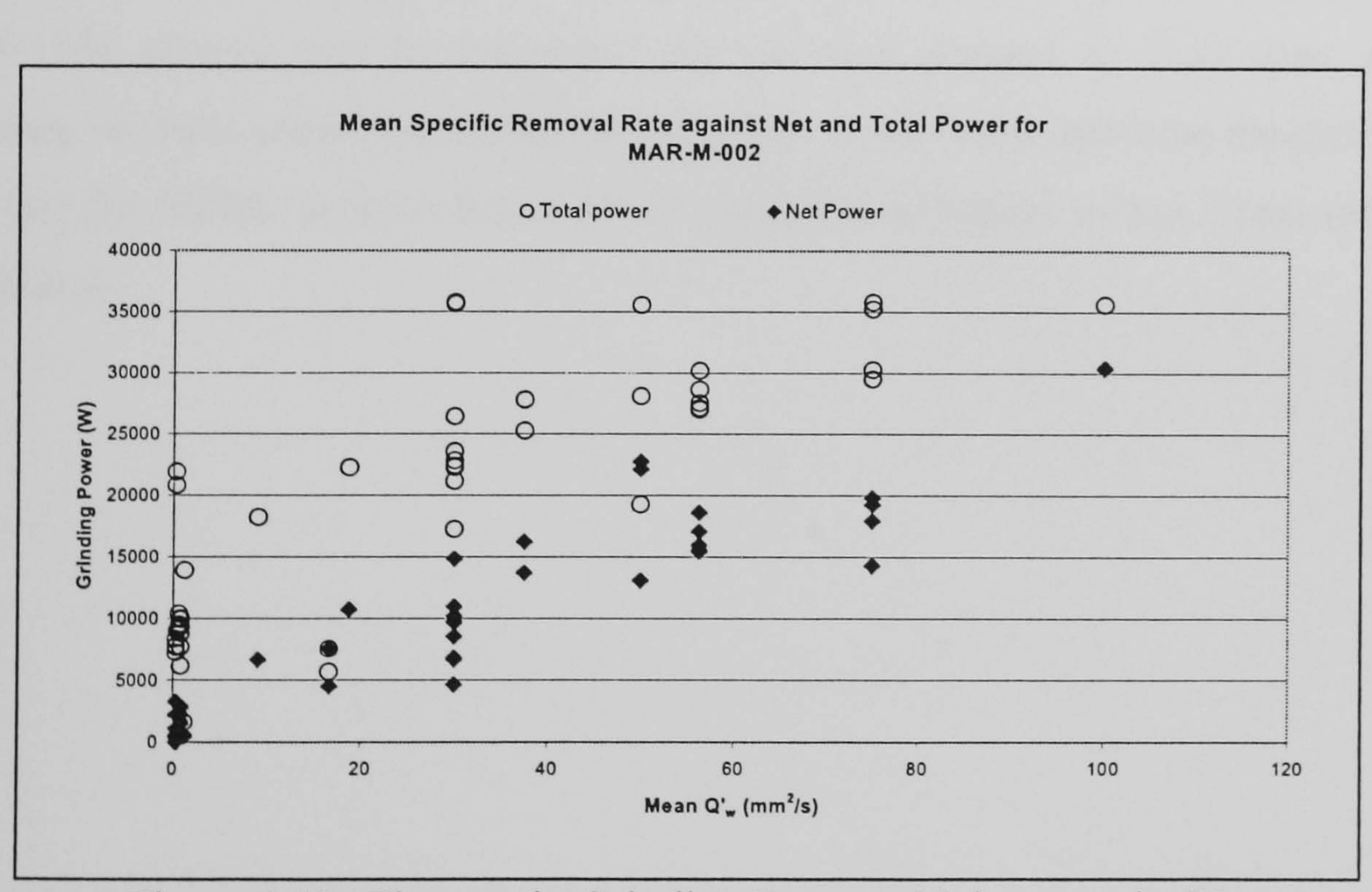

Figure 8.19: Changes in Grinding Power with increase in Q'_w

Figure 8.19 shows the trend of how both the net and total grinding power increases with an increase in specific material removal rate. The maximum spindle power is marked on the machine as being 125% of 27kW; this figure equates to 34kW, and as such,

Figure 8.19 shows that a Q'_w of 100mm^2/s is around the maximum this grinding centre can handle.

8.5 Summary

For the following reasons these tests have been particularly successful. The Viper process used by the turbine blade manufacturer utilised a depth of cut of 1mm at a speed of 16mm/s when grinding blade roots. Using these settings eight roughing passes and a final finishing pass would be required. The process used on the Edgetek machine was one roughing pass and one finishing pass without any degradation in workpiece integrity. The total time required was 10 seconds. Also with the use of X-Ray diffraction techniques measuring the residual stress, a consistent compressive stress regime within the blade root was produced before any final shot-peening operation had been performed. Also, the surface roughness R_a was consistently measured to be below 0.1μm which is a great achievement for the type of machining centre used. In addition, the externally produced report stated that the CBN produced blade roots that had a cleaner cut with less metallurgical surface and sub-surface damage (see Appendix K). Overall this process has far surpassed the previous process in lead time, surface roughness, residual stress and workpiece integrity. In all, these test have yielded further proof that the HEDG process has a definite practical potential within a real industrial environment.

CHAPTER 9 SUMMARY DISCUSSION

The previous experimental chapters have shown that if grinding temperature and hence surface integrity can be controlled, then HEDG in itself can be viewed as a contender as a mainstream manufacturing process. This chapter discusses the thermal modelling, its significance in terms of the grinding process, and compares the thermal responses for the two main materials.

Therefore, 9.1 considers the thermal modelling, Part 9.2 discusses the energy partition ratios, Part 9.3 examines the stress map concept and the industrial application of HEDG is discussed in Part 9.4.

9.1 Thermal Modelling

Using the mean trend lines shown in Figures 5.2 and 6.8 theoretical temperature plots have been calculated to indicate the thermal characteristics of M50 and IN718 during grinding. Figures 9.1 was produced using the mathematical software package MatLab; Figures (i) and (ii) apply to M50 steel and Figures (iii) and (iv) apply to IN718.

Of the minimum and maximum values shown, the minimum value is based on ideal cooling by the fluid i.e. $h_f = 23{,}000 W/m^2K$, whilst the maximum value assumes fluid boiling, i.e. $h_f = 0$ and represents a worst case situation. Parameters such as wheel wear and grinding fluid delivery strategy can have major effects upon the specific grinding energy levels measured. The poorer grinding fluid effectiveness gives rise to greater wheel wear, and this in itself increases the rubbing or sliding fraction of the total specific grinding energy within the grinding zone, which would raise the temperature on the workpiece surface. This escalates the temperature rise by boiling the grinding fluid which enhances the onset of oxidation.

Figure 9.1 (i-iv) shows that the predicted temperature characteristics conform to the trends expected from HEDG reported by Tawakoli (1993) as shown in Chapter 2, Figure 2.6. In fact, if there is any inefficiency within the system then the specific grinding energy will increase or the energy partition coefficients may change and a range of temperatures are possible from one set of grinding parameters. For example,

the convection coefficient of a fluid may change as illustrated in Figure 9.1 or the specific grinding energy may increase as wear flats develop on individual grits. Since grinding is a highly dynamic process, such changes may occur continuously over a period of time. The workpiece temperature may therefore range from well below the burn threshold to temperatures approaching the workpiece melting point under HEDG conditions. The concept of HEDG grinding reported by Tawakoli (1993) therefore represents the ideal conditions but in reality, actual grinding conditions will always be moving towards higher grinding zone temperatures and hence less favourable conditions. This study has highlighted that the major challenge is to control the HEDG process and ensure that the critical burn threshold temperature is not exceeded. From this point of view the need to monitor the grinding process becomes essential and clearly one way of doing this, is to measure the net grinding power and hence changes in specific grinding energy.

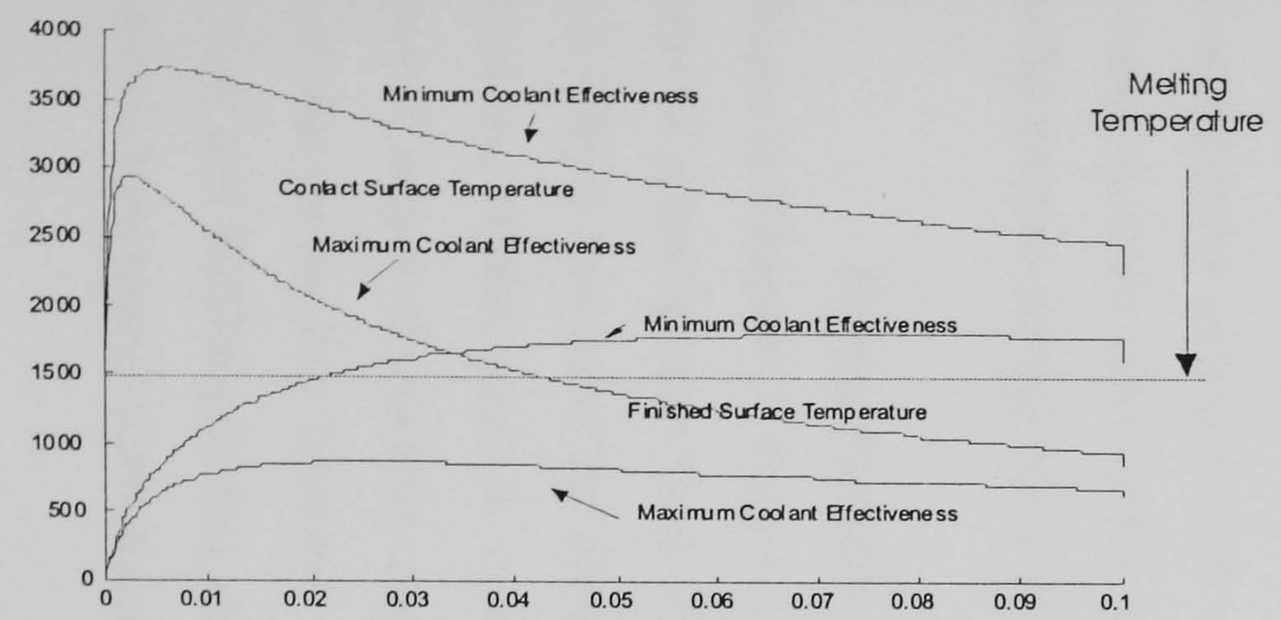

Figure (i): Predicted Temperature over a range of Feedrates for M50

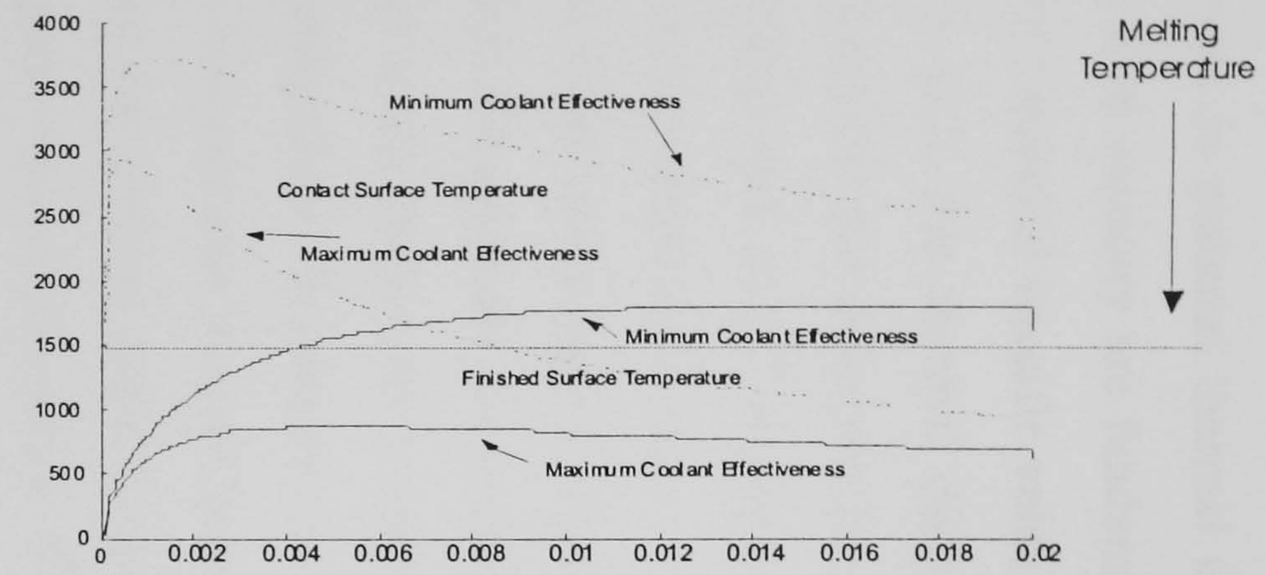

Figure (ii): Predicted Temperature over a range of Depths of Cut for M50

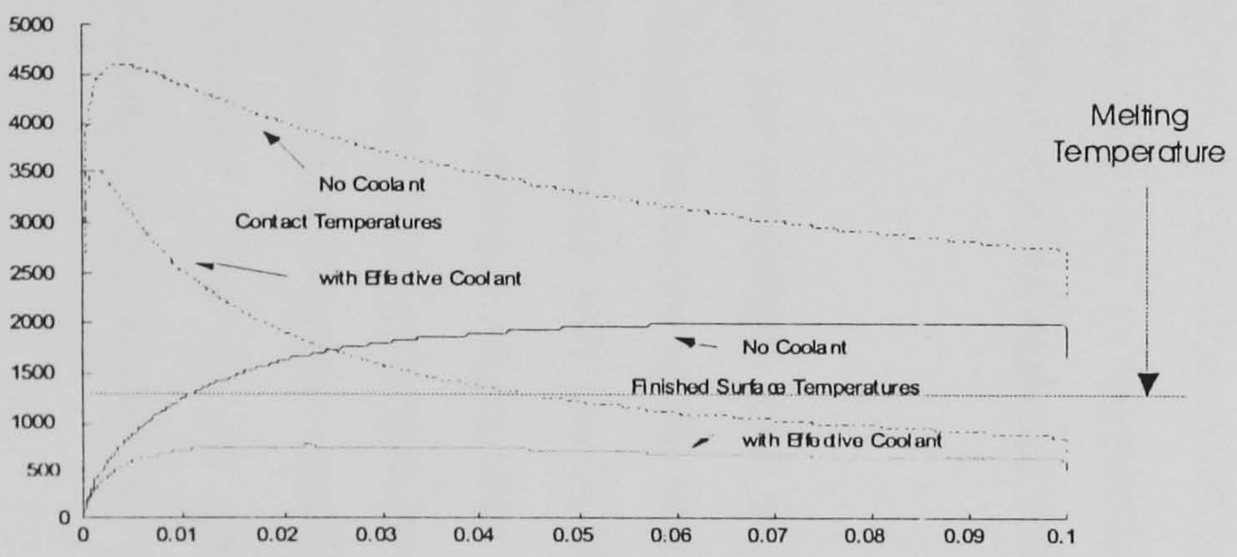

Figure (iii): Predicted Temperature over a range of Feedrates for In718

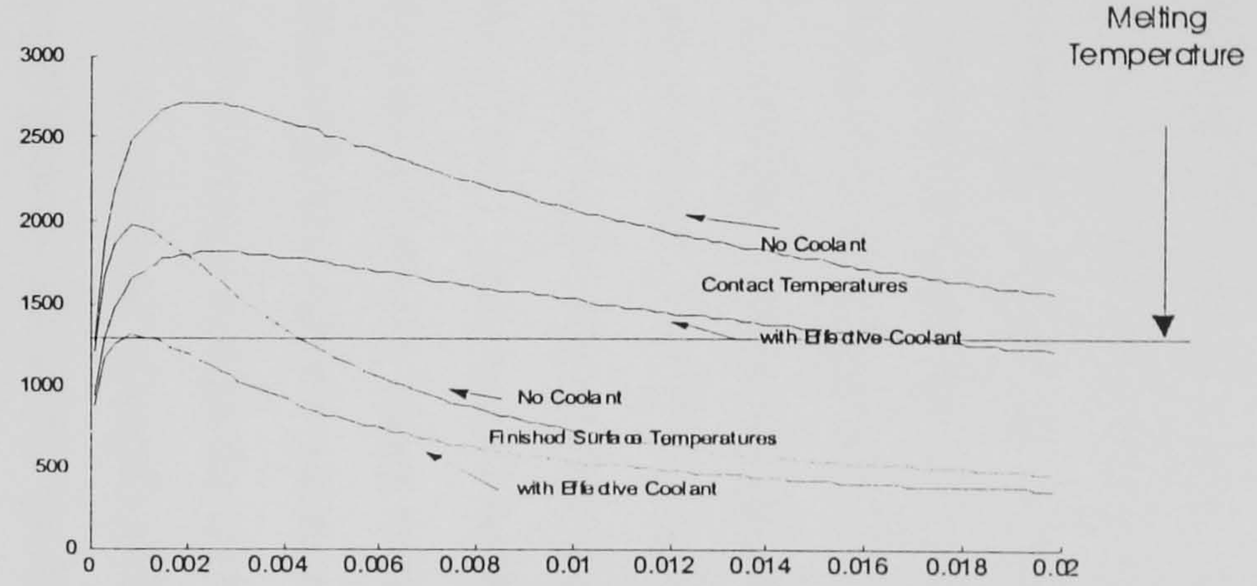

Figure (vi): Predicted Temperature over a range of Depths of Cut for IN718

Figure 9.1: Comparison of Predicted Temperatures

Differences in material thermal characteristics such as the thermal conductivity and specific heat capacity are fundamental in quantifying a material's thermal diffusivity, also, these material specific values vary with temperature. As shown in Appendix H, Equation H.2, the thermal diffusivity (α) is directly proportional to the thermal conductivity (k) and indirectly proportional to the specific heat capacity (c). Therefore, in a material such as IN718 with a low k value the amount of heat dissipated from the surface is calculated to be low. It can be seen that in the case of IN718 in Figure 9.1 (iv) that when using high feedrates the HEDG characteristics are shown quite clearly and lower temperatures are possible at high depths of cut. This would be due to heat retention at the surface for a longer period of time and ultimately being removed with the grinding chips. In addition, as the material is heated at the surface generating higher contact temperatures, it could be argued that with more energy within the material to be removed, the material could be easier to remove i.e. the material strength will be lower as the temperature is increased. The melting point (solidus) of the IN718 is documented as being 1260°C. If the contact surface temperature does reach this melting temperature, such a high temperature could cause damage or loading of the grinding wheel and thereby reduce the life of the grinding wheel. In the case of M50 steel where the k value is more than double that for IN718, the reduction in temperature is lower due to the thermal energy being dissipated more quickly into the material substrate.

9.2 Energy Partition Ratios

As shown in Chapter 2, Figure 2.34, the depth of cut combined with the equivalent diameter of grinding wheel will affect the contact length between wheel and workpiece. Jin et al (2002) stated that the effect of contact angle increases with Peclet Number, and therefore the HEDG process is more sensitive to the contact angle than creep feed grinding. Creep feed grinding operations can have a large contact length but low Peclet Number due to the low feedrate. This means that the heat transfer conditions within creep feed and HEDG grinding are clearly very different. This can be highlighted by considering how energy partition coefficients vary under different grinding conditions.

Predicted temperatures have been calculated from the thermal models and as part of that process, energy partition ratios have been determined for each set of parameters used. This work has shown that at such low values of specific grinding energy, namely between 10 to 15J/mm^3 relevant to HEDG, the energy partition coefficient to the workpiece is also low, typically less than 10%, and that the majority of the thermal energy (>50%) is removed with the grinding chips. The energy partition coefficients can be calculated from the estimated conduction and convection coefficients and equations listed in Appendix H, equations H.1 to H.18. An example of typical values for M50 is shown in Figures 9.2 to 9.4 assuming that $h_f = 23{,}000 W/m^2K$ and as such the grinding fluid does not boil. The value of R_w increases sharply at low specific energies, rising to values around 15% - 20% at high specific grinding energy values, more typical of creep feed conditions.

However, Figure 9.2 also shows that small increases in the specific grinding energy can result in a sharp increase in the fluid energy partition coefficient particularly within the HEDG range of 10 to 20 J/mm^3, and this is likely to influence the workpiece temperature.

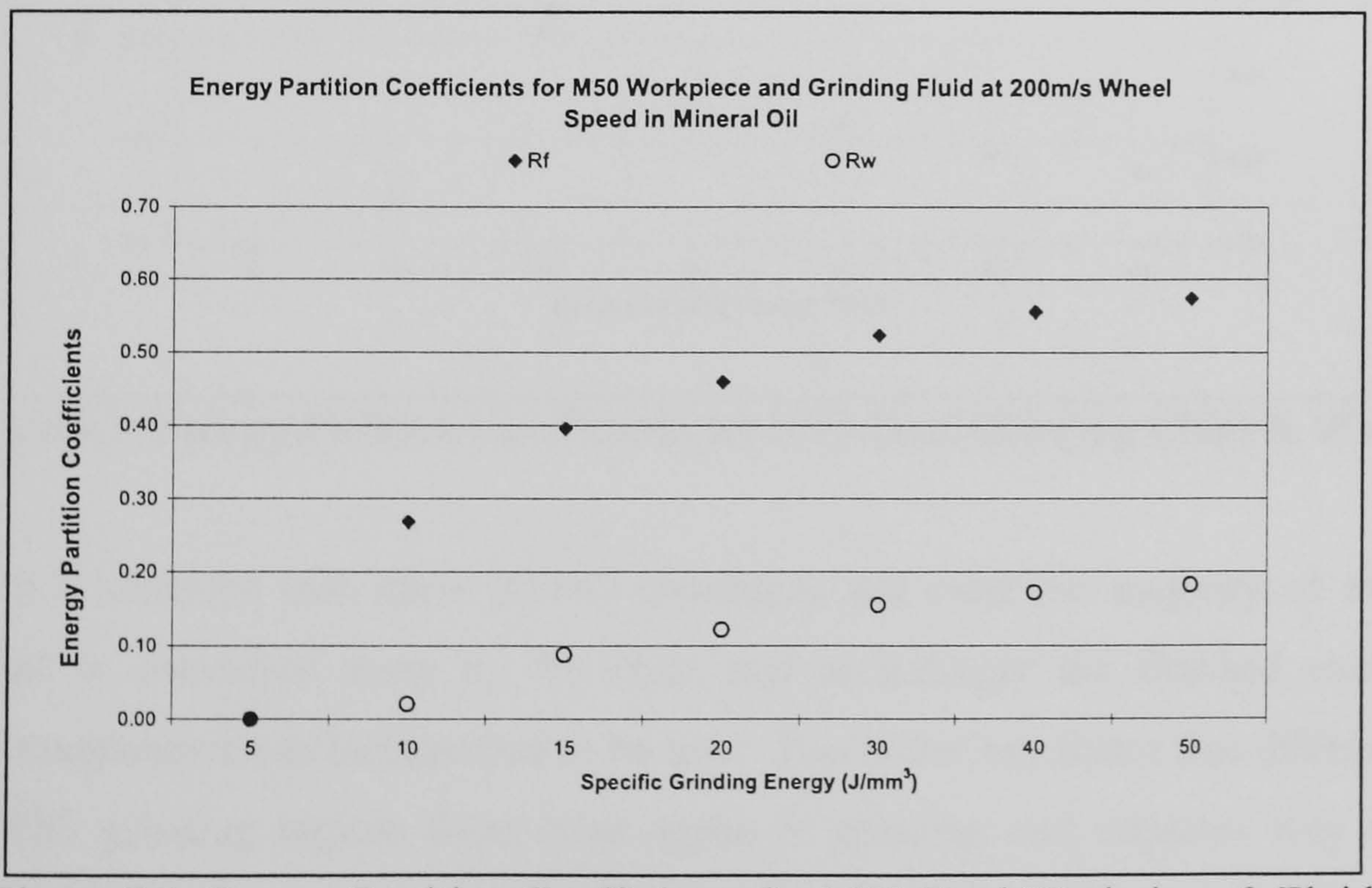

Figure 9.2: Energy Partition Coefficients for M50 Steel Workpiece & Fluid

Figure 9.3 demonstrates that for true HEDG conditions for M50, R_{ch} is 50% to 70%, suggesting that a high percentage of the thermal energy is indeed removed with the chip.

On further inspection of Figures 9.2 and 9.3 one can see the main areas of operation with regard to the specific grinding energy for HEDG and creep feed grinding. Creep feed grinding operates at around the 50 J/mm^3 level and HEDG around 10 – 20 J/mm^3. It can be seen that at the 50 J/mm^3 level the chip removes around 10% of the heat and the fluid convects away around 50%. When applying the HEDG concept the opposite is shown. The fluid removes around 10% and the chip removes between 50 – 70% of the total heat produced.

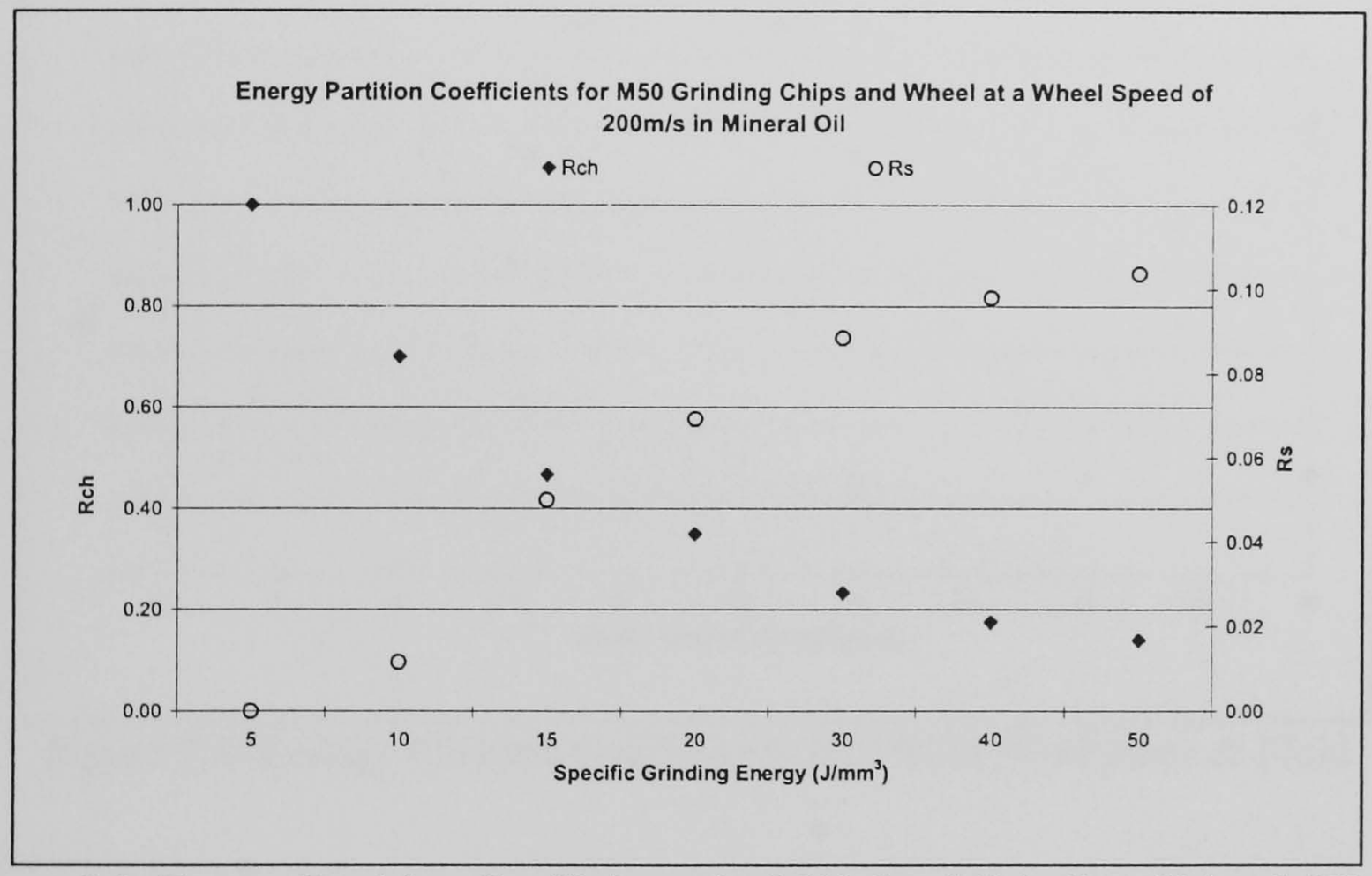

Figure 9.3: Energy Partition Coefficients for M50 Steel Grinding Chips & Wheel

Figure 9.3 indicates that when HEDG conditions are used the majority of the heat generated is convected away by the chip, and accordingly the finished workpiece surface temperature can be expected to be low. This is the key factor that differentiates the HEDG grinding regime from other types of grinding and explains why HEDG grinding is in some ways more akin to a conventional cutting process, e.g. high speed milling, when specific energy values are typically only a few J/mm^3. The exceptionally low values of specific grinding energy during HEDG are consistent with the large

depths of cut and high feedrates which give rise to a large chip thickness, normally associated with conventional cutting processes.

The foregoing discussion has highlighted how changes in specific grinding energy may occur during the grinding process and this may also be associated with significant changes in the energy partition coefficients. Thus, the workpiece surface temperature will change as the conditions within the grinding zone change. The energy partition coefficients can also be determined for the grinding of IN718, as shown in Figures 9.4 and 9.5.

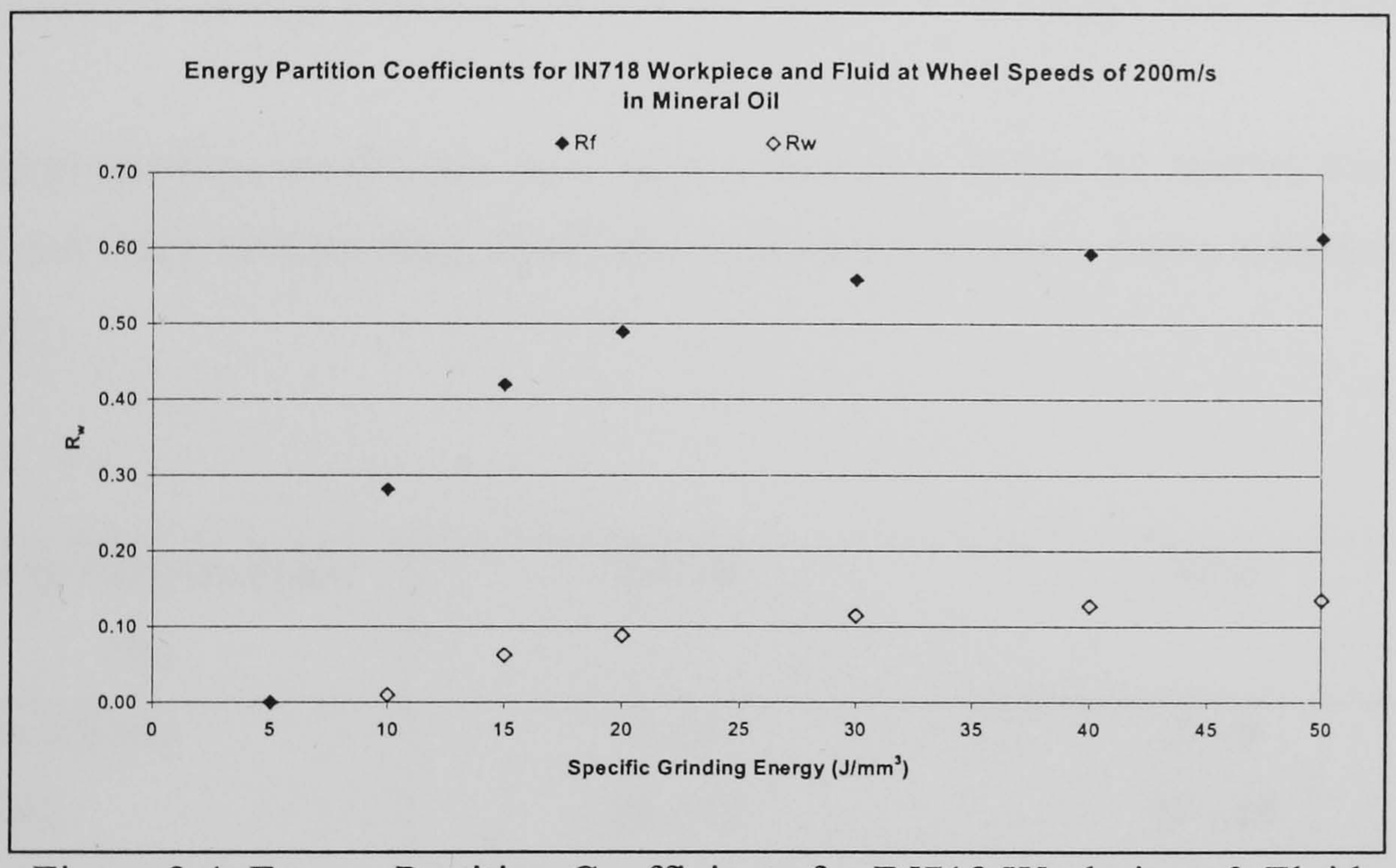

Figure 9.4: Energy Partition Coefficients for IN718 Workpiece & Fluid

Figure 9.4 shows the partition coefficients for workpiece and fluid and Figure 9.5 shows the coefficients for the chip and CBN grinding wheel.

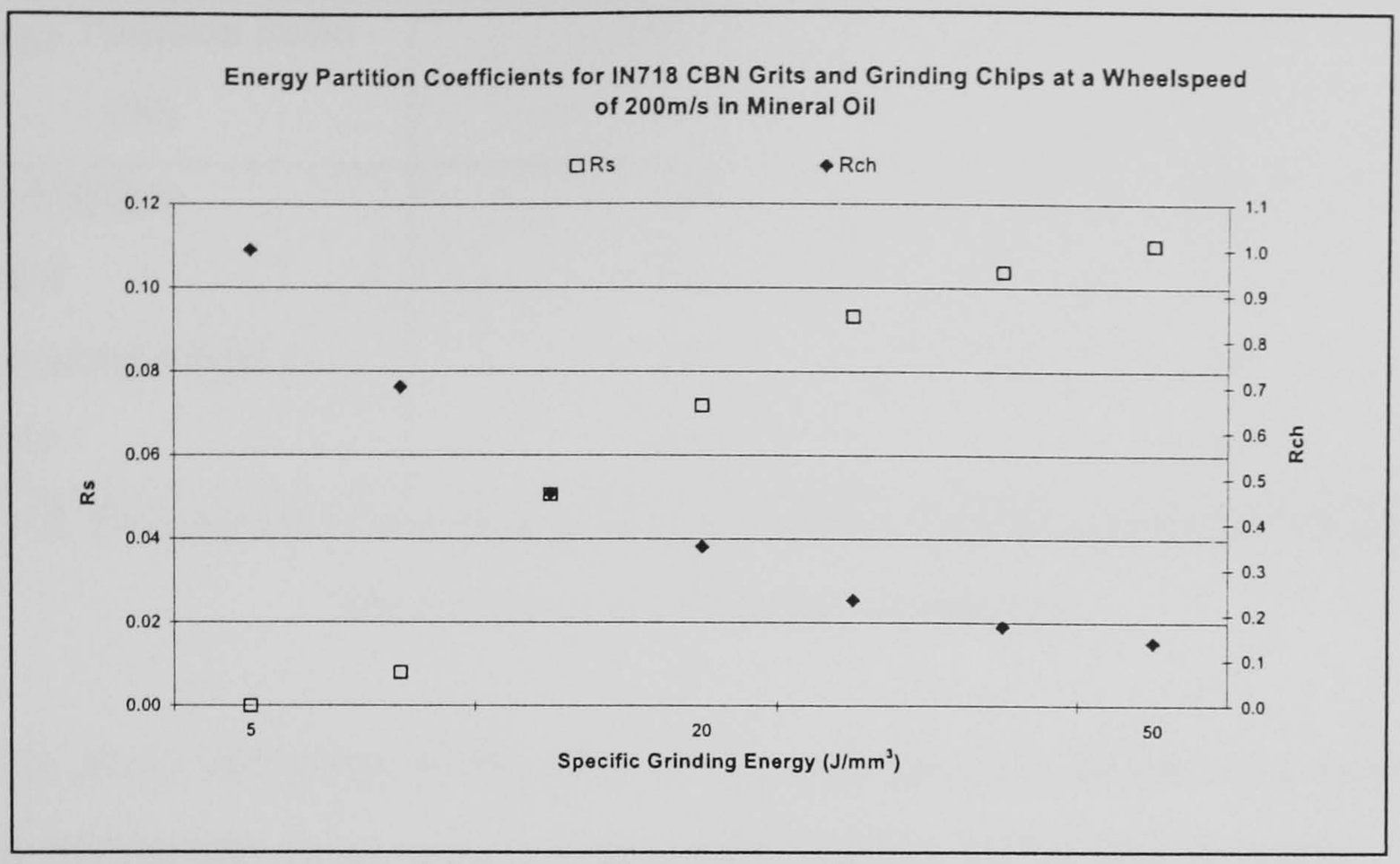

Figure 9.5: Energy Partition Coefficients for IN718 Grinding Chips & Wheel

The energy partition coefficients have been tabulated in Tables 9.1 and 9.2 for typical HEDG and creep feed grinding conditions respectively so that a direct comparison can be made.

Energy Partition Ratio (%)	IN718	M50
R_w - workpiece	1 - 6	2 – 9
R_f - fluid	28 - 42	27 - 40
R_s – grinding wheel	1 - 47	1 – 5
R_c - chip	47 - 70	47 - 70

Table 9.1: Comparison of Percentage Energy Partition Coefficients for IN718 and M50 under HEDG Conditions

Energy Partition Ratio (%)	IN718	M50
R_w - workpiece	14	18
R_f - fluid	61	57
R_s – grinding wheel	11	10
R_c - chip	14	14

Table 9.2: Comparison of Percentage Energy Partition Coefficients for IN718 and M50 under Creep Feed Grinding Conditions

Table 9.1 shows that although the thermal constants are quite different the ratios as to how the heat energy is removed are remarkably similar for the two materials. This is also apparent for creep feed grinding conditions as shown in Table 9.2.

This goes some way to explain why such an extensive range of temperatures are predicted with only slight changes in specific grinding energies. To illustrate these fluctuations in specific grinding energy Table 9.3 takes a Q'_w of 200mm^2/s as an example where the scatter in specific grinding energy is relatively small but the predicted temperature variation is quite large.

Test Number	Depth of Cut (mm)	Feedrate (mm/s)	Fluid Type	Specific Grinding Energy (J/mm^3)	Predicted Temperature (°C)
50-272	2	100	Ester	15.92	1022
50-49	2	100	Mineral	13.20	852
50-260	1.4	125	Mineral	11.93	615
50-255	1.4	125	Mineral	11.87	610
50-262	3	66.67	Mineral	10.99	585

Table 9.3: Results Stream from Q'_w of $200mm^2/s$

One can go further and plot a sample of data from the conditions shown in Appendix F, test numbers 50-167 to 50-243 that compare the predicted temperature rise from the Q'_w values $35mm^2/s$ and $200mm^2/s$.

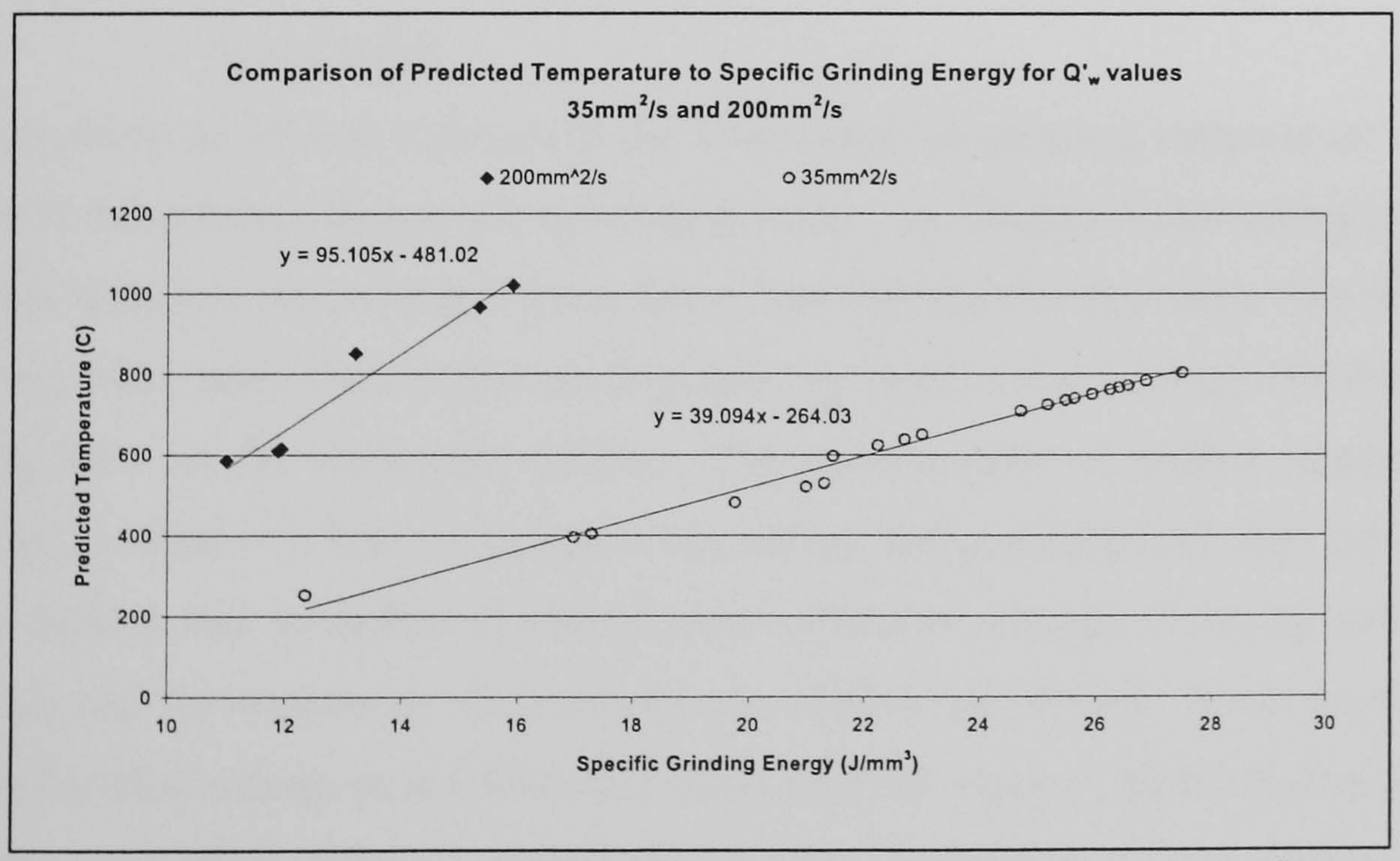

Figure 9.6: Comparison of Temperature Gradients for two Q'_w values

Figure 9.6 illustrates the change in gradient for a comparatively low specific material removal rate to a reasonably high one. The gradient of temperature rise for a relatively

low variation in specific grinding energy is very important as this illustrates the sensitivity of temperature to variations in specific grinding energy within the HEDG process.

Table 9.2 shows the ester based grinding fluid example produced the highest specific grinding energy and although the remaining points had only 3.19J/mm^3 between them the calculated temperature range was over 260°C. Although there are wide variations of specific grinding energy when the specific material removal rates are low, the calculated temperature range is also low. Figure 9.6 shows that the gradient increases by about a factor of 2.5 when the Q'_w value is increased from 35 to 200mm^2/s. Hence, the sensitivity of the grinding temperature to changes in specific grinding energy is much lower for low Q'_w values.

These observations reinforce the need to monitor the grinding process when operating within the HEDG regime since small changes in grinding conditions may have a marked effect on grinding temperatures. The most logical way of achieving this would be to measure the grinding power and hence monitor the change in specific grinding energy.

9.3 Stress Maps

The discussion so far has highlighted the importance of grinding temperature and the control of temperature during the grinding process. In Chapter 5 the concept of burn threshold diagrams was used and from this a burn threshold temperature was obtained. However, these basic burn threshold diagrams are based around visual observation of grinding burn on the workpiece surface. The general issue of surface integrity was discussed in Chapter 5 Part 5.2.6, and it was shown that grinding burn may encompass various factors such as surface oxidation, micro-structural change including white layer formation and the generation of undesirable residual stress profiles. It has been shown recently by McCormack et al (2001) that these different types of grinding damage may commence at quite different workpiece surface temperatures. In particular the generation of tensile residual stresses in steels (EN31) has been shown, under shallow cut grinding conditions, to occur at temperatures over 250°C. Under such conditions, no visible evidence of grinding damage would be present but the component would still

be unfit for service. Hence, in the current research a new approach is suggested which can provide the industrial end user with greater confidence when surface integrity issues are of paramount importance. This new approach is based on the burn threshold diagram principle presented previously, but provides information on surface residual stress. There should be some commonality since residual stress is generally a strong function of the grinding zone temperature.

With a high level of confidence placed in the residual stress measurements, Figures 9.7 and 9.8 show the concept of a stress map for both project materials. These maps were designed to utilise all the basic data acquired during this research in the most productive way for a common wheel speed of 100m/s. All test results contained within this figure were plotted against the f(DaVw) function which took into account the diameter of the wheel, depths of cut used and the various feed rates. The y-axis, specific grinding energy, is a function of the grinding parameters and other factors such as wheel wear characteristics. Both filled and uncoloured dots are indicative of the points tested representing burn and no burn observations respectively. The stress contours are representative of changes in residual stress levels between the points tested and these were calculated using the mathematical software package MathCAD 2000.

From previous results we now understand that for a given Q'_w value the specific grinding energy increases as wear flats develop on the grits. It can be seen that the onset of tensile stress regimes occur before any oxidation can be visually noted. With this type of tool the process engineer can predict and so enhance the possibility of avoiding the formation of tensile stress regimes on the finished component surface, as tensile stresses could have a detrimental effect upon the quality of the manufactured parts. As IN718 has a thermal conductivity value of 11.4W/mK at 20°C any heat generated would produce a much steeper temperature gradient at the surface of the material. As an example Figure 9.1 (iii & iv) show how the produced temperatures for a depth of cut of a few millimetres is much higher for IN718 compared to M50.

This could explain why IN718 normally has tensile stress regimes on the ground surface. Figure 9.1 suggests that only by using very gentle grinding conditions or

severe HEDG conditions, can the temperature be maintained at low values (say <500°C) in order to ensure compressive stresses. These conclusions are consistent with the experimental results shown in Figure 6.11, where the residual stresses were only compressive for Q'_w values less than about 25mm^2/s. It is also interesting to note that IN718 ground under creep feed conditions is known to generate tensile residual stresses, Sullivan (2002). The generation of compressive residual stress within the ground surface of these nickel based superalloys is recognised to be very difficult. This research has indicated that HEDG grinding should be able to generate compressive stresses as long as a grinding machine is available that has the necessary power to achieve the high Q'_w values.

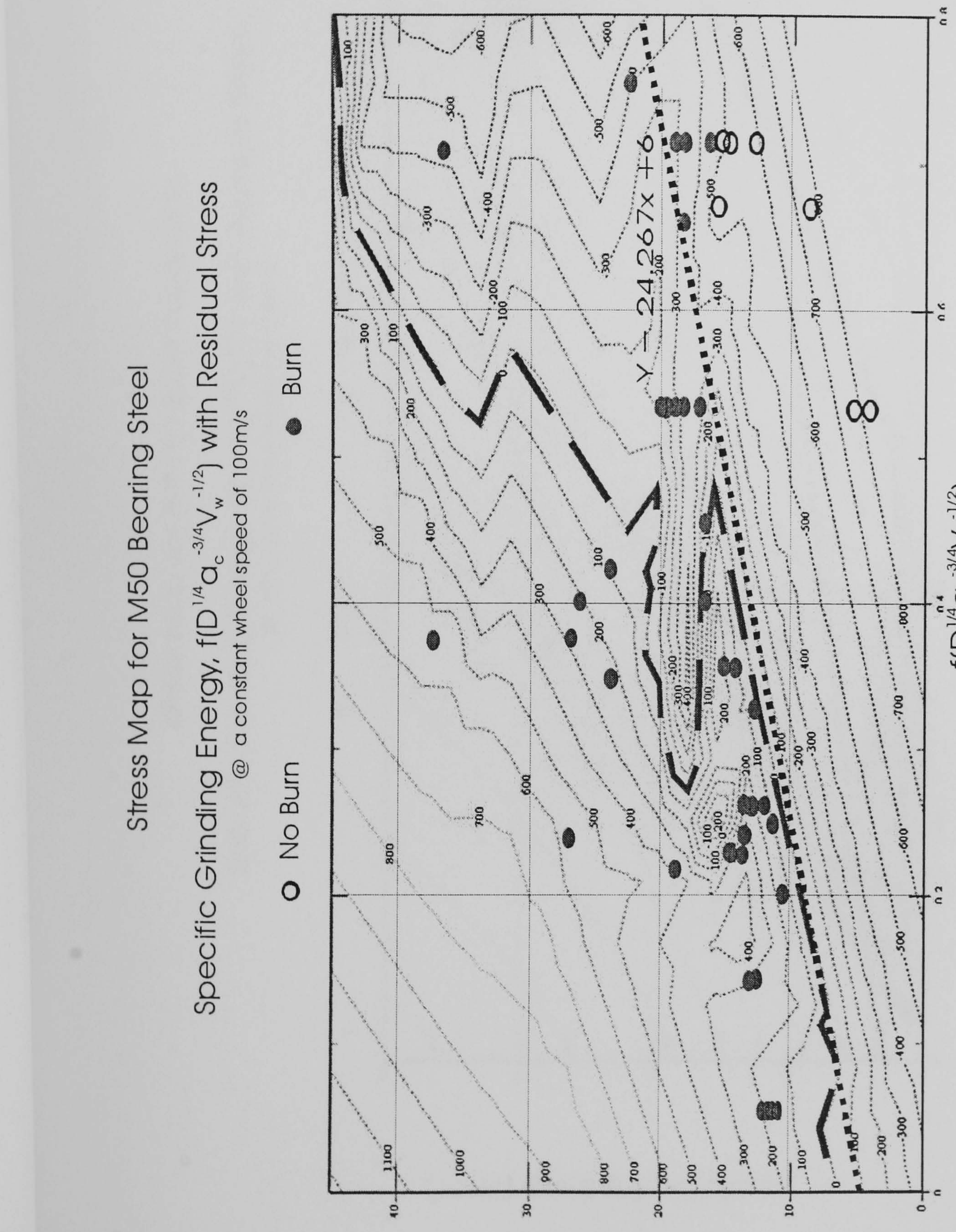

Figure 9.7: Stress Map for M50 Bearing Steel

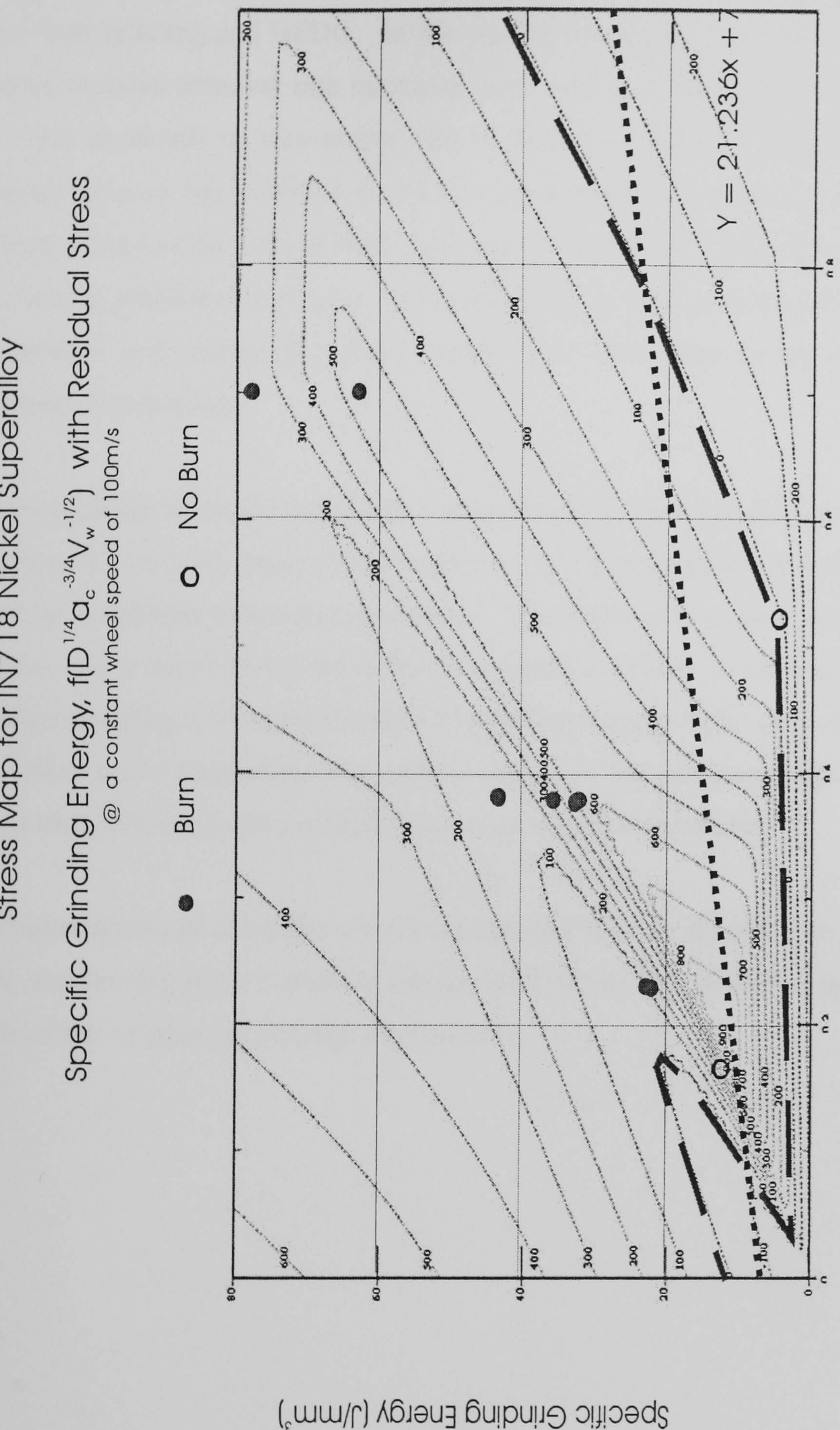

Figure 9.8: Stress Map for IN718 Nickel Superalloy

9.4 Implications for the Industrial Applications of HEDG

Using Figure 9.9 two grinding process regimes can be compared namely shallow cut / creep feed grinding and HEDG. In the case of shallow cut or creep feed grinding, the specific material removal rate increases from zero to a maximum value (steady state) and then decreases to zero at the end of the cut so long as the maximum specific material removal rate is below the critical temperature, e.g. point 3 on Figure 9.9, then no burn should result. When HEDG grinding at point 1 on Figure 9.9 or at even higher Q'_w values, problems may occur during the initial or latter stages of the grind since the temperature will exceed the critical value for a short time as the Q'_w increases or decreases towards zero.

When applying a HEDG procedure incorporating a form grinding process the added problem of a variable depth of cut is present. This type of grinding makes the choice of grinding conditions even more precarious. One could have a small depth of cut at one portion and a depth of cut an order of magnitude greater at another part of the cut. When attempting to monitor this style of grinding through a plot such as Figure 9.9, one can either use a mean specific grinding energy or the minimum depth of cut for the worst case scenario to give an indication of grinding temperatures.

For conventional grinding the critical temperature is never exceeded so when the steady state position at point 3 is reached and the final part of the cut begins, point 4 is reached with no hint of grinding damage what so ever.

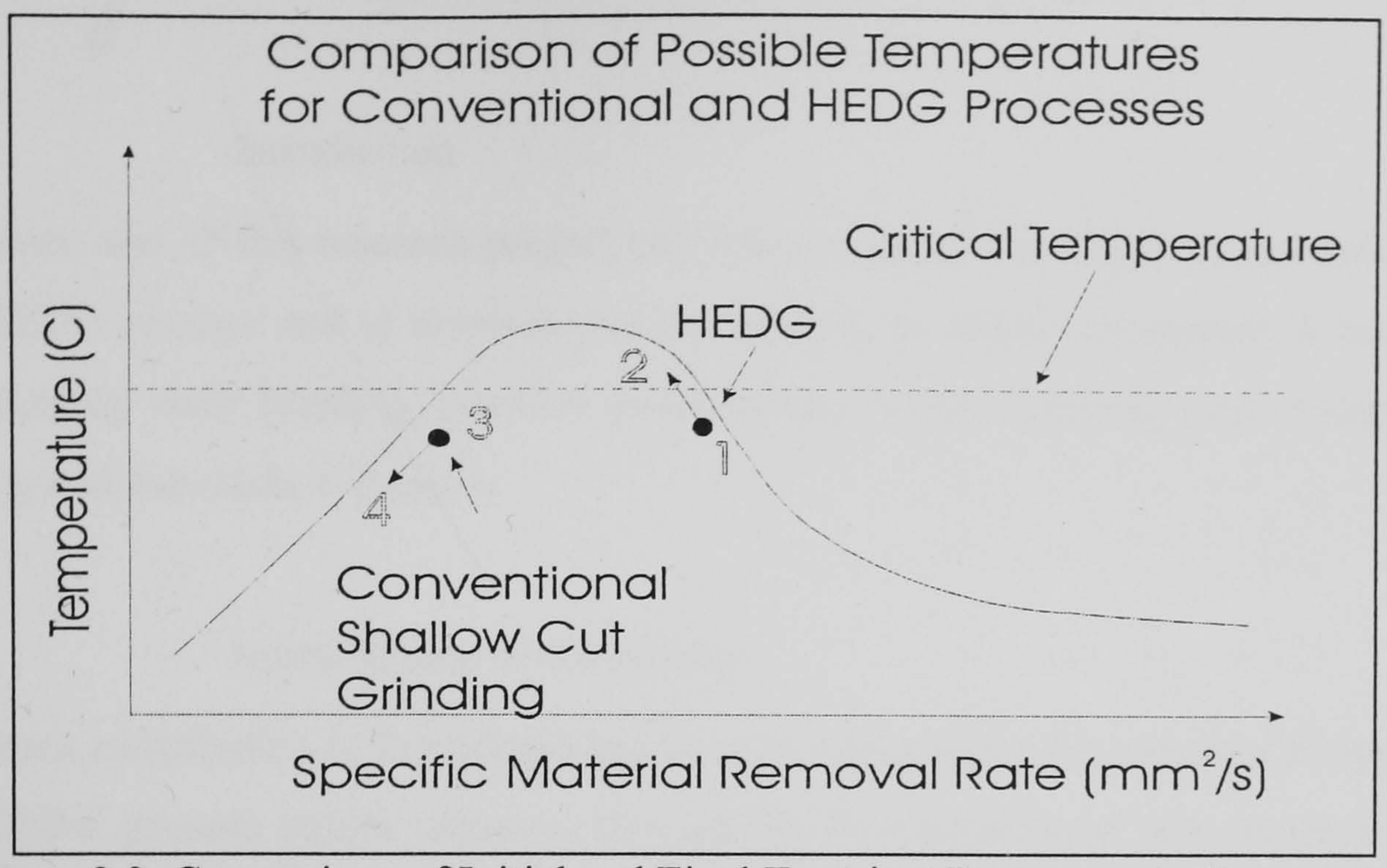

Figure 9.9: Comparison of Initial and Final Transient Responses to Temperature

One way which could counter this issue for HEDG grinding would be in the form of adaptive control which could be used to increase the feedrate thereby increasing the specific material removal rate and reduce the risk of jeopardizing workpiece integrity. Also these models could use other parameters to control the grinding process such as normal force. These outputs could be used to map out the wheel wear rate as laid out in the predictive tools described in previous chapters, thereby controlling this dynamic process to extend wheel life and ultimately to produce higher quality finished workpieces. At this juncture it can be said that the adaptive control system could be a more viable concept, and indeed is a vital development if HEDG grinding is to be adopted by industry.

CHAPTER 10 CONCLUSIONS AND RECOMMENDATIONS

10.1 Introduction

The main aim of this research project has been to gain an in depth understanding of the HEDG process and to develop process models, to enable companies to increase significantly their grinding machine productivity, whilst ensuring good component surface and sub-surface integrity.

10.2 Contributions to Knowledge

The main contribution to knowledge has been to demonstrate the potential of applying the HEDG process within industry, through the development of process models for two advanced materials, in which the processing parameters were mapped against:

- Different grinding fluid strategies
- Burn threshold diagrams
- Residual stress levels
- Specific grinding energies

Researchers may reference this work when investigating different materials. The basic methodology, and results arising from this work should save considerable time when selecting optimum processing parameters for a wide range of materials.

10.3 Conclusions

Through the experimental approach taken, workpiece characterisation and theoretical results the following conclusions can be made:

1. The HEDG process has the potential to be a robust industrial manufacturing process, and it has been shown that Q'_w values of at least one order of magnitude greater are possible when compared to creep feed grinding.

2. Specific grinding energy is a good indicator for the on-set of grinding burn. Hence the monitoring of the power during the process is a critical factor in controlling system output and reducing the possibility of burn within the HEDG regime.

3. When taking the changes in microstructure into account a good all round correlation has been shown between Barkhausen Noise results and surface residual stress measurements. In turn the predicted temperatures show the same trend as the residual stress measurements when plotted against specific material removal rate. The transition temperature at which residual stress changes from compressive to tensile values is shown not to be the same as the real burn threshold temperature. Therefore when the process engineer selects parameters for an operation, the engineer can take into account the possible micro-structural effects of these choices and thereby exercise a greater amount of control over the HEDG process.

4. A major advantage of HEDG is that one can combine a highly efficient material removal process (similar to conventional cutting processes) with the precision and surface integrity benefits associated with conventional grinding processes.

5. HEDG is associated with low values of specific grinding energy, for example $10J/mm^3$ or less, and it has been shown from the thermal modelling from this research that the majority of the total energy is removed with the grinding chips, typically 50 to 70%. The successful application of HEDG relies on the ability to reduce and maintain specific grinding energy at a low level. At intermediate to high stock removal rates typically 200 to $1250mm^2/s$, small changes in the specific grinding energy may result in a large increase in grinding temperature.

6. Grinding temperatures predicted using the circular arc of contact model correlate well with experimental observations of grinding burn. Thermal modelling has demonstrated the potential benefits of HEDG, using high work speeds and large depth of cut to minimise the workpiece finished surface temperature.

7. Under true HEDG conditions only a few percent of the total thermal energy enters the workpiece. However this increases as the specific grinding energy increases, up to a limiting value dependent on the wheel speed, wheel wear and type of abrasive. For CBN abrasives the workpiece energy partition coefficients have been calculated to be typically between 5 and 20%. CBN is an extremely hard, tough wear resistant material with excellent thermal properties which enhance the grinding process through the removal of a greater amount of heat in comparison to aluminium oxide grits.

10.4 Recommendations

The concept of HEDG is a relatively recent derivative of grinding and as such there are many interesting areas to investigate. There is a real requirement to further enhance the theoretical temperature modeling so that the actual grinding process can be characterized more completely. One area in particular is boiling of a grinding fluid, and its effect on the fluid convection factor.

Choi et al (2001) researched the area of light reciprocating grinding using compressed air as a grinding fluid. Although this technology seems more suited to the conventional shallow grinding spectrum it is an attempt at finding an alternative grinding fluid supply. Shaji et al (2002) published an article detailing work carried out on AISI 52100 steel using a light depth of cut and low feed rates whilst using graphite as a solid grinding fluid. Indications were that the graphite gave reduced forces in the normal and tangential directions as well as a marked reduction in the specific grinding energy. This indicates that the use of a solid grinding fluid could enhance the efficiency of the grinding process as a whole. This research paper highlights the possible uses of solid grinding fluids as another major area to research. The use of greases such as boric acid, molybdenum disulphide or even graphite

should reduce the power requirement of the process as a whole and the ecological benefits are quite obvious. Further work would be worthwhile to investigate the influence of solid grinding additives on the HEDG process, and also the mechanical properties of the superabrasive grits used, such as CBN or PCD.

Characteristics of wheel wear and how this relates to the rise in specific energy, also as an extension of this, the mapping of the complete life cycle of a wheel relating to a particular process with set parameters, such as to the limits of acceptable workpiece integrity levels, for specific applications, could of great interest to industry. In this way process engineers could map out wheel life, and adapt this information to reduce further the possible onset of oxidation and tensile residual stresses.

It has been previously shown that hardness profiles and the measurement of residual stresses give an indication of the effects of a machining process. One new area of research could be to examine the stress depth profiles using a new non-destructive Barkhausen Noise process called Micro-Scan and to correlate this with the more conventional applications such as XRD residual stress measurements and Vickers Micro-hardness profiles.

It has been noted in this research program that the BNA response can be sensitive to changes in hardness, micro-structural changes and residual stress levels. Research into this area to quantify the relevance of each of these factors and their possible interactions would enhance the confidence of BNA techniques and could further its use in the industrial arena.

One area which could be enhanced with more research is the area of grinding fluid shoe nozzle technology with regard to HEDG. Although there have been studies published (Brinskmeier et al (1999)) more research is required into the actual influence of nozzle flowrate, fluid velocity, nozzle area and fluid pressure on workpiece integrity.

Butler et al (2002) investigated the characterisation of grinding wheel topography by using 3D surface measurements. This research studied the influence of stock removal in relation to wheel wear and found there to be a reasonable correlation.

Chattapadhyay et al (1990 & 1991) investigated this area using equi-spaced grits bonded on to the grinding wheel hub. These experiments improved grit protrusion through reduced bond loading during this stage of wheel manufacture. Taking the results of these studies in a HEDG context, it is suggested that the quality of the grinding wheel manufacture and grit laying process could be questioned. The quality control used in these areas could be reviewed to take into account the large volumes of space required to facilitate the removal of the large chips which are evident within the HEDG process, and the ingress of grinding fluid.

Finally the complete dataset would be a great asset within a modern adaptive control grinding system. In this way up to date data arising from the research results could be used to decrease the possibility of grinding damage.

REFERENCES

Althaus, P. G., (1985). Residual Stresses in Internal Grinding, *Industrial Diamond Review, March*, 124-127.

Barbacki, A., Kawalec, M. & Hamrol, A., (2002). Turning and Grinding as a source of Microstructural Changes in the Surface Layer of Hardened Steel, *Journal of Materials Processing Technology,* 5795, 1-5.

Barkhausen, H., (1919). Two Phenomena revealed with the help of New Amplifiers, Physik Zeitschrift 20, 401-403.

Bailley, M.W. & Juchem, H.O., (1998). The Advantage of CBN Grinding: Low Cutting Forces and Improved Workpiece Integrity, *Industrial Diamond Review.*

Bailey, M., (2000). High Speed Precision Grinding, *Materials Processing Initiative*, School of Industrial and Manufacturing Science, Cranfield University, June 21 2000.

Bartz, W., (1998). Lubricants and the Environment, *Tribolog International*, 31, 35-47.

Bienkowski, K., (1993). Coolants & Lubricants - The Truth, *Manufacturing Engineering.*

Brinksmeier, E. & Minke, E., (1993). High Performance Surface Grinding – The Influence of Coolant on the Abrasive Process, *Annals of CIRP*, 42(1), 367-370.

Brinksmeier, E., Walter, A. & Brockhoff, T., (1997). Minimum Quantity Lubrication in Grinding. *In: 2nd International Machining & Grinding Conference*, Dearborn, Michigan, September 8-11 1997 MR97-230.

Brinksmeier, E., Heinzel, C. & Wittmann, M., (1999). Friction, Cooling and Lubrication in Grinding, *Annals of CIRP*, 48(2), 1-18.

Brinksmeier, E., Heinzel, C. & Wittmann, M., (2000). Visualisation of Coolant Flow in Shoe Nozzles and their Effect on the Residual Grinding Stresses, *Production Engineering*, 7(1), 9-12.

BS 6897: Part 2 1990 ISO 7626-2: 1990, Experimental Determination of Mechanical mobility. Part 2. Measurements using single point translation excitation with an attached vibration exciter.

Campbell, J.D., (1997). Tools to Measure and Improve Coolant Application Effectiveness, *In: 2nd International Machining & Grinding Conference*, Dearborn, Michigan, September 8-11 1997 MR97-230.

Carius, A.C., (1989). Effect of Grinding Fluid Type and Delivery on CBN Wheel Performance, *In: Society of Manufacturing Engineers, Modern Grinding Technology*, Novi, Michigan, October 1989.

Carslaw, H. & Jaeger, J.C., (1959). *Conduction of Heat in Solids*, 1st Ed. Oxford University Press, Oxford.

Chattopadhyay, A.K., Chollét, L. & Hintermann, H.E., (1991). On Performance of Chemically Bonded Single Layer CBN Grinding Wheels, *Annals of CIRP*, 39(1), 309-312.

Chattopadhyay, A.K., Chollét, L. & Hintermann, H.E., (1991). On Performance of Brazed Bonded Monolayer Diamond Grinding Wheel, *Annals of CIRP*, 40(1), 347-350.

Chen, X., Rowe, W.B. & McCormack, D. F., (2000). Analysis of the Transitional Temperature for Tensile Residual Stress in Grinding, *Journal of Materials Processing Technology*, 107, 216-221.

Choi, H.Z., Lee, S.W. & Jeong, H.D., (2001). A Comparison of the Cooling Effects of Compressed Cold Air and Coolant for Cylindrical Grinding with a CBN Wheel, *Journal of Materials Processing Technology*, 111, 265-268.

Chou, Y. K. & Evans, C. J., (1997). Tool Wear Mechanism in Continuous Cutting of Hardened Tool Steels. *Wear*, 212, 59-65.

Chou, Y. K. & Evans, C. J., (1999). Cubic Boron Nitride Tool Wear in Interrupted Hard Cutting. *Wear*, 225-229, 234-245.

Chou, Y. K. & Evans, C. J., (1999a). White Layers and Thermal Modelling of Hard Turned Surfaces. *International Journal of Machine Tools & Manufacture*, 39, 1863-1881.

Desvaux, S., Gualandri, H. & Carrerot, H., (1999). Follow-up of the Barkhausen Noise Signal on Bearings after Operation. *In: The 2nd International Conference on Barkhausen Noise & Magnetic Testing*. Newcastle, United Kingdom 1999.

Ebbrell, S., Woolley, N.H., Tridimas, Y.D., Allanson, D.R. & Rowe, W.B., (1999). The Effects of Cutting Fluid Applications Methods on the Grinding Process, *Int. Journal of Machine Tools & Manufacture – Design Research and Application*, 40, 209-223.

Field, M., Kahles, J.F. & Cammet, J.T., (1972). A Review of Measuring Methods for Surface Integrity. *Annals of CIRP*, 21(2), 219-238.

Fix, R.M. (2000). Applications of Barkhausen Noise Analysis (BNA), A Review of Three Cases having Industrial Significance. *Abrasives Magazine*, Dec/Jan 30-41.

Fuh, K. & Huang, J., (1994). Thermal Analysis of Creep Feed Grinding, *Journal of Materials Processing Technology*, 43, 109–124.

Ganesan, M., Guo, C. & Malkin, S., (1995). Measurement of Hydrodynamic Forces in Grinding, *Transactions of NAMRI/SME,* 22,103-107.

Genevro, G.W. & Heineman, S.S., (1991). *Machine tools – Processes and Applications*, Prentice-Hall, Englewood Cliffs.

Gu, D.Y. & Wager, J.G., (1990). Further Evidence on the Contact Zone in Surface Grinding, *Annals of CIRP*, 39(1), 349-352.

Guo, C., Wu,Y., Varghese, V. & Malkin, S., (1999). Temperatures and Energy Partitioning for Grinding with Vitrified CBN Wheels, *Annals of CIRP*, 48(1), 247-250.

Gupta, H., Zhang, M., Parakka, A.P., (1996). Barkhausen Effect in Ground Steels. *Acta Materials*, 45(5), 1917-1921.

Hallet, J. F., (2000). Process Improvement for Crankshaft Grinding using Barkhausen Noise Analysis. *In: The 1st International Conference on Barkhausen Noise & Magnetic Testing*. Hannover, Germany 2000.

Hahn, R.S., (1962). On the Nature of the Grinding Process, *Proceedings of the 3rd Machine Tool Design and Research Conference*, Birmingham, 1962, 129-154.

Hayama, M., Yamanaka, Y. & Oi, T., (1997). Development of New Grinding Fluid for CBN Grinding Wheels – Part2, *Lubrication Engineering.*

Hayama, M., Yamanaka, Y. & Oi, T., (1998). Development of New Grinding Fluid for CBN Grinding Wheels – Part 3: Study of Concentration of Metalworking Additives on Grinding Performance, *Lubrication Engineering.*

Hensel, K.B., (2000). Surface Treatments - Electropolishing, *Metal Finishing,* 98 (1), 440-448.

Hillman, R., (2000). Combined NDT Testing of Crankshafts. *In: The 1st International Conference on Barkhausen Noise & Magnetic Testing*. Hannover, Germany 2000.

Howes, T.H. & Gupta, H., (1991). Avoiding Thermal Damage in Grinding, *Abrasive Engineering Society.*

Howes, T.H. & Mindek Jnr., R., (1993). Creep Feed Exam, *Cutting Tool Engineering.*

Howes, T.H., Neailey, K. & Harrison, A.J., (1987). Fluid Boiling in Shallow Cut Grinding, *Annals of CIRP*, 36(1), 223-226.

Howes, T.H., (1990). Assessment of the Cooling and Lubricative Properties of Grinding Fluids, *Annals of CIRP*, 39(1), 313-316.

Howes, T.H., Tönshof, H.K. & Heuer, W., (1991). Environmental Aspects of Grinding Fluids, *Annals of CIRP*, 40(2), 623-630.

Hwang, T., Evans, C. J., Malkin, S., (2000). An Investigation of High Speed Grinding with Electroplated Diamond Wheels, *Annals of CIRP*, 49(1), 245-248.

Hwang, T., Evans, C. J., Whitenton, E.P. & Malkin, S., (2000).High Speed Grinding of Silicon Nitride with Electroplated Diamond Wheels, Part 1: Wear and Wheel Life, *Transactions of the ASME Journal of Manufacturing Science & Engineering*, 122, 32-50

Innatec Bulletin, (1995). Coolant Delivery for Super Abrasives (CBN & Diamond), *INNATEC Industries.*

Inasaki, I., Tönshoff, H.K. & Howes, T.D., (1993). Abrasive Machining in the Future, *Annals of CIRP*, 42(2).

Jaeger, J.C., (1942). Moving Sources of Heat and Temperature at Sliding Contacts, *Proceedings of the Royal Society of New South Wales,* 76, 203-224.

Jin, T., Rowe, W.B. & M^{c}Cormack, D., (2002). Temperatures in Deep Grinding of Finite Workpieces, *International Journal of Machine Tools & Manufacture*, 42, 53-59.

Jin, T., Stephenson, D.J. & Corbett, J., (2002). Burn Threshold of High Carbon Steel in High Efficiency Deep Grinding, *Proceedings Institute of Mechanical Engineers, Part B, Journal of Engineering Manufacture, in press.*

Karpuschewski, B., (2000). Introduction to Micro magnetic Techniques. *In: The 1st International Conference on Barkhausen Noise & Magnetic Testing*. Hannover, Germany 2000.

Klocke, F., Baus, A. & Beck, T., (2000). Coolant Induced Forces in CBN High Speed Grinding with Shoe Nozzles, *Annals of CIRP*, 49(1), 241-244.

Klocke, F., Beck, T., Eisenblatter, G., Fritsch, R., Lung, D. & Pöhls, M., (2000). Applications of Minimal Quantity of Lubrication (MQL) in Cutting and Grinding, Tribology 2000 : Plus. The 12th International Colloquium. Technische Akademie Esslingen, January 11-13.

Klocke, F., Brinksmeier. E., Evans, C., Howes, T., Inaski, I., Minke, E., Tönshoff, H. K., Webster, J.A. & Stuff, D., (1997). High Speed Grinding – Fundamentals and State of the Art in Europe, Japan and the USA, *Annals of CIRP*, 46(2), 715-724.

Klocke, F. & König, W., (1995). Appropriate Conditioning Strategies Increase the Performance Capabilities of Vitrified-Bond CBN Grinding Wheels, *Annals of CIRP*, 44(1), 305-310.

Krusyński, B.W. & van Luttervelt, C.A., (1991). An attempt to Predict Residual Stresses in Grinding of Metals with the Aid of a New Grinding Parameter, *Annals of CIRP*, 40(1), 335-337.

Krusyński, B.W. & Wójcik, R., (2001). Residual Stress in Grinding, *Journal of Materials Processing Technology*, 109, 254-257.

Lamagnere, P., Girodin, D., Meynaud, P., Vergne, F. & Vincent, A., (1996). Study of Elastic-plastic Properties of Microheterogeneities by means of Nano-indentation Measurements Application to Bearing Steels, *Materials and Science,* A215, 134-142.

Lezanski, P. & Rafalowicz, J., (1993). An Intelligent Monitoring System for Cylindrical Grinding, *Annals of CIRP*, 42(1), 393-396.

Li, Y., Rowe, W.B. & Mills, B., (1999). Study and Selection of Grinding Conditions Part 1: Grinding Conditions and Selection Strategy, Proceedings of the Institution of the Mechanical Engineers Part B, 213, 119-129.

Li, Y., Rowe, W.B. Chen, X. & Mills, B., (1999). Study and Selection of Grinding Conditions Part 2: A Hybrid Intelligent System for Selection of Grinding Conditions, Proceedings of the Institution of the Mechanical Engineers Part B, 213, 131-142.

Mahdi, M., & Zhang, L., (1996). Thermal Applied Mechanics in Grinding – V. Thermal Residual Stresses, *International Journal of Machine Tools Manufacture*, 37(5), 619-633.

Malkin, S., (1974). Thermal Aspects of Grinding part 2 – Surface Temperatures and Workpiece Burn, *Trans. ASME – Journal of Engineering for Industry*, 96, 484.

Malkin, S. & Anderson, R.B., (1974). Thermal Aspects of Grinding, *Journal of Engineering for Industry Transactions of the ASME,* Nov. 1974, 1177-1183.

Malkin, S. & Koren, Y., (1980). Off-Line Grinding Optimisation with a Micro-Computer, *Annals of CIRP*, 29(1), 213-216.

Malkin, S., (1981). Grinding Cycle Optimisation, *Annals of CIRP*, .30(1), 223-226.

Mason, F., (1993). First High Efficiency Deep Grinding (HEDG) Machine, *American Machinist,* May, 37-40.

Mason, F., (1997). Are They Grinding or Milling, *Manufacturing Engineering,* 118(3)52-66.

Matsuo, T., Shibahara, H. & Ohbuchi, Y., (1987). Curvature in Section Grinding of Thin Workpieces with Superabrasive Wheels, *Annals of CIRP*, 36(1), 231-234.

Mayer, J.E., Purushothman, G. & Gopalakrishnan, S., (1999). Model of Grinding Thermal. Damage for Precision Gear Materials, *Annals of CIRP*, 48(1), 251-254.

Meyer, J. E. & Price, A., H., (2001). Specific Grinding Energy causing Thermal Damage in Helicopter Gear Steels, *In: 4th International Machining & Grinding Conference*, Troy, MI., USA 7th - 9th May 2001.

McCormack, D., F., Rowe, W., B. & Jin, T., (2001). Controlling the Surface Integrity of Ground Components, *In: 4th International Machining & Grinding Conference*, Troy, MI., USA 7th - 9th May 2001.

Moore, M.G. & Evans, W.P., (1958). Mathematical Correction for Stress in Removed Layers in X-Ray Diffraction Residual Stress Analysis, *SAE Transactions* 66, 340-345.

Morgan, M.N., Rowe, W.B., Black, S.C.E. & Allanson, D.R., (1998). Effective Thermal Properties of Grinding Wheels and Grains, *Proceedings of the Institution of Mechanical Engineers*, 212, 661-669.

Österle, W. & Li, P. X., (1997). Mechanical and Thermal Response of a Nickel-base Superalloy upon Grinding with High Removal Rates. *Materials Science and Engineering,* A238, 357-366.

Österle, W., Li, P. X. & Nolze, G., (1999). Influence of Surface Finishing on Residual Stress Depth Profiles of a Coarse-grained Nickel-base Superalloy. *Materials Science and Engineering,* A262, 308-311.

Petzow, G. (1978). *Metallographic Etching, 1st* Edition. American Society for Metals.

Prevey, P.S., (1986). X-Ray Diffraction Residual Stress Techniques, Metals Handbook 10, Metals Park: American Society for Metals, 380-392.

Ramanath, S., Ramaraj, T.C. & Shaw, M.C., (1987). What Grinding Swarf Reveals, *Annals of CIRP*, 36(1), 245-247.

Ramesh, K., Yeo, S.H., Zhong, Z.W. & Sim, K.C., (2001). Coolant Shoe Development for High Efficiency Grinding, *Journal of Materials Processing Technology*, 114, 240-245.

Rowe, W.B., Black, S.C.E., Mills, B., Qi, H.S. & Morgan, M.N., (1995). Experimental Investigation of Heat Transfer in Grinding, *Annals of CIRP*, 44(1), 329-332.

Rowe, W.B. & Chen, X., (2000). Application and Performance of CBN Wheels, *Abrasives Magazine*, Oct./Nov. 36-41.

Rowe, W.B., (2001). Thermal Analysis of High Efficiency Deep Grinding, *International Journal of Machine Tools & Manufacture*, 41, 1-19.

Rowe, W.B., (2001). Temperature Case Studies in Grinding including an Inclined Heat Source Model, *Proceedings of the Institution of Mechanical Engineers*, 215, 473-491.

Rowe, W.B. & Jin, T., (2001). Temperatures in High Efficiency Deep Grinding, *Annals of CIRP*, 50(1), 205-208.

Savington, D., (1999). Maximising the Grinding Process, Tooling and Accessories Group, Abmart.

Shaji, S. & Radhakrishnan, V., (2002). An Investigation on Surface Grinding using Graphite as Lubricant. *International Journal of Machine Tools & Manufacture*, 42, 733-740.

Shaw, B.A., Benson, M. & Hofmann, D.A., (1999). Calibration of the Barkhausen Noise Method as a Tool for Assessing the Surface Integrity of Gear Steels. *In: The 2nd International Conference on Barkhausen Noise and Micromagnetic Testing*, Newcastle upon Tyne, United Kingdom. 25-26 October 1999.

Shaw, B.A., Evans, J.T. & Yates, D.E., (1996). The Influence of Grinding on the Formation of Residual Stress Distributions in Ground Surfaces. *In: The Drives & Controls Conference*, Telford, United Kingdom. 1996, Session 4, Paper 4, 21-26.

Shaw, M.C., (1972). Fundamentals of Grinding, New Developments of Grinding. *In: The Proceedings of the International Grinding Conference*, Carnegie-Mellon University, Pittsburg, PA. 1972, 220-258.

Shaw, M.C., (1975). Cost Reduction in Stock Removal Grinding, *Annals of CIRP*, 24(2), 539-542.

Shaw, M.C. & Vyas, A., (1993). Heat Affected Zones in Grinding Steel, *Annals of CIRP*, 43(1), 279-282.

Shore, Paul. (1995). *Machining of Optical Surfaces in Brittle Materials using an Ultra Precision Tool,* PhD Thesis, Cranfield University.

Shibata, J., Chao-Kun, K., Inasaki, I. & Yonestu, S., (1980). Adaptive Control for Conveyer-Type Belt Grinding, *Annals of CIRP*, 29 (1), 217-220.

Snoeys, R., (1978). Thermally Induced Damage in Grinding, *Annals of CIRP*, 27 (2), 571-581.

Stephenson, D. J., Laine, E., Johnstone, I., Baldwin, A. & Corbett, J., (2001). Burn threshold studies for super abrasive grinding using electroplated CBN wheels. In: 4th International Machining & Grinding Conference, Troy, MI., USA 7th - 9th May 2001.

Stephenson, D. J., Jin, T. & Corbett, J., (2002). High Efficiency Deep Grinding of Low Alloy Steel with Plated CBN Wheels, *Accepted for Publication by Annals of CIRP*.

Sullivan, J., (2002). Verbal reference as to the ease at which nickel based superalloys generate tensile stresses on the finished ground surface.

Tabesh, A.D., (1990). Important Characteristics of Successful Applications of CBN Production Grinding. *In: The Proceedings of the 28th Abrasive Engineering Society Conference*, 1990 Joint Industry -- AES Conference Cleveland Ohio. May 16-18 1990, 68-94.

Tawakoli, T., (1993). High Efficiency Deep Grinding, *Advanced Engineering & Technic, Bremen Germany.*

Tönshoff, H.K., Peters, J., Inaski, I. & Paul, T., (1992). Modelling and Simulation of Grinding Processes, *Annals of CIRP*, 41(2), 667-688.

Tönshoff, H.K. & Falkenberg, Y., (1996). High Speed Grinding of Cast Iron Crankshafts with CBN Tools, *Industrial Diamond Review*, April, 115-119.

Tönshoff, H.K., Karpuschewski, B. & Mandrysch, T., (1998). Grinding Process Achievements and their Consequences on Machine Tool Challenges and Opportunities, *Annals of CIRP*, 47(2), 651-668.

Uhlmann, E. & Laufer, J., (1998). Technological and Ecological Aspects of Cooling Lubrication during Grinding of Ultra Hard Materials, *Finer Points*, 10(3), 18-29.

Varghese,B., Pathere, S., Gao, R., Guo, C. & Malkin, S., (2000). Development of a Sensor-Integrated "Intelligent" Grinding Wheel for In-Process Monitoring, *Annals of CIRP*, 49(1), 231-234.

Vanek, D.L., (2000). Selective Electropolishing, *Metal Finishing*, 98 (1), 361-374.

Wager, J.G. & Gu, D.Y., (1991). Influence of Up-Grinding And Down-Grinding on the Contact Zone, *Annals of CIRP*, 40(1), 323-326.

Wang, S. & Kou, H., (1997). Cooling Effectiveness of Cutting Fluid in Creep Feed Grinding, *Int. Communication of Heat Mass Transfer*, 24, 771-783.

Wang, S-B. & Fuh, K-H., (1998). The Workpiece Temperature, Fluid Cooling Effectiveness and Burning Threshold of Grinding Energy in Creep Feed Grinding, *Institute of Mechanical Engineers*, 212 Part B, 383-391.

Webster, J.A., Mindek Jnr, R.B. & Cui, C., (1995). Grinding Fluid Application System Design, *Annals of CIRP*, 44(1), 333-338.

Webster, J.A., & Cui, C., (1995). Flow Rate and Jet Velocity determining for Design of a Grinding Cooling System, *In: 1st International Machining & Grinding Conference*, Dearborn, Michigan September 12-14 1995.

Werner, G. & Lauer-Schmaltz, H., (1980). Advanced Application of Coolants and Prevention of Wheel Loading in Grinding. *In: The International Symposium on Metalworking Lubrication*, San Francisco, August 18-19 1980.

Werner, G. & Tawakoli, T., (1988). Deep Grinding Narrow Slots with CBN Wheels, Industrial Diamond Review, June.

Wissner, P. & Ong, W.C., (1998). Biodegradable Lubricants, *Lubrication Engineering*, 54(7), 10-22.

Yoon, S.C. & Krueger, M., (1998). A Killer Combination for Ideal Grinding Conditions, *American Machinist.*

Yui, A. & Lee, H., (1996). Surface Grinding with Ultra High Speed CBN Wheel, *Journal of Materials Processing Technology*, 62, 393-396.

Zhang, B., (2001). An Investigation of the Effect of Machine Loop Stiffness on Grinding of Ceramics, *Annals of CIRP*, 50(1), 209-212.

BIBLIOGRAPHY

Andrew, Howes, & Pearce. (1986). *Creep Feed Grinding.* 1st Edition Holt Technology.

Cullity, B.D. (1967). *Elements of X-Ray Diffraction.* 3rd Edition Addison Wesley Publishing Co.Inc.

Holz, R. & Sauren, J. (1988). *Grinding with Diamond & CBN.* 1st Edition Brendes-Druck Norderstedt for Winter Diamond Tools.

King, R.I. & Hahn, R.S. (1986). *Modern Grinding Technology.* 1st Edition Chapman & Hall.

Mainsah, E., Greenwood, J.A. & Chetwynd, D.G. (2001). *Metrology and Properties of Engineering Surfaces*. Kluwer Academic Publishers.

Malkin, S. (1989). *Grinding Technology – Theory and Applications of Machining with Abrasives.* Ellis Horwood Limited, Chichester.

Metzger, J. L. (1986). *Superabrasive Grinding*, 1st Edition. Butterworth & Co (Publishers) Ltd).

Sims & Hagel. (1972). *The Super Alloy,* 1st Edition. John Wiley & Sons, Inc.

Shaw, Milton C. (1996). *Principles of Abrasive Processing.* Oxford Science Publications.

Tawakoli, Taghi. (1993). *High Efficiency Deep Grinding,* 2nd Edition. Biddles Ltd, Guildford and Kings Lynn.

Woodbury, Robert S. (1959). *History of the Grinding Machine,* 1st Edition. MIT Press, Cambridge MA.

THESIS APPENDICES

Appendix A – Edgetek Test Programme

Edgetek Test Programme

The following test programme is based around the initial schedule prepared by SKF and Rolls-Royce in July 1999. The work programmes will involve grinding studies on both IN718 and a bearing steel, M50.

The basic grinding research outlined in Tasks 1 - 6 will be undertaken on flat blocks, 100 x 40 x 40 mm to be provided by SKF and Rolls-Royce. Standard conditions will use electroplated CBN wheels and a mineral oil coolant eg Castrol Ilogrind 500FG or Ilogrind 600SP. Other types of coolant and grinding wheel will be evaluated within the programme.

For each specimen, the grinding forces will be measured and related to grinding power, grinding zone temperature and grinding wheel performance. Surface roughness measurements will also be made together with a visual assessment of surface burn. Selected samples will be studied in greater detail to provide further information on surface and sub-surface grinding damage through a combination of optical and electron microscopy and surface analysis. Residual stress measurements will be undertaken by Rolls-Royce and SKF.

The following series of tasks will be completed for each of the two workpiece materials.

Task 1. Assess machine dynamic performance

Task Leader- Cranfield

Duration- 0.5 months

It is proposed that the dynamic performance of the Edgetek machine be analysed by modal testing, the objective being to identify the maximum loop compliance, its frequency, the first few such `resonant' peaks, and the mode shapes and thus physical origin of these peaks, on a fully active machine. This modal testing, expected to take around 2 weeks on a commissioned machine, will be achieved using spectral analysis of the transfer function between variously located accelerometers, and calibrated force excitation, applied using `shaker' coil and instrumented hammer.

This process will identify 'weak' points among the machine's structure and elements, and give quantitative comparisons with other machines, which can be related to machining performance.

Task 2. Initial grinding assessment

Task Leader- Cranfield

Duration- 1 month

2.1 Influence of depth of cut

Material removal rate, Q'_w = 50 mm3/mm.s for Inco 718 and 5 mm3/mm.s for M50

Grit size = B252 (for Inco 718) and B151 (for M50)

Wheel speed, Vc = 100 m/s

Grinding will be undertaken at 3 depths of cut ac with feed rate maintained to give the required Q'_w value as follows:

ac (mm) (Inco 718)	ac (mm) (M50)	Vw(mm/s)
1	0.1	50
2.5	-	20
5	0.5	10
-	1	5

2.2 Influence of wheel speed

Material removal rate, QIN718 = 50 mm^3/mm.s, QM50 = 5 mm^3/mm.s

Depth of cut, ac = 5 mm / 0.5mm

Feed rate, Vw = 10 mm/s

Grit size = B252 (for Inco 718) and B151 (for M50)

3 different wheel speeds will be considered: Vc (m/s) = 50, 100, 150

Influence of grit size

Material removal rate, QIN718= 50 mm^3/mm.s, QM50 = 5 mm^3/mm.s

Depth of cut, ac = 5 mm / 0.5mm

Wheel speed, Vc = 100 m/s

Feed rate, Vw = 10 mm/s

2.4 different grit sizes will be considered, as follows:

Inco 718 - B181, B252, B301

M50 - B126, B151, B181

2.5 Influence of material removal rate

Grit size = B252 (for Inco 718) and B151 (for M50)

Wheel speed, Vc = 100 m/s

Depth of cut, ac = 10 mm & 0.5mm

Different feed rates will be used at a constant depth of cut to vary the material removal rate, Q'_w as follows:

Vw (mm/s)	QIN718 (mm^3/mm.s)	QM50 (mm^3/mm.s)
5	50	2.5
10	100	5
50	500	25

Depending on the results from this sub-task, further tests will be undertaken to identify the critical value of Q at which surface integrity issues become important.

The experiments in Task 2 will provide an understanding of how basic grinding parameters influence the surface produced.

Task 3. Wheel life and coolant type

Task Leaders Unicorn, Castrol and Rolls-Royce

Duration 1.5 months

This task will study grinding wheel life and relate wheel performance to surface integrity. Wheel life will be monitored through the measurement of the variation in power and normal grinding force and degradation of surface quality. The influence of coolant type on wheel life will also be studied.

Material removal rate	QIN718 = 50 mm^3/mm.s	QM50 = 5 mm^3/mm.s
Wheel speed Vc = 100 m/s		
Grit size, g	B252 (for Inco 718)	B151 (for M50)
Coolants:	Mineral oil, Ilogrind 500FG or Ilogrind 600SP	
	Ester based, CareCut ES2	
	Water based, Hysol X	

Extended grinding trials will be made to determine wheel performance as a function of usage. Repeatability of wheel performance will be assessed on three samples and using the three different coolants.

Task 4. Optimisation of coolant application

Task Leaders- Unicorn, Wanner and SKF

Duration- 1 month

This task will investigate the influence of coolant application on surface quality.

Material removal rate	QIN718 = 50 mm^3/mm.s	QM50 = 5 mm^3 /mm.s

Wheel speed Vc will be varied between 50 and 150 m/s and for a given depth of cut

Grit size, g	B252 (for Inco 718)	B151 (for M50)

Six levels of coolant application will be studied by control of exit velocity and flow rate using nozzles provided by Unicorn. Three depths of cut, (1, 2.5 and 5 mm for IN718 and 0.1, 0.5 and 1mm for M50) will be studied. The type of coolant will be determined following an assessment in Task 3.

Task 5. Grinding wheel optimisation

Task Leaders- DeBeers and Unicorn

Duration- 1 month

Task 5 will evaluate the performance of various grinding wheel types and highlight the influence of bond type and abrasive.

Material removal rate, QIN718 = 50 mm3/mm.s, QM50 = 5 mm3/mm.s

Depth of cut ac = 5 mm & 0.5mm

Wheel speed, Vc = 100 m/s

Three bond types and three grain types will be supplied to evaluate the importance of wheel design in HEDG. These are likely to be one electroplated wheel and two vitrified bond wheels for each material. The coolant and application method will be determined following Tasks 3 and 4.

Task 6. Loading avoidance

Task Leader	-	Cranfield and Wanner
Duration	-	1 month testing

This task will investigate the problem of wheel loading, its influence on surface quality and evaluate methods to overcome the problem. Grinding conditions will be determined following results from tasks 2 - 5.

The work programme will investigate type and frequency of dressing, high pressure cleaning of the wheel and will build on observations of wheel performance in previous work, particularly task 3.

Task 7. Rolls-Royce 'Specific component test'

Task Leader	-	Rolls-Royce
Duration	-	2 month testing
Objective:	-	Activities to be defined.

Task 8. SKF (Avio) 'Specific component tests'

Task Leader	-	SKF
Duration	-	1 month testing
Objective:	-	Activities to be defined.

Appendix B – Wrought IN718 Data Sheets

Density8220kg/m^3 Melting Point (Solidus)1260°C

Specific Heat Capacity

Temperature(°C)	Specific heat (kJ/(kg.K))
20.0	0.4240
100.0	0.4340
200.0	0.4480
300.0	0.4630
400.0	0.480
500.0	0.50
550.0	0.5110
600.0	0.5250
650.0	0.5410
700.0	0.560
750.0	0.5820
800.0	0.6050
850.0	0.6250

Thermal Conductivity

Temperature(°C)	Conductivity (W/(m.K))
20.0	11.45
100.0	12.75
200.0	14.36
300.0	15.96
400.0	17.60
500.0	19.18
550.0	19.98
600.0	20.77
650.0	21.56
700.0	22.36
750.0	23.15
800.0	23.95
900.0	25.10
1000.0	26.83
1100.0	28.56

ELASTIC DATA All at 20°C

Young's Modulus207.6GPa

Torsion Modulus80.0GPa

Poisson's Ratio0.29

TENSILE DATA All at 20°C

0.2% Proof Stress1172MPa

Ultimate Strength1441MPa

Appendix C – MAR-M-002 Data Sheets

Density8560kg/m^3 Melting Point (Solidus)1270°C

Specific Heat Capacity

Temperature(°C)	Specific heat (kJ/(kg.K))
20	0.416
100	0.428
200	0.443
300	0.458
400	0.473
500	0.488
600	0.505
700	0.533
800	0.58
900	0.646
1000	0.72
1100	0.797
1200	0.875

Thermal Conductivity

Temperature(°C)	Conductivity (W/(m.K))
20	12.6
100	13.7
200	14.9
300	16.1
400	17.4
500	18.4
600	19.5
700	20.8
800	22.1
900	24.1
1000	25.4
1100	27.5
1200	30

ELASTIC DATA All at 20°C

Young's Modulus207.5Gpa

Torsion Modulus83.0Gpa

Poisson's Ratio0.25

TENSILE DATA All at 20°C

0.2% Proof Stress823.2MPa

Ultimate Strength947MPa

Appendix D – M50 Data Sheets

Density7870kg/m^3

Melting Point (Solidus)1570°C

Specific Heat

Temperature (°C)	Thermal Conductivity W/(m.K)
20	25.7
50	26.6
100	28.1
150	29.2
200	30.3
250	31
300	31.6
350	32
400	32.2
450	32.5
500	32.6
550	32.6
600	32.6
650	32.6
700	32.6
750	32.7
800	32.9
850	33.2
900	33.7
950	34.3
1000	35

Thermal Conductivity	
Temperature (°C)	Specific heat kJ/(kg.K)
20	0.437
50	0.447
100	0.467
150	0.488
200	0.508
250	0.529
300	0.55
350	0.572
400	0.593
450	0.615
500	0.637
550	0.658
600	0.68

Appendix E – Taguchi Style Screening Tests

M50 Screening Test Parameters using Mineral Oil Grinding Fluid

	Inputs									Responses				
Test Number	Wheel Speed	Grit Size	Depth of Cut	Nozzle Angle	Nozzle Height	Feed Rate	Nozzle Diameter	Coolant Pressure	Barkhausen Noise Amplitude	Material Removed	Total Material Removed	Net Spindle Power	Calculated Temperature	Specific Grinding Energy
	(m/s)	??m)	(mm)	(degrees)	(mm)	(mm/s)	(mm)	(bar)		(mm^3)	(mm^3)	(kW)	(degrees C)	(J/mm^3)
1	75	151	0.55	7	108	25.25	7	10.8	43	825	825	0.972	80	9.72
4	50	126	1	5	110	0.5	5	14.0	40.2	1500	1500	2.025	650	360.00
5	50	126	0.1	8	105	0.5	8	14.0	47	150	1650	0.675	578	1800.00
15	100	126	1	5	105	0.5	8	7.5	45	1500	3150	4.995	1560	864.00
9	100	126	0.1	8	110	0.5	5	7.5	38	150	3300	1.215	1156	3600.00
14	100	126	1	8	110	50	8	14.0	50	1500	4800	13.365	358	19.80
17	50	126	1	8	105	50	5	7.5	62	1500	6300	15.525	390	21.60
13	50	126	0.1	5	110	50	8	7.5	73	150	6450	4.725	231	72.00
11	100	126	0.1	5	105	50	5	14.0	31.5	150	6600	3.915	231	72.00
10a	75	151	0.55	7	108	25.25	7	10.8	58	825	1650	7.047	319	38.88
10b	75	151	0.55	7	108	25.25	7	10.8	35	825	2475	6.507	297	36.29
10c	75	151	0.55	7	108	25.25	7	10.8	52	825	3300	6.777	308	37.59
10d	75	151	0.55	7	108	25.25	7	10.8	37	825	4125	7.047	319	38.88
6	100	181	0.1	5	110	0.5	8	14.0	31.5	150	150	4.725	2659	8280.00
7	50	181	0.1	5	105	0.5	5	7.5	70.3	150	300	1.350	867	2700.00
12	100	181	1	8	105	0.5	5	14.0	10.2	1500	1800	4.725	1495	828.00
18	50	181	1	8	110	0.5	8	7.5	28.3	1500	3300	2.295	715	396.00
3	100	181	1	5	110	50	5	7.5	44.7	1500	4800	13.365	358	19.80
2	50	181	0.1	8.0	110.0	50	5.0	14.0	39.6	150	4950	3.375	173	54.00
8	50	181	1	5	105	50	8	14.0	21.3	1500	6450	15.525	390	21.60
16	100	181	0.1	8	105	50	8	7.5	87.2	150	6600	5.535	301	93.60
19	75	151	0.55	7	108	25.25	7	10.8	32.4	825	4950	6.237	287	35.00
Q150	100	151	2.5	8	107.5	60	9	6	47	3750	8700	31.055	622	15.80

Table E.1: Inputs and Responses for M50 Screening Test

APPENDIX E

IN718 Screening Test Results in Mineral Grinding Fluid

		Responses	
Test Number	Net Grinding Spindle Power (kW)	Calculated Temperature (degrees C)	Specific Grinding Energy (J/mm^3)
1	1.207	47.50	5.80
6	0.082	35.33	110.00
7	0.110	47.10	146.67
12	0.358	86.09	47.67
18	0.803	193.37	107.07
3	2.778	66.88	3.70
8	8.800	211.91	11.73
2	0.523	22.37	6.97
16	1.650	70.66	22.00
10a	3.850	151.49	18.48
10b	4.730	186.12	22.71
10c	5.060	199.10	24.29
10d	5.500	216.42	26.40
4	0.611	147.01	81.40
15	0.330	79.47	44.00
5	0.479	204.90	638.00
9	0.113	48.28	150.33
14	13.778	331.77	18.37
17	14.960	360.25	19.95
11	1.788	76.54	23.83
13	1.843	78.90	24.57
19	5.363	211.01	25.74

Table E.2: Responses for IN718 Screening Test

Appendix F – M50 Experimental Parameters

Test Number	Q Prime	Depth of cut	Feed Rate Vw	Wheel Speed	Width of Cut	Barkhausen Noise Amplitude	Residual Stress σx	Surface Roughness	Surface Roughness	Specific Grinding Energy	Specific Fv	Specific Fh		Temperature Finished Surface	Temperature Contact Surface
								R_a	R_t						
	(mm^2/s)	(mm)	(mm/s)	(m/s)	(mm)		$E_{(HKL)}$ (Mpa)	(microns)	(microns)	(J/mm^3)	(N/mm)	(N/mm)	Peclet No	(C)	(C)
50-1	150	2.500	60.00	100	15.0	47	-461	1.55	15.8	15.80			44.88	350	1692
50-2	150	2.500	60.00	100	15.0	87	484	1.55	15.8	15.80			44.88	858	1692
50-3	13.89	0.550	25.25	75	15.0	43	-604	2.1	19	9.72			8.86	112	200
50-4	13.89	0.550	25.25	100	15.0	37		2.02	18	38.88			8.86	774	1232
50-5	13.89	0.550	25.25	100	15.0	52		1.58	14.8	37.59			8.86	746	1186
50-6	13.89	0.550	25.25	50	15.0	35		2.08	17.5	36.29			8.86	610	970
50-7	13.89	0.550	25.25	50	15.0	58		1.92	15	38.88			8.86	658	1047
50-8	13.89	0.550	25.25	100	15.0	32.4		1.55	15.8	35.00	8.959	1.181	8.86	689	1095
50-9	50	1.000	50.00	100	15.0	44.7	-640	1.51	17	19.80			23.66	682	1158
50-10	50	1.000	50.00	75	15.0	21.3		1.59	15.5	21.60			23.66	715	1213
50-11	5	0.100	50.00	50	15.0	39.6	-455	2	19	54.00			7.48	365	592
50-12	5	0.100	50.00	100	15.0	87.2		1.4	14.5	93.60			7.48	794	1213
50-13	50	1.000	50.00	50	15.0	50		2.4	24	19.80			23.66	580	985
50-14	50	1.000	50.00	50	15.0	50		2.22	21	21.60	39.365	8.979	23.66	648	1099
50-15	5	0.100	50.00	100	15.0	31.5		3.2	32	72.00	1.447	0.546	7.48	608	929
50-16	5	0.100	50.00	50	15.0	73		3.5	32	72.00	2.928	0.293	7.48	518	792
50-17	150	2.500	60	100.00	15.0	64				14.03	106.059	6.507	44.88	1053	2077
50-18	125	2.500	50	100.00	15.0	125				17.26	110.613	4.555	37.40	1227	2363
50-19	50	1.000	50	100.00	15.0	66				21.60	48.149	3.145	23.66	917	1555
50-20	60	1.000	60	100.00	15.0	129				20.35	52.053	5.856	28.39	940	1611
50-21	150	2.500	60	100.00	15.0	135	62			14.17	144.448	6.181	44.88	1064	2098
50-22	50	1.000	50	100.00	15.0	109	-125			22.81	63.765	4.229	23.66	971	1647
50-23	60	1.000	60	100.00	15.0	159				23.28	64.416	7.157	28.39	1081	1853
50-24	125	2.500	50	100.00	15.0	149				17.07	143.227	3.563	37.40	1212	2335
50-25	0.4	0.200	2	100.00	7.5					27.50	1.640	0.433	0.42	75	144
50-26	0.9	0.300	3	100.00	7.5					16.30	2.038	0.268	0.78	70	132
50-27	0.4	0.200	2	100.00	7.5					18.33	0.751	0.214	0.42	58	106
50-28	3	1.500	2	100.00	7.5					23.22	11.865	0.375	1.16	162	422
50-29	0.4	0.200	2	100.00	7.5					36.67	2.681	0.322	0.42	93	183
50-30	0.3	0.300	1	100.00	7.5					42.78	2.904	0.405	0.26	89	193
50-31	0.1	0.100	1	100.00	7.5					73.33	6.251	0.215	0.15	80	153
50-32	0.4	0.200	2	100.00	7.5					32.08	1.930	0.147	0.42	84	164
50-33	0.4	0.200	2	100.00	7.5					41.25	3.432	1.251	0.42	102	202
50-34	0.3	0.100	3	100.00	7.5					42.78	0.858	0.090	0.45	92	167
50-35	0.4	0.200	2	100.00	7.5					36.67	1.716	0.215	0.42	93	183
50-36	0.9	0.200	4.5	100.00	7.5					24.44	2.681	2.896	0.95	97	180
50-37	0.9	0.300	3	100.00	7.5					24.44	4.628	1.662	0.78	98	193
50-38	0.1	0.100	1	100.00	7.5					91.67	1.427	0.380	0.15	93	180
50-39	0.32	0.200	1.6	100.00	7.5					51.56	3.539	1.448	0.34	108	221
50-40	0.4	0.200	2	100.00	7.5					27.50	0.782	0.143	0.42	76	147

Test Number	Q Prime	Depth of cut	Feed Rate Vw	Wheel Speed	Width of Cut	Barkhausen Noise Amplitude	Residual Stress σx $E_{(HKL)}$ (Mpa)	Surface Roughness R_a (microns)	Surface Roughness R_t (microns)	Specific Grinding Energy (J/mm^3)	Specific Fv (N/mm)	Specific Fh (N/mm)	Peclet No	Temperature Finished Surface (C)	Temperature Contact Surface (C)
	(mm^2/s)	(mm)	(mm/s)	(m/s)	(mm)										
50-41	0.3	0.100	3	100.00	7.5					30.56	1.609	0.490	0.45	73	129
50-42	0.4	0.200	2	100.00	7.5					41.25	2.789	0.053	0.42	102	202
50-43	1	0.500	2	100.00	7.5					33.00	6.328	0.161	0.67	132	294
50-44	0.3	0.300	1	100.00	7.5					42.78	2.788	0.107	0.26	89	193
50-45	13.89	0.550	25.25	100.00	7.5					8.95	11.691	1.233	8.86	102	183
50-46	13.89	0.550	25.25	100.00	7.5					10.30	10.940	0.643	8.86	128	230
50-47	13.89	0.550	25.25	100.00	7.5					11.09	12.441	0.217	8.86	142	258
50-48	13.89	0.550	25.25	100.00	7.5					11.49	16.628	0.196	8.86	150	272
50-49	200	2.000	100.00	100.00	7.0			2.05	15.057	13.20	148.652	12.656	66.91	852	1379
50-50	20	2.000	10.00	100.00	7.0			1.822	13.898	62.86	40.002	12.844	6.69	2244	3385
50-51	10	1.000	10.00	100.00	7.0		198	1.3	9.54	62.86	18.167	0.619	4.73	1365	2046
50-52	100	1.000	100.00	100.00	7.0		-647	1.192	10.2	30.68	93.203	5.309	47.31	1527	2716
50-53	82.5	1.500	55.00	100.00	7.0		117	1.052	8.942	43.48	99.538	6.221	31.87	2286	4090
50-54	200	2.000	100.00	100.00	7.0		226	1.256	9.763	22.65	163.024	11.905	66.91	1818	2942
50-55	10	1.000	10.00	100.00	7.0		-792	1.441	13.224	81.71	21.987	0.268	4.73	1600	2699
50-56	100	1.000	100.00	100.00	7.0			1.252	10.121	31.43	90.857	8.151	47.31	1571	2794
50-57	20	2.000	10.00	100.00	7.0		-587	1.048	8.241	78.77	43.079	0.267	6.69	2654	4304
50-58	1	4.000	0.25	30.00		57		2.004	16.209	11.24			0.24	43	108
50-59	20	4.000	5.00	30.00		58		1.42	15.705	5.69			4.73	40	77
50-60	50	4.000	12.50	30.00		53		1.585	12.785	0.92			11.83		
50-61	100	4.000	25.00	30.00		52		1.552	15.316	2.43			23.66		
50-62	1	4.000	0.25			52		1.406	9.802	188.20					
50-63	20	4.000	5.00	146.00		62		0.949	8.025	8.71			4.73	119	313
50-64	50	4.000	12.50	146.00		57		0.921	7.117	6.34			11.83	125	303
50-65	100	4.000	25.00			61		0.862	6.079						
50-66	25	4.000	6.25	146.00		n/a	-1163	0.785	5.937	7.73			5.91	104	262
50-67	25	4.000	6.25	146.00		57		1.058	8.673	3.73			5.91		
50-68	25	4.000	6.25	146.00		61		0.953	8.517	8.29			5.91	121	309
50-69	25	4.000	6.25	146.00		65		0.856	6.835	9.21			5.91	148	385
50-70	25	4.000	6.25	146.00		65		0.808	6.212	5.47			5.91	38	76
50-71	25	4.000	6.25	146.00		62		0.864	6.705	10.19			5.91	176	466
50-72	25	4.000	6.25	146.00		65		0.793	6.098	13.01			5.91	259	699
50-73	25	4.000	6.25	146.00		n/a	-1127	0.794	6.434	7.92			5.91	110	278
50-74	10	4.000	2.50	146.00		n/a	-1009	0.858	6.684	19.07			2.37	249	783
50-75	10	4.000	2.50	146.00		58		0.804	6.775	15.65			2.37	195	602
50-76	10	4.000	2.50	146.00		62		0.750	6.545	23.65			2.37	325	1034
50-77	10	4.000	2.50	146.00		n/a	-1118	0.774	6.395	17.19			2.37	220	683
50-78	10	4.000	2.50	146.00		72		0.754	5.863	17.19			2.37	220	683
50-79	10	4.000	2.50	146.00		65		0.756	5.688	17.22			2.37	220	685
50-80	10	4.000	2.50	146.00		64		0.772	6.142	20.34			2.37	269	849

Test Number	Q Prime	Depth of cut	Feed Rate Vw	Wheel Speed	Width of Cut	Barkhausen Noise Amplitude	Residual Stress σx	Surface Roughness R_a	Surface Roughness R_t	Specific Grinding Energy	Specific Fv	Specific Fh		Temperature Finished Surface	Temperature Contact Surface
	(mm^2/s)	(mm)	(mm/s)	(m/s)	(mm)		$E_{(HKL)}$ (Mpa)	(microns)	(microns)	(J/mm^3)	(N/mm)	(N/mm)	Peclet No	(C)	(C)
50-81	10	4.000	2.50	146.00		65		0.727	5.730	17.19			2.37	220	683
50-82	20	4.000	5.00	146.00		49		1.734	12.952	5.27			4.73	32	58
50-83	20	4.000	5.00	146.00		52		1.257	8.600	8.47			4.73	113	295
50-84	20	4.000	5.00	146.00		52		1.247	9.213	8.86			4.73	123	325
50-85	20	4.000	5.00	146.00		51		1.202	9.257	9.17			4.73	131	347
50-86	10	4.000	2.50	146.00		50		1.312	8.603	5.39			2.37	34	62
50-87	10	4.000	2.50	146.00		52		1.296	10.23	14.21			2.37	173	527
50-88	10	4.000	2.50	146.00		53		1.282	10.009	15.87			2.37	199	614
50-89	10	4.000	2.50	146.00		54		1.214	8.326	14.21			2.37	173	527
50-90	0.5	1.000	0.5	50.00	5.0			2.420	18.646	64.80	1.940	0.968	0.24	135	378
50-91	0.5	1.000	0.5	100.00	5.0			2.187	15.679	140.40	1.940	0.960	0.24	284	933
50-92	0.05	0.100	0.5	50.00	5.0			2.045	16.205	108.00	1.948	1.960	0.07	31	47
50-93	50	1.000	50	50.00	5.0			1.352	11.233	14.69	42.932	5.840	23.66	349	658
50-94	5	0.100	50	100.00	5.0			1.167	9.130	0.09	3.904	1.952	7.48	143	232
50-95	5	0.100	50	100.00	5.0			1.146	8.732	0.09	7.808	0.980	7.48	134	217
50-96	5	0.100	50	100.00	5.0			1.152	8.913	0.11	7.808	0.004	7.48	170	276
50-97	5	0.100	50	100.00	5.0			1.135	8.621	0.09	9.760	0.972	7.48	143	232
50-98	5	0.100	50	100.00	5.0			1.094	8.543	0.10	7.808	0.004	7.48	152	247
50-99	5	0.100	50	100.00	5.0			1.109	9.250	0.12	9.010	0.154	7.48	188	306
50-100	5	0.100	50	100.00	5.0			1.092	8.757	0.10	8.260	0.230	7.48	152	247
50-101	5	0.100	50	100.00	5.0			1.123	8.866	0.11	9.460	5.784	7.48	170	276
50-102	5	0.100	50	100.00	5.0			1.065	9.074	0.12	5.255	1.026	7.48	197	321
50-103	5	0.100	50	100.00	5.0			1.054	8.812	0.11	7.808	1.852	7.48	179	291
50-104	5	0.100	50	100.00	5.0			1.046	9.046	0.11	5.843	1.076	7.48	170	276
50-105	5	0.100	50	100.00	5.0			1.019	8.588	0.11	3.904	0.876	7.48	179	291
50-106	5	0.100	50	100.00	5.0			1.024	9.301	0.12	9.760	0.700	7.48	197	321
50-107	5	0.100	50	100.00	5.0			1.023	9.063	0.12	7.808	1.852	7.48	197	321
50-108	5	0.100	50	100.00	5.0			1.035	8.802	0.12	3.904	0.100	7.48	197	321
50-109	5	0.100	50	100.00	5.0			1.038	9.288	0.12	7.808	1.952	7.48	197	321
50-110	50	1.000	50	100.00	5.0		-280	1.017	9.137	19.12	48.800	5.880	23.66	652	1106
50-111	50	1.000	50	100.00	5.0		-91	1.095	8.882	20.52	46.848	4.904	23.66	714	1212
50-112	50	1.000	50	100.00	5.0		-182	1.032	8.773	21.60	44.896	6.832	23.66	763	1294
50-113	50	0.400	125	100.00	5.0		225	1.066	9.013	18.04	52.704	4.880	37.40	531	826
50-114	50	1.000	50	100.00	5.0					21.92	56.608	3.904	23.66	820	1392
50-115	50	1.000	50	100.00	5.0					22.90	66.368	3.904	23.66	876	1486
50-116	50	1.000	50	100.00	5.0					23.76	50.752	4.880	23.66	931	1580
50-117	50	1.000	50	100.00	5.0					23.11	58.560	3.904	23.66	830	1408
50-118	50	1.000	50	100.00	5.0					23.87	60.512	2.928	23.66	986	1674
50-119	50	1.000	50	100.00	5.0					24.41	60.504	4.880	23.66	1042	1767
50-120	50	1.000	50	100.00	5.0			1.082	1.347	25.27	60.512	3.904	23.66	1097	1861

Test Number	Q Prime (mm³/s)	Depth of cut (mm)	Feed Rate Vw (mm/s)	Wheel Speed (m/s)	Width of Cut (mm)	Barkhausen Noise Amplitude	Residual Stress σx Eрнкц (Mpa)	Surface Roughness R_a (microns)	Surface Roughness R_t (microns)	Specific Grinding Energy (J/mm³)	Specific Fv (N/mm)	Specific Fh (N/mm)	Peclet No	Temperature Finished Surface (C)	Temperature Contact Surface (C)
50-121	50	1.000	50	100.00	5.0					24.62	62.464	4.880	23.66	897	1522
50-122	50	1.000	50	100.00	5.0			0.877	1.097	25.38	66.368	4.880	23.66	1153	1955
50-123	50	1.000	50	101.00	5.0					24.73	56.608	4.880	23.66	1155	1960
50-124	50	1.000	50	102.00	5.0					25.16	76.128	5.856	23.66	1157	1964
50-125	50	1.000	50	103.00	5.0					25.70	70.272	6.832	23.66	1160	1967
50-126	50	1.000	50	104.00	5.0					26.14	56.608	4.880	23.66	1162	1971
50-127	50	1.000	50	105.00	5.0					25.70	42.464	0.976	23.66	1164	1975
50-128	50	1.000	50	106.00	5.0					26.46	62.464	4.880	23.66	1166	1979
50-129	50	1.000	50	107.00	5.0					26.78	66.368	4.880	23.66	1169	1983
50-130	50	1.000	50	108.00	5.0			0.986	1.249	27.22	82.458	6.632	23.66	1171	1986
50-131	50	1.000	50	109.00	5.0					26.03	54.656	3.904	23.66	1173	1990
50-132	50	1.000	50	110.00	5.0					25.60	62.464	4.880	23.66	1175	1993
50-133	50	1.000	50	111.00	5.0					27.54	64.416	5.856	23.66	1177	1997
50-134	50	1.000	50	112.00	5.0					26.46	66.368	6.832	23.66	1179	2001
50-135	50	1.000	50	113.00	5.0					27.43	62.464	4.880	23.66	1181	2004
50-136	50	1.000	50	114.00	5.0					26.89	58.560	5.856	23.66	1183	2007
50-137	50	1.000	50	115.00	5.0			0.920	1.191	26.24	68.320	5.856	23.66	1185	2011
50-138	50	1.000	50	116.00	5.0					26.46	76.128	8.784	23.66	1187	2014
50-139	50	1.000	50	117.00	5.0					26.46	70.272	6.832	23.66	1189	2018
50-140	50	1.000	50	118.00	5.0					26.46	70.272	9.608	23.66	1191	2021
50-141	50	1.000	50	119.00	5.0					27.65	62.464	8.784	23.66	1193	2024
50-142	50	1.000	50	120.00	5.0					27.97	74.176	5.856	23.66	1195	2027
50-143	50	1.000	50	121.00	5.0			0.853	1.086	28.30	70.320	4.880	23.66	1197	2031
50-144	50	1.000	50	122.00	5.0					27.65	64.416	6.832	23.66	1199	2034
50-145	50	1.000	50	123.00	5.0					28.62	62.464	5.856	23.66	1201	2037
50-146	50	1.000	50	124.00	5.0					28.62	68.320	5.856	23.66	1202	2040
50-147	50	1.000	50	125.00	5.0					27.00	66.128	6.832	23.66	1204	2043
50-148	50	1.000	50	126.00	5.0			0.863	1.084	28.51	62.464	8.784	23.66	1206	2046
50-149	50	1.000	50	127.00	5.0					27.76	70.272	6.832	23.66	1208	2049
50-150	50	1.000	50	128.00	5.0					28.73	70.272	7.808	23.66	1210	2052
50-151	50	1.000	50	129.00	5.0			0.844	1.063	28.73	64.516	5.856	23.66	1211	2055
50-152	50	1.000	50	130.00	5.0					29.05	80.032	7.808	23.66	1213	2058
50-153	50	1.000	50	131.00	5.0					26.14	60.512	4.880	23.66	1215	2061
50-154	50	1.000	50	132.00	5.0					28.94	68.080	2.928	23.66	1217	2064
50-155	50	1.000	50	133.00	5.0			0.877	1.097	28.30	70.272	5.856	23.66	1218	2067
50-156	50	1.000	50	134.00	5.0					27.22	66.368	5.856	23.66	1220	2070
50-157	50	1.000	50	135.00	5.0					28.94	78.080	0.968	23.66	1222	2072
50-158	50	1.000	50	136.00	5.0					27.65	64.416	6.832	23.66	1223	2075
50-159	50	1.000	50	137.00	5.0					28.94	78.080	6.832	23.66	1225	2078
50-160	50	1.000	50	138.00	5.0					28.08	74.176	4.880	23.66	1226	2081

Test Number	Q Prime	Depth of cut	Feed Rate Vw	Wheel Speed	Width of Cut	Barkhausen Noise Amplitude	Residual Stress σx	Surface Roughness R_a	Surface Roughness R_t	Specific Grinding Energy	Specific Fv	Specific Fh		Temperature Finished Surface	Temperature Contact Surface
	(mm²/s)	(mm)	(mm/s)	(m/s)	(mm)		$E_{(HKL)}$ (Mpa)	(microns)	(microns)	(J/mm³)	(N/mm)	(N/mm)	Peclet No	(C)	(C)
50-161	50	1.000	50	139.00	5.0					29.38	74.176	5.856	23.66	1228	2083
50-162	50	1.000	50	140.00	5.0					28.94	62.464	6.856	23.66	1230	2086
50-163	50	1.000	50	141.00	5.0					28.62	68.320	8.784	23.66	1231	2089
50-164	50	1.000	50	142.00	5.0			0.872	6.786	27.86	60.512	7.808	23.66	1233	2091
50-165	50	1.000	50	143.00	5.0					29.05	80.032	3.904	23.66	1234	2094
50-166	50	1.000	50	144.00	5.0			0.875	5.662	29.38	78.080	6.832	23.66	1236	2097
50-167	34.98	0.636	55	100.00	5.0			1.433	9.492	12.35	21.472	3.904	20.75	253	460
50-168	34.98	0.636	55	100.00	5.0			1.294	9.963	15.13	19.520	5.856	20.75	338	618
50-169	34.98	0.636	55	100.00	5.0			1.166	10.250	17.29	25.376	4.880	20.75	405	741
50-170	34.98	0.636	55	100.00	5.0			1.112	8.808	18.83	31.232	4.880	20.75	453	829
50-171	34.98	0.636	55	100.00	5.0			1.019	6.958	19.76	35.136	5.856	20.75	482	882
50-172	34.98	0.636	55	100.00	5.0			1.133	8.217	19.61	33.184	3.904	20.75	477	873
50-173	34.98	0.636	55	100.00	5.0			1.141	8.565	20.99	35.136	5.856	20.75	520	952
50-174	34.98	0.636	55	100.00	5.0			1.074	10.304	19.30	40.992	3.904	20.75	467	856
50-175	34.98	0.636	55	100.00	5.0			1.133	9.675	19.76	37.088	12.880	20.75	482	882
50-176	34.98	0.636	55	100.00	5.0			1.159	9.377	21.30	34.136	4.880	20.75	529	970
50-177	34.98	0.636	55	100.00	5.0			1.122	8.181	21.30	35.136	5.856	20.75	529	970
50-178	34.98	0.636	55	100.00	5.0			1.115	7.582	20.84	37.088	3.904	20.75	515	943
50-179	34.98	0.636	55	100.00	5.0		-301	1.146	7.623	16.98	39.040	4.880	20.75	396	724
50-180	34.98	0.636	55	100.00	5.0		-283	1.094	7.031	22.08	40.992	2.928	20.75	553	1014
50-181	34.98	0.636	55	100.00	5.0		-288	1.099	7.785	21.92	40.992	2.868	20.75	548	1005
50-182	34.98	0.636	55	100.00	5.0		-153	1.082	7.167	21.46	42.944	2.928	20.75	534	979
50-183	34.98	0.636	55	100.00	5.0					23.16	21.472	3.904	20.75	586	1075
50-184	34.98	0.636	55	100.00	5.0					23.00	48.800	3.904	20.75	582	1067
50-185	34.98	0.636	55	100.00	5.0					23.16	46.850	5.856	20.75	586	1075
50-186	34.98	0.636	55	100.00	5.0					24.39	44.888	6.832	20.75	625	1146
50-187	34.98	0.636	55	100.00	5.0					23.77	44.896	5.856	20.75	606	1111
50-188	34.98	0.636	55	100.00	5.0					23.46	42.944	4.856	20.75	596	1093
50-189	34.98	0.636	55	100.00	5.0					24.70	40.992	4.880	20.75	708	1163
50-190	34.98	0.636	55	100.00	5.0					24.55	37.088	3.128	20.75	703	1155
50-191	34.98	0.636	55	100.00	5.0					24.70	37.088	12.880	20.75	708	1163
50-192	34.98	0.636	55	100.00	5.0			1.081	8.074	23.46	35.136	4.880	20.75	666	1093
50-193	34.98	0.636	55	100.00	5.0					22.23	35.136	1.952	20.75	623	1023
50-194	34.98	0.636	55	100.00	5.0					24.08	46.848	3.904	20.75	687	1128
50-195	34.98	0.636	55	100.00	5.0					23.16	44.896	3.904	20.75	655	1075
50-196	34.98	0.636	55	100.00	5.0					24.70	48.800	4.880	20.75	708	1163
50-197	34.98	0.636	55	100.00	5.0					24.70	40.994	5.856	20.75	708	1163
50-198	34.98	0.636	55	100.00	5.0					23.31	52.704	1.952	20.75	660	1084
50-199	34.98	0.636	55	100.00	5.0					24.85	46.848	2.928	20.75	714	1172
50-200	34.98	0.636	55	100.00	5.0					24.85	42.944	5.856	20.75	714	1172

Test Number	Q Prime	Depth of cut	Feed Rate Vw	Wheel Speed	Width of Cut	Barkhausen Noise Amplitude	Residual Stress σx $E_{(HKL)}$ (Mpa)	Surface Roughness R_a (microns)	Surface Roughness R_t (microns)	Specific Grinding Energy (J/mm³)	Specific Fv (N/mm)	Specific Fh (N/mm)	Peclet No	Temperature Finished Surface (C)	Temperature Contact Surface (C)
	(mm³/s)	(mm)	(mm/s)	(m/s)	(mm)										
50-201	34.98	0.636	55	100.00	5.0			1.025	7.74	22.69	46.860	5.856	20.75	639	1049
50-202	34.98	0.636	55	100.00	5.0			1.034	8.096	22.23	42.944	2.928	20.75	623	1023
50-203	34.98	0.636	55	100.00	5.0					25.16	40.992	6.832	20.75	725	1190
50-204	34.98	0.636	55	100.00	5.0					24.24	39.040	6.832	20.75	692	1137
50-205	34.98	0.636	55	100.00	5.0					25.16	46.848	2.928	20.75	725	1190
50-206	34.98	0.636	55	100.00	5.0					24.39	38.800	3.928	20.75	698	1146
50-207	34.98	0.636	55	100.00	5.0					23.62	50.752	4.880	20.75	671	1102
50-208	34.98	0.636	55	100.00	5.0					24.70	46.848	3.904	20.75	708	1163
50-209	34.98	0.636	55	100.00	5.0					23.00	48.800	4.880	20.75	650	1067
50-210	34.98	0.636	55	100.00	5.0					25.47	48.800	4.880	20.75	735	1207
50-211	34.98	0.636	55	100.00	5.0					23.00	48.800	2.928	20.75	650	1067
50-212	34.98	0.636	55	100.00	5.0			1.045	7.795	25.16	56.608	5.856	20.75	725	1190
50-213	34.98	0.636	55	100.00	5.0					21.46	42.944	5.880	20.75	596	979
50-214	34.98	0.636	55	100.00	5.0					26.09	46.848	5.856	20.75	757	1243
50-215	34.98	0.636	55	100.00	5.0					25.93	48.800	4.880	20.75	751	1234
50-216	34.98	0.636	55	100.00	5.0					25.32	46.848	1.952	20.75	730	1199
50-217	34.98	0.636	55	100.00	5.0					25.47	56.256	3.904	20.75	735	1207
50-218	34.98	0.636	55	100.00	5.0					21.92	46.848	7.808	20.75	612	1005
50-219	34.98	0.636	55	100.00	5.0					26.24	54.456	2.934	20.75	762	1251
50-220	34.98	0.636	55	100.00	5.0					25.93	56.608	3.904	20.75	751	1234
50-221	34.98	0.636	55	100.00	5.0			1.029	7.582	25.63	54.656	5.856	20.75	741	1216
50-222	34.98	0.636	55	100.00	5.0			1.030	7.162	21.77	48.800	5.856	20.75	607	996
50-223	34.98	0.636	55	100.00	5.0					26.86	46.848	4.880	20.75	783	1266
50-224	34.98	0.636	55	100.00	5.0					26.09	56.608	2.928	20.75	757	1243
50-225	34.98	0.636	55	100.00	5.0					25.78	52.704	5.856	20.75	746	1225
50-226	34.98	0.636	55	100.00	5.0					27.02	50.752	3.904	20.75	789	1295
50-227	34.98	0.636	55	100.00	5.0					26.40	50.752	7.808	20.75	767	1260
50-228	34.98	0.636	55	100.00	5.0					25.47	54.664	3.904	20.75	735	1207
50-229	34.98	0.636	55	100.00	5.0					27.02	56.608	5.856	20.75	789	1295
50-230	34.98	0.636	55	100.00	5.0					23.31	44.896	7.796	20.75	660	1084
50-231	34.98	0.636	55	100.00	5.0					27.48	52.704	6.832	20.75	805	1322
50-232	34.98	0.636	55	100.00	5.0					25.78	52.704	3.904	20.75	746	1225
50-233	34.98	0.636	55	100.00	5.0					24.55	50.752	4.880	20.75	703	1155
50-234	34.98	0.636	55	100.00	5.0					19.91	56.608	5.856	20.75	542	891
50-235	34.98	0.636	55	100.00	5.0					25.93	56.608	6.832	20.75	751	1234
50-236	34.98	0.636	55	100.00	5.0					26.24	46.848	3.904	20.75	762	1251
50-237	34.98	0.636	55	100.00	5.0					25.47	54.656	4.880	20.75	735	1207
50-238	34.98	0.636	55	100.00	5.0					26.40	50.752	4.880	20.75	767	1260
50-239	34.98	0.636	55	100.00	5.0					26.55	54.556	2.928	20.75	773	1269
50-240	34.98	0.636	55	100.00	5.0					26.09	50.752	3.904	20.75	757	1243

Test Number	Q Prime (mm²/s)	Depth of cut (mm)	Feed Rate Vw (mm/s)	Wheel Speed (m/s)	Width of Cut (mm)	Barkhausen Noise Amplitude	Residual Stress σx $E_{[HK]}$ (Mpa)	Surface Roughness R_a (microns)	Surface Roughness R_t (microns)	Specific Grinding Energy (J/mm³)	Specific Fv (N/mm)	Specific Fh (N/mm)	Peclet No	Temperature Finished Surface (C)	Temperatur Contact Surface (C)
50-241	34.98	0.636	55	100.00	5.0			1.021	7.34	27.32	54.660	4.896	20.75	800	1313
50-242	34.98	0.636	55	100.00	5.0			1.071	7.08	25.32	52.704	3.904	20.75	730	1199
50-243	34.98	0.636	55	100.00	5.0			1.050	7.27	25.93	54.656	5.856	20.75	751	1234
50-244	32.50	0.500	65	100	3.0		-348			17.65	1.220	0.976	21.75	390	696
50-245	37.50	0.750	50	100	3.0		-369			21.22	13.544	11.712	20.49	626	1036
50-246	70.00	1.000	70	100	3.0		552			19.33	56.608	7.808	33.12	754	1305
50-247	120.00	1.200	100	100	3.0		588			16.76	29.280	6.832	51.83	779	1423
50-248	187.50	1.500	125	100	3.0		1066			15.34	64.320	5.856	72.43	814	1589
50-249	1250.00	10.000	125	100	2.0		1432	1.817	12.237	13.38	442.128	213.940	187.02	1069	3319
50-250	1250.00	10.000	125	100	2.0		2238	1.437	11.129	13.29	262.544	31.062	187.02	1058	3284
50-251	1250.00	10.000	125	146	2.0		456	0.798	9.608	12.58	221.796	17.934	187.02	1047	3250
50-252	1250.00	10.000	125	100	2.0		1233	0.886	6.610	13.21	192.955	101.870	187.02	1047	3251
50-253	1250.00	10.000	125	146	2.0		987	0.771	7.414	12.55	172.752	73.688	187.02	1042	3233
50-254	50.00	0.400	125	100	4.0					9.57	15.555	4.575	37.40	186	318
50-255	200.00	1.600	125	100	4.0					11.87	108.825	9.760	74.81	610	1142
50-256	375.00	3.000	125	100	4.0					9.53	191.235	9.303	102.44	515	1107
50-257	200.00	3.000	66.667	100	4.0					10.99	120.370	6.710	54.63	585	1146
50-258	50.00	3.000	16.667	100	4.0					12.51	62.830	1.970	13.66	453	786
50-259	50.00	0.400	125	100	4.0		-159	1.328	9.503	15.07	176.270	4.270	37.40	378	652
50-260	200.00	1.600	125	100	4.0		1600	1.341	9.163	11.93	129.930	37.515	74.81	615	1152
50-261	375.00	3.000	125	100	4.0		933	1.415	9.413	13.33	220.515	73.353	102.44	942	2026
50-262	200.00	3.000	66.667	100	4.0		1603	1.360	9.313	10.99	127.795	49.715	54.63	585	1146
50-263	50.00	3.000	16.667	100	4.0		-848	1.109	8.013	19.14	52.765	20.435	13.66	835	1449
50-264	5	0.100	50.00	100.00	7.5		-644	5.0		27.13	0.047	8.609	7.48	216	353
50-265	50	1.000	50.00	100.00	7.5		371			23.32	54.456	4.505	23.66	839	1424
50-266	13.8875	0.550	25.25	100.00	7.5		309			30.36	22.623	1.852	8.86	529	933
50-267	200	2.000	100	100.00	7.0		572	2.015	14.261	15.34	100.857	2.397	66.91	967	1564
50-268	20	2.000	10	100.00	7.0		-615	1.756	13.124	17.43	36.471	1.341	6.69	459	692
50-269	10	1.000	10	100.00	7.0		-813	1.774	17.422	32.23	13.953	0.787	4.73	466	912
50-270	100	1.000	100	100.00	7.0		296	1.741	14.808	16.85	70.197	5.414	47.31	649	1154
50-271	82.5	1.500	55	100.00	7.0			1.876	16.200	24.55	80.327	4.719	31.87	1074	1922
50-272	200	2.000	100	100.00	7.0		567	1.926	12.875	15.92	86.093	7.296	66.91	1022	1654
50-273	10	1.000	10	100.00	7.0		-948	1.671	12.718	49.55	21.037	1.481	4.73	981	1472
50-274	100	1.000	100	100.00	7.0		1476	1.861	13.363	18.34	66.067	6.167	47.31	731	1299
50-275	20	2.000	10	100.00	7.0		-417	2.229	14.056	46.73	21.356	1.027	6.69	1507	2273
50-276	200	2.000	100	100.00	7.0			2.936	23.785	21.26	65.746	10.940	66.91		
50-277	20	2.000	10	100.00	7.0			1.656	11.343	40.27	38.718	3.593	6.69	1379	2079
50-278	10	1.000	10	100.00	7.0			1.505	10.172	39.29	17.853	1.638	4.73	821	1231
50-279	100	1.000	100	100.00	7.0			1.534	11.46	22.16	64.219	8.902	47.31	1026	1825
50-280	82.5	1.500	55	100.00	7.0			1.806	13.414	26.76	78.323	9.974	31.87	1301	2328

Test Number	Q Prime	Depth of cut	Feed Rate Vw	Wheel Speed	Width of Cut	Barkhausen Noise Amplitude	Residual Stress σx	Surface Roughness R_a	Surface Roughness R_t	Specific Grinding Energy	Specific Fv	Specific Fh		Temperature Finished Surface	Temperatur Contact Surface
	(mm³/s)	(mm)	(mm/s)	(m/s)	(mm)		$E_{(HKL)}$ (Mpa)	(microns)	(microns)	(J/mm³)	(N/mm)	(N/mm)	Peclet No	(C)	(C)
50-281	200	2.000	100	100.00	7.0			1.974	16.691	21.23	112.186	9.385	66.91	314	2708
50-282	10	1.000	10	100.00	7.0		-840	1.631	11.48	48.71	17.161	2.091	4.73	100	1557
50-283	100	1.000	100	100.00	7.0			2.271	21.284	22.51	62.636	10.028	47.31	1047	1862
50-284	20	2.000	10	100.00	7.0			2.192	16.041	42.63	30.032	3.647	6.69	1469	2215
50-285	30	6.000	5	100.00	7.0			4.89	35.73	39.29	48.264	2.520	5.79	1786	3188
50-286	32.5	6.500	5	100.00	7.0			2.841	22.249	47.63	64.996	3.700	6.03	2320	4184
50-287	55	5.500	10	100.00	7.0			2.671	18.099	33.86	79.260	0.858	11.10	1864	3475
50-288	60	6.000	10	100.00	7.0			3.254	23.636	35.68	84.515	1.180	11.59	2071	3917
50-289	75	5.000	15	100.00	7.0			2.67	20.053	31.32	84.301	2.252	15.87	1861	3558
50-290	90	6.000	15	100.00	7.0			2.412	17.441	30.16	93.739	1.555	17.38	1935	3832
50-291	100	5.000	20	100.00	7.0			1.949	15.672	29.23	99.210	5.309	21.16	1873	3705
50-292	120	6.000	20	100.00	7.0			2.046	15.72	33.69	140.394	3.325	23.18	2386	4914
50-293	25	1.000	25	100.00	7.0		-523	6.046	19.72	25.93	25.955	3.316	11.83	716	1176
50-294	55.5	3.700	15	100.00	7.0		-648	5.046	18.72	28.38	62.850	0.107	13.65	1610	2584
50-295	44.333333	3.800	11.67	100.00	7.0		-179	4.046	17.72	30.31	61.027	0.643	10.76	1418	2539
50-296	40	4.000	10	100.00	7.0		-552	3.046	16.72	27.70	43.974	0.590	9.46	1652	2641
50-297	120	3.000	40.00	100.00	5.0		-195	1.752	14.157	14.91	80.033	5.931	32.78	917	1783
50-298	20	1.000	20.00	100.00	5.0		-526	1.2	1.469	30.67	38.269	4.505	9.46	108	1293
50-299	120	3.000	40.00	100.00	5.0			1.879	15.631	20.41	88.742	3.604	32.78	1392	2705
50-300	50	1.000	50.00	100.00	5.0			1.89	15.341	24.91	75.077	8.961	23.66	910	1543
50-301	250	5.000	50.00	100.00	5.0		481	1.984	13.451	13.08	187.830	0.901	52.90	106	1769
50-302	100	5.000	20.00	100.00	5.0		707	1.458	10.951	32.00	125.228	1.577	21.16	1133	2770
50-303	20	1.000	20.00	100.00	5.0			1.36	12.019	47.14	57.197	6.156	9.46	1390	2091
50-304	250	5.000	50.00	100.00	5.0			1.948	16.786	12.95	322.756	7.863	52.90	763	1748
50-305	250	5.000	50.00	100.00	5.0			1.879	12.374	14.36	116.349	2.853	52.90	895	2051
50-306	100	5.000	20.00	100.00	5.0			1.476	1.917	25.54	77.329	0.751	21.16	863	2112
50-307	250	5.000	50.00	100.00	5.0			1.876	14.106	19.20	161.116	0.450	52.90	1349	3090
50-308	50	1.000	50.00	100.00	5.0			1.777	14.487	25.69	82.735	13.213	23.66	945	1604
50-309	120	3.000	40.00	100.00	5.0			1.507	11.853	22.83	145.199	3.904	32.78	1603	3114
50-310	120	3.000	40.00	100.00	5.0			1.159	8.97	16.81	88.441	7.132	32.78	1083	2105
50-311	20	1.000	20.00	100.00	5.0		-741	0.834	7.043	24.99	40.842	3.979	9.46	85	1015
50-312	20	1.000	20.00	100.00	5.0		-738	0.811	6.272	36.83	36.038	5.931	9.46	975	1589
50-313	120	3.000	40.00	100.00	5.0			1.096	8.574	17.56	95.047	8.333	32.78	1151	2236
50-314	50	1.000	50.00	100.00	5.0			1.285	9.757	26.75	68.321	12.864	23.66	994	1687
50-315	120	3.000	40.00	100.00	5.0			1.206	9.319	17.60	91.993	8.960	32.78	1151	2236
50-316	100	5.000	20.00	100.00	5.0			1.34	11.522	22.86	77.329	0.125	21.16	756	1848
50-317	120	3.000	40.00	100.00	5.0			1.462	11.155	20.68	102.705	7.583	32.78	1415	2748
50-318	50	1.000	50.00	100.00	5.0			1.511	12.56	25.69	25.137	15.766	23.66	945	1604
50-319	100	5.000	20.00	100.00	5.0			1.247	9.399	27.26	105.264	1.126	21.16	938	2294

Appendix G – IN718 Experimental Parameters

Test Number	Q Prime	Depth of cut (mm)	Feed Rate Vw (mm/s)	Wheel Speed (m/s)	Width of Cut (mm)	Residual Stress MU (Mpa) V	Surface Roughness R_a (micron)	Surface Roughness R_t (micron)	Specific Grinding Energy (J/mm^3)	Specific Fn (N/mm)	Specific Ft (N/mm)	Pe	Temperature Finished Surface coolant	Temperature Finished Surface boiling
718-1	13.9	0.55	25.25	75	15	-496	4.3	64	5.80	4.580	1.542	18.457	126	154
718-2	13.9	0.55	25.25	100	15		2.52	31	26.40	2.373	1.091	14.788	471	596
718-3	13.9	0.55	25.25	100	15		3.4	28	24.29	2.796	0.009	14.788	436	550
718-4	13.9	0.55	25.25	50	15		3.51	35.5	22.71	3.292	0.007	15.730	365	446
718-5	13.9	0.55	25.25	50	15		3.25	35	18.48	3.494	0.876	15.730	302	368
718-6	13.9	0.55	25.25	100	15		3.9	28	25.74	16.653	2.968	14.788	460	581
718-7	50.0	1	50.00	100	15	-430	4.5	71	3.70	12.723	2.412	49.282	146	176
718-8	50.0	1	50.00	75	15		4.25	63	11.73	13.974	2.758	42.001	380	456
718-9	5.0	0.1	50.00	50	15	-118	7.1	41	6.97	16.791	2.788	15.584	84	91
718-10	5.0	0.1	50.00	100	15		3.55	45	22.00	1.153	0.436	14.283	224	251
718-11	50.0	1	50.00	50	15		3	39.5	18.37	65.347	11.061	39.485	525	619
718-12	50.0	1	50.00	50	15		2.55	33	19.95	3.093	0.941	37.742	560	658
718-13	5.0	0.1	50.00	100	15		1.98	20.75	23.83	5.924	2.165	14.283	240	269
718-14	5.0	0.1	50.00	50	15		1.92	34.5	24.57	15.876	3.268	14.283	213	234
718-23	7.2	0.4	18	90	15				24.90	10.478	2.310	9.563	317	407
718-24	7.2	0.4	18	60	15				31.40	21.063	4.350	9.563	363	457
718-25	24.0	0.8	30	75	15		1.593	13.257	21.90	43.710	7.706	21.190	493	615
718-26	21.6	1.2	18	90	15		1.528	10.386	27.54	43.173	4.835	14.432	578	780
718-27	24.0	0.8	30	75	15		1.486	10.714	27.75	64.987	7.862	19.639	593	732
718-28	16.8	0.4	42	90	15		1.402	13.061	29.46	39.345	6.505	19.442	528	619
718-29	16.8	0.4	42	60	15		1.462	11.273	31.16	67.190	11.129	20.051	526	612
718-30	24.0	0.8	30	75	15		1.418	11.881	33.87	84.763	10.515	19.459	698	857
718-31	50.4	1.2	42	90	15		1.339	10.59	27.28	136.063	10.907	33.365	816	995
718-32	50.4	1.2	42	60	15		1.373	13.137	26.39	191.050	17.750	33.675	752	907
718-33	24.0	0.8	30	75	15		1.382	11.784	34.54	88.822	9.220	19.459	712	874
718-34	3.0	0.1	30	75	15		1.221	8.527	48.21	13.440	2.578	7.969	323	371
718-35	24.0	0.8	30	75	15		1.266	11.486	42.44	114.942	12.619	19.627	840	1025
718-36	24.00	0.8	30	100	15		1.127	9.006	46.26	93.318	9.228	19.347	943	1159
718-37	24.00	0.8	30	50	15		1.272	9.559	41.25	180.044	19.240	19.627	758	909
718-38	40.00	0.8	50	75	15				35.29	180.218	16.220	32.712	881	1030
718-39	8.00	0.8	10	75	15				68.75	60.812	7.644	6.449	745	1025
718-40	24.00	0.8	30	75	15		1.011	8.395	50.93	160.475	15.329	18.099	979	1187

Test Number	Q Prime	Depth of cut	Feed Rate Vw	Wheel Speed	Width of Cut (mm)	Residual Stress MU (Mpa) V	Surface Roughness R_a (micron)	Surface Roughness R_t (micron)	Specific Grinding Energy (J/mm³)	Specific Fn (N/mm)	Specific Ft (N/mm)	Pe	Temperature Finished Surface coolant	Temperature Finished Surface boiling
		(mm)	(mm/s)	(m/s)			(micron)	(micron)	(J/mm³)	(N/mm)	(N/mm)			
718-41	45.00	1.5	30	75	15		1.154	8.355	43.00	254.972	10.989	24.784	1116	1390
718-42	13.89	0.55	25.25	75	15		0.969	7.756	60.58	103.944	12.771	13.502	876	1065
718-43	13.89	0.55	25.25	75	15		1.1	8.536	61.75	108.960	13.134	13.502	893	1085
718-44	13.89	0.55	25.25	75	15		1.055	9.346	61.46	113.977	13.497	13.502	889	1080
718-45	13.89	0.55	25.25	75	15		1.097	9.463	69.38	113.820	12.561	12.631	989	1198
718-46	5.00	0.1	50	50	15		1.104	10.202	85.15	70.275	12.429	11.573	601	660
718-47	2.63	0.075	35	75	15		1.058	9.381	72.95	24.858	3.985	7.569	416	468
718-48	2.0	0.1	20	100	15		1.059	7.568	79.44	12.243	2.009	4.995	427	510
718-49	1.0	0.05	20	50	15		0.981	7.035	91.67	15.090	2.487	3.757	281	318
718-50	2.63	0.075	35	75	15		0.975	7.118	77.60	24.388	3.785	7.235	429	482
718-51	2.5	0.05	50	100	15		0.94	7.482	74.15	16.245	2.681	8.629	413	455
718-52	2.63	0.075	35	75	15		0.95	7.268	77.60	24.668	3.919	7.235	429	482
718-53	5.00	0.1	50	100	15		1.089	9.287	64.78	30.326	4.265	11.935	552	618
718-54	1.0	0.05	20	100	15		1.053	7.356	87.59	6.707	1.250	3.757	311	362
718-55	2.50	0.05	50	50	15		0.975	7.929	95.33	35.641	7.066	8.439	437	473
718-56	2.00	0.1	20	50	15		0.948	7.759	105.93	29.115	5.486	4.774	475	549
718-57	24.00	0.8	30	100	15		0.982	8.082	63.23	152.985	12.334	17.003	1255	1534
718-58	24.00	0.8	30	145	15		0.93	7.461	63.15	121.839	5.631	17.003	1322	1638
718-59	5.00	0.1	50	100	15		1.045	7.937	70.89	32.489	8.258	11.573	511	566
718-60	5.0	0.1	50	145	15		0.968	8.619	69.67	26.491	1.180	11.488	603	677
718-61	2.50	0.05	50	100	15		1.025	7.988	110.81	19.627	6.167	8.123	558	611
718-62	2.5	0.05	50	145	15		0.952	8.651	72.52	15.873	0.322	8.829	433	482
718-63	2.00	0.1	20	100	15		0.977	7.649	104.91	18.018	6.092	4.595	518	611
718-64	1.0	0.05	20	50	15		0.914	7.461	112.04	18.127	0.965	3.532	329	372
718-65	2.50	0.05	50	100	15		0.965	7.34	88.81	1.609	0.483	8.439	474	522
718-66	1.0	0.05	20	100	15		0.876	7.524	101.85	9.001	1.180	3.532	347	402
718-67	8.00	0.8	10	75	15		0.907	7.293	112.80	92.345	8.958	5.668	1332	1822
718-68	8.00	0.8	10	75	15		0.977	8.962	111.27	121.839	12.334	5.668	1314	1797
718-69	8.00	0.8	10	75	15		0.967	7.871	101.85	32.489	5.631	5.668	1206	1648
718-70	13.75	0.275	50	75	15		0.991	7.265	75.56	108.433	12.017	16.615	990	1113
718-71	12.18	0.3	40.6	75	15		0.932	8.273	78.10	121.839	5.631	14.091	973	1110
718-72	13.79	0.35	39.4	75	15		0.968	7.664	74.89	32.489	8.258	14.770	1010	1161
718-73	21.08	0.9	23.42	75	15		0.922	7.553	74.22	26.491	1.180	14.079	1322	1647
718-74	9.76	1.2	8.13	75	15		0.899	7.649	108.58	19.627	6.167	5.643	1265	1837
718-75	13.23	1.15	11.5	75	15		0.9	6.911	90.72	15.873	0.322	7.815	1264	1737
718-76	8.00	0.8	10	75	15		0.888	8.008	129.10	78.831	10.403	5.668	1347	1843
718-77	8.00	0.8	10	75	15		0.933	8.066	119.42	121.839	5.631	5.668	1248	1707
718-78	8.00	0.8	10	75	15		0.957	6.972	118.91	77.651	11.422	5.668	1243	1700
718-79	1.2	0.03	35	146	15		2.588	18.704	50.76	0.215	0.161	5.864	223	250
718-80	21.0	0.6	35	146	15		2.415	15.778	20.95	15.015	0.375	21.410	496	620

Test Number	Q Prime	Depth of cut (mm)	Feed Rate Vw (mm/s)	Wheel Speed (m/s)	Width of Cut (mm)	Residual Stress MU (Mpa) V	Surface Roughness R_a (micron)	Surface Roughness R_t (micron)	Specific Grinding Energy (J/mm^3)	Specific Fn (N/mm)	Specific Ft (N/mm)	Pe	Temperature Finished Surface coolant	Temperature Finished Surface boiling
718-81	20.0	1	20	146	15	-976	1.913	13.927	45.22	19.634	1.233	13.491	885	1162
718-82	4.0	0.2	20	146	15		1.978	14.725	36.16	9.116	0.483	7.513	345	433
718-83	21.0	0.6	35	146	15		1.877	15.415	25.61	24.775	1.555	20.077	669	828
718-84	33.7	0.6	56.2	146	15	-835	1.372	10.259	25.49	29.280	1.126	31.868	707	838
718-85	21.0	0.6	35	146	15		1.341	9.883	34.24	24.561	1.019	19.736	717	876
718-86	40.8	1.17	35	146	15		1.502	10.8	24.77	38.182	2.306	27.403	735	929
718-87	10.0	0.2	50	146	15				69.26	15.213	0.664	16.278	808	924
718-88	21.0	0.6	35	146	15				15.62	26.062	0.429	22.774	395	483
718-89	8.3	0.6	13.8	146	15		1.268	9.264	45.55	15.337	0.214	7.776	581	785
718-90	23.8	0.69	34.397273	146	15		0.894121508	6.966354749	28.70	25.419	0.322	21.195	689	862
718-91	24.7	0.714	34.524091	146	15		0.75925419	6.047374302	28.62	49.443	0.429	21.604	699	875
718-92	312.50	2.5	125	100	3	-388	1.746	16.619	11.29	175.680	14.640	166.023	494	565
718-93	375.00	3	125	100	3				14.52	133.387	14.640	170.977	610	695
718-94	437.50	3.5	125	100	3				18.65	702.720	17.893	176.524	746	847
718-95	500.00	4	125	100	3				23.50	852.373	100.853	181.299	869	977
718-96	200	2	100	100.00	7		4.891	34.77	13.40	164.311	6.167	104.732	602	695
718-97	20	2	10	100.00	7		4.671	29.808	90.55	95.991	9.331	8.961	1608	2394
718-98	10	1	10	100.00	7		3.87	24.012	111.96	63.065	4.773	6.337	1384	1956
718-99	100	1	100	100.00	7		2.591	17.345	28.99	201.529	2.467	63.367	1052	1181
718-100	82.5	1.5	55	100.00	7	244	2.934	25.327	37.86	181.579	5.684	42.684	1292	1531
718-101	200	2	100	100.00	7	427	2.51	19.079	22.71	306.636	1.394	89.614	945	1073
718-102	10	1	10	100.00	7	-1410	2.823	24.875	110.39	58.131	0.376	6.337	1365	1929
718-103	100	1	100	100.00	7	658	2.239	15.48	35.32	234.883	6.489	63.367	1276	1434
718-104	20	2	10	100.00	7	-802	3.015	26.21	63.84	116.155	1.609	8.961	1141	1695
718-105	200	2	100	100.00	7		4.89	35.73	13.20	163.453	5.470	104.732	176	685
718-106	20	2	10	100.00	7		2.841	22.249	62.86	61.243	5.684	13.939	172	2158
718-107	10	1	10	100.00	7		2.671	18.099	62.86	28.851	2.359	9.856	143	1469
718-108	100	1	100	100.00	7		3.254	23.636	30.68	220.404	9.706	63.367	371	1249
718-109	82.5	1.5	55	100.00	7	565	2.67	20.053	43.48	201.099	6.703	42.684	386	1755
718-110	200	2	100	100.00	7	618	2.412	17.441	22.65	360.798	0.054	89.614	296	1070
718-111	10	1	10	100.00	7	-1241	1.949	15.672	81.71	42.291	9.277	9.856	178	1902
718-112	100	1	100	100.00	7	63	2.046	15.72	31.43	304.383	18.608	63.367	380	1278
718-113	20	2	10	100.00	7	-747	3.269	20.721	78.77	111.035	0.965	8.961	215	2086

Appendix H – Thermal Modelling Procedure

Initially the contact length can be calculated using:

$$l_c = \sqrt{D_e a_e} \qquad \text{Eqn. H.1}$$

Where:

D_c	Effective Diameter of Grinding Wheel
a_c	Depth of Cut

Also the thermal constants can be calculated.

The thermal diffusivity of the material is calculated using:

$$\alpha = \frac{k}{\rho c} \qquad \text{Eqn. H.2}$$

Where:

k	Thermal Conductivity
ρ	Density
c	Specific Heat Capacity

The mean thermal property is calculated using:

$$\beta = \sqrt{k \rho c} \qquad \text{Eqn. H.3}$$

Where:

k	Thermal Conductivity
ρ	Density
c	Specific Heat Capacity

The Peclet Number is a dimensionless value given by:

$$P_e = \frac{v_w l_c}{4\alpha} \qquad \text{Eqn. H.4}$$

Where:

α	Thermal Diffusivity
v_w	Feed Rate
l_c	Contact Length

The grinding angle phi in radians is calculated by:

$$\phi = \sin^{-1}\left(\frac{a_e}{l_c}\right) \qquad \text{Eqn. H.5}$$

Where:

a_c	Depth of Cut
l_c	Contact Length

Using the net spindle power the total heat flux in the system is calculated by:

$$q_t = \frac{W}{l_c b} \qquad \text{Eqn. H.6}$$

Where:

W	Spindle Power
l_c	Contact Length
b	Breadth of Cut

The heat flux going in to the workpiece, wheel, chip and fluid are given by:

$$q_w = h_w T_{\max} \qquad \text{Eqn. H.7}$$

$$q_s = h_s T_{\max} \qquad \text{Eqn. H.8}$$

$$q_c = h_c T_{\max} \qquad \text{Eqn. H.9}$$

$$q_f = h_f T_{\max} \qquad \text{Eqn. H.10}$$

Where:

q	Heat Flux
h	Heat Convection Factor
T_{max}	Maximum Contact Surface Temperature

Subscripts	Contact Length
w	workpiece
f	fluid
c	chip
s	wheel

The convection factor for the work piece can be calculated by:

$$h_w = \frac{\beta_w}{c}\sqrt{\frac{v_w}{l_c}} \qquad \text{Eqn. H.11}$$

Where:

β	Mean Thermal Property
c	Specific Heat Capacity
v_w	Feed Rate
l_c	Contact Length

The maximum contact temperature based upon Jaegers sliding heat source is given by:

$$T_{\max} = C\frac{q_w}{\beta_w}\sqrt{\frac{l_c}{v_w}} \qquad \text{Eqn. H.12}$$

Where:

C	the Conduction / Convection factor
q_w	Heat Flux Entering Workpiece
β	Mean Thermal Property
l_c	Contact Length
v_w	Feed Rate

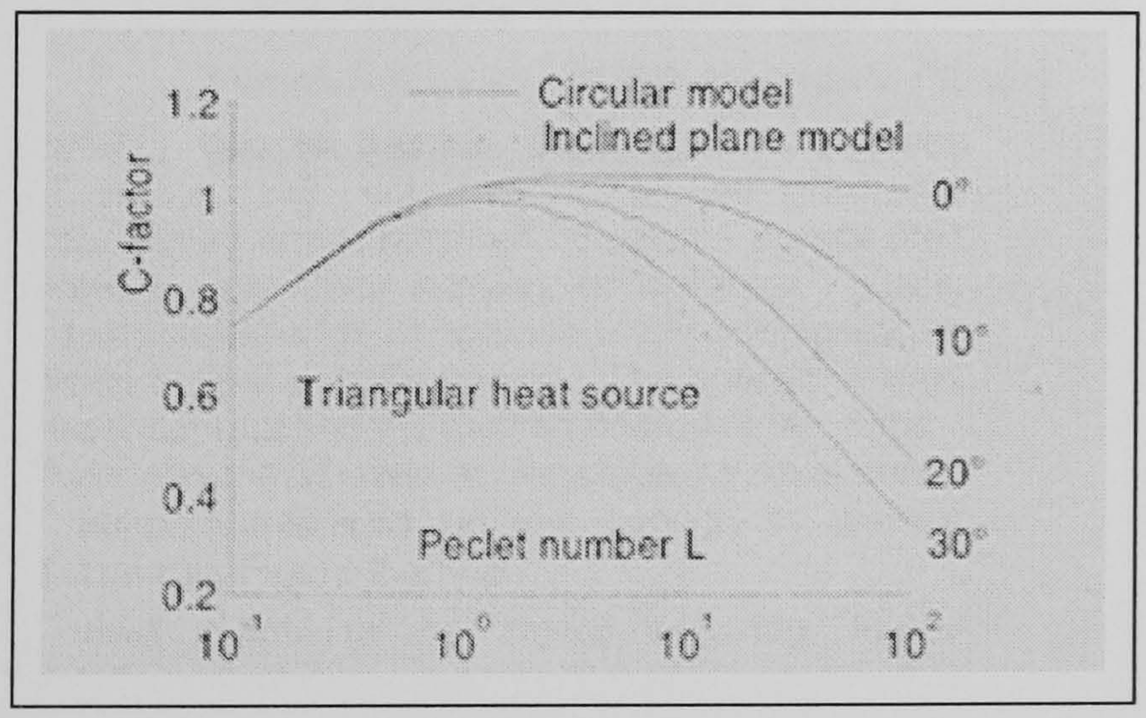

Figure H.1: C Co-efficient Diagram

The value of C can be taken from Figure H.1 by cross referring the values of Peclet Number and grinding angle phi.

Hahn's model for the percentage heat flux entering both the workpiece and the wheel is given by:

$$R_{ws} = \frac{q_w}{q_{ws}} = \frac{q_w}{q_w + q_s} = \frac{h_w}{h_w + h_s} = \left[1 + \frac{0.97 k_g}{\beta_w \sqrt{r_o v_s}}\right] \qquad \text{Eqn. H.13}$$

Where:

qw	Heat Flux Entering Workpiece
qs	Heat Flux Entering Wheel
hw	Convection Factor for heat flux entering Workpiece
hs	Convection Factor for heat flux entering Wheel
kg	Thermal Conductivity of grit
βw	Mean Thermal Property for Workpiece
ro	Radius of grit
vs	Wheel Speed

The convection factor for the heat entering the wheel is given by:

$$h_s = h_w \left[\frac{1}{R_{ws}} - 1\right] \qquad \text{Eqn. H.14}$$

Where:

Rws	Percentage of Heat Flux entering both Workpiece and Wheel
hw	Convection Factor for heat flux entering Workpiece
hs	Convection Factor for heat flux entering Wheel
qs	Heat Flux Entering Wheel

Values for the flux entering the chip h_c were published by Malkin (1989) to be close to the melting point of the workpiece material. For ferrous metals this is quoted by Malkin (1984) as being 13J/mm^3. For other materials the value of h_c is calculated using Equation H.9, with initially calculating q_{ch} given by:

$$q_{ch} = e_{ch}\frac{a_e v_w}{l_c} \qquad \text{Eqn. H.15}$$

Where:

ech	Energy within Chip
ae	Depth of Cut
vw	Feed Rate
lc	Contact Length

The fluid convection factor has been experimentally obtained by Rowe (2001) for various fluid types. In general the value for water based fluids is 290,000W/m^{2}K, for oil fluids the general value is 23,000W/m^{2}K.

It should be remembered that heat convection from the contact zone will only occur by the fluid before the boiling temperature of the coolant is exceeded, after which there will be no cooling affect when $q_f = 0$.

Therefore before fluid boiling the heat removed by the fluid is given by:

$$q_f = h_f T_{\max} \qquad \text{Eqn. H.16}$$

Therefore two values of T_{max} can be calculated, one with coolant and one with no coolant. It can be seen that the T_{max} value with coolant would be the value before the onset of burn and vice versa.

The value of T_{max} with the effects of coolant is given by:

$$T_{\max} = \frac{q_t - h_{ch}T_{mp}}{\frac{h_w}{R_{ws}} + h_f} \qquad \text{Eqn. H.17}$$

The value of Tmax with no effects of coolant is given by:

$$T_{\max} = \frac{q_t - h_{ch} T_{mp}}{\frac{h_w}{R_{ws}}} \qquad \text{Eqn. H.18}$$

Where:

Tmax	Maximum Finished Surface Temperature
qt	Total Heat Flux
hch	Convection Factor for heat flux entering Chip
Tmp	Melting Temperature of Workpiece Material
hw	Convection Factor for heat flux entering Workpiece
Rws	Percentage of Heat Flux entering both Workpiece and Wheel

As stated in Rowe & Jin (2001) the fluid conduction/convection factor is related to the mean contact surface temperature. The threshold at the boiling point of the fluid or when the fluid burns out is $T_{mean} = T_{boil}$ and the finished surface temperatures rise sharply. Therefore $T_{mean} = 0.667T_{max}$.

Rowe & Jin (2001) published Figure H.2 which shows the relationship between the ratio T_{fin}/T_{max}, the Peclet Number and grind angle phi. This figure gives the maximum finished surface temperature as a fraction of the maximum contact surface temperature for various values of phi and Peclet Number.

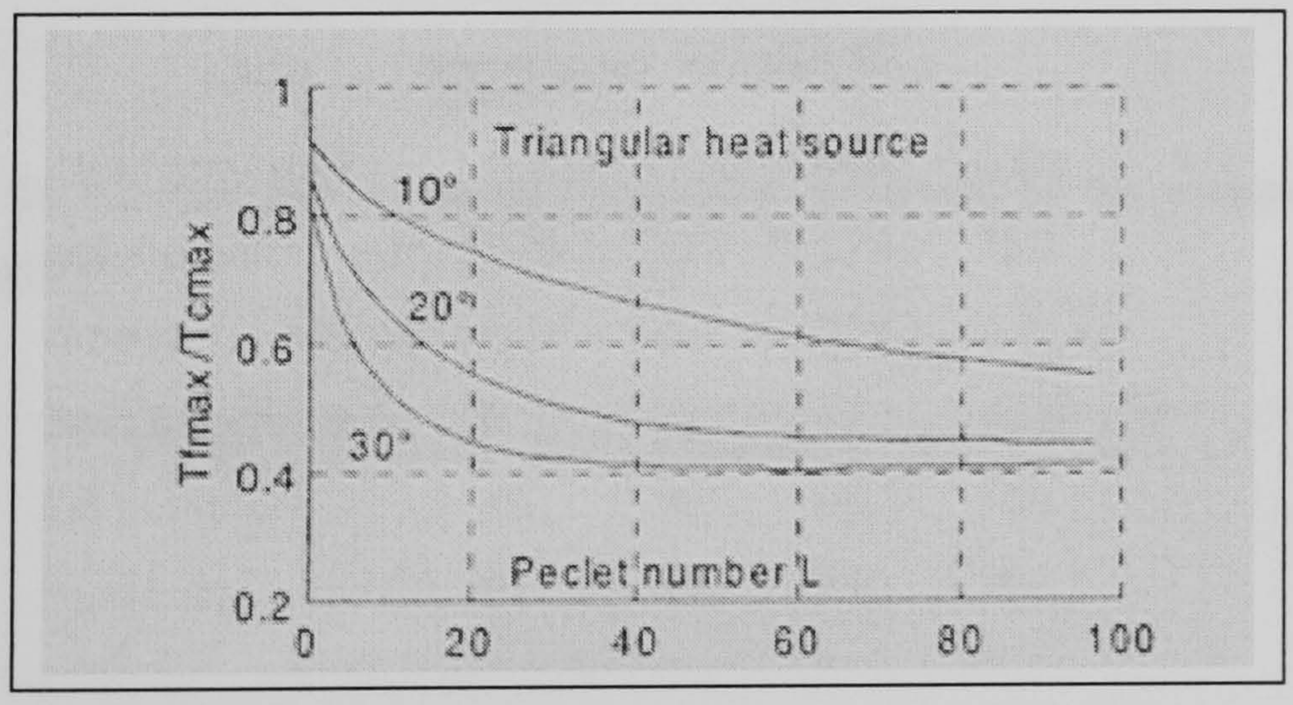

Figure H.2: Relationship of T_{fin}/ T_{max}, Peclet Number and phi.

α	Thermal Diffusivity for M50 Steel	$7.47 \times 10^{-6} m^2/s$
y	Depth of Damaged Layer	$0.09 \times 10^{-3} m$
D	Diameter of Wheel	0.2m
a	Depth of Cut	$0.03 \times 10^{-3} m$
V	Feedrate	0.125m/s
t	Temperature at which Martensite begins to form	800°C
l	Contact Length	0.024m
T	the time constant or the time in which the heat source is concentrated above each part of the sample surface	$T := \frac{l}{v}$ 0.196/s
z	the terms which are proportional the temperature change	$z := \frac{y}{2 \cdot \sqrt{\alpha \cdot T}}$

The main temperature response is equated to initiation temperature divided by 1 minus the Gaussian error function (erf) of z.

$$\frac{t}{1 - erf(z)} = 835.029°C$$

Therefore for this example the actual temperature witnessed by the workpiece surface would be 835°C

Figure H.3: Heat Transfer Equation Worked Example

Appendix I – Bearing Manufacture

APPENDIX I

Test Number	Wheel Speed (m/s)	Q Prime (mm^2/s)	Depth Of Cut (mm)	Feed Rate (mm/s)	Barklhausen Noise Amplitude	Residual Stress σx $E_{\{HKL\}}$ (Mpa)	Surface Roughness R_a (microns)	Surface Roughness R_t (microns)	Specific Grinding Power (W/mm)	Specific Grinding Energy (J/mm^3)
50-58	30.00	1	4.000	0.25	57		2.004	16.209	11.24	11.24
50-59	30.00	20	4.000	5.00	58		1.42	15.705	113.76	5.69
50-60	30.00	50	4.000	12.50	53		1.585	12.785	46.07	0.92
50-61	30.00	100	4.000	25.00	52		1.552	15.316	242.70	2.43
50-62		1	4.000	0.25	52		1.406	9.802	188.20	188.20
50-63	146.00	20	4.000	5.00	62		0.949	8.025	174.16	8.71
50-64	146.00	50	4.000	12.50	57		0.921	7.117	316.85	6.34
50-65		100	4.000	25.00	61		0.862	6.079		
50-66	146.00	25	4.000	6.25	n/a	-1163	0.785	5.937	193.26	7.73
50-67	146.00	25	4.000	6.25	57		1.058	8.673	93.26	3.73
50-68	146.00	25	4.000	6.25	61		0.953	8.517	207.30	8.29
50-69	146.00	25	4.000	6.25	65		0.856	6.835	230.34	9.21
50-70	146.00	25	4.000	6.25	65		0.808	6.212	136.80	5.47
50-71	146.00	25	4.000	6.25	62		0.864	6.705	254.78	10.19
50-72	146.00	25	4.000	6.25	65		0.793	6.098	325.28	13.01
50-73	146.00	25	4.000	6.25	n/a	-1127	0.794	6.434	198.03	7.92
50-74	146.00	10	4.000	2.50	n/a	-1009	0.858	6.884	190.73	19.07
50-75	146.00	10	4.000	2.50	58		0.804	6.775	156.46	15.65
50-76	146.00	10	4.000	2.50	62		0.750	6.545	238.48	23.85
50-77	146.00	10	4.000	2.50	n/a	-1118	0.774	6.395	171.91	17.19
50-78	146.00	10	4.000	2.50	72		0.754	5.863	171.91	17.19
50-79	146.00	10	4.000	2.50	65		0.756	5.688	172.19	17.22
50-80	146.00	10	4.000	2.50	64		0.772	6.142	203.37	20.34
50-81	146.00	10	4.000	2.50	65		0.727	5.730	171.91	17.19
50-82	146.00	20	4.000	5.00	49		1.734	12.952	105.34	5.27
50-83	146.00	20	4.000	5.00	52		1.257	8.600	169.38	8.47
50-84	146.00	20	4.000	5.00	52		1.247	9.213	177.25	8.86
50-85	146.00	20	4.000	5.00	51		1.202	9.257	183.43	9.17
50-86	146.00	10	4.000	2.50	50		1.312	8.603	53.93	5.39
50-87	146.00	10	4.000	2.50	52		1.296	10.23	142.13	14.21
50-88	146.00	10	4.000	2.50	53		1.282	10.009	158.71	15.87
50-89	146.00	10	4.000	2.50	54		1.214	8.326	142.13	14.21

Table I.1: Results from Experimental Stage

	Tests	Initial Dia (mm)	Half Wear (mm)	Total Wear (mm)	Final Dia (mm)	Intial Vol (mm^3)	Final Vol (mm^3)	Difference (mm^3)	Material removed (mm^3)	G-Ratio
Wheel 1	After range of Q's (1, 10, 25 ,100) x2	200	0.038	0.076	199.924	1571428.57	1570234.51	1194.06	6504	5.45
	After above and 8xQ10 and 8xQ25	200	0.086	0.172	199.828	1571428.57	1568726.88	2701.69	19512	7.22
	After only 8xQ10 and 8xQ25	200	0.048	0.096	199.904	1571428.57	1569920.36	1508.21	13008	8.62
Wheel 2	After 4 x Q25	200	0.01	0.02	199.98	1571428.57	1571114.30	314.27	3252	10.35
	After 4 x Q25 and 4 x Q10	200	0.014	0.028	199.972	1571428.57	1570988.60	439.97	6504	14.78
	After 4 x Q10	200	0.004	0.008	199.992	1571428.57	1571302.86	125.71	3252	25.87

Table I.2: Wheel Wear and G-Ratio Figures

Appendix J – Fir Tree Root Manufacture

Test Number	Roughing of Finishing	Ra	Rt	Material Removed (mm^3)	Finishing Material Removed (mm^3)	Wheel Material Removed (mm^3)	Max Q Prime ($mm^3/mm.s$)	Mean Q Prime ($mm^3/mm.s$)	Feed Rate Vw (mm/min)	Wheel Speed Vc (m/s)	Wheel dia D (m)	Specific Grinding Power (W/mm)	Mean Specific Grinding Energy (J/mm^3)	Normal Force Fz (N)
002-11	1R	0.886	7.694	1430.246	1430		5.85	3.38	45	130	0.27			429.44
002-12	1R			1430.246	2860									
002-13	2R	0.853	7.161	1254.396	4115		11.70	6.75	90	129	0.27			429.44
002-14	2R	0.678	5.006	1254.396	5369		15.60	9.00	120	130	0.27	634.89	70.5	429.44
002-15	2R	0.637	5.121	1254.396	6624		32.50	18.75	250	130	0.27	1020.60	54.4	546.56
002-16	2R	0.605	5.365	1254.396	7878		65.00	37.50	500	130	0.27	1306.03	34.8	741.36
002-17	2R			1254.396	9132		97.50	56.25	750	130	0.27	1486.03	26.4	858.88
002-18	2R			1254.396	10387		97.50	56.25	750	130	0.27	1627.46	28.9	917.44
002-19	2F	0.09	1.122	23.44666		23.45	0.63	0.63	750	100	0.20	15.43	24.7	204.96
002-20	2R			1254.396	11641		65.00	37.50	500	130	0.27	1547.74	41.3	839.84
002-21	2F			23.44666		46.89	0.42	0.42	500	100	0.20	2.57	6.2	107.84
002-22	2R			1254.396	1254		97.50	56.25	750	130	0.27	1522.03	27.1	1005.28
002-23	2F-1			23.44666		70.34	0.63	0.63	750	100	0.20	23.14	37.0	204.96
002-24	2F-2			23.44666		93.79	0.63	0.63	750	100	0.20	25.71	41.1	156.16
002-25	2F-3	0.087	0.785	23.44666		117.23	0.63	0.63	750	100	0.20	131.14	209.8	185.44

Table J.1: Results from Wheel #1

Test Number	Roughing of Finishing	Ra	Rt	Material Removed (mm^3)	Finishing Material Removed (mm^3)	Wheel Material Removed (mm^3)	Max Q Prime ($mm^3/mm.s$)	Mean Q Prime ($mm^3/mm.s$)	Feed Rate Vw (mm/min)	Wheel Speed Vc (m/s)	Wheel dia D (m)	Specific Grinding Power (W/mm)	Mean Specific Grinding Energy (J/mm^3)	Normal Force Fz (N)
002-01	Rough			375	375		16.67	16.67	1000	39	0.2	501.48	30.1	380.64
002-02	Rough			1500	1875		100.00	100.00	1500	100	0.2	2026.8	20.3	2069.12
002-03	Rough			750	2625		50.00	50.00	1500	146	0.2	1517.4	30.3	1776.32
002-04	Rough			375	3000		16.67	16.67	1000	39	0.2	300.6	18.0	302.56
002-05	Finish	0.834	6.191	23.45		23	0.83	0.83	1000	39	0.2	36	43.2	19.52
002-06	Rough			750	3750		50.00	50.00	1500	100	0.2	873	17.5	575.84
002-07	Finish	0.833	5.898	23.45		47	1.25	1.25	1500	100	0.2	30.6	24.5	78.08
002-08	Rough			750	4500		50.00	50.00	1500	146	0.2	1476	29.5	556.32
002-09	Finish	0.897	5.912	23.45		70	1.25	1.25	1500	146	0.2	39.6	31.7	65.72

Table J.2:Results from Flat Cuts

Test Number	Roughing of Finishing	Ra	Rt	Material Removed (mm^3)	Finishing Material Removed (mm^3)	Wheel Material Removed (mm^2)	Max Q Prime ($mm^3/mm.s$)	Mean Q Prime ($mm^3/mm.s$)	Feed Rate Vw (mm/min)	Wheel Speed Vc (m/s)	Wheel dia D (m)	Specific Grinding Power (W/mm)	Mean Specific Grinding Energy (J/mm^3)	Normal Force Fz (N)
002-26	1R	0.583	4.417	1430.246	1430		97.50	56.25	750	130	0.27	1773.77	31.5	458.72
002-27	2R			1254.396	2685		97.50	56.25	750	130	0.27	1470.60	26.1	507.52
002-28	2F			23.45		23.45	0.63	0.63	750	100	0.20	50.40	80.6	117.12
002-29	2F			23.45		46.89	0.63	0.63	750	100	0.20	44.36	71.0	87.84
002-30	2F	0.299	2.526	23.45		70.34	0.63	0.63	750	100	0.20	46.29	74.1	97.8
002-31	1R	0.565	4.335	1430.246	4115		52.00	30.00	400	130	0.27	1415.31	47.2	390.4
002-32	1R			1430.246	5545		52.00	30.00	400	130	0.27	443.31	14.8	1
002-33	1F	0.673	4.748	23.45		93.79	0.33	0.33	400	100	0.20	0.33	1.0	83.84
002-34	2R			1254.396	6800		52.00	30.00	400	130	0.27	815.14	27.2	253.76
002-35	2F	0.752	6.476	23.45		117.23	0.33	0.33	400	100	0.20	0.77	2.3	102.4
002-36	1R			1430.246	8230		52.00	30.00	400	130	0.27	920.57	30.7	273.28
002-37	1F	0.802	6.786	23.45		140.68	0.33	0.33	400	100	0.20	53.49	160.5	141.44
002-38	2R			1254.396	9484		52.00	30.00	400	130	0.27	933.43	31.1	409.92
002-39	2F	0.693	6.951	23.45		164.13	0.33	0.33	400	100	0.20	41.91	125.7	141.44
002-40	1R			1430.246	10914		52.00	30.00	400	130	0.27	973.54	32.5	390.4
002-41	1F	0.739	5.673	23.45		187.57	0.33	0.33	400	100	0.20	106.46	319.4	151.2
002-42	2R			1254.396	12169		52.00	30.00	400	130	0.27	1044.51	34.8	351.36
002-43	2F	0.791	6.254	23.45		211.02	0.33	0.33	400	100	0.20	106.46	319.4	141.44
002-44	2R			1430.246	13599		130.00	75.00	1000	130	0.27	1710.00	22.8	351.36
002-45	2F	0.774	5.503	23.45		234.47	0.83	0.83	1000	100	0.20	141.43	169.7	141.44

Table J.3:Results from Wheel #2

Test Number	Roughing of Finishing	Ra	Rt	Material Removed (mm^3)	Finishing Material Removed (mm^3)	Wheel Material Removed (mm^3)	Max Q Prime ($mm^3/mm.s$)	Mean Q Prime ($mm^3/mm.s$)	Feed Rate Vw (mm/min)	Wheel Speed Vc (m/s)	Wheel dia D (m)	Specific Grinding Power (W/mm)	Mean Specific Grinding Energy (J/mm^3)	Normal Force Fz (N)
002-46	1R			1430.246	1430		52.00	30.00	400	196.4	0.27	649.29	21.6	390.4
002-47	1F	0.749	4.478	23.45		23.45	0.33	0.33	400	145.5	0.20	208.80	626.4	151.2
002-48	2R			1254.396	2685		52.00	30.00	400	196.4	0.27	636.43	21.2	390.4
002-49	2F	0.694	5.215	23.45		46.89	0.33	0.33	400	145.5	0.20	313.20	939.6	151.2
002-50	2R			1430.25	4115		130.00	75.00	1000	146	0.27	1362.86	18.2	497.76
002-51	2F	0.604	4.754	23.45		70.34	0.83	0.83	1000	108	0.20	52.20	62.6	195.2
002-52	2R			1254.40	5369		130.00	75.00	1000	146	0.27	1886.91	25.2	497.76
002-53	2F	0.118	1.563	23.45		93.79	0.83	0.83	1000	108	0.20	159.94	191.9	195.88
002-54	2R			1430.25	6800		130.00	75.00	1000	146	0.27	1834.46	24.5	858.88
002-55	2F	0.125	1.485	23.45		117.23	0.83	0.83	1000	108	0.20	55.03	66.0	263.52
002-56	2R			1254.40	8054		130.00	75.00	1000	146	0.27	1886.91	25.2	858.88
002-57	2F	0.112	1.554	23.45		140.68	0.83	0.83	1000	108	0.20	213.43	256.1	244
002-58	2R			1430.25	9484		130.00	75.00	1000	146	0.27	1886.91	25.2	927.6
002-59	2F1			23.45		164.13	0.83	0.83	1000	108	0.20	156.86	188.2	214.72
002-60	2F2			23.45	9508	187.57	0.83	0.83	1000	146	0.27	208.80	250.6	253.76
002-61	2F3	0.111	0.865	23.45		211.02	0.83	0.83	1000	108	0.20	208.80	250.6	224.48
002-62	2R			1254.40	10762		130.00	75.00	1000	146	0.27	1835.49	24.5	1015.04
002-63	2F1			23.45		234.47	0.83	0.83	1000	108	0.20	264.86	317.8	214.72
002-64	2F2			23.45		257.91	0.83	0.83	1000	146	0.27	264.86	317.8	185.44
002-65	2F3	0.12	0.875	23.45		281.36	0.83	0.83	1000	108	0.20	277.71	333.3	165.92

Table J.4:Results from Wheel #3

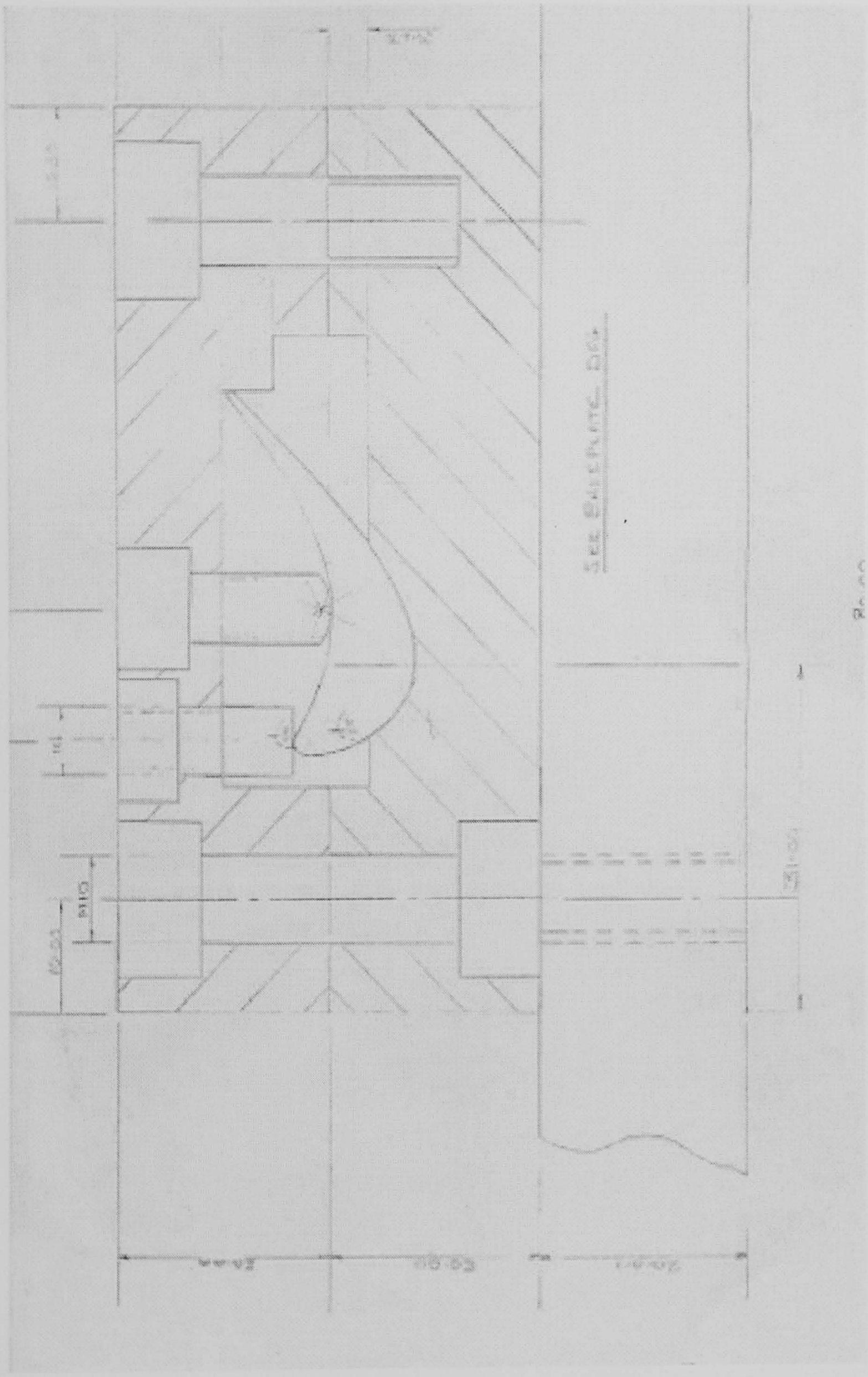

Figure J.1:Front Elevation

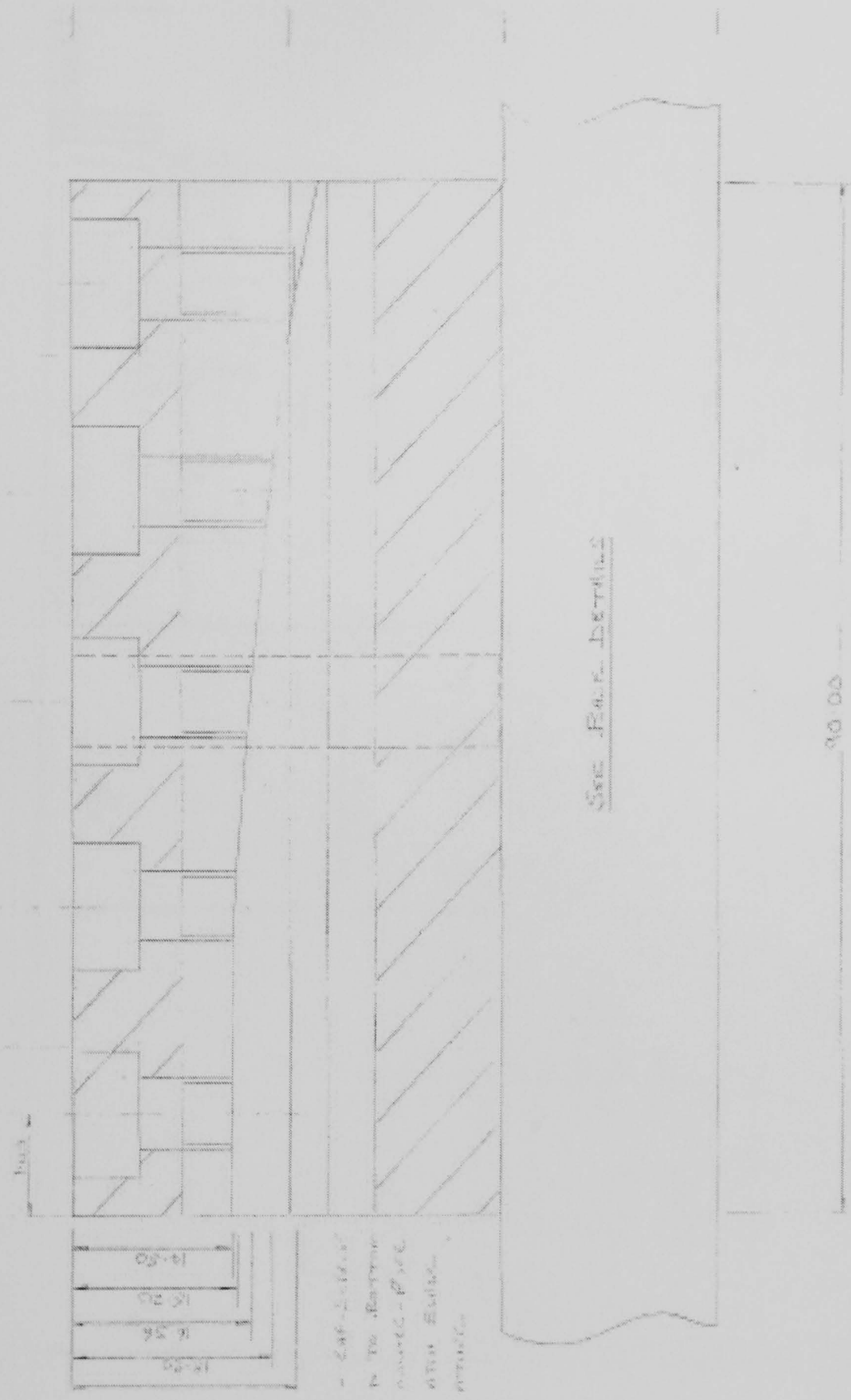

Figure J.2:Side Elevation of Fixture

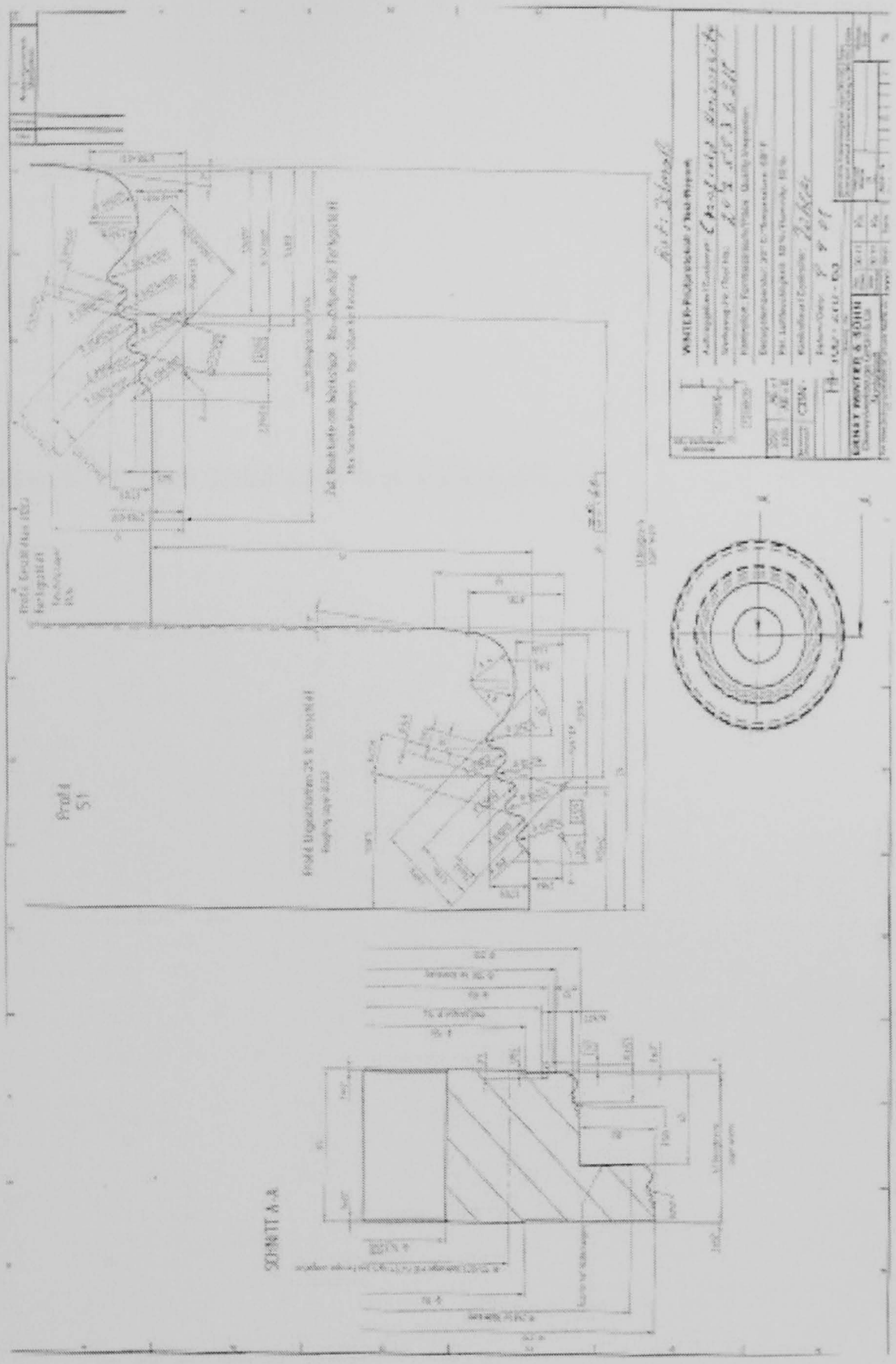

Figure J.3: Wheel Profile

Appendix K – Minton, Treharne & Davies Limited Report

Our ref: x 1299

Order Number: 5000056238

Manufacturing Technology
Rolls-Royce
PO Box 3
Filton
Bristol
BS35 7QE

MTD

MINTON,
TREHARNE &
DAVIES LIMITED
Consulting Scientists,
Mariners & Engineers
Analytical & Testing
Laboratories
Public Analysts

For the attention of Mr. John Sullivan EW4 - 14.

4th April 2001.

METALLOGRAPHIC COMPARISON OF SURFACES PRODUCED BY CBN AND VIPER GRINDING

1. SUMMARY

The roots of two blades in Mar M002 material were finished by grinding. One was ground on both sides using Viper grinding technology and the other was ground using a wheel impregnated by CBN particles. They were submitted to MTD for metallographic assessment of the surface condition and comparison to CME 5043. This report details the results of this investigation where it appeared that both techniques comfortably satisfied CME 5043.

2. CONCLUSIONS

2.1. Both techniques were acceptable to CME 5043 subject to the provisos detailed in the report.

2.2. The work hardening effect of the Viper grinding was estimated by metallographic examination to be approximately 5pm.

2.3. The work hardening effect of CBN grinding was estimated by metallographic examination to be approximately 10~tm.

2.4. There were indications that the CBN grinding resulted in a cleaner cut than the Viper grinding.

3. RECOMMENDATIONS

3.1. The actual values for the hardening must be obtained by X ray Diffraction Techniques. Scanning electron microscope can only give the depth but more accurately than metallographic techniques.

K.C.Moloney

Minton, Treharne and Davies Ltd

4. EXAMINATION

The blade aerofoil was removed from each blade. The root was cut in half vertically. One half was kept for Electron Diffraction techniques to obtain the true depth of hardening. The other halves were placed on their bottom faces, mounted together one mount and then polished back to the base of the first groove. (This then enabled a measurement to be taken at right angles to the grinding surface). The samples were prepared for metallographic examination using colloidal silica for final polish.

The sections were examined in the unetched condition.

Figure 1 shows some features that were witnessed on the Viper ground surface. There were four instances of "smearing" or surface drag along the face. The depth 2Ftm and the length was 100~tm. The debris at the end of the cut was measured at 15pm. Plucking was measured at 4l.tm.

Figure 2 shows typical feature seen on the CBN ground surface. Plucking to a depth of 4 pin was seen together with some small laps at a "height" of 5pm.

Figure 3 shows typical features of the Viper ground surface in the etched condition. The depth of the visually disturbed layer was estimated at 5pm.

Figure 4 details some typical features of the CBN ground surface. The depth of visual disturbed layer was estimated at lOμm.

5.DISCUSSION

Both samples appeared to be comfortably within the levels set in appendix 1 of CME 5043. There are two provisos. Firstly, the surfaces were not examined for "black" spot defects because this entails macro etching. This will interfere with the depth of strained lattice values to be accomplished by Electron Diffraction techniques. Secondly, an in-depth microhardness traverse of the surface was not possible because of the very segregated nature of the microstructure. It was attempted but the results were unsatisfactory and are not included in the report.

The defects seen on the surface were usually associated with the various phases seen in the material. This was exemplified by the smearing or surface drag defect that appeared to be associated with the large gamma prime particles.

Minton, Treharne and Davies Ltd

This was only seen in the Viper ground specimens. This may indicate that the CBN grinding may give a cleaner cut than the Viper grinding.

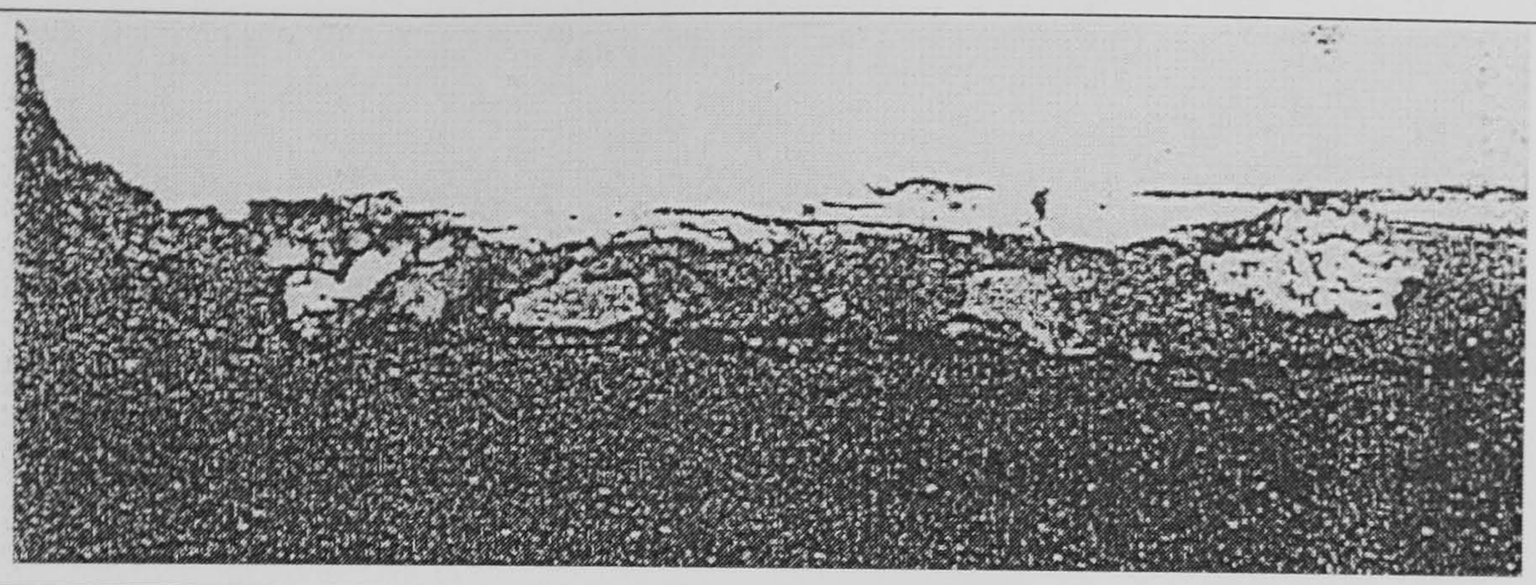

Debris at end of Cut

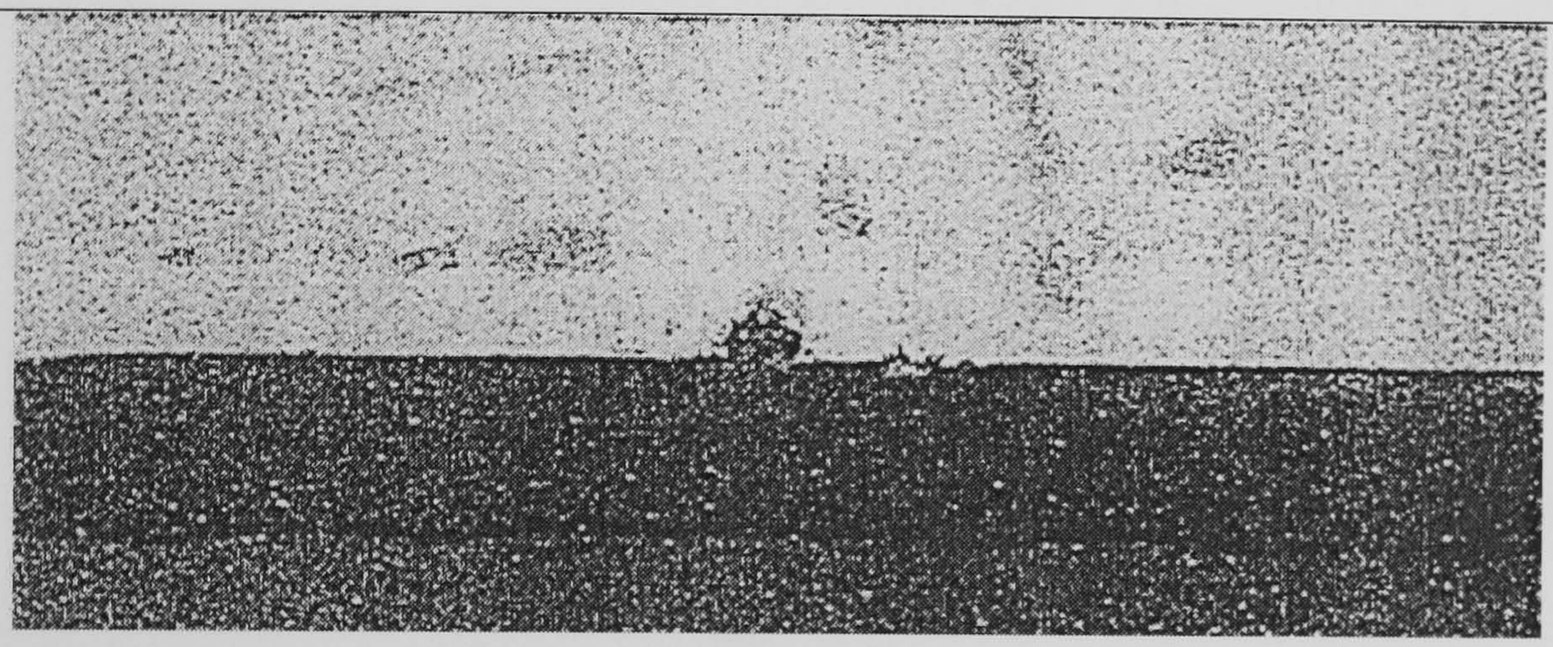

Plucking

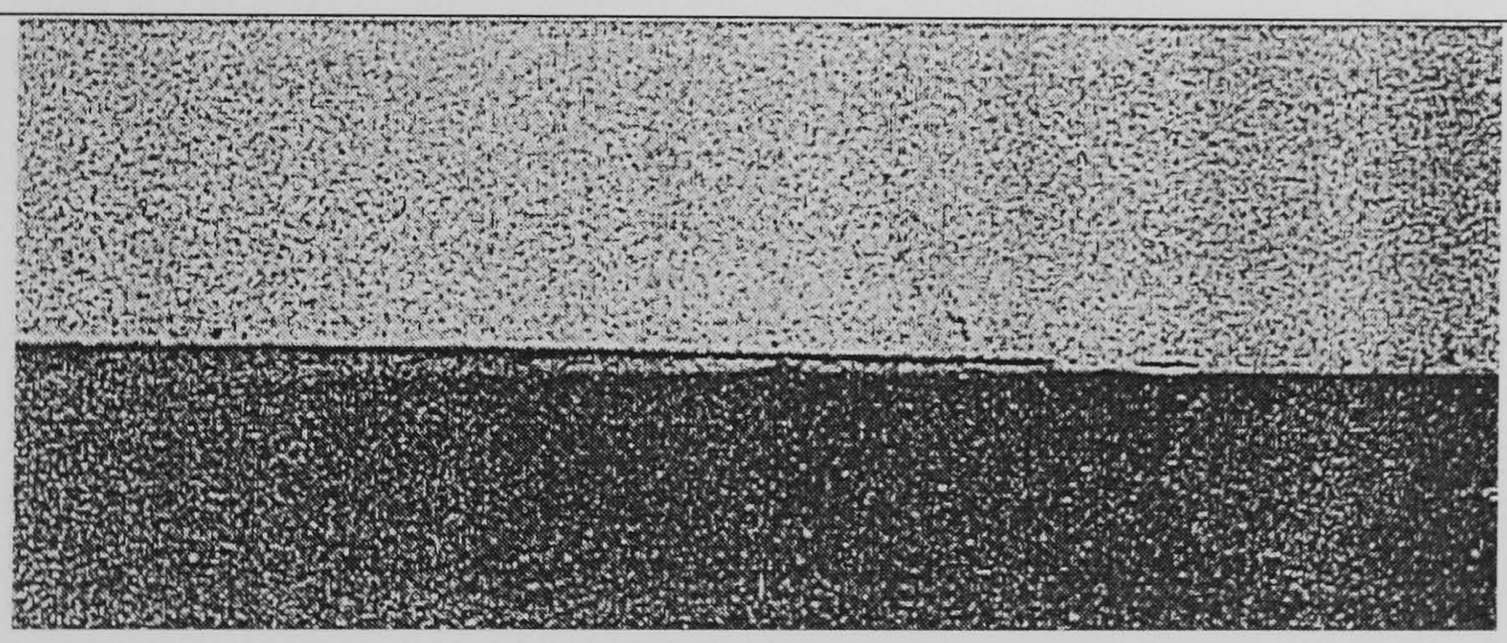

Smearing

Figure 1. Examples of features after Viper grinding.

Magnification x 1000. Unetched

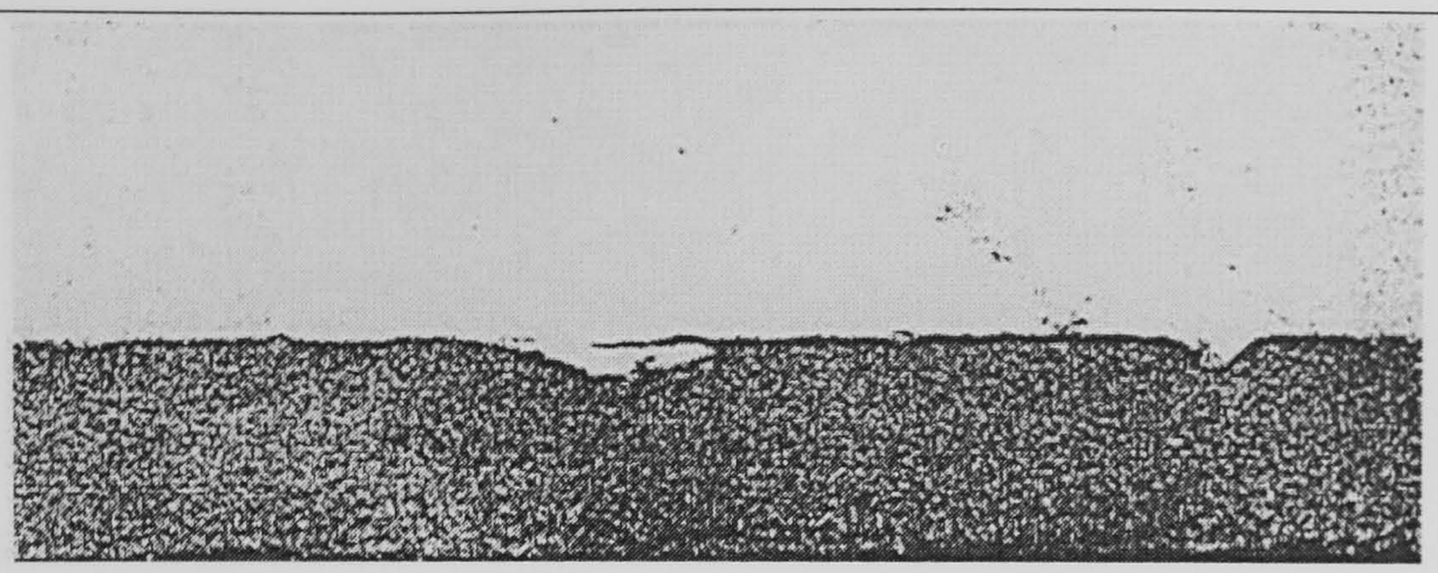

Laps

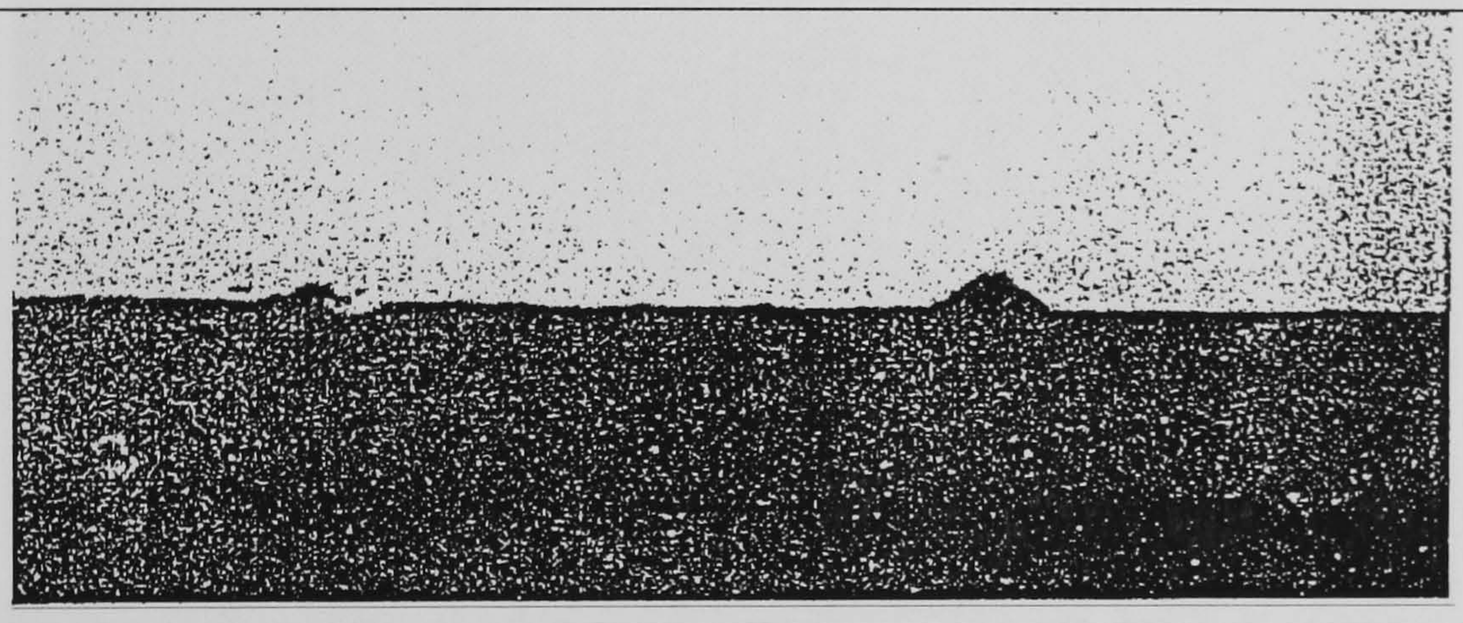

Plucking

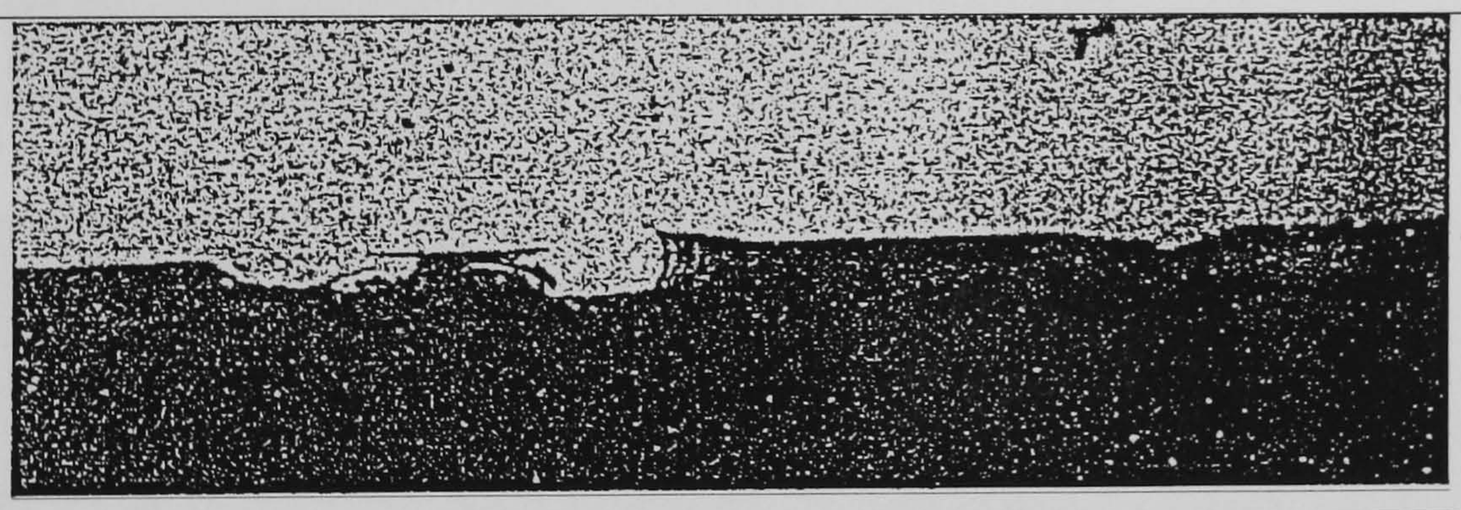

Laps

Figure 2. Examples of surface condition after CBN grinding.

Magnification x 1000. Unetched

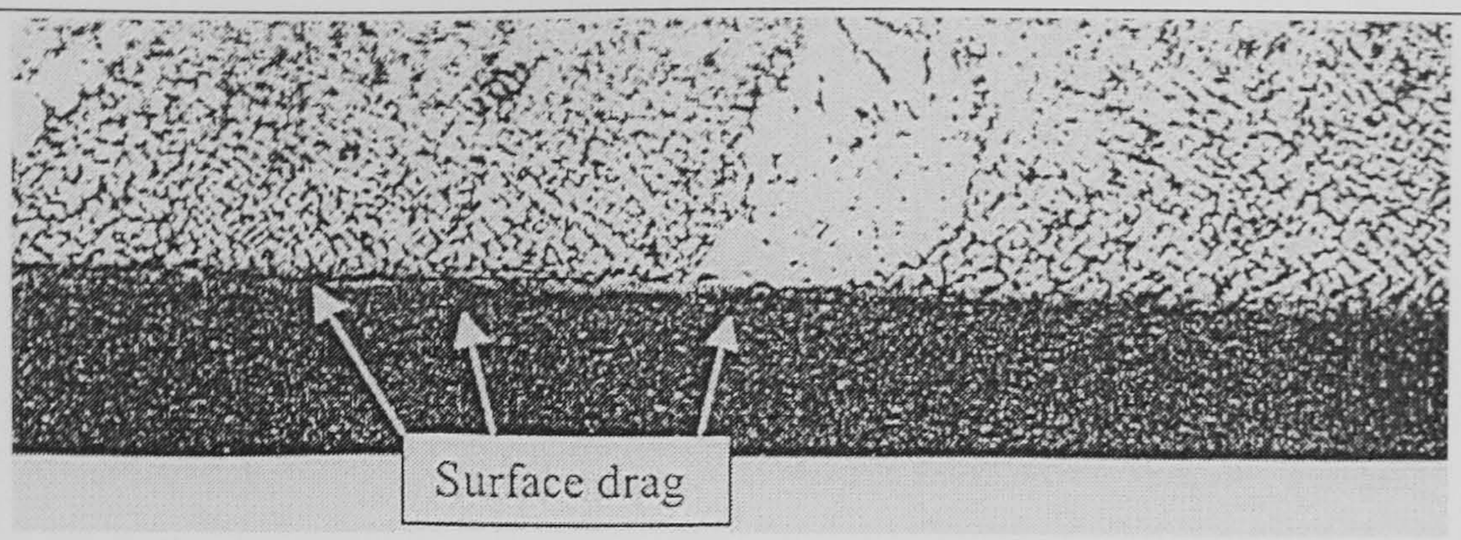

Figure 3. Examples of surface condition after Viper grinding.

Magnification x 1000. Etch:- Electrolytic Etch 10% Oxalic Acid

Appendix L – Mineral Grinding Fluid Datasheets

Castrol International
Marketing and Technology Division

Product Information

CASTROL ILOGRIND 600 SP

Low viscosity chlorine and zinc free neat grinding oil most suited to high speed ,creep feed and especially gear grinding using the latest technology machines from KAPP and NILES. Its low viscosity also gives it good performance in the process of belt or tape finishing where a thin oil with exceptional flushing properties is required.
NOTE - Product can stain yellow metals such as copper and brass

BENEFITS

Excellent lubricity and flushing has given this product a proven advantage in helping resist burning on gear teeth from the grinding process

Gives good wheel life and can extend life between regrinds ,dramatically so compared with water based products

Backed by approvals from the major manufacturers of gear grinding machines in Germany

Low misting and foaming even when used at high pressures and flowrates found on the latest technology machinery.

Zinc and chlorine free formulation can reduce the problem of disposal in certain countries.

PROPERTY	STANDARD	TYPICAL DATA
KINEMATIC VISCOSITY AT- 40 C	IP 71	9.4 cSt
APPEARANCE	BAM 300	CLEAR AMBER LIQUID
DENSITY AT 20 C	IP 365	.87 g/ml
FLASH POINT (PM CLOSED)	IP 34	>130 degC

Castrol International
Marketing and Technology Division

Product Specification

Brand: CASTROL ILOGRIND 600 SP

Version: 2

Technical Responsiblity: Metalworking

Product Classification:

Quality Control Tests

Test	Method	Minimum	Maximum	Typical
Appearance	BAM 300	Clear amber liquid		
Odour	BAM 300	Bland		
Density at 20 °C (g/ml)	IP 365			0.87
Kinematic Viscosity at 40 °C (cSt)	IP 71	7	11	9.4
Flash Point (PM Closed) (°C)	IP 34	130		>130
Foam Sequence 1 - Tendency (ml)	IP 146		50	
Foam Sequence 2 - Tendency (ml)	IP 146		50	
Foam Sequence 3 - Tendency (ml)	IP 146		50	
Sulphur (%wt)	BAM 037	1.05	1.15	
Phosphorus (%wt)	BAM 036	0.085	0.095	

Type Approval Tests

Test	Method	Minimum	Maximum	Typical
Kinematic Viscosity at 20 °C (cSt)	IP 71	16	23	
Cleveland Open Cup Flash Point (°C)	IP 36	140		

Reason For Change

No longer classed as Asia Pacific core range product

Castrol (U.K.) Limited

The Leading Lubrication Specialist

SAFETY DATA SHEET

1: IDENTIFICATION OF THE SUBSTANCE / PREPARATION AND OF THE COMPANY / UNDERTAKING

Product Name: **Variocut G600 SP** Code: **7470-UK**

Application: Metalworking fluid - Neat.

Company: **Castrol (U.K.) Limited**

Address: Burmah Castrol House, Pipers Way, Swindon, Wiltshire, SN3 1RE

Telephone (24 hours): **01793 512712** Fax: 01793 491442

2: COMPOSITION/INFORMATION ON INGREDIENTS

Composition: Highly refined mineral oil and additives.

Hazardous Ingredient(s)	Symbol	Risk Phrases	Other Information	%
This product contains ingredients classified as hazardous. However, they are NOT present in sufficient quantities to warrant classifying the product as hazardous.				

All constituents of this product are listed in EINECS (European Inventory of Existing Commercial Chemical Substances) or ELINCS (European List of Notified Chemical Substances) or are exempt.

Refer to Section 8 for Occupational Exposure Limits.

3: HAZARDS IDENTIFICATION

This product is NOT classified as hazardous.

4: FIRST AID MEASURES

Eyes: Irrigate immediately with copious quantities of water for several minutes.

Skin: Wash thoroughly with soap and water or suitable skin cleanser as soon as possible.

Inhalation: Remove from exposure.

Ingestion: Obtain medical attention. Do NOT induce vomiting.

5: FIRE FIGHTING MEASURES

Suitable Extinguishing Media: Carbon dioxide, powder, foam or water fog - Do not use water jets.

Special Exposure Hazards: None.

Special Protective Equipment: None.

6: ACCIDENTAL RELEASE MEASURES

Personal Precautions: Spilt product presents a significant slip hazard.

Environmental Precautions: Prevent entry into drains, sewers and water courses.

Decontamination Procedures: Soak up with inert absorbent or contain and remove by best available means.

7: HANDLING AND STORAGE

Handling: Avoid breathing spray mist.
To avoid the possibility of skin disorders, repeated or prolonged contact with products of this type must be avoided. It is essential to maintain a high standard of personal hygiene.

Storage: No special precautions.

8: EXPOSURE CONTROLS/PERSONAL PROTECTION

Occupational Exposure Limits:-

Substance	8 Hr.TWA	STEL	Source/Other Information
Mineral oil (see Oil mist, mineral)	5mg/m³	10mg/m³	EH40 (OES)

Engineering Control Measures: Mechanical methods to minimise exposure must take precedence over personal protective measures.
Local exhaust ventilation is recommended.

Personal Protective Equipment: Safety glasses. Plastic apron. Wear impervious gloves (eg of PVC), in case of repeated or prolonged contact.
Change contaminated clothing and clean before re-use.

9: PHYSICAL AND CHEMICAL PROPERTIES

Physical State:	Liquid
Colour:	Amber
Odour:	Mild
Boiling Point/Range (°C):	Above 250
Pour Point: (°C):	Below minus 9
Kinematic Viscosity @ 40°C (cSt):	9.4
Flash Point (closed, °C):	Above 130
Autoignition (°C):	Above 230
Explosive Properties (%):	Explosive limit range (%): Approximately 0.6 - 10.0
Vapour Pressure (kPa at 20°C):	Below 0.1
Relative Density (at 20°C):	0.87
Water Solubility:	Insoluble
Fat Solubility:	Not determined

10: STABILITY AND REACTIVITY

Stability:	Stable, will not polymerise.
Conditions to Avoid:	Temperatures (°C) above 60.
Materials to Avoid:	Strong oxidising agents.
Hazardous Decomposition Products:	Irritant fumes.

11: TOXICOLOGICAL INFORMATION

The following toxicological assessment is based on a knowledge of the toxicity of the product's components.
Expected oral LD_{50}, rat > 2g/kg. Expected dermal LD_{50}, rabbit > 2g/kg.

Health Effects

On Eyes: May cause transient irritation.

On Skin:	Unlikely to cause harm on brief or occasional contact.
By Inhalation:	Mist and vapours may cause irritation to nose and respiratory tract.
By Ingestion:	May cause nausea, vomiting and diarrhoea.
Chronic:	Repeated and prolonged skin contact may lead to skin disorders.
Other:	None known.

12: ECOLOGICAL INFORMATION

Environmental Assessment:	When used and disposed of as intended, no adverse environmental effects are foreseen.
Mobility:	Non-volatile. Liquid. Insoluble in water.
Persistence and Degradability:	Inherently biodegradable.
Bioaccumulative Potential:	Bioaccumulation is unlikely to be significant because of the low water solubility of this product.
Ecotoxicity:	Not expected to be toxic to aquatic organisms. Not expected to be inhibitory to sewage bacteria.

13: DISPOSAL CONSIDERATIONS

Disposal must be in accordance with local and national legislation.

Unused Product:	May be sent for reclamation.
Used/Contaminated Product:	Dispose of through an authorised waste contractor to a licensed site. May be incinerated. For further information see Section 16.
Packaging:	Must be disposed of through an authorised waste contractor. May be steam cleaned and recycled.

14: TRANSPORT INFORMATION

This product is NOT classified as dangerous for transport.

15: REGULATORY INFORMATION

This product is NOT classified as dangerous for supply in the UK.

Hazard Label Data:-

EC Directives:	Waste Oil Directive, 87/101/EEC. Framework Waste Directive, 91/156/EEC.
Statutory Instruments:	Health & Safety at Work, etc. Act 1974. Consumer Protection Act 1987. Environmental Protection Act 1990.
Codes of Practice:	Waste Management. The Duty of Care.
Guidance Notes:	Occupational exposure limits (EH 40). Carcinogenicity of mineral oils (EH 58). Metalworking fluids - health precautions (EH 62). Skin cancer caused by oil [MS(B)5]. Save your skin! - Occupational Contact Dermatitis [MS(B)6]. Dermatitis - cautionary notice [SHW 367]. Effects of mineral oil on the skin [SHW 397]. Health and safety in engineering workshops [HS(G)129].

The above publications are available from HMSO or HSE

Appendix M – Ester Grinding Fluid Datasheet

Castrol (U.K.) Limited

The Leading Lubrication Specialist

SAFETY DATA SHEET

1: IDENTIFICATION OF THE SUBSTANCE / PREPARATION AND OF THE COMPANY / UNDERTAKING

Product Name: **Carecut ES1** Code: 7443-UK

Application: Metalworking fluid - Neat.

Company: **Castrol (U.K.) Limited**

Address: Burmah Castrol House, Pipers Way, Swindon, Wiltshire, SN3 1RE

Telephone (24 hours): 01793 512712 Fax: 01793 491442

2: COMPOSITION/INFORMATION ON INGREDIENTS

Composition: Ester basestocks and additives.

Hazardous Ingredient(s)	Symbol	Risk Phrases	Other Information	%
This product contains ingredients classified as hazardous. However, they are NOT present in sufficient quantities to warrant classifying the product as hazardous.				

All constituents of this product are listed in EINECS (European Inventory of Existing Commercial Chemical Substances) or ELINCS (European List of Notified Chemical Substances) or are exempt.

Refer to Section 8 for Occupational Exposure Limits.

3: HAZARDS IDENTIFICATION

This product is NOT classified as hazardous.

4: FIRST AID MEASURES

Eyes: Irrigate immediately with copious quantities of water for several minutes.

Skin: Wash thoroughly with soap and water or suitable skin cleanser as soon as possible.

Inhalation: Remove from exposure.

Ingestion: Obtain medical attention. Do NOT induce vomiting.

5: FIRE FIGHTING MEASURES

Suitable Extinguishing Media: Carbon dioxide, powder, foam or water fog - Do not use water jets.

Special Exposure Hazards: None.

Special Protective Equipment: None.

6: ACCIDENTAL RELEASE MEASURES

Personal Precautions: Spilt product presents a significant slip hazard.

Environmental Precautions: Prevent entry into drains, sewers and water courses.

Decontamination Procedures: Soak up with inert absorbent or contain and remove by best available means.

7: HANDLING AND STORAGE

Handling: Avoid breathing spray mist.
To avoid the possibility of skin disorders, repeated or prolonged contact with products of this type must be avoided. It is essential to maintain a high standard of personal hygiene.

Storage: No special precautions.

8: EXPOSURE CONTROLS/PERSONAL PROTECTION

Occupational Exposure Limits:- None.

Engineering Control Measures: Mechanical methods to minimise exposure must take precedence over personal protective measures.
Local exhaust ventilation is recommended.

Personal Protective Equipment: Safety glasses. Plastic apron. Wear impervious gloves (eg of PVC), in case of repeated or prolonged contact.
Change contaminated clothing and clean before re-use.

9: PHYSICAL AND CHEMICAL PROPERTIES

Physical State:	Liquid
Colour:	Straw
Odour:	Mild
Boiling Point/Range (°C):	Above 200
Kinematic Viscosity @ 40°C (cSt):	27
Kinematic Viscosity @ 100°C (cSt):	6
Flash Point (closed, °C):	240
Autoignition (°C):	Above 250
Explosive Properties (%):	Not determined
Vapour Pressure (kPa at 20°C):	Below 0.1
Relative Density (at 20°C):	Below 1.0
Water Solubility:	Insoluble
Fat Solubility:	Not determined

10: STABILITY AND REACTIVITY

Stability:	Stable, will not polymerise.
Conditions to Avoid:	Temperatures (°C) above 120
Materials to Avoid:	Strong oxidising agents.
Hazardous Decomposition Products:	Irritant fumes.

11: TOXICOLOGICAL INFORMATION

The following toxicological assessment is based on a knowledge of the toxicity of the product's components.
Expected oral LD_{50}, rat > 2g/kg.

Health Effects

On Eyes: May cause transient irritation.

On Skin: Unlikely to cause harm on brief or occasional contact.

By Inhalation: Mist and vapours may cause irritation to nose and respiratory tract.

By Ingestion:	May cause nausea, vomiting and diarrhoea.
Chronic:	Repeated and prolonged skin contact may lead to skin disorders.
Other:	None known.

12: ECOLOGICAL INFORMATION

Environmental Assessment:	When used and disposed of as intended, no adverse environmental effects are foreseen.
Mobility:	Non-volatile. Mobile liquid. Insoluble in water.
Persistence and Degradability:	Not known.
Bioaccumulative Potential:	Not determined.
Ecotoxicity:	Not expected to be toxic to aquatic organisms. Not expected to be inhibitory to sewage bacteria.

13: DISPOSAL CONSIDERATIONS

Disposal must be in accordance with local and national legislation.

Unused Product:	May be sent for reclamation.
Used/Contaminated Product:	Dispose of through an authorised waste contractor to a licensed site. May be incinerated. For further information see Section 16.
Packaging:	Must be disposed of through an authorised waste contractor. May be steam cleaned and recycled.

14: TRANSPORT INFORMATION

This product is NOT classified as dangerous for transport.

15: REGULATORY INFORMATION

This product is NOT classified as dangerous for supply in the UK.

Hazard Label Data:-

EC Directives:	Framework Waste Directive, 91/156/EEC.
Statutory Instruments:	Health & Safety at Work, etc. Act 1974. Consumer Protection Act 1987. Environmental Protection Act 1990.
Codes of Practice:	Waste Management. The Duty of Care.
Guidance Notes:	Save your skin! - Occupational Contact Dermatitis [MS(B)6]. Dermatitis - cautionary notice [SHW 367]. Health and safety in engineering workshops [HS(G)129].

The above publications are available from HMSO or HSE

16: OTHER INFORMATION

Castrol Advice Sheet: The Disposal of Used Metalworking Fluids.
Castrol publication: Talking about Cutting Fluids.
Code of Practice for Metalworking Fluids (IP).
Several publications relating to the use of metalworking fluids are available from the HSE.

Appendix N – Water Based Grinding Fluid Datasheet

Castrol (U.K.) Limited

The Leading Lubrication Specialist

SAFETY DATA SHEET

1: IDENTIFICATION OF THE SUBSTANCE / PREPARATION AND OF THE COMPANY / UNDERTAKING

Product Name: **Hysol XH** Code: **7049-UK**

Application: Metalworking fluid - Soluble.

Company: **Castrol (U.K.) Limited**

Address: Burmah Castrol House, Pipers Way, Swindon, Wiltshire, SN3 1RE

Telephone (24 hours): **01793 512712** Fax: 01793 491442

2: COMPOSITION/INFORMATION ON INGREDIENTS

Composition: Highly refined mineral oil, emulsifiers and additives.
Contains biocide. Contains Polysulphide.

Hazardous Ingredient(s)	Symbol	Risk Phrases	Other Information	%
This product contains ingredients classified as hazardous. However, they are NOT present in sufficient quantities to warrant classifying the product as hazardous.				

All constituents of this product are listed in EINECS (European Inventory of Existing Commercial Chemical Substances) or ELINCS (European List of Notified Chemical Substances) or are exempt.

Refer to Section 8 for Occupational Exposure Limits.

3: HAZARDS IDENTIFICATION

This product is NOT classified as hazardous.

4: FIRST AID MEASURES

Eyes: Irrigate immediately with copious quantities of water for several minutes.
Obtain medical attention if irritation persists.

Skin: Wash thoroughly with soap and water or suitable skin cleanser as soon as possible.

Inhalation: Remove from exposure.

Ingestion: Obtain medical attention. Do NOT induce vomiting. Wash out mouth with water.

5: FIRE FIGHTING MEASURES

Suitable Extinguishing Media: Carbon dioxide, powder, foam or water fog - Do not use water jets.
Prevent contaminated extinguishing media from entering drains, sewers and water courses.

Special Exposure Hazards: Sulphur compounds including hydrogen sulphide.
Nitrogen compounds.

Special Protective Equipment: Self-contained breathing apparatus.

6: ACCIDENTAL RELEASE MEASURES

Personal Precautions:	Spilt product presents a significant slip hazard.
Environmental Precautions:	Prevent entry into drains, sewers and water courses.
Decontamination Procedures:	Soak up with inert absorbent or contain and remove by best available means.

7: HANDLING AND STORAGE

Handling: Avoid breathing spray mist.
To avoid the possibility of skin disorders, repeated or prolonged contact with products of this type must be avoided. It is essential to maintain a high standard of personal hygiene.
This product has been formulated to be used diluted with water. The dilution rate will need to be varied depending on the application. For this information, please refer to the Castrol Technical Data Sheet.

Storage: Protect from frost. Store out of direct sunlight. Store between (°C): 5 - 40.

8: EXPOSURE CONTROLS/PERSONAL PROTECTION

Occupational Exposure Limits:-

Substance	8 Hr.TWA	STEL	Source/Other Information
Mineral oil (see Oil mist, mineral)	5mg/m^3	10mg/m^3	EH40 (OES)
Formaldehyde (formed in solution)	2ppm	2ppm	EH40 (MEL)

Engineering Control Measures:	Mechanical methods to minimise exposure must take precedence over personal protective measures. Local exhaust ventilation is recommended.
Personal Protective Equipment:	Safety glasses. Plastic apron. Wear impervious gloves (eg of PVC), in case of repeated or prolonged contact. Change contaminated clothing and clean before re-use.

9: PHYSICAL AND CHEMICAL PROPERTIES

Physical State:	Liquid
Colour:	Amber
Odour:	Mild
pH(working dilution):	9.3 (5%)
Boiling Point/Range (°C):	Above 100
Pour Point: (°C):	Below 0
Flash Point (closed, °C):	Above 100
Autoignition (°C):	Not determined
Explosive Properties (%):	Not determined
Vapour Pressure (kPa at 20°C):	Not determined
Relative Density (at 20°C):	0.97
Water Solubility:	Emulsifiable
Fat Solubility:	Not determined

10: STABILITY AND REACTIVITY

Stability:	Stable, will not polymerise.
Conditions to Avoid:	Temperatures (°C) above 50.

Materials to Avoid:	Strong oxidising agents. Strong acids.
Hazardous Decomposition Products:	Sulphur compounds including hydrogen sulphide. Nitrogen compounds.

11: TOXICOLOGICAL INFORMATION

The following toxicological assessment is based on a knowledge of the toxicity of the product's components. Expected oral LD_{50}, rat > 2g/kg. Expected dermal LD_{50}, rabbit > 2g/kg.
Not classified as an eye or skin irritant.

Health Effects

On Eyes:	May cause transient irritation.
On Skin:	May defat the skin.
By Inhalation:	Mist and vapours may cause irritation to nose and respiratory tract.
By Ingestion:	May cause nausea, vomiting and diarrhoea.
Chronic:	Repeated and prolonged skin contact may lead to skin disorders.
Other:	None known.

12: ECOLOGICAL INFORMATION

Environmental Assessment:	May cause ecological damage in aquatic systems and must be used and disposed of in accordance with the recommendations made in this safety data sheet.
Mobility:	Mobile liquid. Emulsifiable in water.
Persistence and Degradability:	Inherently biodegradable.
Bioaccumulative Potential:	Not determined.
Ecotoxicity:	Not determined.

13: DISPOSAL CONSIDERATIONS

Disposal must be in accordance with local and national legislation.

Unused Product:	Dispose of through an authorised waste contractor to a licensed site. European Waste Code: 12 01 07.
Used/Contaminated Product:	Diluted product may be separated by chemical means before removal by an authorised waste contractor. For further information see Section 16. European Waste Code: 12 01 09.
Packaging:	Must be disposed of through an authorised waste contractor. May be steam cleaned and recycled.

14: TRANSPORT INFORMATION

This product is NOT classified as dangerous for transport.

15: REGULATORY INFORMATION

This product is NOT classified as dangerous for supply in the UK.

Hazard Label Data:-

EC Directives:	Waste Oil Directive, 87/101/EEC.
Statutory Instruments:	Health & Safety at Work, etc. Act 1974. Consumer Protection Act 1987. Environmental Protection Act 1990.
Codes of Practice:	Waste Management. The Duty of Care.